Design and Optimization of Cell-Free Systems: Channel Estimation, Duplexing Scheme, and Synchronization

A Thesis

Submitted for the Degree of

Doctor of Philosophy

in the **Faculty of Engineering**

by

Anubhab Chowdhury

under the Guidance of

Chandra R. Murthy

Electrical Communication Engineering
Indian Institute of Science, Bangalore
Bangalore – 560 012 (INDIA)

June 2024

To My Family

Acknowledgments

First and foremost, my sincere gratitude is to my advisor, *Prof. Chandra Murthy*, whose continuous technical and moral support was the driving force throughout my Ph.D. study. His dedication to research is exemplary and inspiring. He has been remarkably patient with all my mistakes, helped me learn from them, and taught me how to improve. I immensely value his counsel on formulating meaningful research problems and how one should write and present research, balancing the lucidity of presentation with the technical intricacies. He was extremely kind to accommodate all the impromptu meeting requests I made, and everything I learned during our personal meetings will be invaluable ammunition for my future career.

I want to convey my gratitude to my collaborators, *Dr. Ribhu Chopra* and *Dr. Pradip Sasmal*, whose expertise complemented the contents of certain chapters of this thesis. Further, a special thanks goes to *Dr. Ribhu Chopra*, who nurtured my passion for research during my M.Tech. project, and also introduced me to *Prof. Chandra Murthy's* vibrant research group. I also sincerely thank my review committee members, *Prof. K. V. S Hari*, *Prof. Sundeep Chepuri*, and *Prof. Chandramani Singh*, for their constructive feedback. I also thank *Prof. Neelesh Mehta* and *Prof. K. V. S Hari* for their support and recommendations. Finally, I thank *Dr. Sanjeev Gopinath* for offering me a visiting instructor position multiple times at PESU to help me fulfill my PMRF teaching requirements.

I sincerely thank ECE office members, especially *Mr. Srinivasa Murthy* and *Ms. Rajani*, for their administrative support.

Being part of the Signal Processing for Communication (SPC) laboratory has been a pleasure. I am incredibly grateful to its alums and current members: *Lekshmi, Sai, Unnikrishnan, Pradip, Abhinav, Soumendu, Chandrasekhar, Rupam, Chirag, Dheeraj, Sameera, Yashvanth, Niladri, Krishna Praveen, Shankhadeep*, and *Prabhat*. They all deserve a few words of appreciation. I would have struggled during the initial days of my Ph.D. without the spontaneous technical and nontechnical help from *Lekshmi, Sai, Arun, Pradip,* and *Chirag*. Although senior in age and experience, *Sameera* has been the much-needed batch-mate whose sense of humor relieved the stress of coursework and exams. A special thanks to *Soumendu* for being a good friend and often entertaining me in his rented

flat on weekends. My occasional weekend outings with *Sai, Chirag, Pradip, Yashvanth*, and *Soumendu* were always refreshing. *Yashvanth* has been unfailingly affirmative to my countless requests for coffee breaks and has been, and still is, a patient listener to my ramblings about life in general and an excellent friend.

I want to thank the Next Gen. Lab. colleagues, *Sarvendranath, Sayantan, Sruthi, Suji, Sandip*, and *Samaresh*, with whom I shared several fond memories during SPCOM volunteering. My thanks go to my batch-mates, *Krishnan, Elizabeth*, and *Prashob*. I was often involved in seemingly unending discussions with them, ranging from deep technical matters to the quality of mess food. I thank *Nagabhushan*, with whom I collaboratively taught several courses as a part of our PMRF deliverables.

I am indebted to my family. I am immensely grateful to my parents, *Subhendu* and *Banabani*, who put their best efforts into bringing me up in a cosmopolitan and academically liberal atmosphere. My loving sister, *Anyatama*, has never failed to take my side in every little aspect of family life and will soon become a doctor herself. My late grandfathers would have been very proud today, as they were for whatever I have achieved. I thank my grandmothers for their unconditional love. My late maternal uncle has taught me the values of sacrifice and simple life. Finally, my dearest pet cats have been a source of absolute peace, and without them, I would have certainly lost my sanity during the crazy days of the COVID lockdown.

Abstract

Cell-free massive multiple-input multiple-output (CF-mMIMO) systems, where multiple access points (APs) jointly and coherently serve a large number of user-equipments (UEs) in a geographical area, offer multi-fold improvement in spectral efficiency (SE) compared to cellular mMIMO systems. This is because of its unique ability to convert multi-cell interference of a cellular system to useful information-bearing signals while performing joint data processing at the central processing unit (CPU). Further, the proximity of the UEs and the distributed APs improves macro-diversity and link reliability, which in turn provides a uniform quality of service (QoS) to all the UEs while maintaining a high peak data rate. However, several signal processing challenges need to be thoroughly understood and addressed, in order to make CF-mMIMO practically viable. In this regard, this thesis addresses three problems in CF-mMIMO systems: channel estimation, enabling dynamic time division duplexing (DTDD), and synchronization.

In CF-mMIMO systems, a natural UE grouping by the serving base stations (BSs) does not exist, unlike a cellular mMIMO system. Also, in cellular mMIMO, only the serving BS aims to estimate the channel from a given UE, while in a CF-mMIMO system, all the APs in the vicinity of a given UE need to obtain good channel estimates. Therefore, there is a need to revisit the allocation of pilot sequences across UEs to mitigate pilot contamination in CF-mMIMO systems. We address the problem of channel estimation from three different viewpoints: (i) design of quasi-orthogonal pilots, (ii) development of a low complexity algorithm for pilot allocation, and (iii) pilot length minimization while ensuring that physically proximal UEs do not suffer from pilot contamination. We first develop a clustering algorithm for APs and UEs and propose a novel mutually unbiased orthonormal bases (MUOB)-based pilot (quasi-orthogonal) design, where the pilots are orthogonal within a cluster of APs and UEs and minimally correlated across clusters. Theoretically, we show that pilot sets forming MUOB minimize inter- and intra-cluster pilot contamination. The key advantage of MUOB is that, once these AP-UE clusters are formed, the effect of pilot contamination on the channel estimates is *allocation-agnostic* due to the constant correlation properties of the MUOB pilots. We also develop iterative algorithms for pilot allocation where clustering of APs and UEs is not required. Now,

the preceding two schemes are for a predetermined length of pilot sequences. Hence, we next formulate a pilot length minimization problem and propose a novel pilot design and allocation algorithm that ensures no pilot contamination among any pair of UEs that are proximal to a common AP, and this is guaranteed at all APs. Further, our algorithm procures the pilot allocation with a minimum number of orthogonal pilots being reused across the UEs. We numerically validate the superiority of the proposed algorithms over several existing schemes in the literature and also provide a comparative study of our proposed algorithms.

We next analyze the performance of DTDD-enabled CF-mMIMO systems, where the uplink (UL) reception and downlink (DL) transmission modes of the half-duplex (HD) APs can be scheduled based on the local UL/DL traffic load. Thus, a DTDD-enabled CF system operates like a virtual full-duplex (FD) system that can concurrently serve UL and DL UEs; however, with HD hardware. However, the sum UL-DL SE is limited by inter-AP interference (InAI) and inter-UE interference (InUI), commonly referred to as cross-link interferences (CLIs). We analyze the effects of CLIs on the sum UL-DL SE of DTDD CF systems. We also develop greedy AP scheduling algorithms and UL-DL power allocation strategies to maximize the sum UL-DL SE. Our algorithms come with closed-form update equations and are shown to converge to local optima. Numerical experiments illustrate that sum SE with DTDD can match and even *outperform* an FD CF system and also an FD cellular system with similar antenna density. This is because DTDD can schedule the APs in UL or DL based on the localized traffic load and achieve better array gain for a given antenna density. Further, in DTDD, CF has better InAI suppression capability as only the subset of APs that are operating in DL interferes with the subset of APs that are operating in UL. In contrast, all the APs contribute to InAI in an FD CF system. Hence, although DTDD and FD enable the CF system to concurrently serve UL and DL UEs, DTDD is preferable because it can meet and even outperform FD without requiring IrAI cancellation hardware.

We next address the synchronization issues in a UL CF-mMIMO system using orthogonal frequency division multiplexing (OFDM). The distributed nature of the CF system results in different propagation delays in the signals received at the APs. This delay in receiving signals from different UEs can exceed the cyclic prefix duration, leading to interference from adjacent subcarriers and consecutive OFDM symbols. We develop a mathematical framework to analyze the impact of inter-carrier and inter-symbol interference (ICI and ISI) in the UL SE of the CF-mMIMO OFDM system. Our analysis shows that ignoring this crucial aspect leads to a gross overestimation of the achievable UL SE. We also develop an interference-aware combining scheme to alleviate ISI and ICI in addition to multi-UE

interference. We then account for the scenario in which each UE performs a timing-advance with respect to its nearest AP. Numerically, we illustrate that ICI and ISI can significantly limit the achievable SE, but their impact can be significantly mitigated by employing the nearest AP-based timing advance and interference-aware combining. In fact, in many scenarios, the performance is close to that of a time-aligned CF-mMIMO system.

In summary, in this thesis, we address three aspects of CF-mMIMO systems: channel estimation, DTDD, and UL synchronization. Overall, the key takeaways are as follows:

- We develop novel pilot design and allocation algorithms for CF-mMIMO systems. In particular, *our algorithm based on vertex-coloring ensures no contamination among the UEs that are being served by one or more common AP(s) and, at the same time, procures an optimal allocation with the least number of orthogonal pilots.*

- We analyze the sum UL-DL SE of DTDD-enabled CF systems and develop algorithms for APs' UL/DL mode scheduling and UL-DL power allocation. Our *major* finding is that *DTDD-enabled CF is more resilient to CLIs and can even outperform FD cellular as well as FD CF systems with similar antenna densities.*

- Finally, we develop a theoretical framework to analyze the effects of asynchronous reception on the UL SE of the CF-mMIMO systems. Our analysis and experiments *underscore the importance of the proposed interference-aware combining scheme that is able to mitigate the resulting ICI and ISI considerably, obtaining a near synchronous/ideal performance.*

For all the above cases, we benchmark the performances of our proposed schemes with several existing comparable methods and validate the superiority of the developed algorithms in terms of achievable SE, complexity, and convergence.

Glossary

Acronym	Definition
3GPP	Third Generation Partnership Project
5G NR	Fifth Generation New Radio
ADMM	Alternating Direction Method of Multipliers
AO	Alternating Optimization
AP	Access-Point
AWGN	Additive White Gaussian Noise
BS	Base Station
CDF	Cumulative Distribution Function
CF	Cell-Free
CLI	Cross Link Interference
CoMP	Coordinated Multipoint
CP	Cyclic Prefix
CPU	Central Processing Unit
CSI	Channel State Information
DAA	Distributed Antenna Arrays
DL	Downlink
DTDD	Dynamic Time Division Duplex
EE	Energy Efficiency
FD	Full-Duplex
FP	Fractional Programming
ICI	Inter-Carrier Interference
ISI	Inter-Symbol Interference
InAI	Inter-AP Interference
InUI	Inter-user Interference
IrAI	Intra-AP Interference

LMMSE	Linear Minimum Mean Squared Error
LSFD	Large-Scale Fading Decoding
LTE	Long-Term Evolution
MFP	Matched-Filter Precoding
MIMO	Multiple-Input Multiple-Output
mMIMO	Massive Multiple-Input Multiple-Output
MU-MIMO	Multi-User Multiple-Input Multiple-Output
MMSE	Minimum Mean Squared Error
MRC	Maximal Ratio Combining
MSE	Mean Squared Error
MUOB	Mutually Unbiased Orthonormal Basis
NMSE	Normalized Mean Squared Error
NP-hard	Non-Deterministic Polynomial-Time hard
OFDM	Orthogonal Frequency Division Multiplexing
OPR	Orthogonal Pilot Reuse
QCQP	Quadratically Constrained Quadratic Program
QoS	Quality of Service
RZF	Regularized Zero-Forcing
SE	Spectral Efficiency
SI	Self-Intereference
SINR	Signal-to-Interference-plus-Noise Ratio
SNR	Signal-to-Noise Ratio
TDD	Time Division Duplex
UE	User-Equipment
UL	Uplink
ZC	Zadoff-Chu
ZF	Zero Forcing
ZFC	Zero Forcing Combining
ZFP	Zero Forcing Precoding

Notation

Vectors and matrices are denoted by boldface small and capital letters, respectively. Sets are denoted by calligraphy letters. The rest of the notation is listed below.

Vectors

$[\mathbf{a}]_i$	:	ith element of a vector $\mathbf{a}$
$\langle \mathbf{a}, \mathbf{b} \rangle$	:	Inner product between two vectors $\mathbf{a}$ and $\mathbf{b}$
$\|\mathbf{a}\|_2$	:	l_2 norm of a vctor $\mathbf{a}$
$\mathbf{e}_i$	:	ith column of identity matrix
$\mathbf{0}_N$	:	All zero vector of length N

Matrices

$\mathbf{I}_N$	:	Identity matrix of dimension $N \times N$
$\mathbf{A} = [\mathbf{a}_1, \ldots, \mathbf{a}_N]$	:	A matrix $\mathbf{A}$ whose columns are $\mathbf{a}_1, \ldots, \mathbf{a}_N$
$[\mathbf{A}]_{m,n}$	:	(m, n)th entry of $\mathbf{A}$
$[\mathbf{A}]_{:,n}$	:	nth column of $\mathbf{A}$
$[\mathbf{A}]_{m,:}$	:	mth row of $\mathbf{A}$
$\mathbf{A}^T$	:	Transpose of a matrix $\mathbf{A}$
$\mathbf{A}^{-1}$	:	Inverse of a matrix $\mathbf{A}$
$\mathbf{A}^*$	:	Conjugation of a matrix $\mathbf{A}$
$\mathbf{A}^H$	:	Conjugate transpose (Hermitian) of a matrix $\mathbf{A}$
$\mathtt{tr}(\mathbf{A})$	:	Trace of a matrix $\mathbf{A}$
$\mathsf{diag}(\mathbf{a})$	:	Diagonal matrix with entries of the vector $\mathbf{a}$ on the diagonal
$\mathbf{0}_{N \times N}$	:	All zero matrix of dimension $N \times N$

Field

$\mathbb{R}$	:	Field of real numbers
$\mathbb{C}$	:	Field of complex numbers

Probability

$\mathbb{E}[.]$	:	Expectation of a random variable/vector
$\texttt{var}(.)$	:	Variance of a random variable/vector
$\mathcal{CN}(\mathbf{0}, \mathbf{\Sigma})$	:	Zero mean circularly symmetric complex normal with covariance $\mathbf{\Sigma}$
$\xrightarrow{\mathsf{P}}$	:	Convergence in probability

Set

$\lvert\mathcal{A}\rvert$	:	Cardinality of the set $\mathcal{A}$
$\mathcal{A} \cup \mathcal{B}$	:	Union of the set $\mathcal{A}$ and $\mathcal{B}$
$\mathcal{A} \cap \mathcal{B}$	:	Intersection of the set $\mathcal{A}$ and $\mathcal{B}$
$\mathcal{A} \backslash \mathcal{B}$	:	Set difference: set of elements in $\mathcal{A}$ that are not in $\mathcal{B}$
$\mathcal{A}'$	:	Complement of the set $\mathcal{A}$
$\mathcal{A} \subseteq \mathcal{B}$	:	$\mathcal{A}$ is subset of $\mathcal{B}$
$\{j\} \notin \mathcal{I}$	:	j is not an element of the index set $\mathcal{I}$
$\emptyset$	:	Null set or empty set

Miscellaneous

$\mathbb{R}^{N \times M}$	:	The set of real-valued $N \times M$ matrices
$\mathbb{C}^{N \times M}$	:	The set of complex-valued $N \times M$ matrices
$\lvert x\rvert$	:	Absolute value of a complex scalar x
$\lceil x \rceil$	:	The smallest integer not less than the scalar $x \in \mathbb{R}$
$\forall x$	:	The statement holds for all x (in the set that x belongs to)
$\mathcal{O}(.)$	:	Big-O notation or Bachmann–Landau notation
$\log_2(x)$	:	Logarithm of x using the base 2

Thesis-Specific Notation

The following notations are common across chapters. Any notation used only in a specific chapter is explicitly defined in the corresponding chapter.

M	:	Number of APs in the system
$\mathcal{A}$	:	Set of all AP indices
$\mathcal{A}_{\mathsf{u}}$	:	Set of AP indices operating in UL mode
$\mathcal{A}_{\mathsf{d}}$	:	Set of AP indices operating in DL mode
K	:	Total number of UEs in the system
$\mathcal{U}$	:	Set of all UE indices
$\mathcal{U}_{\mathsf{u}}$	:	Set of UL UE indices
$\mathcal{U}_{\mathsf{d}}$	:	Set of DL UE indices
N	:	Number of antennas per AP
$\mathbf{f}_{mk} \in \mathbb{C}^N$	:	The channel (includes both fast and slow fading) between
	:	the kth UE to mth AP
$\mathbf{h}_{mk} \in \mathbb{C}^N$	:	The fast fading channel ($\mathcal{CN}(\mathbf{0}_N, \mathbf{I}_N)$) between the kth UE to mth AP
β_{mk}	:	Slow fading coefficient (includes path loss and shadowing) between
	:	the kth UE to mth AP
$\hat{\mathbf{f}}_{mk} \in \mathbb{C}^N$	:	MMSE estimate of the channel $\mathbf{f}_{mk}$
$\tilde{\mathbf{f}}_{mk} \in \mathbb{C}^N$	:	MMSE estimation error of the channel $\mathbf{f}_{mk}$
τ_p	:	Length of the pilot signals
τ	:	Length of the coherence interval
N_0	:	AWGN variance
N_{s}	:	Number of sub-carriers
N_{cp}	:	Cyclic-prefix length
N_{o}	:	OFDM symbol duration (time domain)

Contents

List of Figures

List of Tables

1 Cellular to Cell-Free: A Paradigm Shift

Chapter Highlights

This chapter reviews the state-of-the-art cellular wireless systems that use massive multiple-input multiple-output (mMIMO) technology. Within the purview of mMIMO, several different topologies, such as coordinated multipoint (CoMP) access, virtual MIMO, small-cell/ultra-dense network, etc., have evolved in the last decade to improve the spectral efficency (SE), coverage, and quality of service (QoS) of cellular systems. However, there are two fundamental limitations of cellular mMIMO deployments, even with cooperation among the base stations (BSs): (a) inter-cell interference and (b) poor signal-to-noise ratio (SNR) of the cell-edge UEs. Procuring uniform QoS along with a high peak data rate for all the UEs in a geographical area requires an altogether different topology that can reap the benefits of mMIMO and, at the same time, the advantages of joint signal processing like a CoMP system. In this regard, *cell-free mMIMO (CF-mMIMO)* has emerged as a potential candidate where distributed access points (APs) jointly and coherently serve the UEs in a given area. Since the UEs communicate with multiple distributed APs, a CF system offers a much higher degree of macro-diversity compared to its cellular counterpart. This, in turn, can be exploited to obtain higher spatial-multiplexing gains, mitigating the detrimental effects of path loss and shadow fading; and eventually offering multi-fold improvement in the SE. Here, we survey the current literature on CF-mMIMO systems, discuss various signal processing challenges, and summarize the major contributions of this thesis in providing new and novel techniques, especially related to channel estimation, duplexing scheme, and synchronization, in the context of CF systems.

1.1 Cellular Massive MIMO

Massive multiple-input multiple-output (mMIMO) technology, where the base stations (BSs) are equipped with a large number of antennas and are capable of serving multiple user-equipments (UEs) in the same time-frequency resource via aggressive spatial multiplexing, has evolved from being an ambitious academic idea [1–3] to become a key enabler for the *cellular* 5G new radio (NR) [4]. Two immediate effects of massive antennas at the BS are the so-called *channel hardening* [5][1] and *favorable propagation*[2], which makes linear precoding and receive combining near-optimal, significantly reducing the complexity of power and resource allocation and, in turn, making mMIMO scalable compared to the conventional multi-user MIMO (MU-MIMO) systems. Further, the array gain in mMIMO improves linearly with the number of BS antennas, while the number of independent interfering signals does not, leading to a multi-fold improvement in the spectral efficiency (SE) compared to MU-MIMO systems.

However, mMIMO in its cellular form does not provide uniform quality of service (QoS) due to the significant path loss encountered by the UEs near the cell edge. Inter-cell interference further deteriorates the achievable SEs for these UEs. One way to reduce inter-cell interference and boost the cell-edge signal-to-noise ratio (SNR) is to consider cooperation among the neighboring BSs. An alternative is to deploy several pico or micro BSs in each cell. In the last two decades, these architectures promoted a plethora of new technologies, such as coordinated multipoint (CoMP) [7], virtual MIMO [8], and distributed antenna array (DAA) [9], all under the umbrella of network MIMO [10]. However, although network MIMO improves the overall SE compared to conventional cellular MIMO, it comes at the cost of exchanging the instantaneous channel state information (CSI) among the

[1] Channel hardening refers to the phenomenon where the fluctuation between the instantaneous and average channel gain is negligible. Formally, suppose $\mathbf{h}$ is a N dimensional channel vector. We say that the channel hardens if $\|\mathbf{h}\|_2^2 / \mathbb{E}\left[\|\mathbf{h}\|_2^2\right] \xrightarrow{\mathsf{P}} 1$ as $N \to \infty$ [6].

[2] Due to large number of antennas at the BS, the UEs' channels become approximately orthogonal, which in turn reduce multi-user interference and facilitate spatial multiplexing [3].

cooperating BSs, imposing a high front-haul load and detrimentally affecting the system latency. Further, the SE attained via cooperation among BSs is still limited to a finite value even if the transmit power is infinite and the power of out-of-cluster interfering BSs scales with that of the in-cluster (cooperating BSs) signals [11]. Another way to improve achievable SE is via cell densification along with CoMP. In this case, a large macro cell is partitioned into smaller pico or micro-cells, which reduces the relative distances between the BSs and the UEs and mitigates the limiting effects of path loss. Such deployments are known as small cells or ultra-dense networks, which can even be aided with CoMP via small-cell clustering. Ideally, the network capacity should grow proportionally to the number of small-cell BSs. However, the SE gain drastically reduces after a certain threshold of cell densification due to inordinately high inter-cell interference [12]. The fundamental drawback of all these variants of cellular mMIMO is that they fail to turn the outer-cell interference or outer-cluster interference (for CoMP) into useful information-bearing signals that can improve the SE via joint data processing.

Now, to overcome the above limitation of cellular MIMO and provide uniformly high SE throughout the geographical area, the next generations of wireless systems need to be built on an altogether new premise. A promising candidate for this is the *cell-free* mMIMO (CF-mMIMO) network [13], a new paradigm that enjoys the benefits of mMIMO, CoMP, and also ultra-dense networks; and naturally eliminates inter-cell interference.[3]

1.2 CF-mMIMO: Benefits and Challenges

CF-mMIMO refers to a network topology where distributed access points (APs)[4], connected to a central processing unit (CPU) via front-haul links, jointly and coherently

[3]Here, "no inter-cell interference" does not imply the absence of multi-UE interference. The suppression of multi-UE interference depends on the choice of combiners and precoders. However, via joint processing, CF-mMIMO takes the data streams of all other UEs into account while decoding the data stream of a particular UE, enabling it to largely overcome multi-UE interference effects.

[4]In this thesis, following the convention and for clarity of understanding, we use the term AP for the distributed antenna arrays in CF systems and BS for the centralized antenna arrays in cellular systems.

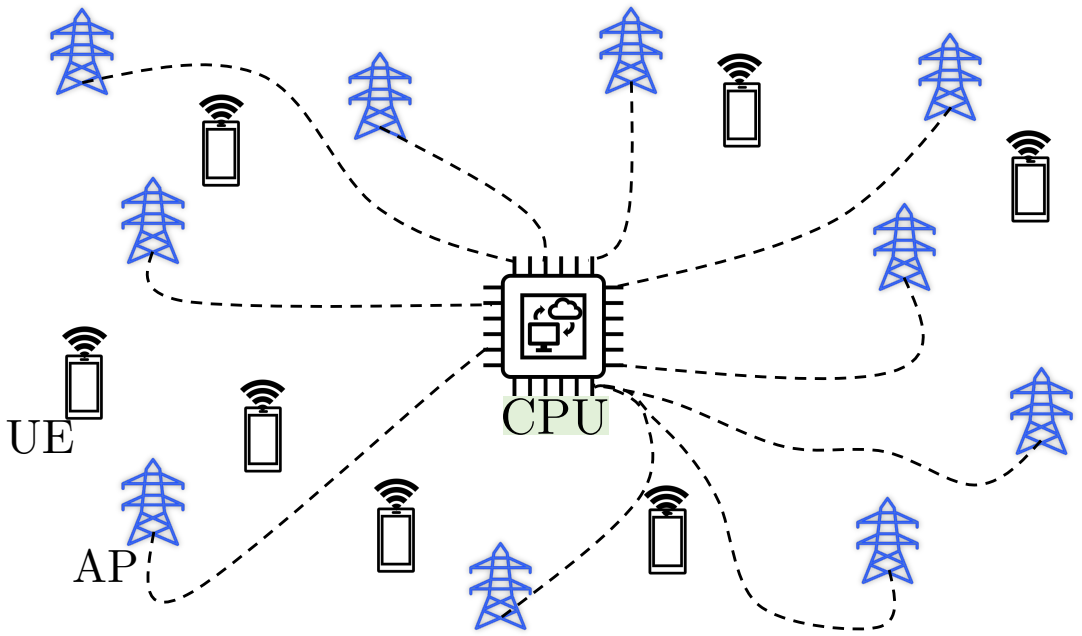

Figure 1.1: Illustration of a CF-mMIMO set-up. The dashed lines connecting the APs and the CPU depict the front-haul links.

serve the UEs using the same time-frequency resources in a geographical area [14]. The model is illustrated in Figure 1.1. The APs in the CF system are typically equipped with fewer antennas than a central BS in the cellular mMIMO system. However, the collective spatial antenna density of the APs is more than the density of UEs; thus, the overall architecture is referred to as CF *massive* MIMO. Indeed, with multiple distributed antennas, the CF system inherits the benefits of mMIMO, such as favorable propagation and channel hardening [15]. The proximity of the UEs and the APs improves the macro-diversity and inherently offers near-uniform SNR and hence QoS across UEs [16]. It has been reported that with practical system parameters of comparable settings, the CF-mMIMO procures an SNR of 24.5 dB at 95% of all UE locations, while mMIMO only guarantees 6.5 dB [17]. Further, a consequence of joint signal processing by multiple APs is that the inter-cell interference is now turned into useful/information-bearing signals, substantially improving the accuracy of the joint data detection at the CPU. This is analogous to how MIMO

interference channels can be turned into multiple access channels via the cooperation of the distributed antennas [18]. As a result, per-UE SE improves, and initial experiments in [19] reported *tenfold* enhancement in 95%-liekly SE in the CF system compared to the small cell counterpart.

We note that signal processing tasks such as channel estimation, combining and precoding, and data detection can either be fully orchestrated by the CPU or shared among the APs and the CPU. In the former case, the APs act as relays, and the instantaneous CSI of all AP UE links is communicated to the CPU via front-haul links. On the other hand, in the latter case of distributed processing, the APs combine the UL signals based on locally available CSI and transmit the combined signal to the CPU; and the CPU performs joint data detection. Similarly, in DL, the CPU sends the precoded data symbols to the APs for joint DL transmission. In this setting, the CPU does not require knowledge of instantaneous CSI between every UE and every AP. Hence, compared to the fully centralized system, distributed processing incurs considerably less front-haul load, which is essential for the scalable implementation of CF systems. One can also consider a semi-centralized system, where the CPU has the global knowledge of the statistical CSI, which is utilized along with the combined soft symbols from the APs for data detection. We will evaluate the performance with various levels of signal processing under different duplexing schemes later in the thesis. Finally, we note that local combining and precoding capabilities at the AP make CF systems scalable compared to network MIMO, where the BSs need to exchange the individual cell-level CSI and data vectors among themselves to facilitate joint combining, precoding, and interference management.

Thus, in a nutshell, the key aspects of CF-mMIMO are:

i. Low variation in the SNRs across UEs, leading to uniform QoS.

ii. Superior interference management capability via joint and coherent data processing.

iii. Inherits the benefits of mMIMO with dense AP deployment.

iv. Distributed signal processing between APs and the CPU makes the system scalable.

Having discussed the promise of CF-mMIMO systems, we next discuss the signal processing challenges that need to be understood and addressed in making CF-mMIMO practically deployable. Broadly speaking, they include channel estimation, choice of duplexing scheme, joint AP-UE clustering, constraints on the front-haul load, high mobility support, hardware impairment and calibration, synchronization, etc. A few of these issues can be resolved with a slight variation in the established signal processing tools originally developed for cellular systems. On the other hand, several of these problems are more challenging than cellular systems and demand special attention and separate analysis. We next discuss three such signal processing challenges in CF-mMIMO: channel estimation, choice of duplexing scheme, and synchronization, which form the core of this thesis.

First, the interference management capability of the overall CF system largely depends on the choice of precoders and combiners, which in turn depend on the CSI available at the APs and the CPU. The choice of the channel estimator and underlying pilot allocation technique dictates the quality of the available CSI. Now, channel estimation in a distributed mMIMO system fundamentally differs from that of a cellular mMIMO system. In a cellular system, each BS/cell is interested in estimating the channels of the UEs connected to it. If we randomly allocate orthogonal pilots in each cell and reuse them across cells, this naive pilot allocation scheme of complexity $\mathcal{O}(1)$ can eliminate intra-cell pilot contamination. However, in a CF system, it is not just the nearest AP that is interested in estimating the channel of a given UE; all the (nearby) APs need to estimate the channel in order to combine the signals from all the UEs correctly. Here, allotting orthogonal pilots to all UEs (the equivalent of allocating orthogonal pilots across all cells rather than per cell) in the entire geographical zone could lead to an inordinately high pilot overhead, as the length of orthogonal pilots scales linearly with the total number of UEs. On the other hand, randomly reusing a set of orthogonal pilots can result in pilot-sharing UEs being in proximity, leading to high pilot contamination, which can erase or even negate the benefits

of CF systems. An exhaustive search-based pilot allocation is computationally prohibitive. Hence, there is a need to revisit the problem of pilot allocation across UEs in the context of CF systems.

Second, wireless systems for 5G NR and beyond are required to serve heterogeneous devices with diverse QoS requirements. This can only be met by supporting highly flexible UL-DL resource allocation schemes that adapt to diverse and rapidly changing requirements for UL and DL access from the UEs. Thus, for CF-mMIMO to become the next-generation physical layer solution for meeting the heterogeneous data demands from the UEs, we need to rethink the underlying duplexing scheme that can enable a CF system to serve UL and DL data load simultaneously. Most of the works in CF-mMIMO consider time division duplexing (TDD) [19–22], where in a given slot, either all the APs operate in UL or all the APs operate in DL. Needless to say, TDD CF-mMIMO cannot serve UL and DL UEs concurrently, and a limitation that can be overcome by equipping the APs with full-duplex (FD) capabilities. However, the critical challenge for FD deployment is self-interference (SI) or intra-AP interference (IrAI) caused by the signal leakage from the transmit antenna arrays to the receive antenna arrays of an AP [23]. Now, IrAI cancelation often entails additional signal processing overhead and power-hungry hardware. Further, the use of FD transceivers gives rise to additional sources of interference, termed as cross-link interference (CLI), i.e., the interference received by the receiving antennas of one AP from the transmitting antennas of all the other FD APs, as well as the interference received by a DL UE from other UL UEs. In the sequel, we term the former as inter-AP interference (InAI) and the latter as inter-UE interference (InUI). It has been shown in the literature that if SI is not mitigated satisfactorily, the sum UL-DL SE of FD can even fall below that attained by a TDD-based HD-CF mMIMO system [24]. Suitable signal processing techniques and resource allocation strategies need to be developed to mitigate SI and CLI, making it a nontrivial challenge to attain SE improvement in FD CF-mMIMO

compared to the conventional half-duplex (HD) CF-mMIMO. Hence, it is pertinent to investigate whether it is possible to develop a duplexing scheme that can enable the overall CF system to serve UL and DL UEs simultaneously without incurring SI, in other words, using HD hardware.

Third, a critical challenge of the CF-mMIMO system is synchronization, which is essential for joint and coherent transmission/reception. We note that clock synchronization among the APs and CPU is relatively straightforward and can be done using network synchronization techniques such as precision time protocol (PTP) [25], satellite-based global positioning system (GPS), or even using an inexpensive 802.11-grade clock via over-the-air endogenous synchronization techniques [26]. However, the key challenge is the joint synchronization of the APs and UEs. Essentially, due to the distributed nature of the system, the UL(/DL) transmitted signals from the UEs(/APs) experience different delays and arrive at the APs(/UEs) at different time instants. Now, for instance, if we consider a UL CF-mMIMO system using orthogonal frequency division multiple (OFDM), then due to relative distances between the APs and UEs, propagation delays at a subset of APs can exceed the cyclic prefix (CP) duration. In turn, this could break the orthogonality of the subcarriers, resulting in inter-carrier interference (ICI) and inter-symbol interference (ISI). Here, we note that cellular networks such as 4G Long Term Evolution (LTE) use a mechanism called timing advance (TA) that mandates the UEs to advance the transmission of its signal based on the propagation time between the BS and the UEs so that the received signals at the BS arrive in the correct time-frequency resource according to the frame structure at its connected base station. However, such a TA mechanism will not work for a CF system because a UE is served not only by the nearest AP but also by all other APs in its vicinity. Hence, timing mismatch is inevitable in CF, and the established cellular TA techniques cannot ensure the time-synchronous reception of a given UE's signal at all the nearby APs. Thus, to make CF-mMIMO practically viable, we need to quantify and analyze the effect of timing mismatch on the achievable SE and develop combining

schemes that take this mismatch into account.

As mentioned earlier, there are other challenges involved in a CF-mMIMO system, such as mobility management and finite front-haul capacity effects, to name a few. However, considering the scope of this thesis, we refrain from detailed discussions on these topics. Interested readers are referred to the excellent survey on CF-mMIMO in [27].

We next introduce, without delving into mathematical details, the research problems explored in this thesis and our original contributions regarding the methodologies developed to address them. More elaborate discussions are relegated to the dedicated chapters.

1.3 Scope and Contributions of the Thesis

This thesis focuses on three central themes: channel estimation and pilot allocation, analysis of various duplexing schemes, and synchronization, all within the context of the CF-mMIMO system. Here, we give a brief overview of each of these and highlight our main contributions.

1.3.a Channel Estimation and Pilot Assignment

As alluded to earlier, finding a suitable pilot allocation with limited-length orthogonal pilots is a challenging problem for CF systems. Further, due to distributed architecture, we cannot directly apply the centralized (BS-centric) algorithms available for cellular systems. Thus, we need to revisit the problem of pilot allocation and develop new techniques suitable for CF systems. In this regard, Chapter 2 of this thesis explores the pilot design and allocation problem from three different viewpoints, as summarized below.

1.3.a.i Quasi-orthogonal Pilots with Clustering

Random allocation of pilots can lead to a scenario where UEs in proximity share the same orthogonal pilot sequence. This will lead to high pilot contamination at all the nearby APs, which in turn can eliminate the advantages of joint processing. Here, we note that the

convenience of random allocation is that it is the least complex; however, it could perform poorly compared to a greedy or iterative algorithm that systematically allocates pilots based on a suitable design criterion. Thus, we first analyze the best performance that can be achieved via random allocation. We design pilot codebooks such that the channel estimates are allocation-agnostic, as is the case with orthogonal pilot sequences. However, given a pilot length, say τ_p, we can only generate τ_p orthogonal sequences. Thus, we consider a quasi-orthogonal pilot design, where each pilot codebook consists of τ_p mutually orthogonal pilot sequences, and inter-codebook pilots are non-orthogonal but have a fixed, low cross-correlation. Next, if we can form AP-UE clusters and then assign one quasi-orthogonal pilot codebook to each cluster, i.e., pilots within each cluster are orthogonal, and all outer-cluster pilots have a fixed low correlation, then, even if we allocate pilots randomly within each cluster, we can eliminate intra-cluster pilot contamination, and the strength of outer-cluster pilot contamination becomes nearly allocation-agnostic.

This idea motivates us to develop a pilot design and allocation scheme using mutually unbiased orthonormal bases (MUOB) that enables us to generate quasi-orthogonal pilot codebooks, with the property that pilot sequences within each codebook are orthogonal and the cross-correlation between the pilot sequences of two different codebooks is inversely proportional to the square root of the length of the pilots. It can also be shown that this is the minimum cross-correlation that can be attained. We present the construction of MUOB pilot codebooks in Section 2.2 of Chapter 2. Now, we summarize our main contributions in that part of this thesis.

i. We pose the problem of pilot design that minimizes the maximum pilot contamination across APs and for all UEs. We derive a lower bound on the mean squared pilot contamination power in a CF-mMIMO system with non-orthogonal pilots under arbitrary pilot assignment. We show that pilots drawn from a MUOB codebook achieve this lower bound. This proves the optimality of the MUOB codebook design and is the main theoretical result of Section 2.2 of Chapter 2.

ii. We also develop a low complexity AP-centric UE clustering algorithm for pilot allocation to the UEs. For comparison purposes, we provide an adaptive orthogonal pilot reuse (OPR) algorithm that improves the performance of OPR with fixed-duration pilots at the cost of additional pilot length.

Our numerical results reveal that MUOB-based pilots can achieve better system throughput as well as fairness across users, compared to the adaptive OPR method. The takeaway from Section 2.2 of Chapter 2 is that MUOB pilots can minimize the effects of pilot contamination in a CF-mMIMO system for a given pilot length with a very low computational cost since we can assign pilots to the UEs in each cluster in an arbitrary manner. This is in contrast with OPR, where, even after AP-UE clustering, complex algorithms are required to ensure that cluster edge UEs do not share the same pilot sequences.

1.3.a.ii Orthognal Pilots Allocation without Clustering

The above-mentioned analysis of MUOB-based pilot allocation reveals the best that can be achieved via quasi-orthogonal pilots. Also, the attractive aspect of MUOB is that once the AP-UE clusters are formed, the power of the interference due to pilot contamination is agnostic to the pilot allocation among the UEs. However, an initial AP-UE clustering is required for designing appropriate MUOB pilots. Hence, we revisit the channel estimation procedure from a different perspective. We consider orthogonal pilots of fixed length, and we develop algorithms where the pilot reuse strategy does not require AP-UE clustering, unlike MUOB-based allocation or adaptive OPR. However, we incur complexity in the allocation of pilots across UEs. Such techniques provide an idea of how, and by how much, we can improve over random and adaptive OPR. This is presented in Section 2.3. Key features of the proposed algorithm are:

i. It reuses orthogonal pilots among UEs to iteratively refine the locally available channel estimates at the APs. Essentially, the algorithm minimizes the normalized mean squared error (NMSE) of the estimated channels across APs.

ii. This algorithm does not require extra signaling overhead in terms of inter-AP coordination and also requires only the large-scale fading coefficient information. Thus, the allocation needs to be executed in the time scale of large-scale fading coefficients, which generally remain constant for several coherence intervals.

We empirically validate the superiority of the proposed method over random OPR and report substantial improvement in performance in terms of achievable SE.

Now, we note that the theory and algorithmic development for channel estimation so far assumes a fixed pilot length. This is also the case with most of the works available in literature; a summary of existing pilot assignment methods for CF-mMIMO systems is presented in Table 2.2. Thus, next, we look at the problem of pilot length optimization.

1.3.a.iii Pilot Length Minimization

As noted earlier, we cannot afford to allocate orthogonal pilots to all the UEs because it leads to inordinately long pilot sequences, reducing the time duration available for data transmissions. Thus, although the channel estimation is simplified because the channels are pilot contamination-free, the achievable SE can degrade substantially if the pilot length becomes comparable to the coherence duration of the channel. Therefore, we should look at algorithms that not only reduce pilot contamination but also do so by using the least number of orthogonal pilots. This idea is thoroughly developed in Section 2.4. Our main contributions are:

i. We propose a UE-centric clustering of APs and formulate a pilot length minimization problem with the constraint that intra-cluster UEs (i.e., the UEs connected to a common AP) are allocated orthogonal pilots. Also, the clustering algorithm presented in Section 2.4 gives us the flexibility to optimally decide the cluster size so that if the number of UEs in the system is small, the algorithm can generate a fully connected bipartite graph, implying orthogonal pilot allocation across all the UEs. Thus, the

algorithm in this section is more general than the clustering algorithm in 1.3.a.i, where the cluster size and the pilot length were fixed.

ii. We recast the problem as a graph-vertex coloring problem and solve it via a low-complexity algorithm known to be optimal for all bipartite graphs. Unlike existing solutions, our algorithm does not require additional signaling overhead, e.g., signal-to-interference plus noise ratio exchanges, for pilot assignment.

Our numerical results show that the proposed algorithm outperforms existing random or greedy pilot allocation methods in terms of the minimum mean squared error (MMSE) of the estimated channels and the achievable SE. Finally, the algorithm is attractive for practical deployment as it only requires the locations (path losses) of the UEs for pilot allocation and not the instantaneous channel states.

At this point, we switch our attention from channel estimation to the UL and DL data transmission phases, which can either be partitioned orthogonally in time or frequency or executed simultaneously using the same time-frequency resource. Consequently, the achievable sum UL-DL SE depends on the choice of the duplexing scheme, which is the main focus of Chapter 3, Chapter 4, and Chapter 5 in this thesis.

1.3.b Virtual FD: Enabling DTDD in CF-mMIMO

As noted earlier, traditional TDD-based CF-mMIMO cannot simultaneously serve UL and DL UEs. While FD CF-mMIMO can simultaneously serve UL and DL traffic at the APs, SI/IrAI cancelation demands power-hungry hardware and additional signal processing overhead. We explore an alternative strategy to FD that can simultaneously serve the UL and DL UEs using the same time-frequency resources using only HD hardware, thereby obviating the need for IrAI cancelation. Specifically, a duplexing scheme that enables an HD CF mMIMO with concurrent UL/DL data processing capability is *dynamic TDD (DTDD)*. In a DTDD CF-mMIMO system, the APs are HD; however, unlike TDD, it is not necessary that the APs must be scheduled to either all operate in the UL mode

or all operate in the DL mode, in a given time slot. The UL and DL modes of the APs can be scheduled independently, based on the local UL and DL traffic load in the vicinity of an AP (or a subset of nearby APs), so that a reasonable utility metric such as the sum UL-DL SE can be maximized. Here, we note that similar to an FD CF system, DTDD also encounters InAI and InUI; however, the latter has a better interference management capability. This is because, in a DTDD CF system, only the subset of APs scheduled in DL contribute to InAI, whereas *all* the neighboring APs contribute to InAI in an FD CF system. Therefore, adopting DTDD along with CF-mMIMO can offer the benefits of FD operation without incurring its hardware and signal processing complexity; hence, the name *virtual FD*.[5]

This thesis explores the benefits of DTDD CF systems, and addresses signal processing challenges involved, such as AP scheduling, combiner, precoder design, UL and DL power control, etc. In Chapter 3, we begin by developing an AP-scheduling algorithm under the perfect CSI and perfect CLI cancelation assumptions, in order to expose the fundamental design challenges involved in the UL-DL mode scheduling problem. Then, in subsequent chapters, we consider more practical situations, addressing the effects of statistical CSI, pilot contamination, and imperfect InAI cancelation on the system performance. We also address the problem of optimal combining and precoder design, and UL-DL power control. Further, under all these scenarios, we derive closed-form expressions for the sum UL-DL SE and comment on the optimality of the AP-scheduling algorithm. We finally benchmark the performance of DTDD with TDD and FD cellular and TDD and FD CF systems. Our major theoretical contributions and findings on DTDD CF systems are as follows:

1.3.b.i DTDD CF versus TDD CF

Chapter 3 introduces the concept of DTDD-enabled CF mMIMO systems. In Section 3.2, we present the UL and DL sum SEs considering the scenario in which the APs locally

[5]The term virtual FD has previously been used in a completely different context in [28], where the authors consider a multi-hop HD relay network to achieve FD performance.

estimate channels to all the UEs using orthogonal pilots and use maximal ratio combining (MRC) in the UL and matched filter precoding (MFP) in the DL. Then, we develop a greedy algorithm for scheduling the UL and DL modes of the APs, where, at each iteration, an AP is activated in either UL or DL if that AP offers the highest incremental gain (among all the remaining APs) in the sum UL-DL SE. This pragmatic approach circumvents the exponential complexity (2^M, M is the number of unscheduled APs) of exhaustive search-based AP mode selection and determines the UL/DL AP schedule in linear time ($\mathcal{O}(M)$). We numerically validate the efficacy of the greedy algorithm and observe that the sum UL-DL SE attained via the greedy algorithm matches with that achieved via a brute force search over all possible UL and DL AP schedules.

Although the algorithm presented in Section 3.2 solves the scheduling problem in polynomial time, there is no guarantee regarding the optimality of the solution, i.e., the set of scheduled UL and DL APs, in terms of the sum UL-DL SE. It turns out that the naive[6] joint data detection scheme at the CPU considered in Section 3.2 is the bottleneck: it does not exhibit tractable properties in the overall sum UL-DL SE that can be leveraged to establish the optimality of the scheduling algorithm. We overcome this limitation in Section 3.3, where we consider optimal weighted combining and precoding. With weighted combining and precoding, we are able to provide guarantees regarding the optimality of the AP scheduling algorithm by exploiting the monotonicity and submodular properties of the signal-to-interference-plus-noise ratio (SINR) and the sum UL-DL SEs. In summary, our contributions are:

i. We analyze the UL SINR and sum UL SE with MRC at the APs and an SINR-maximizing weighted combining scheme at the CPU. We prove that, under a weighted combining scheme, UL SINR is a monotonically non-decreasing modular function of the activated AP set, and the sum UL SE is a sub-modular function of the activated

[6]Here, we refer to the classical joint decoding scheme where all the locally combined or estimated data streams from all the APs are given equal weightage at the CPU.

AP set. A similar weighted precoding scheme is developed for DL, which leads us to prove that sum DL SE, and hence sum UL-DL SE, is a sub-modular function of the scheduled UL and DL AP sets.

ii. We leverage the sub-modularity property to theoretically prove that the algorithm developed in Section 3.2 is guaranteed to achieve within $(1 - 1/e)$ of the sum SE attained via a full-complexity brute-force search, under SINR-maximizing weights applied at the CPU. Our analysis holds for perfect, statistical, and trained CSI.

We empirically show that DTDD-enabled CF-mMIMO nearly doubles the sum of UL-DL SE compared to the canonical TDD-based system. Essentially, DTDD CF-mMIMO exploits both the joint signal processing of a CF system and the adaptive UL-DL slot selection at the APs based on local traffic demands, leading to better and more efficient time resource utilization than TDD CF systems.

1.3.b.ii DTDD CF versus FD Cellular

In developing the theory in Chapter 3, two major assumptions are orthogonal pilot allocation across UEs and perfect InAI cancelation. Although the robustness of the proposed algorithms is numerically verified with imperfect InAI cancelation, it is critical to evolve the theory further, accounting for the effects of pilot contamination and imperfect CLI cancelation. This is the main focus of Chapter 4. Further, we theoretically compare the performance of DTDD CF systems with FD cellular systems. Our main contributions are:

i. We first derive closed-form expressions for the sum UL-DL SE considering the effects of pilot contamination and imperfect InAI cancelation with MRC and MFP.

ii. We argue that the achievable sum UL-DL SE is a monotonic nondecreasing function of the set of scheduled APs, even with pilot contamination and imperfect InAI cancelation. Then, we observe that the dependence of the sum UL- DL SE on the scheduled AP-set is non-linear in nature (a consequence of pilot contamination), and therefore

proving properties such as sub-modularity becomes mathematically intractable. To circumvent this difficulty, we derive the following results:

(a) We lower bound the sum UL-DL SE and prove that maximizing the lower bound is equivalent to maximizing the product of the SINRs.

(b) We prove that the product of the SINRs of all UEs is a sub-modular set function of the APs scheduled in the system. This leads us to develop a greedy algorithm for AP scheduling.

(c) We numerically illustrate the efficacy of the scheduling algorithm, by showing that the sum UL-DL SE obtained via exhaustive search over all UL-DL AP-configurations and considering the effects of CLIs matches closely with that obtained via the greedy algorithm based on the sub-modularity of the lower bound.

Our further experimental results show that DTDD CF-mMIMO substantially enhances the system performance compared to an FD cellular mMIMO system. This is because DTDD CF-mMIMO exploits the joint signal processing benefits of a CF system coupled with the adaptive scheduling of UL-DL slots based on the localized traffic demands at the APs. Another key advantage of DTDD CF over the FD cellular system is that we no longer need additional hardware at each AP to cancel the SI or InAI.

1.3.b.iii DTDD CF versus FD CF

The theoretical and numerical results discussed so far considered fixed power allocation in UL and DL and considered MRC and MFP. However, power control is needed for better interference management. This is addressed in Chapter 5. Also, we explore whether DTDD CF can outperform an FD CF system and analyze the role of InAI, IrAI, and InUI on the overall system performance. Our major findings are as follows:

i. We analyze the sum UL-DL SE considering distributed MMSE combiners and RZF precoders. We also derive closed-form expressions for the sum UL-DL SE with ZF

combiners and precoders. These expressions uncover the effects of InAI, IrAI, and InUI on the UL-DL SEs and how power control and UL/DL scheduling of the APs (for DTDD) dictate the strengths of these CLIs. Also, in the UL, we present an SINR optimal weighting scheme, which ensures that the received SINR at the CPU is maximized.

ii. Next, we focus on the sum UL-DL SE maximization with set constraints on the UL/DL APs and transmit power constraints on the APs and UEs. This problem of joint AP scheduling and power control is non-convex and NP-hard. We decouple it into two sub-problems. Our proposed solutions enjoy the following computational as well as theoretical advantages:

   (a) We use fractional programming (FP) to solve the UL and DL power control problem. FP convexifies the non-convex cost function such that the optimal solution of the surrogate cost function and the original cost function are the same.

   (b) Our algorithms admit closed-form updates for UL and DL power control and all auxiliary variables, which are derived using the alternating direction method of multipliers (ADMM) in the DL and augmented Lagrange multiplier in the UL. Furthermore, the resulting algorithms for each sub-problem are shown to converge to local optima.

   (c) Our proposed FP-based algorithms are precoder/combiner scheme agnostic and require only a few auxiliary variables, which makes our solutions scalable to large distributed systems.

   (d) For AP scheduling, we develop a greedy AP mode (UL/DL) selection algorithm, where, at each iteration, we select the AP and the corresponding mode such that the incremental gain in the sum UL-DL SE (with optimal power control) is maximum. This pragmatic low-complexity approach solves an otherwise exponentially complex scheduling algorithm in polynomial time.

(e) Our algorithms need to be applied in the time scale of large-scale fading, which remains constant for several coherence intervals. In contrast, instantaneous CSI-based approaches require the scheduling of APs and the computation of the UL and DL power control coefficients in every coherence interval.

We perform extensive numerical experiments that reveal the superiority of the UL/DL power control algorithms over several existing schemes. Surprisingly, our results show that for the same number of APs and antenna density, DTDD procures a better sum UL-DL SE compared to an FD CF system. Further, we observe that even with double the antenna density, the performance of the FD system can be limited by InAI and IrAI, while DTDD is more resilient to InAI. Thus, we can obtain the benefits of FD via DTDD itself, obviating the need for IrAI suppression at the APs.

1.3.c Synchronization

In the last part of the thesis, we switch gears and address a critical issue in the practical viability of CF-mMIMO systems, namely, synchronization. Almost all the existing works in CF-mMIMO assume that every AP receives the transmitted signals from all the UEs at the same time. This is not feasible due to the different relative distances between the APs and the UEs. Thus, the propagation delays between the APs and UEs can potentially exceed the CP duration for an OFDM-based CF system. This breaks the orthogonality among the subcarriers, eventually leading to ICI and ISI. For instance, 5G NR supports 30 kHz subcarrier spacing with the OFDM symbol duration being 33.3 μs and the CP duration being 2.3 μs. Thus, the propagation delay at an AP that is at an excess distance (relative to its nearest AP to a UE) of 750 m will be 2.5 μs, which exceeds the CP duration. Further, for 60 kHz subcarrier spacing and 1.2 μs CP duration, propagation delay at an AP at an excess distance of more than even 360 m will exceed the CP duration. Thus, the performance gain attained by CF-mMIMO with OFDM over the cellular setup with the assumption of synchronous reception at the APs is an overestimate

of the actual performance. Hence, it is crucial to account for the effects of propagation delays in the system performance while deriving the SINR at the CPU, and then develop techniques to mitigate the additional interferences arising due to asynchronous reception. Chapter 6 considers the impact of asynchronous reception in the UL CF-mMIMO system using OFDM. Our main contributions are:

i. We develop a mathematical framework that captures the relative propagation delays between the APs and UEs, manifesting as ICI and ISI in the UL SE.

ii. We analyze a scheme where each UE time-advances its transmit signal with respect to the time reference at its nearest AP. This ensures that for every UE, there is no delay on the received signal in the nearest AP and also reduces the propagation delays on the subsequent APs that are farther away. The effectiveness of the scheme is validated via numerical experiments.

iii. We derive the achievable per-UE SE with MRC and ZF combining. We extend our analysis to design an ICI and ISI-aware combiner that minimizes the mean squared error (MSE) between the transmitted and the estimated symbols at the CPU.

Our numerical experiments show that ICI and ISI can severely limit the performance of a CF system. Increasing the CP length mitigates the ICI; this, however, reduces the fractional symbol duration. Further, an interference aware combining with nearest AP-based timing-advance can reduce the effects of ICI and ISI and offer a performance that almost matches the time-aligned CF system. Hence, it is essential to perform appropriate timing-advance and ICI and ISI-aware signal processing at the CPU in order to mitigate the loss in SE due to ICI and ISI.

1.4 List of Publications from this Thesis

Journal Articles

J1: A. Chowdhury, P. Sasmal, C. R. Murthy and R. Chopra, "On the Performance of Distributed Antenna Array Systems With Quasi-Orthogonal Pilots," *IEEE Trans. Veh. Technol.*, vol. 71, no. 3, pp. 3326-3331, Mar. 2022.

J2: A. Chowdhury, R. Chopra, and C. R. Murthy, "Can Dynamic TDD Enabled Half-Duplex Cell-Free Massive MIMO Outperform Full-Duplex Cellular Massive MIMO?," *IEEE Trans. Commun.*, vol. 70, no. 7, pp. 4867-4883, Jul. 2022.

J3: A. Chowdhury and C. R. Murthy, "On the Sum Spectral Efficiency of Dynamic TDD-Enabled Cell-Free Massive MIMO Systems," *IEEE Wireless Commun. Lett.*, vol. 12, no. 3, pp. 481-485, Mar. 2023.

J4: A. Chowdhury and C. R. Murthy, "Half-Duplex APs with Dynamic TDD vs. Full-Duplex APs in Cell-Free Systems," *accepted for publication to IEEE Trans. Commun.*, Jan. 2024.

Conference Proceedings

C1: A. Chowdhury, P. Sasmal and C. R. Murthy, "Comparison of Orthogonal vs. Union of Subspace Based Pilots for Multi-Cell Massive MIMO Systems," in *Proc. IEEE 21st Int. Workshop Signal Process. Adv. Wireless Commun. (SPAWC)*, Atlanta, GA, USA, May 2020, pp. 1-5.

C2: A. Chowdhury, C. R. Murthy and R. Chopra, "Dynamic TDD Enabled Distributed Antenna Array Massive MIMO System," in *Proc. IEEE 12th Sensor Array Multichannel Signal Process. Workshop (SAM)*, Trondheim, Norway, Jun. 2022, pp. 131-135.

C3: A. Chowdhury and C. R. Murthy, "Comparative Study of Dynamic TDD with Full-Duplex in Cell-Free Massive MIMO Systems," in *Proc. Nat. Conf. Commun. (NCC)*, Guwahati, India, Feb. 2023, pp. 1-6.

C4: A. Chowdhury and C. R. Murthy, "How Resilient are Cell-Free Massive MIMO OFDM Systems to Propagation Delays?," in *Proc. IEEE 24th Int. Workshop Signal Process. Adv. Wireless Commun. (SPAWC)*, Shanghai, China, 2023, pp. 581-585.

C5: A. Chowdhury and C. R. Murthy, "Pilot Length Minimization via AP-UE Clustering in Cell-Free Systems," *accepted* in *IEEE Int. Conf. Acoust. Speech Signal Process. (ICASSP)*, Seoul, Korea, Apr. 2024.

2 Pilot Design and Channel Estimation

Chapter Highlights

This chapter investigates the problem of pilot design and pilot allocation in a CF-MIMO set-up considering quasi-orthogonal and orthogonal pilots with different utility matrices. In contrast to a cellular system where only the serving BS/AP requires CSI from a given UE, in CF systems, accurate CSI is required at all the APs in the vicinity of the UE, rendering the pilot design and allocation problem a more challenging task.

The first part of this chapter presents a novel MUOB-based pilot (quasi-orthogonal) design and its performance compared to conventional OPR. Specifically, we propose to use pilots that are not only orthogonal within a cluster of APs and UEs but also minimally correlated across clusters. Theoretically, we show that pilot sets forming MUOB minimize inter- and intra-cluster pilot contamination. Following this, we develop an AP-centered clustering algorithm that facilitates the pilot allocation across clusters from MUOB pilot codebooks. The advantage of MUOB is that, once these AP-UE clusters are formed, *the channel estimation is allocation agnostic due to the constant correlation properties of the MUOB pilots.*

Then, we look at the problem of pilot allocation from a different viewpoint and develop algorithms for pilot allocation where no clustering of APs and UEs is required. Specifically, we propose an iterative algorithm and show that the *method substantially improves the performance over random OPR and other existing schemes..*

Finally, we note that the preceding pilot allocation schemes are for a predetermined number of pilot sequences (i.e., a predetermined pilot length.) Thus, finally, we formulate a pilot length minimization problem and propose a novel pilot allocation algorithm that ensures no pilot contamination among the UEs near one AP or a subset of APs. At the same time, our algorithm procures the pilot allocation with a minimum number of orthogonal pilots being reused across the UEs. We numerically *validate the superiority of the proposed algorithms over several existing schemes in the literature and also provide a comparative analysis of our proposed algorithms.*

2.1 Introduction

CF-mMIMO systems offer excellent macro-diversity and uniformly good SE compared to canonical co-located or cellular MIMO systems. However, the benefits of the CF mMIMO system critically depend on the quality of the estimated channel at the APs, which in turn depends on the underlying pilot design and allocation scheme. One can assign orthogonal pilots to all UEs per cell in a cellular system, ensuring zero intra-cell pilot contamination. In contrast, in a CF system, multiple APs jointly serve multiple UEs. Hence, ensuring no pilot contamination across all the APs in the vicinity of every UE demands practically infeasible pilot length, resulting in a corresponding reduction of data duration per coherence block, reducing the data rate, and potentially erasing the benefits of CF MIMO. Hence, the pilot assignment problem in a CF MIMO system fundamentally differs from cellular MIMO systems.

Almost all the works on CF-mMIMO consider orthogonal pilots for channel estimation. If we randomly assign pilots to the UEs, the same pilots can be reused by UEs in proximity, resulting in high pilot contamination in all nearby APs. Thus, although the random pilot assignment is the least complex solution, it can lead to severe degradation in the SE. To this end, the authors in [22] proposed an iterative algorithm to allocate pilots to maximize achievable sum SE across UEs. On a similar track, the authors in [19] and [29] proposed a greedy pilot assignment strategy that iteratively refines the allocation of pilots based on the worst achievable SE and overall sum SE of the system, respectively. The method presented in [30] further improved the iterative search method to reduce the complexity of finding the pilot reuse strategy. However, all these pilot allocation techniques require the exchange of SINR of every AP and UE pair even before the actual data transmission phase. On the other hand, the algorithms available in current literature that require only UE locations for pilot allocation [31–33] do not consider pilot length optimization.

In this thesis, we address the pilot assignment in a CF-mMIMO from three different

viewpoints, as follows:

1. Keeping in mind that random pilot allocation is the least complex, we first ask whether we can design pilot codebooks that can procure good channel estimates across APs via random allocation. We consider a quasi-orthogonal pilot design, where each pilot codebook consists of τ_p mutually orthogonal pilot sequences, and inter-codebook pilots are non-orthogonal with a fixed cross-correlation. Now we note that if we can form AP-UE clusters and then assign one quasi-orthogonal pilot codebook to each cluster, i.e., pilots within each cluster are orthogonal, and all outer-cluster pilots have a fixed low correlation; then even if we allocate pilots randomly within each cluster, we can eliminate intra-cluster pilot contamination and control the outer-cluster pilot contamination. This notion is developed in Section 2.2.

2. Next, we switch our attention to OPR[1] and ask the question of whether we can develop an algorithm for OPR that can improve the performance over random allocation without incurring heavy signal processing overhead in terms of SINR exchanges among the APs and CPU and also can rule out the need for initial AP-UE clustering. This is addressed in Section 2.3. This is in contrast with Section 2.2, wherein the complexity was primarily due to the clustering, and then the channel estimates were allocation agnostic. Now, we incur complexity in allocating the orthogonal pilots; however, we do not need AP-UE clustering and show substantial improvement over random OPR.

3. Finally, we consider the problem of pilot length minimization, in contrast to the theoretical development in the preceding sections, where the algorithms were developed for a predetermined length of pilots. We present a low-complexity (again without requiring SINR exchanges) yet effective pilot allocation scheme that ensures no contamination among the subset of APs in the vicinity of every UE and also attains

[1]Here, we recapitulate from Section 1.3.a.i, that OPR refers to a scheme where we reuse a set of orthogonal pilots across UEs. Hence the name orthogonal pilot reuse (OPR).

such an allocation while minimizing the required pilot length. This is addressed in Section 2.4.

Next, we present our developed algorithms and compare performance with several existing benchmark schemes. We also study the relative performances of the proposed schemes.

2.2 Channel Estimation with Quasi-orthogonal Pilots

One way of looking at the problem of pilot allocation in CF-mMIMO systems is to allocate pilots from a set of non-orthogonal yet distinct sequences (in the sequel, we will refer to these as quasi-orthonormal sequences) to minimize the effect of pilot contamination. It has been shown that MUOB [34] can be used to generate pilot sequences satisfying this property. We first briefly show that in cellular mMIMO systems, the use of MUOB pilots can deliver *uniform QoS irrespective of the underlying pilot assignment strategy [35]*, which will later motivate and help us build the clustering algorithm for the CF-mMIMO system.

2.2.a Pilot Design from Union of Orthogonal Bases

We begin with a brief introduction to MUOB and how such vectors can be constructed.

Definition 2.1. *(Mutually Unbiased Orthonormal Bases [36]) A collection of orthonormal bases* $\{\mathcal{B}_j\}_{j=1,\ldots,n}$ *of the Hilbert space* $\mathbb{C}^K$ *are said to be mutually unbiased if and only if* $|\langle \boldsymbol{\phi}, \boldsymbol{\psi} \rangle|^2 = 1/K$ *for* $\boldsymbol{\phi} \in \mathcal{B}_l$ *and* $\boldsymbol{\psi} \in \mathcal{B}_k$*, with* $l \neq k$*.*

Theorem 2.1. *[34] Let* $q = p^n$*, where* p *is an odd prime and* n *is a positive integer, and* $\mathbb{F}_q$ *is a field with* q *elements. Let* $\Phi_l \triangleq \{\varphi_{l,m} | m \in \mathbb{F}_q\}$ *be the set of vectors given by*

$$\varphi_{l,m} = \frac{1}{\sqrt{q}} [\omega_p^{\mathtt{Tr}(lx^2+mx)}]_{x \in \mathbb{F}_q}, \tag{2.1}$$

where, for $\alpha \in \mathbb{F}_q$, $\mathrm{Tr}(\alpha) \triangleq \alpha + \alpha^2 + \ldots + \alpha^{q-1}$*. Then, the standard basis and the sets* Φ_l*, with* $l \in \mathbb{F}_q$*, form a set of* $q+1$ *mutually unbiased bases of* $\mathbb{C}^q$*. Here,* $\omega_k \triangleq exp(\sqrt{-1}(2\pi/k))$ *denotes the* k*-th primitive root of unity.*

The construction of MUOBs is not limited to odd prime power-based design. For thorough treatments of existing constructions, readers are referred to [34,36] and the references therein. ZC sequences with different roots have been found to be efficient implementations of MUOB and have been employed in 3GPP LTE and 5G NR [37, 38]. In this chapter, our goal is to evaluate the utility of these constructions as pilots to mitigate pilot contamination so that a uniform QoS can be provided to all UEs, which is a consequence of the mutual unbiasedness ensures that the interference power due to pilot contamination decreases inversely with the length of the pilot sequence.

2.2.b MUOB: Uniform QoS

We present expository numerical experiments manifesting the benefits of MUOB-based pilots in a cellular MIMO system. Detailed theoretical developments are available in [35]. These results motivate us to develop an AP-centric clustering algorithm (analogous to inherent BS-UE clusters per cell; however, here, APs jointly serve the UEs) for the CF-mMIMO system, which will be discussed afterward.

We consider a multi-cell system consisting of one central hexagonal cell surrounded by 6 neighboring cells and with a wrap-around of interference. The distance from the cell center to a corner point of the cell is assumed to be 1 km. The BSs are deployed at the cell center, and the UEs are randomly dropped within each cell, keeping a reference distance of 100 m. The carrier frequency and the signal bandwidth are 2 GHz and 1 MHz, respectively, with Nyquist rate sampling at the BS. The path loss exponent is assumed to be 3.76 [39]. We assume path loss inversion-based power control, and therefore, the received SNR at the BS to which they are attached is 10 dB for all UEs, irrespective of their locations.

In Figure 2.1, we plot the CCDF of MMSE channel estimation variances for different levels of pilot contamination. We consider 101 UEs in each cell and take 10^5 random UE instantiations for computing the empirical CDF. We observe that when the pilot

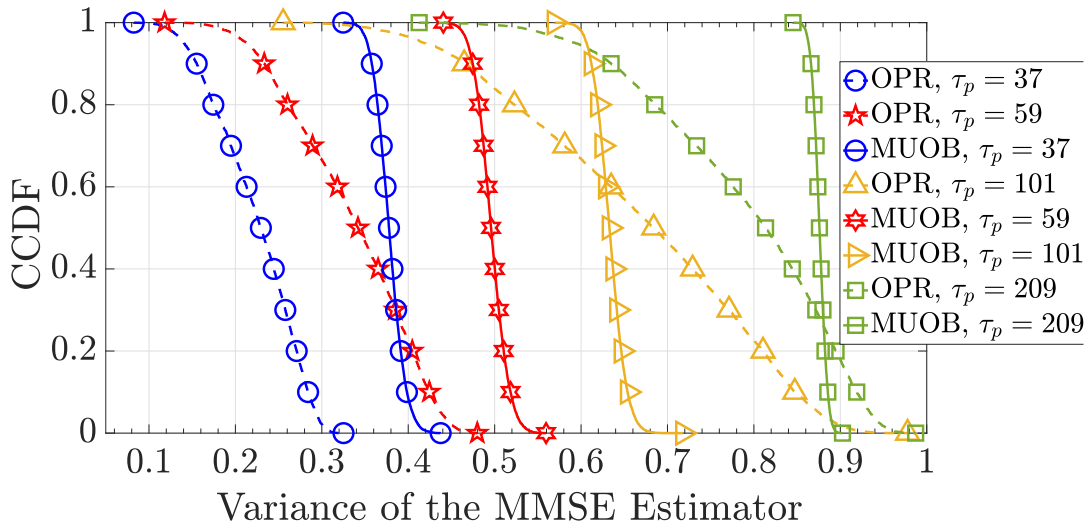

Figure 2.1: CCDF of the channel estimation variance of OPR and MUOB with different pilot lengths.

length equals a number of UEs/cell, estimated channel variance with OPR ranges between $[0.3, 0.95]$, and with MUOB pilots, it lies within $[0.65, 0.75]$. Therefore, MUOB pilots lead to channel estimates of similar quality for all UEs and neither as good as the best UEs nor as bad as the worst UEs under OPR. We next consider the case when the available pilot length is double the number of UEs/cells. We notice a striking improvement (estimated channel variance in the range $[0.85, 0.95]$) in the performance of MUOB pilots because of its inverse scaling of mutual cross-correlation with pilot lengths. Also, even with longer pilots, pilot contamination from cell edge UEs in neighboring cells still affects the overall estimation of some UEs under OPR. Finally, we consider pilots lengths less than the number of UEs per cell. In such cases, MUOB outperforms OPR because the latter is much more affected by intra-cell pilot contamination than MUOB. Also, note that as the pilot length increases, the variance of the MMSE estimator improves (becomes close to 1), and, correspondingly, the variance of the error in the estimated channel decreases.

Remark 2.1. *The pilot lengths used in Figure 2.1 are prime numbers because we follow the basis design according to (2.1). However, there are several methods for constructing*

unbiased bases using finite fields with odd and even prime powers.

Next, to compare the fairness of OPR and MUOB-based pilot transmission schemes across UEs, we present the two most commonly used fairness measures, namely, Jain's index and max-min index [40]. For a set of input values $\mathcal{X} = (x_1, \ldots, x_N)$, Jain's fairness index is defined as $\mathcal{J}(\mathcal{X}) = \frac{(\sum_{l=1}^{N} x_l)^2}{|\mathcal{X}| \sum_{l=1}^{N} x_l^2}$. When the input values are all equal, Jain's index equals one. For our experiment, we generate random UE locations at each instantiation, measure their respective channel variances, and numerically evaluate Jain's index. We observe in Figure 2.2 that in the case of MUOB, even for a small number of instantiations, the Jain's index converges to a value ≥ 0.99, and with an increasing number of UEs, it saturates to a value ≥ 0.996 with less than 500 Monte-Carlo realizations. However, in a conventional OPR scheme, Jain's index never crosses 0.96, and the convergence to 0.955 happens only after 6000 realizations. This reveals that, on average, MUOB pilots achieve equal quality of channel estimates almost irrespective of where the UEs are located. In OPR, the relative placement of UEs and their pilot assignments plays a critical role in obtaining good channel estimates.

Next, we consider the max-min fairness metric, defined at the center cell as $\mathcal{U}_{\text{max-min}} = \frac{\min_k(\sigma_{jk}^2)}{\max_k(\sigma_{jk}^2)}$, where σ_{jk}^2 is the estimated channel variance at the jth BS for the kth UE. The large difference between MUOB and OPR in terms of the max-min fairness is evident from Figure 2.3. For example, with 101 UEs/cell, the max-min fairness metric converges to 0.755 with MUOB and 0.234 with OPR. A simple calculation based on this shows that, in the case of MUOB, the worst channel estimate will deviate from the best possible estimate by at most 24.5%. However, with OPR, there exists a UE whose channel estimate at the BS is 76.62% worse than the best-estimated channel. Note that Jain's index requires estimated channel variances of all UEs to quantify the overall fairness achieved by the system. On the other hand, the max-min index reveals to what extent the best-estimated channel deviates from the worst one.

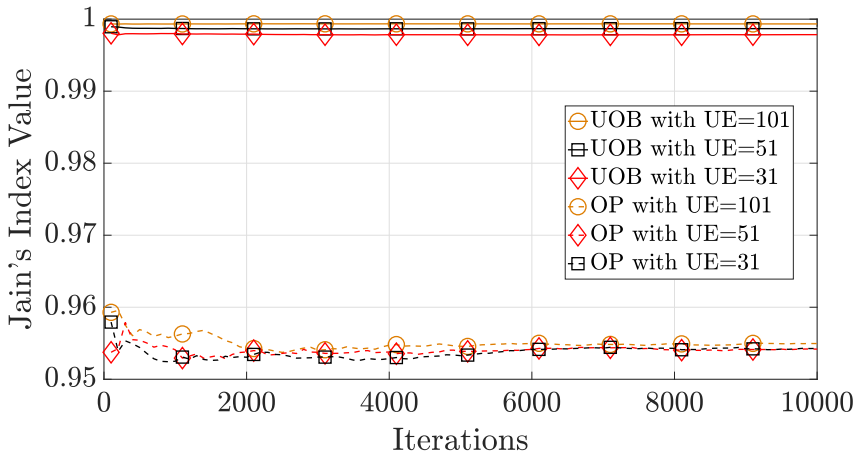

Figure 2.2: Convergence of Jain's fairness index. The pilot length equals the number of UEs per cell.

As the BS chooses its precoding vectors based on the estimated channels, pilot contamination has a direct effect on the achievable spectral efficiency. We examine the per-UE UL-DL sum rates achieved by these MUOB and OPR for different pilot lengths. We consider 101 UEs/cell and a coherence interval of 600 channel uses. (At a UE velocity of 100 m/sec, the Jakes' correlation coefficient is 0.99 after each coherence interval [41]). We define the "best case" as the rate of the UE, which achieves the highest rate, and the "worst case" as the rate of the UE, which achieves the lowest rate, in the center cell. From Figure 2.4, we see that the best achievable rate is obtained by the OPR scheme with $\tau_p = 101$. This is intuitive in the sense that using a pilot length that equals the number of UEs balances the trade-off between pilot overhead and data transmission duration. The crucial point to note is that the gap between the highest achievable rate and the lowest in OPR is much larger than that obtained using MUOB pilots. This also corroborates our observations about the behavior of the empirical cumulative distributions and fairness metrics. Therefore, to provide uniformly good service across all UEs in a cell, pilot construction via MUOB is a promising choice compared to OPR, especially when the pilot length is limited.

These numerical experiments motivate us to consider MUOB-based pilots for CF-mMIMO

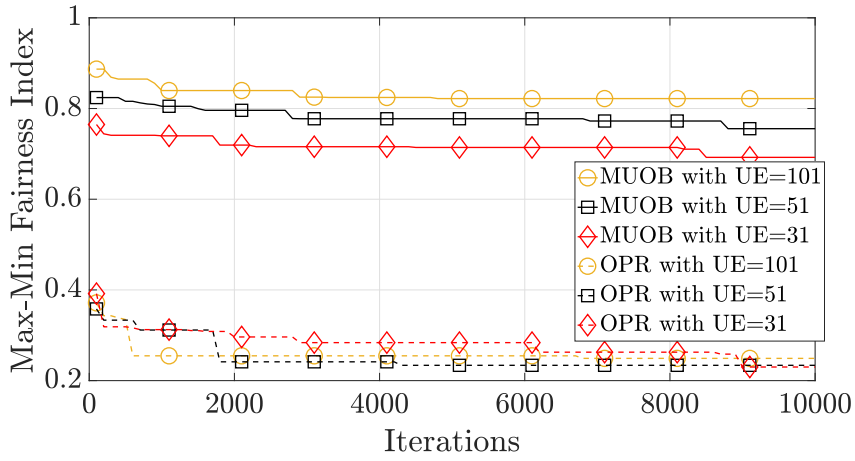

Figure 2.3: Convergence of max-min fairness index. The pilot length equals the number of UEs per cell.

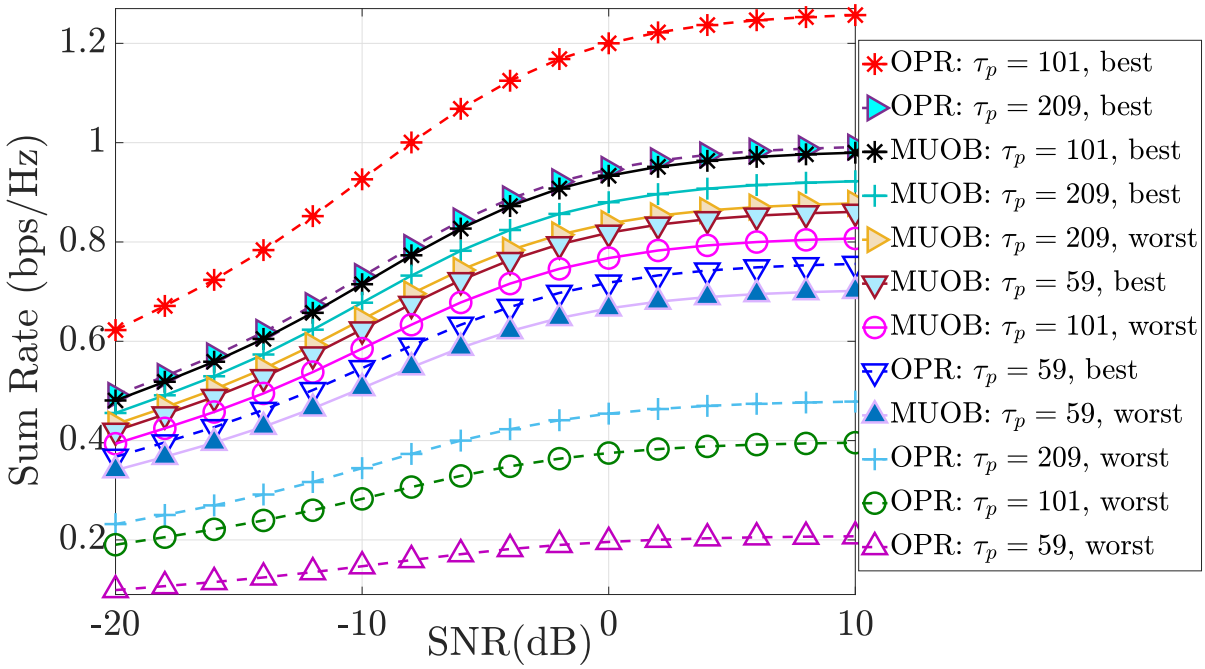

Figure 2.4: Per UE UL-plus-DL achievable sum-throughput vs. SNR.

systems, which we discuss in the next section.

2.2.c MUOB for CF-mMIMO System

Now, note that UEs in cellular mMIMO systems are naturally clustered based on the

BS serving them. However, no such clusters exist in the distributed MIMO case since all the APs can potentially serve all the UEs. Hence, we need to appropriately cluster the UEs before pilot allocation, making the CSI acquisition problem more challenging in CF-mMIMO systems than their cellular counterparts. The current state of the art [42–44] in CF-mMIMO systems considers the use of OPR among different UE clusters. One issue with this approach is that a large amount of pilot contamination can potentially be incurred if adjacent cluster-edge UEs from two physically proximal clusters share the same pilot sequence. This, in turn, substantially degrades the quality of the channel estimates for that UE at all nearby APs. However, this problem can be circumvented via suitably designing non-orthogonal pilots. To the best of our knowledge, the problem of channel estimation with non-orthogonal pilots (and, in particular, mutually unbiased orthogonal bases pilots) has not yet been explored in the context of a CF-mMIMO system. Therefore, our goal in this chapter is to analyze the performance of CF-mMIMO systems with quasi-orthogonal pilots and to develop a strategy for pilot allocation to the UEs that can minimize the effects of pilot contamination.

Our main contributions are:

1. We first derive a lower bound on the mean squared pilot contamination power in a CF-mMIMO system with non-orthogonal pilots and arbitrary pilot assignment. We show that pilots drawn from an MUOB codebook achieve this lower bound. (See Theorem 2.2.)

2. We develop a low complexity AP-centric UE clustering algorithm for pilot allocation to the UEs (See Algorithm 1.). The algorithm aims to minimize the pilot contamination across the UEs for a given pilot length.

3. We derive the achievable UL and DL rates for this system. (See Theorem 2.3.) Note that these expressions are developed for arbitrarily correlated pilots and are applicable for both MUOB and OPR.

Notation	Description
$\texttt{Cont}_{mk}$	Pilot contamination in the kth UE's channel estimated at the mth AP
$\mathcal{U}$	Set of all UE indices
$\mathcal{O}_k$	Set of UE indices whose pilots are orthogonal to the kth UE's pilot
$\mathcal{U}_m$	Indices of the UEs clustered with mth AP
$\tilde{\mathcal{U}}_m$	Indices of the UEs whose data is processed by the mth AP
$\mathcal{A}_k$	Indices of the APs that jointly process the kth UE's data
$\boldsymbol{\Phi}$	The set of all pilot sequences with the kth sequence (column) $\boldsymbol{\varphi}_k \in \mathbb{C}^{\tau_p}$ being allocated to the kth UE

Table 2.1: Symbols used in AP-centric clsutering and MUOB-based pilot design.

4. Via numerical simulations, we validate our derived results and prescribe parameter values that optimize the achievable rates in the system under study. We also benchmark the performance of MUOB against the OPR-based channel estimation technique, which has previously been used in [42,43]. We observe that MUOB pilots with a pilot length 13 achieve a Jain's fairness index value of above 0.999 for a 50 UE CF-mMIMO system, which is comparable to the case with no pilot contamination, i.e., pilot length 50 (see Figure 2.7). Also, with optimized pilot length, both cluster-wise MUOB and unclustered MUOB uniformly outperform adaptive OPR as well as unclustered OPR in terms of the achievable rates (see Figure 2.8).

The key takeaway of this work is that MUOB pilots can minimize the effects of pilot contamination in a CF-mMIMO system for a given pilot length. Also, we can arbitrarily allot pilots to UEs within each cluster, and do not require computationally expensive pilot allocation algorithms. Furthermore, optimizing the pilot length significantly improves the throughput achievable with MUOB pilots due to the inverse scaling of the correlation between non-orthogonal pilots. Such properties make MUOB-codebooks an attractive choice as training signals in distributed systems such as CF-mMIMO.

Notation: The key notations used throughout this section are described in Table 2.1.

2.2.d System Model

We consider a TDD CF-mMIMO system consisting of M APs equipped with N antennas each, jointly serving K single antenna UEs. The channel vector between the mth AP and kth UE is modeled as $\mathbf{f}_{mk} = \sqrt{\beta_{mk}}\mathbf{h}_{mk} \in \mathbb{C}^N$, where the path loss component β_{mk} is assumed to be constant for several coherence blocks, and the fast fading channel, $\mathbf{h}_{mk} \sim \mathcal{CN}(\mathbf{0}, \mathbf{I}_N)$, is estimated at the start of each coherence interval. Let $\mathcal{U} = \{1, 2, \ldots, K\}$ be the index set of all the UEs, and let their corresponding set of pilot sequences be $\mathbf{\Phi} \triangleq \{\boldsymbol{\varphi}_1, \boldsymbol{\varphi}_2, \ldots, \boldsymbol{\varphi}_K\}$, with the pilot sequence $\boldsymbol{\varphi}_k \in \mathbb{C}^{\tau_p}$ allocated to the kth UE, such that $\langle \boldsymbol{\varphi}_k, \boldsymbol{\varphi}_k \rangle = 1$ [42]. Without loss of generality, we group the K pilot sequences (correspondingly, UEs) into L clusters, with each cluster containing at most τ_p sequences, such that any pair of pilots within a cluster are mutually orthogonal. Thus, $\tau_p L \geq K$. Note that $L = 1$ if all the pilot sequences are orthogonal (this requires $\tau_p \geq K$), while $L = K$ if none of the pilot sequences are orthogonal. In the sequel, for simplicity of presentation, we assume that the pilot sequences can be grouped into L clusters, each containing τ_p mutually orthogonal pilots such that $\tau_p L = K$.

Let the kth UE transmit the pilot signal with an energy $\mathcal{E}_{p,k}$. Also, let the index set of UEs whose pilots are orthogonal to the pilot transmitted by the kth UE be denoted as $\mathcal{O}_k$. That is, $\mathcal{O}_k \triangleq \{k' : \langle \boldsymbol{\varphi}_k, \boldsymbol{\varphi}_{k'} \rangle = 0, k' \in \mathcal{U}\}$.

All the APs use the received pilot symbols to obtain minimum mean square error (MMSE) estimates of the channel vectors to the corresponding UEs. Let $\hat{\mathbf{f}}_{mk}$ be the estimate of $\mathbf{f}_{mk}$, such that $\mathbf{f}_{mk} = \hat{\mathbf{f}}_{mk} + \tilde{\mathbf{f}}_{mk}$, with $\tilde{\mathbf{f}}_{mk} \sim \mathcal{CN}(\mathbf{0}, (\beta_{mk} - \alpha_{mk}^2)\mathbf{I}_N)$ being the channel estimation error orthogonal to $\hat{\mathbf{h}}_{mk}$, where

$$\alpha_{mk}^2 \triangleq \frac{\mathcal{E}_{p,k}\beta_{mk}^2\tau_p}{N_0 + \mathcal{E}_{p,k}\beta_{mk}\tau_p + \texttt{Cont}_{mk}}. \tag{2.2}$$

Here $\texttt{Cont}_{mk}$ represents the amount of pilot contamination in the kth UE's channel estimate, and is given as

$$\texttt{Cont}_{mk} = \sum_{j \in \mathcal{U} \setminus \{\mathcal{O}_k \cup k\}} \tau_p \mathcal{E}_{p,j} \beta_{mj} |\langle \boldsymbol{\varphi}_j, \boldsymbol{\varphi}_k \rangle|^2. \tag{2.3}$$

A detailed proof for (2.2) and (2.3) are available at Appendix A.1. Next, we formulate the pilot design problem as one of min-max optimization based on the contamination derived in (2.3).

2.2.e Minimizing Pilot Contamination

The contribution of pilot contamination to the channel estimation error is minimized when the inner product term $|\langle \boldsymbol{\varphi}_j, \boldsymbol{\varphi}_k \rangle|^2$ is uniformly zero. However, this is not possible in a system with $\tau_p < K$. Hence, we seek to minimize the maximum inter-pilot correlation to minimize (2.3), that is,

$$\mathrm{P}: \min_{\boldsymbol{\Phi}} \max_{\substack{k \in \mathcal{U}, \\ j \in \mathcal{U} \setminus \{\mathcal{O}_k \cup k\}}} |\langle \boldsymbol{\varphi}_j, \boldsymbol{\varphi}_k \rangle|^2. \tag{2.4}$$

We have the following theorem.

Theorem 2.2. *For a given pilot length τ_p satisfying $\sqrt{K} \leq \tau_p < K$ and for $\tau_p L = K$, the optimal value of* P *is* $\dfrac{1}{\tau_p}$*, and is attained when distinct MUOB-pilot codebooks are allocated across clusters and the chosen pilot length τ_p is either a prime number or a power of a prime number.*

Proof. See Appendix A.2. ■

Also, from [34], τ_p distinct orthogonal pilot codebooks can be constructed and allotted to τ_p^2 UEs using MUOB-codebooks. In practice, we can choose the smallest prime or prime-powered $\dot{\tau}_p$, for a given number of UEs, such that $\tau_p \geq \dot{\tau}_p$ and $\dot{\tau}_p^2 \geq K$. This way, we can generate sufficiently many pilot sequences of length $\dot{\tau}_p$ to allot to all K UEs.

We note that for prime values of τ_p, ZC sequences allow for a fast implementation of MUOBs [38]. Since sequences generated by circular shifts of a ZC sequence are orthogonal to each other for a given root, and since a ZC sequence of length τ_p has $\tau_p - 1$ roots, we can generate $\tau_p^2 - \tau_p$ MUOB pilots using ZC sequences. These $\tau_p^2 - \tau_p$ sequences coupled with the columns of the $\tau_p \times \tau_p$ identity matrix form τ_p^2 distinct pilots for the given pilot length.

Using the correlation structure of MUOB pilots, we can write the overall pilot contamination at the kth UE as

$$\texttt{Cont}_{mk} = \sum_{j \in \mathcal{U} \setminus \{\mathcal{O}_k \cup k\}} \mathcal{E}_{p,j} \beta_{mj}. \tag{2.5}$$

For comparison, the overall pilot contamination in a system that uses OPR-based pilot assignment is given as

$$\texttt{Cont}_{mk} = \tau_p \sum_{j \text{ s.t.} \langle \boldsymbol{\varphi}_k, \boldsymbol{\varphi}_j \rangle = 1} \mathcal{E}_{p,j} \beta_{mj}. \tag{2.6}$$

Note that the contamination power in (2.6) scales with the number of clusters (also τ_p) in this case, as opposed to (2.5). The latter is due to the fact that the mutual correlation of non-orthogonal MUOB pilots scales inversely as $\sqrt{\tau_p}$.

Having developed a technique for the optimal design of pilot codebooks, in the next section, we present an AP-centric UE-clustering algorithm for pilot assignment to the UEs.

2.2.f AP-Centric Pilot Assignment

We note that the natural UE grouping by associating each UE to its nearest base station (BS) of a cellular mMIMO system is not appropriate in a CF system, as multiple APs cooperatively process each UE's signal. Consequently, AP-centric clustering is necessary to minimize the pilot contamination among geographically close UEs. Thus, we now discuss our proposed AP-centric UE clustering strategy, with each AP forming non-overlapping

clusters with at most τ_p UEs.[2] Hence, given M APs we set $L = M$. Our proposed strategy is summarized in Algorithm 1, with d_{mk} being the distance between the mth AP and the kth UE. We declare an AP as available if the associated cluster size is less than τ_p, and as overloaded if the cluster size exceeds τ_p. In each iteration of this algorithm, we associate unclustered UEs with the nearest available APs and ensure that none of the APs is overloaded. The outputs of this algorithm are index sets $\mathcal{U}_m, m \in \{1 \dots M\}$, containing UE indices clustered with the corresponding AP.

Remark 2.2. *MUOB pilot codebooks are generated via ZC-sequences with τ_p being a prime number satisfying $\tau_p \geq \max\{M-1, K/M\}$. We cluster UEs into M groups, each containing at most τ_p UEs. Now, since $\tau_p \geq K/M$, the UEs within a cluster can be assigned orthonormal pilots. This avoids intra-cluster pilot contamination. Also, since $\tau_p \geq M-1$, we can assign a distinct block of pilots to each cluster.*

Following this, the UEs within each cluster are assigned pilot sequences that are randomly chosen from a unique block of MUOB pilots without replacement. For OPR, a set of orthonormal pilots are assigned to UEs within a cluster and repeated across the clusters [35, 42, 43]. We then employ the largest large-scale fading (LLSF) based AP selection [45] to find the set of the UE indices whose data will be processed by the mth AP, denoted by $\tilde{\mathcal{U}}_m$. This is a superset of the mth AP's pilot cluster. The cardinality of the set $\tilde{\mathcal{U}}_m$ is controlled by a threshold parameter denoted by $\delta \in [0, 1]$. Setting $\delta = 1$ leads $\tilde{\mathcal{U}}_m = \mathcal{U}, \forall m$. Following this, using $\tilde{\mathcal{U}}_m, \forall m$, we can easily find $\mathcal{A}_k$, the set of AP indices associated with the kth UE. As an example, we demonstrate the clusters formed for one given UE distribution, in Figure 2.5, such that each distinctly colored cluster is assigned pilots from one distinct MUOB-pilot codebook. We observe that the UE of interest (as indicated) is jointly served by two APs.

[2]The association/clustering is used only for assigning pilot sequences to the UEs. In a cell-free system, the APs collaboratively serve all UEs.

Algorithm 1: AP-centric UE clustering

Input: τ_p, M, K, $d_{mk}, \forall m$ & $\forall k$

Initialization: $\bar{\mathcal{A}}_m = \{1, 2, ..., M\}, \bar{\mathcal{U}} = \{1, 2, ..., K\}$, $\mathcal{U}_i = \emptyset$, $\forall i \in \bar{\mathcal{A}}_m$.

Check: $\tau_p \geq \max\{M - 1, K/M\}$.

[1]: **while** $(|\bar{\mathcal{U}}| \neq 0)$ **do**

[2]: **for** $i \in \text{length}(\bar{\mathcal{U}})$ **do**

[3]: Find: $m' = \min_{m \in \bar{\mathcal{A}}_m} d_{mi}$

[4]: Update: $\mathcal{U}_{m'} = \mathcal{U}_{m'} \cup \{i\}$, $\bar{\mathcal{U}} = \bar{\mathcal{U}} \setminus \{i\}$

[5]: **end**

`/* Manage the overloaded APs */`

[6]: **for** $j \in \bar{\mathcal{A}}_m$ **do**

[7]: **if** $|\mathcal{U}_j| > \tau_p$ **then**

[8]: Retain only the τ_p nearest UEs in $\mathcal{U}_j$

[9]: Move the dropped UEs back to $\bar{\mathcal{U}}$

[10]: Update the available APs: $\bar{\mathcal{A}}_m = \bar{\mathcal{A}}_m \setminus \{j\}$

[11]: **end**

[12]: **end**

[13]: **end**

Output: $\mathcal{U}_m$: UEs associated with mth AP, $\forall m$.

Remark 2.3. *The clusters formed according to Algorithm 1 are used to allocate MUOB pilots across clusters. Due to the constant correlation (i.e., $1/\tau_p$) among the inter-cluster UEs, the contamination strength is independent of how we assign pilots from each MUOB codebook to the UEs within a given cluster. Therefore, the UEs within each cluster are randomly assigned pilot sequences drawn from one block of MUOB pilots without replacement. Then, there is no pilot contamination from UEs within a cluster and a fixed contamination from UEs in other clusters, regardless of how the pilot sequences are assigned to the UEs within each cluster. This is a key advantage of MUOB, namely, that we completely obviate the need to solve a pilot assignment problem based on inter-cluster UE distances.*

Now, in CF mMIMO systems, OPR may lead to poor performance because each UE is served by multiple APs. Due to this, using $\tau_p \ll K$ may result in multiple UEs being served by the same AP using the same pilot sequence, leading to severe pilot contamination

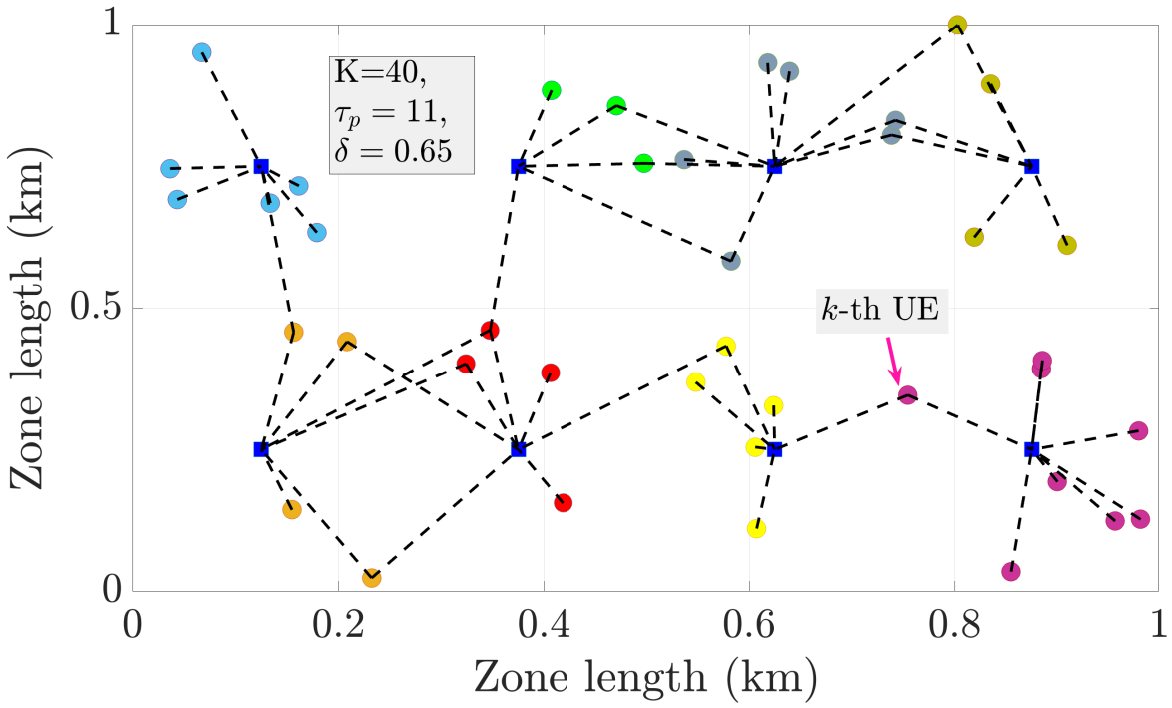

Figure 2.5: A realization of the system model. The blue squares denote the AP positions, and solid circles denote the UEs.

---

and loss of performance. Therefore, for a fair comparison with OPR-based pilot allocation, we allow the pilot length with OPR to exceed τ_p and propose a technique for generating pilot sequences in Algorithm 2, which we call adaptive OPR. The algorithm ensures that if any UE is being jointly served by more than one AP, then the assigned pilot of that particular UE is orthogonal to all the other UEs being served by the corresponding APs. We note that the threshold parameter δ acts as a trade-off between the amount of pilot contamination and the pilot length (τ_p').

Remark 2.4. *Note that in the case of adaptive OPR, the parameter δ also controls the pilot length τ_p', unlike MUOB, where τ_p is independent of δ.*

Remark 2.5. *The worst case order of our proposed clustering Algorithm 1 is $\mathcal{O}(K^2M)$. However, this clustering only needs to be performed in the time scale over which the large-scale fading coefficients change. Further, Algorithm 1 is sufficient to allocate MUOB pilots*

Algorithm 2: Adaptive OPR

Initialization: $\dot{\mathbf{\Phi}}_j = \emptyset, \forall j = 1, 2, \ldots, M$

Find $\tau_p' = \max\{|\tilde{\mathcal{U}}_1|, |\tilde{\mathcal{U}}_2|, \ldots, |\tilde{\mathcal{U}}_M|\}$

Define $\mathcal{I} = \{i_1, \ldots, i_M\}$ s.t. $|\tilde{\mathcal{U}}_{i_1}| \geq |\tilde{\mathcal{U}}_{i_2}| \geq \ldots |\tilde{\mathcal{U}}_{i_M}|$

if $\tau_p' > \tau_p$ **then**

  Generate: New pilot codebook: $\bar{\mathbf{\Phi}} \in \mathbb{C}^{\tau_p' \times \tau_p'}$

else

  Set: $\bar{\mathbf{\Phi}} = \mathbf{\Phi} \in \mathbb{C}^{\tau_p \times \tau_p}$ (initial codebook)

end

for $j = 1 : \text{length}(\mathcal{I})$ **do**

  Find the UEs in $\tilde{\mathcal{U}}_{i_j}$, if any, to which pilots have been assigned in the previous iteration(s)

  Store those pilots in $\dot{\mathbf{\Phi}}_j$

  Randomly assign pilots to the remaing UEs in $\tilde{\mathcal{U}}_{i_j}$ from $\bar{\mathbf{\Phi}} \backslash \dot{\mathbf{\Phi}}_j$ without replacement

end

because of the constant correlation property as discussed in Remark 2.3. For adaptive OPR, we need Algorithm 2 to mitigate inter-cluster pilot contamination, which has worst-case order complexity of $\mathcal{O}(M)$. Therefore, with a very low complexity, the clustering algorithm can procure the benefits offered by MUOB codebooks.

2.2.g Performance Analysis

In this section, we analyze the throughput of the proposed system. Our analysis is applicable to any choice of pilot codebooks, including pilots from MUOB codebooks and pilots allocated using OPR. Let the kth UE's transmitted symbol be $s_{u,k}$ ($\mathbb{E}[|s_{u,k}|^2] = 1$) with energy $\mathcal{E}_{u,k}$. The UL signal transmitted by the kth UE is processed by the APs whose indices are included in the index set $\mathcal{A}_k$. Each AP processes these UL signals via maximal ratio combining. Therefore, the processed kth stream of the received signal at the CPU becomes

$$\sum_{m \in \mathcal{A}_k} \sum_{i \in \mathcal{U}} \sqrt{\mathcal{E}_{u,i}} \hat{\mathbf{f}}_{mk}^H \mathbf{f}_{mi} s_{u,i} + \sum_{m \in \mathcal{A}_k} \hat{\mathbf{f}}_{mk}^H \mathbf{w}_m,$$

with $\mathbf{w}_m \sim \mathcal{CN}(\mathbf{0}, N_0\mathbf{I}_N)$.

Similarly, let the DL symbol indented for the kth UE be denoted by $s_{d,k}$, with $\mathbb{E}[|s_{d,k}|^2] = 1$. In the DL, the mth AP serves the UEs whose indices are contained in the index set $\tilde{\mathcal{U}}_m$. For simplicity, we assume equal power distribution among the APs, and let ρ_d be the maximum normalized (as a multiple of the noise variance N_0) power transmitted by each AP [45]. Assuming reciprocity-based matched filter precoding in the DL, the signal transmitted by the mth AP can be expressed as

$$\mathbf{r}_{d,m} = \sum_{i \in \tilde{\mathcal{U}}_m} \sqrt{\rho_d \zeta_{mi}} \hat{\mathbf{f}}^*_{mi} s_{d,i},$$

where the power control coefficients, $\zeta_{mk}, \forall k \in \tilde{\mathcal{U}}_m$, are designed such that $\mathbb{E}\left[\|\mathbf{r}_{d,m}\|^2\right] \leq \rho_d$. Also since, $\hat{\mathbf{f}}^*_{mi} \in \mathcal{CN}(\mathbf{0}, \alpha^2_{mi}\mathbf{I}_N)$,

$$\sum_{i \in \tilde{\mathcal{U}}_m} \zeta_{mi} \mathbb{E}\left[\|\hat{\mathbf{f}}^*_{mi}\|^2\right] \leq 1 \implies \sum_{i \in \tilde{\mathcal{U}}_m} \zeta_{mi} \alpha^2_{mi} \leq \frac{1}{N}. \tag{2.7}$$

Optimally solving (2.7) is beyond the scope of this chapter, however, considering each AP to transmit at the maximum allowable power, we can set $\zeta_{mk} = 1/(N \sum_{i \in \tilde{\mathcal{U}}_m} \alpha^2_{mi}), \forall k \in \tilde{\mathcal{U}}_m$. We consider that a fraction λ ($\lambda \in [0, 1]$) of data transmission duration, i.e., $(\tau - \tau_p)$, is allotted for UL.

Theorem 2.3. *The achievable rate of the kth UE can be expressed as*

$$R_k = \left(1 - \frac{\tau_p}{\tau}\right) \left[\lambda \log_2(1 + \gamma^u_k) + (1 - \lambda) \log_2(1 + \gamma^d_k)\right],$$

where

$$\gamma^u_k = \frac{N \mathcal{E}_{u,k} (\sum_{m \in \mathcal{A}_k} \alpha^2_{mk})^2}{N \ \mathtt{CohI}^u_k + \mathtt{NCohI}^u_k + N_0 \sum_{m \in \mathcal{A}_k} \alpha^2_{mk}}, \tag{2.8a}$$

$$\gamma^d_k = \frac{N^2 \rho_d (\sum_{m \in \mathcal{A}_k} \sqrt{\zeta_{mk}} \alpha^2_{mk})^2}{N^2 \ \mathtt{CohI}^d_k + N \ \mathtt{NCohI}^d_k + 1}, \tag{2.8b}$$

with the respective terms are evaluated as

$$\texttt{CohI}_k^u \triangleq \sum_{i\in\mathcal{U}\setminus\{k\}} \mathcal{E}_{u,i}|\boldsymbol{\varphi}_k^H\boldsymbol{\varphi}_i|^2 \left(\sum\nolimits_{m\in\mathcal{A}_k} \alpha_{mk}^2\sqrt{\frac{\mathcal{E}_{p,i}}{\mathcal{E}_{p,k}}}\frac{\beta_{mi}}{\beta_{mk}}\right)^2, \tag{2.9a}$$

$$\texttt{NCohI}_k^u \triangleq \sum_{i\in\mathcal{U}}\mathcal{E}_{u,i}\sum_{m\in\mathcal{A}_k}\alpha_{mk}^2\beta_{mi}, \tag{2.9b}$$

$$\texttt{CohI}_k^d \triangleq \sum_{i\in\mathcal{U}\setminus\{k\}} \rho_d|\boldsymbol{\varphi}_i^H\boldsymbol{\varphi}_k|^2 \left(\sum_{m\in\mathcal{A}_i} \alpha_{mi}^2\sqrt{\zeta_{mi}}\sqrt{\frac{\mathcal{E}_{p,k}}{\mathcal{E}_{p,i}}}\frac{\beta_{mk}}{\beta_{mi}}\right)^2, \tag{2.9c}$$

$$\texttt{NCohI}_k^d \triangleq \rho_d\sum_{i\in\mathcal{U}}\sum_{m\in\mathcal{A}_i}\alpha_{mi}^2\zeta_{mi}\beta_{mk}. \tag{2.9d}$$

Proof. The proof is available in Appendix A.3. ■

We observe that the choice of pilot sequences controls the coherent interference power in the UL and the DL, i.e., $\texttt{CohI}_k^u$ and $\texttt{CohI}_k^d$, that in turn determines the achievable rates. We have earlier shown that for any given pilot length, MUOB pilot codebooks minimize the coherent interference regardless of the underlying pilot assignment strategy, hence maximizing the achievable rate.

Remark 2.6. *We note that the results in Theorem 2.3 are based on the channel hardening-based bounds, commonly known as use-and-forget bound. It has been experimentally validated in the literature that the use-and-forget bounds are close to the ergodic capacity under hardening propagation environments (i.e., the independent Rayleigh channels, which is the case with our analysis), even when the number of APs is small. Further, we underscore the fact that hardening-based analysis helps us find insightful closed-form UL and DL SE expressions that, in turn, reveal the interdependence of various system parameters.*

2.2.h Numerical Results

We use the setup in Figure 2.5 with $M = 8$ APs, each equipped with $N = 32$ antennas. The UEs are deployed uniformly at random over a square area of size 1 km^2, and we consider 10^5 realizations of the channels. The path loss exponent and the reference distance

with respect to each AP are taken as 3.76 and 10 m, respectively [42]. We assume a coherence block to consist of 200 channel uses, corresponding to a coherence time of 1 ms [42, 46]. The pilot and data SNRs are taken as 10 dB, with λ being 0.5. We compare the proposed MUOB pilot codebook-based channel estimation with the established OPR technique as presented in [42]. We also compare the performance of MUOB with adaptive OPR where the pilot contamination between inter-cluster UEs is mitigated as described in Section 2.2.f. We now state the three schemes of pilot allocation and data processing employed in our experiments:

1. *Cluster Wise MUOB* $[\tau_p = x, \delta = y]$*:* We form the clusters using Algorithm 1 setting $\tau_p = x$, and then assign pilots from a distinct MUOB codebook at each cluster. Then, we apply an LLSF-based AP section with $\delta = y$ for joint data processing.

2. *Cluster wise OPR* $[\tau_p = x, \delta = y]$: We form the clusters using Algorithm 1 with $\tau_p = x$, and reuse a single set of orthogonal pilots across clusters. After that, we use the LLSF-based AP section method with $\delta = y$ to find the APs that jointly process the data of each UE.

3. *Adaptive OPR* $[\delta = y]$*:* We first form the cluster using Algorithm 1. Next, we apply LLSF-based AP section with $\delta = y$ to find the sets $\tilde{\mathcal{U}}_m, \forall m$. Then we assign pilots using Algorithm 2 which will result in a pilot length $\tau_p' \in [x, |\mathcal{U}|]$ depending on δ.

We first evaluate the effectiveness of MUOB pilots for channel estimation against cluster-wise OPR and adaptive OPR. We do this by plotting the complementary cumulative distribution functions (CCDFs) of the NMSE of estimated channels in Figure 2.6. For each of the three schemes, we measure the NMSE of a particular UE at the APs that are involved in joint processing, and average the error variances over the number of associated APs. Thus, the x-axis of Figure 2.6 is $\frac{1}{|\mathcal{A}_k|}\sum_{m\in\mathcal{A}_k}(1-\alpha_{mk}^2/\beta_{mk}), \forall k \in \mathcal{U}$. We can observe that MUOB pilots render channel estimates with considerably lower error variance as

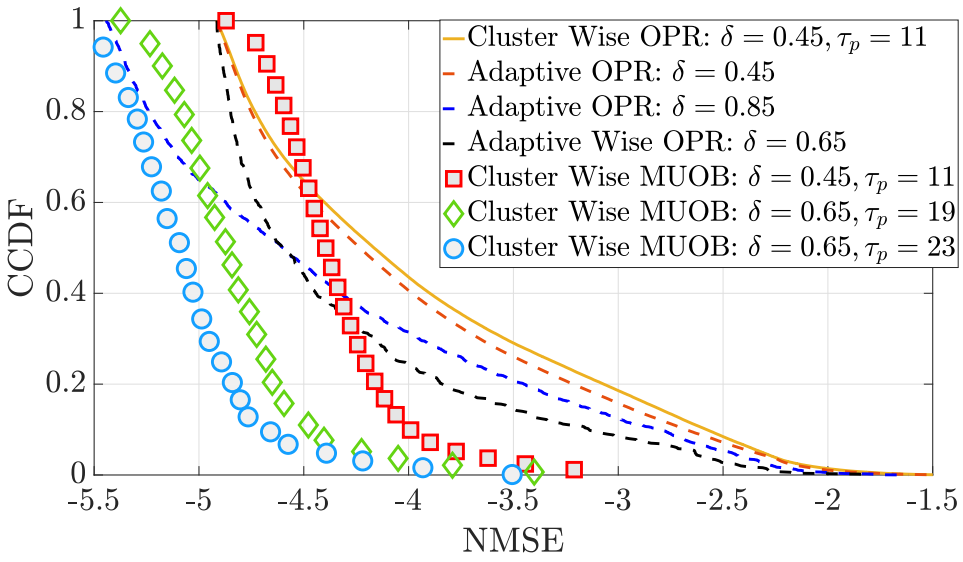

Figure 2.6: CCDF of NMSE of the estimated channels with $K = 40$.

compared to cluster-wise OPR. As adaptive OPR reduces contamination by increasing the pilot length, for certain UEs, it can achieve better channel estimates. However, the probability that the NMSE is greater than -3.5 dB with MUOB is almost zero, whereas the NMSE under adaptive OPR exceeds -3.5dB at least in 20% of the cases even with $\delta = 0.85$. We also observe that if the pilot length is increased, as in adaptive OPR, MUOB significantly outperforms adaptive OPR. Therefore, a simple clustering-based algorithm can attain better channel estimates with MUOB pilots.

Next, in Figure 2.7, we compare the fairness offered by these pilot allocation schemes via Jain's utility index [35], which is defined as $J(\alpha) = (\sum_{k=1}^{K} \alpha_{mk}^2/\beta_{mk})^2 \;/\; K \sum_{k=1}^{K} (\alpha_{mk}^2/\beta_{mk})^2$. For $\delta = 1$, Algorithm 2 generates orthogonal pilot codebooks (i.e. $\tau_p' = K$) for all the UEs, which results in a Jain's index of unity for all UEs. We observe that MUOB pilots can achieve nearly the same fairness as a system with no pilot contamination. Furthermore, even as the number of UEs increases, MUOB pilots retain overall fairness.

We observe that the pilot length represents an important trade-off between the amount of pilot contamination and the usable frame duration. We observe in Theorem 2.3 that $\texttt{CohI}_k^u$ and $\texttt{CohI}_k^d$ are dependent on $|\langle \boldsymbol{\varphi}_k, \boldsymbol{\varphi}_i \rangle|^2$ which scales as $1/\tau_p$ under MUOB. However, if τ_p

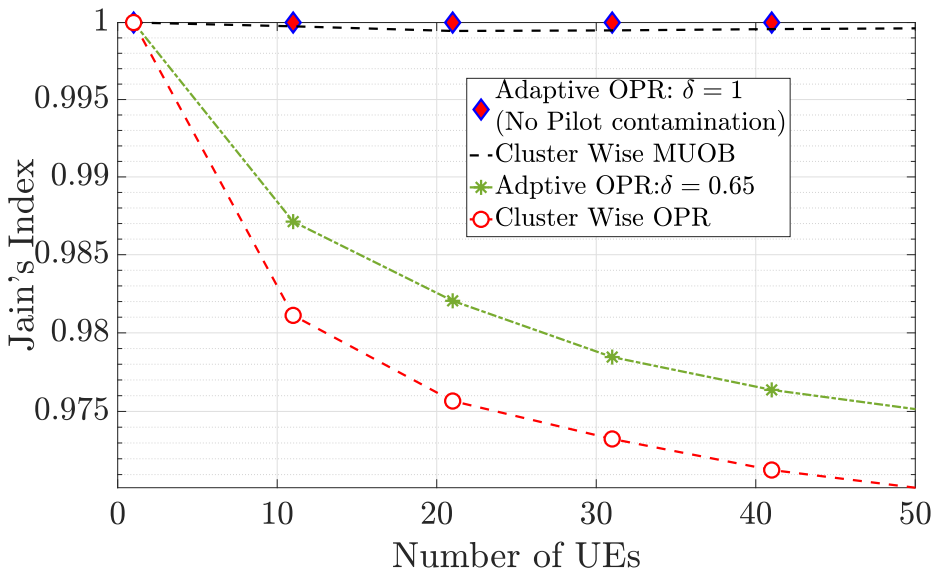

Figure 2.7: CDF of Jain's Index and fairness variation with UE load.

becomes comparable with coherence interval (τ), the pre-log factor $(1 - \tau_p/\tau)$ degrades the SE. Thus, the right choice of the pilot length with MUOB is important for obtaining optimal performance. Although optimally solving for τ_p in Theorem 2.3 is beyond the scope of this work, we numerically solve the following problem:

$$\max_{\tau_p} \sum_{k \in \mathcal{U}} R_k, \tag{2.10}$$

$$\text{subject to } \tau_p \in \begin{cases} [x, \tau], \text{Cluster wise OPR \& Cluser wise MUOB} \\ [\tau_p', \tau], \text{Adaptive OPR}, \end{cases} \tag{2.11}$$

where x and τ_p' are as defined at the beginning of this section. We plot the average optimized SE against the UE load in Figure 2.8. We observe that MUOB pilot codebooks with optimized pilot lengths substantially improve the average throughput compared to adaptive OPR. Also, with increasing δ, more APs contribute to joint data processing, which improves the per UE rate. Furthermore, at optimal pilot length, the coherent interference is also minimized under MUOB-pilot books, unlike any OPR technique, where both the interference and the effective channel gain increase linearly with the pilot length.

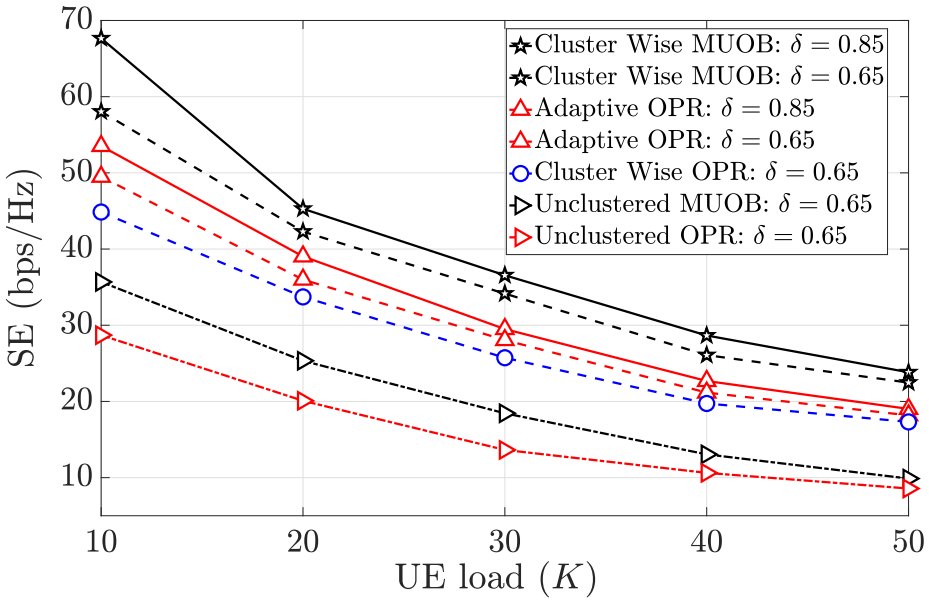

Figure 2.8: Pilot length optimized SE vs. UE load (K).

In summary, our numerical results reveal that MUOB-based pilots can achieve better system fairness as well as throughput compared to conventional OPR.

Now, we note that, although MUOB benchmarks the best that can be done via random allocation and with quasi-orthogonal pilots, we require an initial AP-centric UE clustering for the pilot assignment. On the other hand, although the proposed adaptive OPR improves the performance over random OPR, it incurs additional pilot overhead. Thus, the question we next ask is whether we can improve over random allocation, however, without AP-centric clustering and without incurring additional pilot overhead. We will address this next.

2.3 Iterative NMSE Based Pilot Allocation

We note the algorithm developed in the previous section requires an AP-UE clustering algorithm, and we have shown that MUOB pilots with the clustering algorithms offer superior performance compared to random and adaptive OPR. Now, we look at the pilot allocation algorithm, where we can improve the performance of OPR without the need for

an initial clustering algorithm. This is the main focus of this section.

2.3.a Channel Estimation

The channel estimation procedure remains the same as discussed in Section 2.2.d. However, for notational convenience, we rewrite α_{mk}^2 in (2.2) as follows: $\hat{\mathbf{f}}_{mk} \sim \mathcal{CN}(\mathbf{0}, \alpha_{mk}^2 \mathbf{I}_N)$, where,

$$\alpha_{mk}^2 = c_{mk} \tau_p \mathcal{E}_{p,k} \beta_{mk}^2, \tag{2.12}$$

and

$$c_{mk} \triangleq (\tau_p \mathcal{E}_{p,k} \beta_{mk} + \tau_p \sum_{n \in \mathcal{I}_p \backslash k} \mathcal{E}_{p,n} \beta_{mn} + N_0)^{-1}. \tag{2.13}$$

The estimation error, denoted by $\tilde{\mathbf{f}}_{mk} \triangleq \mathbf{f}_{mk} - \hat{\mathbf{f}}_{mk}$, is distributed as $\mathcal{CN}(\mathbf{0}, \bar{\alpha}_{mk}^2 \mathbf{I}_N)$, with $\bar{\alpha}_{mk} \triangleq \sqrt{\beta_{mk} - \alpha_{mk}^2}$. Here, we denote the indices of the UEs employing the pth pilot sequence by the set $\mathcal{I}_p$. Note that the cardinality of $\mathcal{I}_p$ indicates the repetition factor of the pth pilot sequence, such that $\sum_{p=1}^{\tau_p} |\mathcal{I}_p| = K$. This notation will later come helpful in Chapter 4.

2.3.b Iterative Pilot Allocation Algorithm

Now, a UE with a good channel estimate at the mth AP has a high $\alpha_{mk}^2 = c_{mk} \tau_p \mathcal{E}_{p,k} \beta_{mk}^2$, where c_{mk} accounts for pilot contamination. As the distance between kth and nth ($k, n \in \mathcal{I}_p$) UEs decreases, the values of α_{mk}^2 and α_{mn}^2 decrease, resulting in worsening of the channel estimates for both UEs. Hence, we first arbitrarily allocate pilots to all the K UEs, and then we find the UE $k^\star$ with the least value of α_{mk} to its nearest AP, that is, $k^\star = \arg\min_k \alpha_{mk}$, where m is the index of the AP closest to UE k. If $\boldsymbol{\phi}_{k^\star}$ is the associated pilot for this UE, we reallocate a new pilot sequence to this UE from $\{\boldsymbol{\phi}_1, \ldots, \boldsymbol{\phi}_K\} \backslash \boldsymbol{\phi}_{k^\star}$ so that $\alpha_{mk^\star}$ is maximized. We repeat this iterative process either up to a predetermined number of iterations or if no other pilot sequence from $\{\boldsymbol{\phi}_1, \ldots, \boldsymbol{\phi}_K\} \backslash \boldsymbol{\phi}_{k^\star}$ improves $\alpha_{mk^\star}$, or if $\alpha_{mk^\star}$ exceeds a certain threshold for all UEs. The overall recipe is presented in

Algorithm 3: Iterative Pilot Allocation

Initialization: $\mathcal{I}_p$ for $1 \leq p \leq \tau_p$, Number of iterations $= N_{iter}$, Set: $\mathtt{i} = 0$

Calculate: d_{mk} for all $k \in \mathcal{U}$, $m \in \mathcal{A}$

Define: $m_k^\star = \arg\min_m d_{mk}$

Calculate: $\alpha_{m_k^\star k}$ for all $k \in \mathcal{U}$

Initialization: $\alpha_q = \max_k \alpha_{m_k^\star k}$

[1]: $\alpha_{\min} = \min_k \alpha_{m_k^\star k}$

[2]: **while** $(\alpha_{min} < \alpha_o)$ && $(\alpha_{min} < \alpha_q)$ && $(\mathtt{i} \leq N_{iter})$ **do**

[3]: $k^\star = \arg\min_k \alpha_{mk}$

[4]: $\alpha_q = \alpha_{\min}$

[5]: **for** $1 \leq p \leq \tau_p$ **do**

[6]: $\mathcal{I}_p = \mathcal{I}_p \cup \{k^\star\}$

[7]: $a_p = \alpha_{m_k^\star k}$

[8]: **end**

[9]: $p^\star = \arg\max_p a_p$

[10]: Reallocate k to $\mathcal{I}_{p^\star}$

[11]: **Update:** $\alpha_{\min} = \min_k \alpha_{m_k^\star k}$

[12]: **Set:** $\mathtt{i} = \mathtt{i} + 1$

[13]: **end**

Algorithm 3.

Remark 2.7. *Here, we have assumed that the knowledge of the path loss coefficients is available at the APs, which is a common assumption in CF-literature [16, 19, 21, 47]. Essentially, the path loss coefficients are slow-fading components and remain constant over several coherence intervals; therefore, at the beginning of each coherence interval, only the fast-fading components are estimated at the APs. Also, when a UE* "registers" *with the enB/network, it must exchange the primary/secondary synchronization signals with the APs to perform the random access channel (RACH) procedure and then register itself with the AP/core network. During this process, in the RACH message, the UE can include information about its large-scale fading and path loss coefficient. In this way, the APs can be aware of the path loss coefficients before allocating the pilot and training. The*

randomness in the path loss coefficients depends on the UE distribution, and therefore, the estimation of such parameters requires scholastic geometry-based analysis, which is a completely different line of work in contrast with our current model.

We illustrate the effectiveness of the proposed algorithm in Figure 2.9. In the cell-based allocation scheme, since $\tau - p = 25$, we consider 4 equal-sized cells in the system, assign each UE to its nearest cell center, and allot orthogonal pilots to the UEs within each cell. In case the number of UEs in any cell exceeds the pilot length, we set the pilot length to equal the maximum group size, thus maintaining the orthogonality of the pilots within each cell. This reduces pilot contamination within each cluster of UEs and, therefore, outperforms random pilot allocation. However, we see that pilot allocation according to Algorithm 3 significantly improves the overall SE compared to both cell-based grouping and random pilot allocation schemes. The advantage of our pilot allocation algorithm is that it can be executed without the knowledge of UL/DL SINRs. Later, when we introduce a based CF system, we shall see that an algorithm that can allocate pilots without the requirement for exchange of UL and DL SINRs can help us decouple the problem of pilot assignment and AP scheduling.

Now, we note that both the MUOB-based pilot design and the associated AP-centric clustering and the iterative pilot allocation algorithm proposed in Section 2.3.b consider a *predetermined length of pilot signals*. Hence, we next consider the channel estimation for CF-mMIMO while minimizing the required pilot length. Also, we develop a UE-centric clustering algorithm, unlike AP-centric clustering (see Algorithm 1) in the preceding section, which is scalable with any number of APs and UEs.

2.4 Pilot Length Minimization

Until now, we have developed algorithms with a pre-determined length of pilot signals. Even this is the case with most of the existing algorithms in CF-mMIMO literature, as alluded to in Section 2.1. For the reader's immediate reference, we provide a catalog of

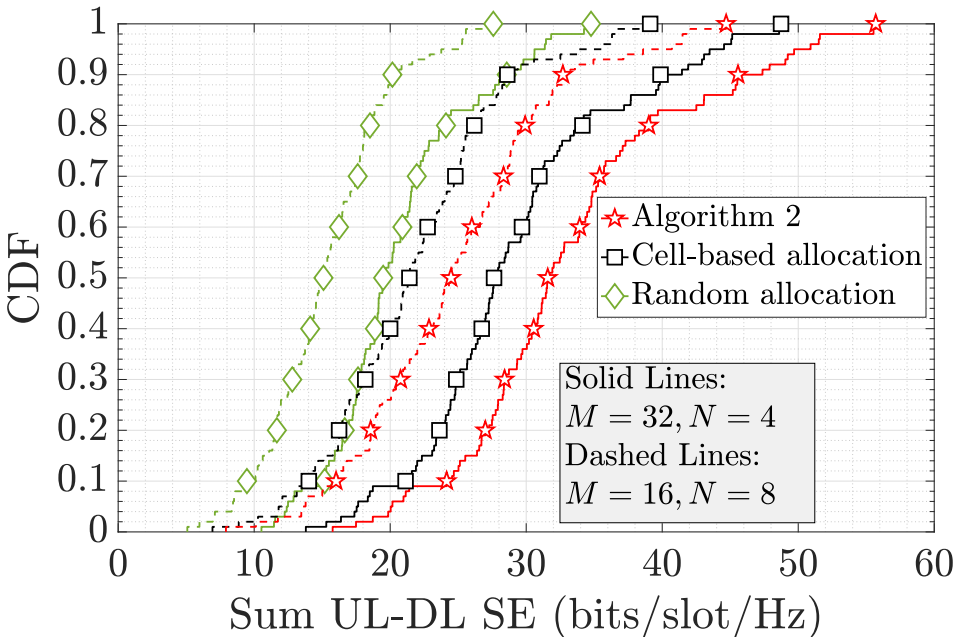

Figure 2.9: CDF of the achievable sum UL-DL SE under the pilot allocation obtained from Algorithm 3. Here, $K = 100, \tau_p = 25, N_{\text{iter}} = 1000$, and pilot SNR = 20 dB.

---

the notable works on channel estimation in CF-mMIMO in Table 2.2. In contrast to the existing works, where algorithms are designed for predetermined pilot length, we posed a pilot length minimization problem and presented a low-complexity yet effective pilot allocation scheme that ensures no contamination among the subset of APs in the vicinity of every UE and also attains such an allocation while minimizing the required pilot length. We viewed the pilot assignment as a vertex (representing the UEs) coloring problem where the vertices connected by an edge (implying that UEs share a common AP) are colored distinctly using a minimum number of colors and solved this NP-complete problem via an algorithm that procures *optimal* coloring for bipartite graphs, which is the case for our problem. The *advantage* of our pilot allocation strategy is that, *we do not incur additional signal processing overhead* in terms of SINR exchange between APs and CPU, and we can decouple the problem of pilot allocation and AP scheduling, which makes our solution attractive from an implementation perspective.

In summary, our key contributions are:

Ref.	Problem considered	Pilot length minimization	Overhead (front-haul load)	Method
Greedy [19, 48]	Maximize the worst UE's rate	No	SINR exchanges are required	Iterative method (no convergence guarantee)
Greedy [33]	Minimize the worst UE's MSE at all APs	No	Only UE locations/large scale information	Iterative method (no convergence guarantee)
Pilot Reuse [22]	Maximize sum UL rate	No	SINR exchanges are required	Either pilot reuse criteria is met or or when all pairs of users are tested
Structured [49]	Maximize the distance between copilot UEs	No	Only UE locations/large scale information	Cluster of UEs based on k-means algorithm
Tabu-search [30]	Maximize UL rate	No	SINR exchanges are required	Iterative method (best solution depends on maximum iteration)
Scalable CF [50]	Distributed pilot assignment	No	Only UE locations/large scale information	Dynamic cooperation clustering
Pilot power [32]	Minimising maximum NMSE	No	Only UE locations/large scale information	Pilot power control over random allocation
Proposed Scheme	Pilot length minimization and joint AP-UE clustering	Yes	Only UE locations/large scale information	Algorithm procures *optimal* result for bipartite graph

Table 2.2: Existing algorithms and our proposed method: a comparative survey.

1. We propose an AP-UE clustering method and formulate a pilot length minimization problem with the constraint that intra-cluster UEs (i.e., the UEs connected to a common AP) are allocated orthogonal pilots.

2. We recast the above problem as a vertex (representing the UEs) coloring problem where the vertices connected by an edge (implying that UEs share a common AP) are colored distinctly using a minimum number of colors. We then solve this NP-complete problem via an algorithm called DSATUR, which procures optimal coloring for bipartite graphs, which is the case for our problem.

Our numerical results show that the proposed algorithm outperforms the random or greedy pilot allocation methods in terms of the minimum mean squared error (MMSE) of the estimated channels and the achievable SE.

Next, we discuss our clustering and pilot length minimization problem and, subsequently, our proposed solutions.

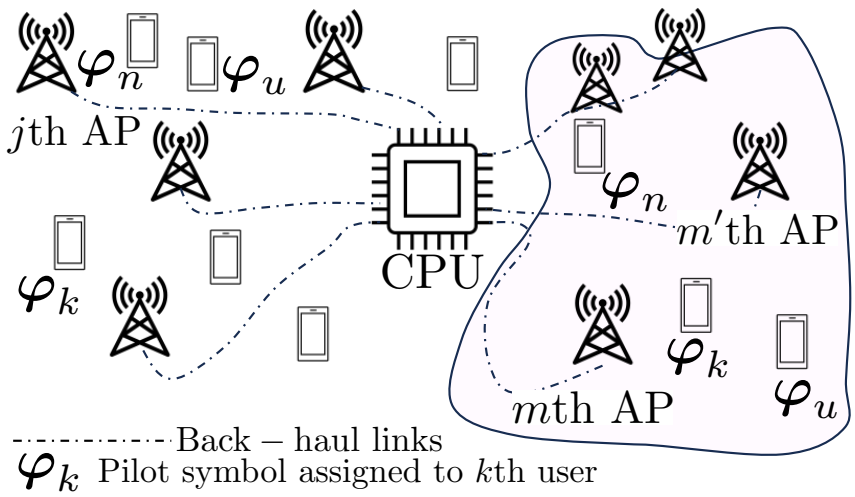

Figure 2.10: CF-MIMO system model. Here, pilot signals φ_k, φ_n, and φ_u are mutually orthogonal.

2.4.a UE-Centric Clustering & Pilot Allocation

As mentioned earlier, in CF systems, APs jointly serve the UEs. Thus, physically proximal UEs should not reuse the same pilot sequences even if their nearest APs are different. On the other hand, assigning pilot sequences so that the received signals at all the APs are contamination-free requires a pilot length at least equal to the number of UEs, which in turn reduces the duration available for data transmission. However, we note that although all the APs can serve all the UEs, only a subset of APs within the vicinity of a UE receive a signal with sufficient strength for decodability. In other words, at a given AP, the pilot contamination caused by a UE located far away is minimal due to path loss and shadowing. This is illustrated in Figure 2.10. Here, although all the APs can potentially serve all the UEs, due to path loss, the pilot contamination due to φ_k, φ_n, and φ_u is negligible at the jth AP's received signal. However, with respect to m and m'th AP, all three marked UEs are in proximity; thus, reusing pilots among these UEs results in severe pilot contamination.

Hence, we consider a UE-centric clustering and ensure that given any UE, the received signals at the APs within its cluster are contamination-free. We emphasize that all the

APs can still participate in data processing to/from all the UEs; we enforce orthogonality within the clusters only for the purpose of pilot allocation. This is illustrated in Figure 2.12, where the kth UE is connected to the mth and m'th AP. Thus, the pilot assigned to the kth UE should be orthonormal to all the UEs served by both the mth and the m'th APs. Next, we discuss how to form such clusters.

We define the following sets:

$$\mathcal{U}_k \triangleq \{m \text{ s.t. } \|\mathbf{u}_k - \mathbf{a}_m\| \leq r_{\mathsf{o}}, \forall m \in \mathcal{A}\}, \ \forall k \in \mathcal{U} \tag{2.14a}$$

$$\mathcal{A}_m \triangleq \{k \text{ s.t. } \|\mathbf{u}_k - \mathbf{a}_m\| \leq r_{\mathsf{o}}, \forall k \in \mathcal{U}\}, \ \forall m \in \mathcal{A}, \tag{2.14b}$$

where $\mathcal{U}$ and $\mathcal{A}$ are the set of UE and AP indices, $\mathbf{u}_k \in \mathbb{R}^2$ and $\mathbf{a}_m \in \mathbb{R}^2$ are the locations of the kth UE and mth AP, respectively, and

$$r_{\mathsf{o}} \triangleq \max\left\{\max_{k\in\mathcal{U}} d_{m_k k}, d_{\mathsf{SNR}_{\mathsf{o}}}\right\}, \tag{2.15}$$

where m_k is the AP index closest to the kth UE, i.e., if $d_{mk} = \|\mathbf{u}_k - \mathbf{a}_m\|$ denotes the distance between the mth AP and the kth UE, then $d_{m_k k} = \min\{d_{mk}, \forall m \in \mathcal{A}\}$. Also, $d_{\mathsf{SNR}_{\mathsf{o}}}$ is the distance from any UE where the received SNR is at least $\gamma_{\min}$, i.e.,

$$d_{\mathsf{SNR}_{\mathsf{o}}} = \max_{d}\left\{\frac{N\mathcal{E}_p\beta(d)}{N_0} \geq \gamma_{\min}\right\},$$

with $\beta(d) = (d/d_0)^{-\mathrm{PL}}$, d_0 is the reference distance, and PL is the path loss exponent. Here, N accounts for the array gain. This choice of r_{o} ensures that:

1. There is no UE that is not connected to any AP. In particular, every UE is connected to at least one AP even if the received signal strength to its nearest AP is below $\gamma_{\min}$, i.e., if $\max_{k\in\mathcal{U}} d_{m_k k} > d_{\mathsf{SNR}_{\mathsf{o}}}$.

2. Every UE is connected to all APs where the received signal strength is $\geq \gamma_{\min}$. However, in a dense deployment where $\max_{k\in\mathcal{U}} d_{m_k k} < d_{\mathsf{SNR}_{\mathsf{o}}}$, unnecessary connections of UEs to APs where the received signal strength is below $\gamma_{\min}$ are avoided.

With the clusters as defined above, our pilot length minimization problem is

$$\begin{aligned} &\min \ \tau_p \\ &\text{subject to } \langle \boldsymbol{\varphi}_{l(k)}, \boldsymbol{\varphi}_{l(k')} \rangle = 0, \forall k, k' \in \mathcal{A}_m, \forall m \in \mathcal{U}_k. \end{aligned} \tag{2.16}$$

The constraint above ensures that any two UEs that are connected to a common AP are assigned orthogonal pilot sequences, thereby avoiding pilot contamination at APs where it is important to form high-quality estimates of the channel from that UE. Note that the above pilot assignment is only based on the UEs' and APs' locations and not on the channel state instantiations.

We recast (2.16) as a graph coloring problem. We define a graph $\mathcal{G} = \{\mathcal{V}, \mathcal{E}\}$, where the vertex set $\mathcal{V}$ represents the UEs, i.e., $\mathcal{U}$, and edge set is defined as

$$\mathcal{E} \triangleq \{e_{kk'} \text{ s.t. } \mathcal{U}_k \cap \mathcal{U}_{k'} \neq \emptyset; \forall k, k' \in \mathcal{U}\}.$$

Thus, if two UEs, indexed by k and k', are connected to at least one common AP, there is an edge between them. A color assigned to a vertex represents the pilot sequence assigned to that UE. Then, to satisfy the constraint in (2.16), we must ensure that any two connected vertices have distinct colors. On the other hand, if two vertices are not connected by an edge, they can potentially reuse the same color (pilot sequence). Now, let $\mathcal{C}$ be the set of distinct colors, and $\mathcal{C}(k)$ indicate the color assigned to the kth UE. Then, the equivalent coloring problem becomes

$$\begin{aligned} &\min \quad |\mathcal{C}| \\ &\text{subject to} \quad \mathcal{C}(k) \neq \mathcal{C}(k'), \text{ if } e_{kk'} \in \mathcal{E}, \forall k, k' \in \mathcal{U}. \end{aligned} \tag{2.17}$$

From the above arguments, we have the following proposition.

Proposition 2.1. *The pilot length minimization problem in* (2.16) *and the graph coloring problem in* (2.17) *are equivalent.*

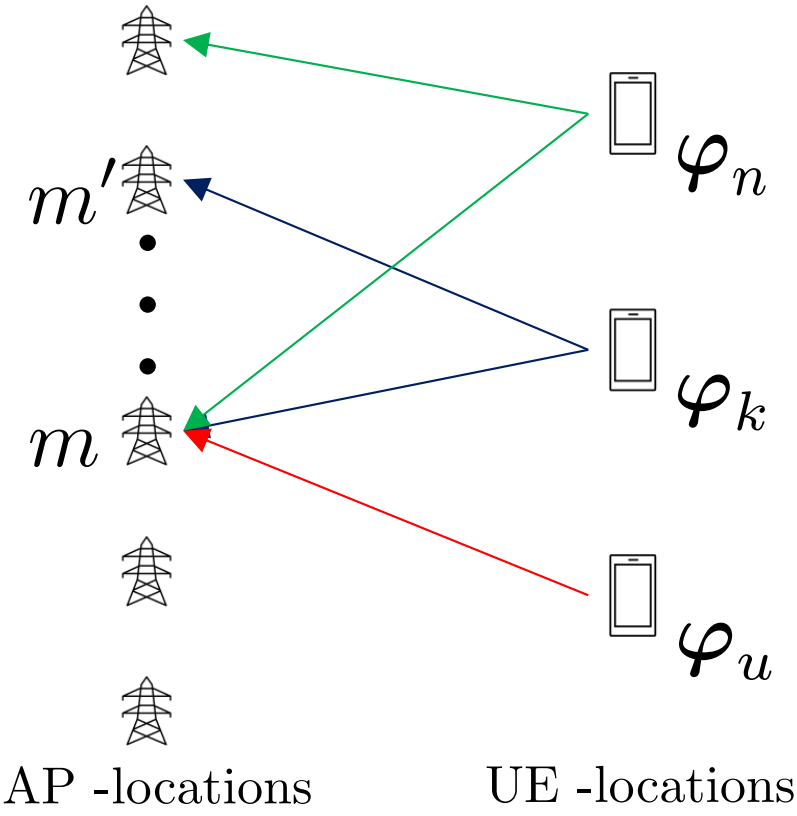

Figure 2.11: Bipartite graph coloring view of the pilot allocation problem.

Proof. Let $\mathcal{P} = \{\boldsymbol{\varphi}_1, \boldsymbol{\varphi}_2, \ldots, \boldsymbol{\varphi}_{\tau_p}\}$ be a set of orthonormal pilots. Every color in the set $\mathcal{C}$ can be mapped to an orthonormal pilot sequence in $\mathcal{P}$. Thus, minimizing τ_p, i.e., the cardinality of $\mathcal{P}$, is equivalent of minimizing the cardinality of $\mathcal{C}$. The constraint in (2.16) says that any two UEs connected to at least one AP are assigned orthonormal pilots. Now, while forming the graph, we connect two vertices (UEs) if and only if both UEs are connected to at least one common AP (say, the mth AP). Thus, requiring that any two vertices connected by an edge be colored differently is equivalent to requiring that any two UEs in the set $\mathcal{A}_m$ be assigned orthonormal pilots. ■

The coloring problem in (2.17) is NP-complete [51, Chapter 3]. Now, we observe that the existing algorithms cannot be directly applied as a solution to our problem, nor are they directly comparable as the involved problems are different (see second column of Table 2.2).

Therefore, to solve (2.17), we first recast the problem in (2.17) as a bipartite graph coloring problem, where there are two sets of nodes representing APs and UEs, and edges between them represent the connections defined by (2.14). That is, we have an edge between the kth UE and the mth AP if the distance between them is $\leq r_{\mathsf{o}}$. This is illustrated in Figure 2.11. This bipartite graph coloring problem can be solved efficiently using low complexity greedy techniques, such as the DSATUR algorithm [52]. We summarize the solution in Algorithm 4.

The DSATUR algorithm procures *optimal* coloring for all *bipartite graphs* [52] in terms of minimizing the number of distinct colors. In each iteration, Algorithm 4 operates as follows. It first selects the vertex among the uncolored vertices based on the number of connected colored or uncolored vertices. Once a vertex is chosen, it is assigned a color that has not been assigned to the vertices connected to it and has been reused the least number of times. If no such color is available, a new color is assigned, and the set $\mathcal{C}$ is updated. Finally, we generate $|\mathcal{C}|$ orthonormal pilot sequences each of length $|\mathcal{C}|$ and assign pilot sequences to UEs based on the UE-to-color mapping returned by the algorithm.

The attractive features of Algorithm 4 are: the algorithm does not require an exchange of instantaneous UL/DL SINRs for pilot allocation, unlike existing algorithms [22,29,30]. As a consequence, apart from time-division duplex (TDD), this algorithm is applicable for a wide range of duplexing schemes, including dynamic TDD [33] and full-duplex [23,24,53], where channel estimation is often performed at the beginning of each coherence interval, and the DL precoder is designed based on reciprocity.

Complexity Analysis: We note that complexity of Algorithm 4 is $\mathcal{O}(K^2)$, which is substantially less compared $\mathcal{O}(\tau_p^K)$, complexity of an exhaustive search. The complexity of the greedy methods presented in [19] and [33] are $\mathcal{O}(MK)$, and random search is $\mathcal{O}(K)$. In the section, we empirically show that Algorithm 4 uniformly outperforms both [33] and random allocation, and even fully orthogonal allocation at a high UE load. Further comparisons are provided in Table 2.3.

Algorithm 4: Pilot Allocation via Graph Coloring

Input: $\bar{\mathcal{U}} = \{1, 2, \ldots, K\}$, $\mathcal{C} = \emptyset$

while $\bar{\mathcal{U}} \neq \emptyset$ **do**

`/* Stage 1: Select the uncolored vertex */`

Select the $k \in \bar{\mathcal{U}}$ that has the maximum number of distinct colored vertices connected to it.

If there is more than one such vertex, choose the $k \in \bar{\mathcal{U}}$ within the subset of vertices with the maximum number of distinct colors with the maximum number of vertices connected to it.

Choose any $k \in \bar{\mathcal{U}}$ at random if there is more than one such vertex.

`/* Stage 2: Assign the least used color from the set of available colors */`

Assign color $c(k)$ to kth vertex such that

$$\begin{aligned} c(k) = \min \quad & c(p) \in \mathcal{C} \\ \text{subject to } & c(k') \neq c(p), \\ & \forall k' \in \{l \text{ s.t. } e_{kl} \in \mathcal{E}\}. \end{aligned} \tag{2.18}$$

`/* Stage 2a: Assign a new color */`

if $c(k) = \emptyset$ **then**

Assign a new color $c(k)$ to vertex k

Update: $\mathcal{C} \leftarrow \mathcal{C} \cup c(k)$

end

end

Method	Complexity	Method	Complexity
Random assignment	$\mathcal{O}(K)$	A. Lozano et al. [49]	$\mathcal{O}(MK(K\tau_p + 1))$
Greedy (rate based) [19, 48]	$\mathcal{O}(KM)$	Y. Zhang et al. [31]	$\mathcal{O}(KM(\tau_p + 2)$
Greedy (NMSE based) [33]	$\mathcal{O}(KM)$	H. Liu et al. [46]	$\mathcal{O}(K(K + 2M) + KM \log_2 M)$
Exhaustive	$\mathcal{O}(\tau_p^K)$	Proposed	$\mathcal{O}(K^2)$

Table 2.3: Complexity of various pilot assignment schemes. Here, M, K, and τ_p correspond to the number of (UL and DL) APs, (UL and DL) UEs, and the pilot length. Here, NMSE based method corresponds to Algorithm 3 described in the preceeding section.

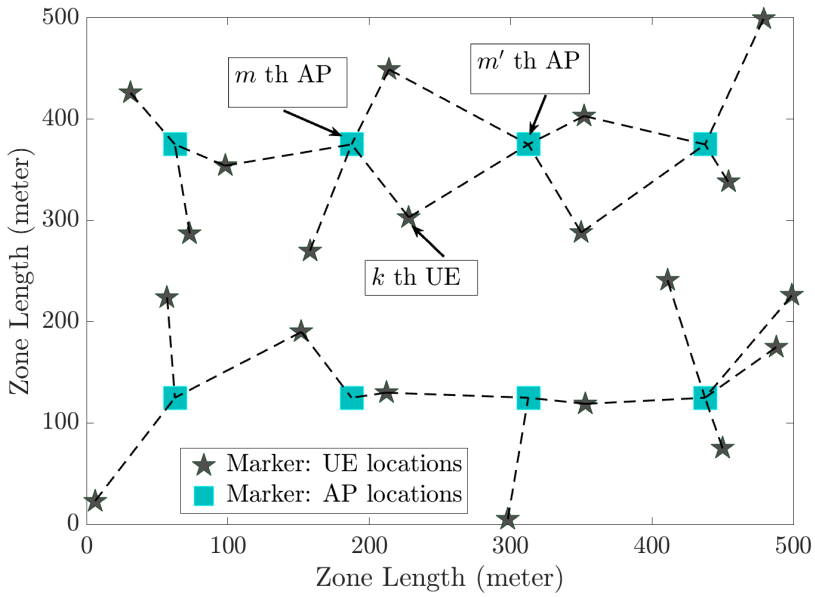

Figure 2.12: Uncolored AP-UE connections: the lines between the APs and UEs denote the clusters formed by r_o.

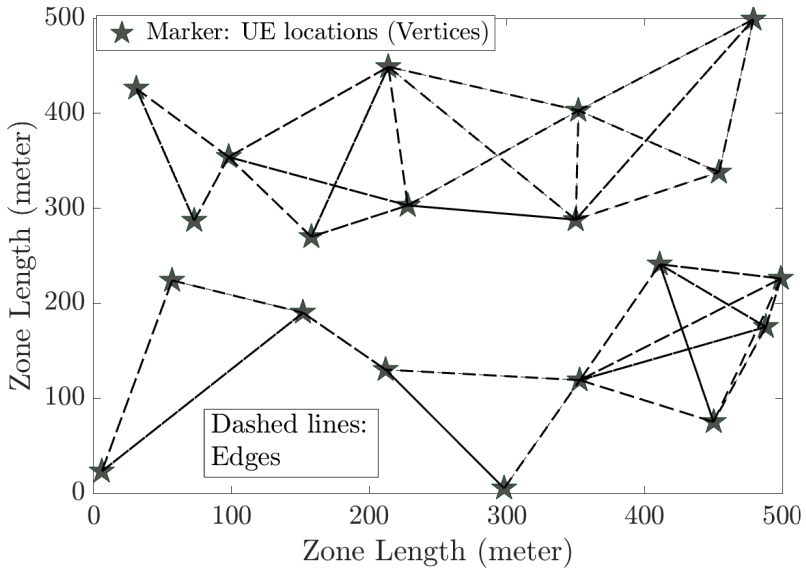

Figure 2.13: Graph formed by connecting UEs (vertices) that share common AP(s).

Remark 2.8. *The key difference between Algorithm 1 and the clustering rule presented in Section 2.4.a is that the former is an AP-centric clustering and applies for only a*

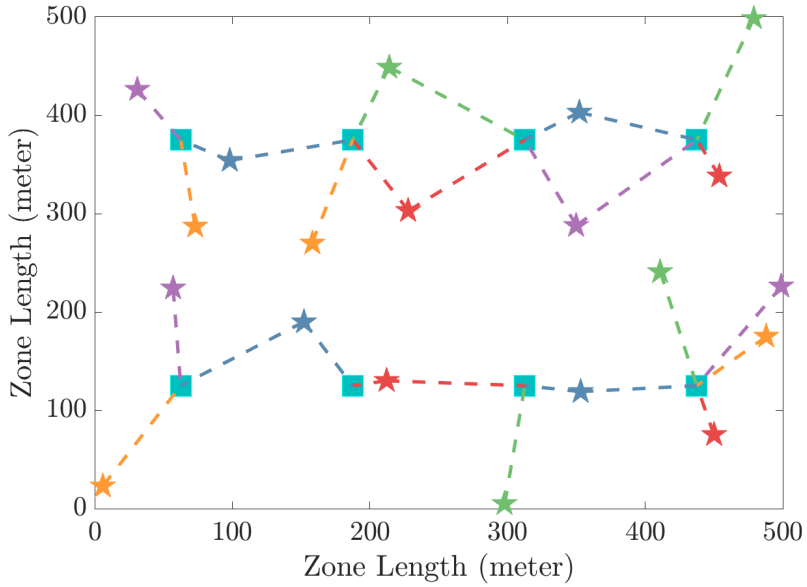

Figure 2.14: Colored AP-UE connections: Distinct colors correspond to distinct orthonormal pilot sequences.

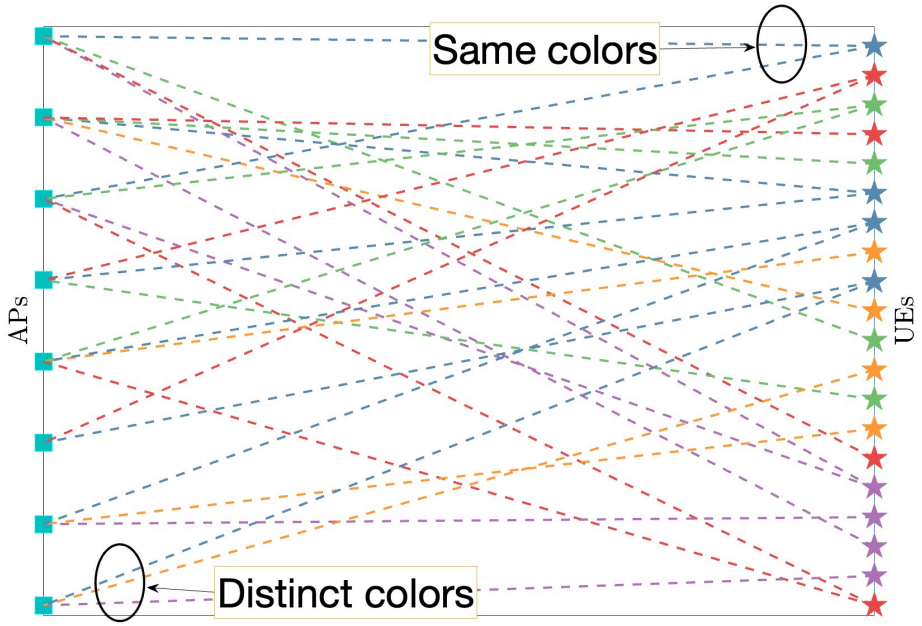

Figure 2.15: All lines emerging from a UE have the same color, and all the lines merging into an AP have distinct colors.

pre-determined pilot length. However, the joint AP-UE clustering in Section 2.4.a is UE-centric and thus more suitable for CF-mMIMO. Further, the cluster sizes can be optimized by choosing r_{o} in (2.15) for a given pilot length and coherence duration.

2.4.b Numerical Results

Here, we present a few experimental results based on the algorithm developed in the previous section to illustrate the efficacy of our pilot allocation scheme. We consider a square area of side 1 km where UEs are dropped uniformly at random locations. The APs are placed on a square grid for uniform coverage [33]. We take $5,000$ random channel instantiations for Monte Carlo averaging. The large scale fading between the mth AP and the kth UE is modeled as $\beta_{mk} = 10^{\frac{\mathsf{PL}_{mk} + \alpha_{\mathsf{sh.}} z_{mk}}{10}}$, where the path loss PL_{mk} follows the three-slope model in [19], $\alpha_{\mathsf{sh.}} = 6$ dB, and $z_{mk} \sim \mathcal{N}(0,1)$. The system bandwidth and noise figure are taken as 20 MHz and 9 dB, respectively, which gives a noise variance of -92 dBm. The coherence interval (denoted by τ) consists of 200 channel uses [20].

In Figure 2.12, Figure 2.13, Figure 2.14, and Figure 2.15, we illustrate the AP-UE connectivity and the pilot assignment via an example. To understand the allocation on a small scale, we take 8 APs over a 500 square meter area. Figure 2.13 illustrates the formation of the uncolored graph where two vertices (UEs) are connected if they share at least one common AP as per Figure 2.12. Figure 2.14 shows the assignment of the pilot sequences via the corresponding colors of the UEs. Next, Figure 2.15 demonstrates the outcome of the algorithm via a bipartite graph, where the nodes on the left-hand-side represent APs, and the right-hand-side nodes are for UEs. There is an edge if an AP and UE are connected via the set $\mathcal{A}_m$. We observe that all the edges emanating from an AP have distinct colors, which implies that all UEs connected to that AP are assigned orthonormal pilots. On the other hand, all the edges emanating from a UE have the same color, i.e., a single orthonormal pilot sequence is used by a UE.

We compare the proposed algorithm with the greedy pilot allocation presented in [33].

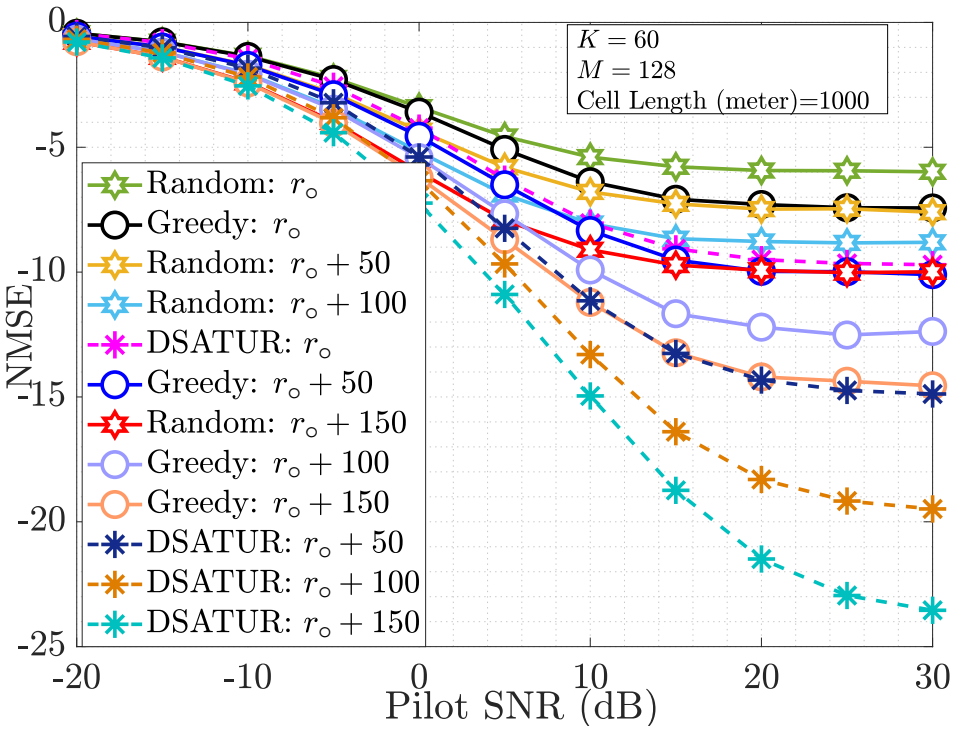

Figure 2.16: NMSE in the channel estimate as a function of pilot SNR and comparison with existing approaches.

We also compare against a random pilot allocation scheme.[3] In Figure 2.16, we compare the performance of the pilot allocation scheme in terms of the NMSE in channel estimation at the APs as a function of pilot SNR. The pilot allocation returned by Algorithm 4 leads to considerably lower NMSE than the greedy method. Also, as we increase the value of $r_\circ$, the cardinality of $\mathcal{U}_k$ in (2.14a) increases. This leads to a higher value of pilot length, and hence, the NMSE decreases even further. Figure 2.17 illustrates the minimum pilot length required for a given UE density and $r_\circ$. Even with a large number of UEs, say 500, the pilot length is only *one-tenth* that required for allocating fully orthonormal pilots.

Next, in Figure 2.18, we illustrate the effect of the pilot allocation rendered by Algorithm 4 on the sum UL SE of a time-division duplex (TDD) based CF-MIMO system

[3]For both the greedy and random allocation schemes, we take the pilot length returned by our algorithm and assign that many pilots across the UEs.

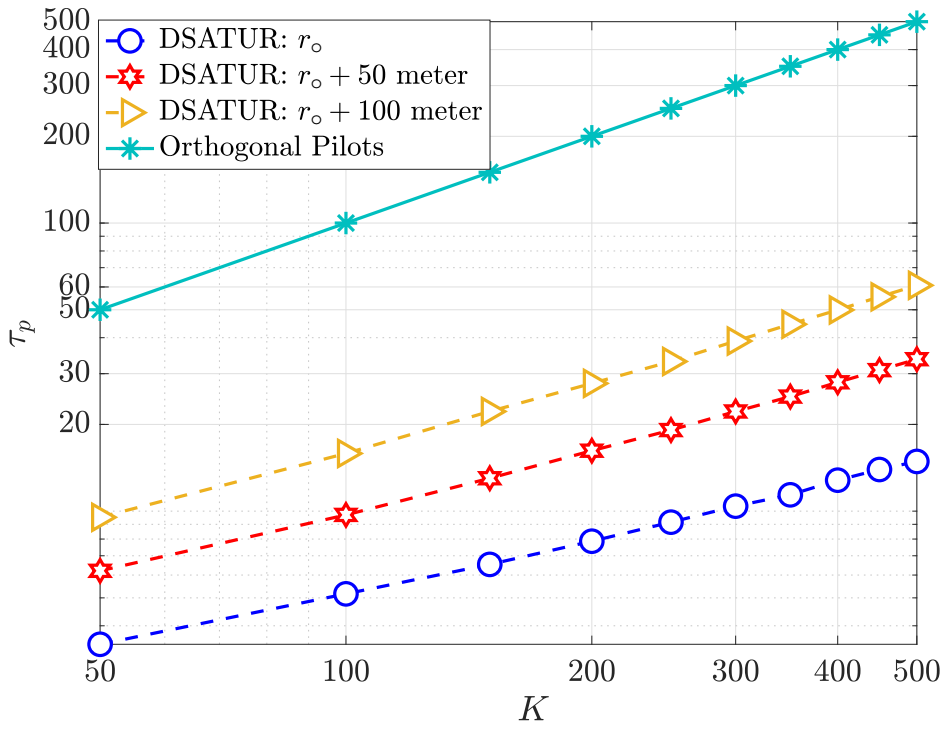

Figure 2.17: Scaling of pilot length with number of UEs (K). Algorithm 4 requires less than 20 pilots for the assumed choice of $r_\circ$, which is 4% of the total UEs at $K = 500$.

considering zero-forcing combining. We also plot the sum UL SE attained via orthogonal pilot allocation. The sum UL SE is evaluated as $\frac{\tau - \tau_p}{\tau} \sum_{k=1}^{K} \log_2 (1 + \mathsf{SINR}_{\mathsf{u},k})$, where the UL signal to noise plus interference ratio (SINR) of the kth UE is given in (2.19).[4][5] Observe that, in the case of orthogonal pilots, SE does not suffer from coherent interference (see $(N - \tau_p) \sum_{i \in \mathcal{P}_{l(k)} \setminus k} \mathcal{E}_{\mathsf{u},i} \left(\sum_{m=1}^{M} \alpha_{mi}^2 \right)^2$ in (2.19)), unlike the case where pilots are being reused. However, for orthogonal pilots, as $\tau_p = K$, the beamforming gain is also reduced by a factor $(N - K)$. Further, the pre-log factor $\frac{\tau - \tau_p}{\tau}$ can substantially degrade the SE as K becomes comparable to τ, as K gets large. This trade-off is noticeable in Figure 2.18, where, as the UE load increases, the SE attained when we use the Algorithm 4

[4]The derivation of the UL SINR for TDD case is a generalization of what is presented in Chapter 5 in the sense that $\mathsf{SINR}_{\mathsf{u},k}$ can be obtained considering only UL APs and UL UEs in the system.

[5]Here, $\mathcal{E}_{u,k}$ is the UL transmit power of the kth UE. All the UEs transmit at the same power, with $\mathcal{E}_{\mathsf{u},k}/N_0 = 20$ dB for all $k \in \mathcal{U}$.

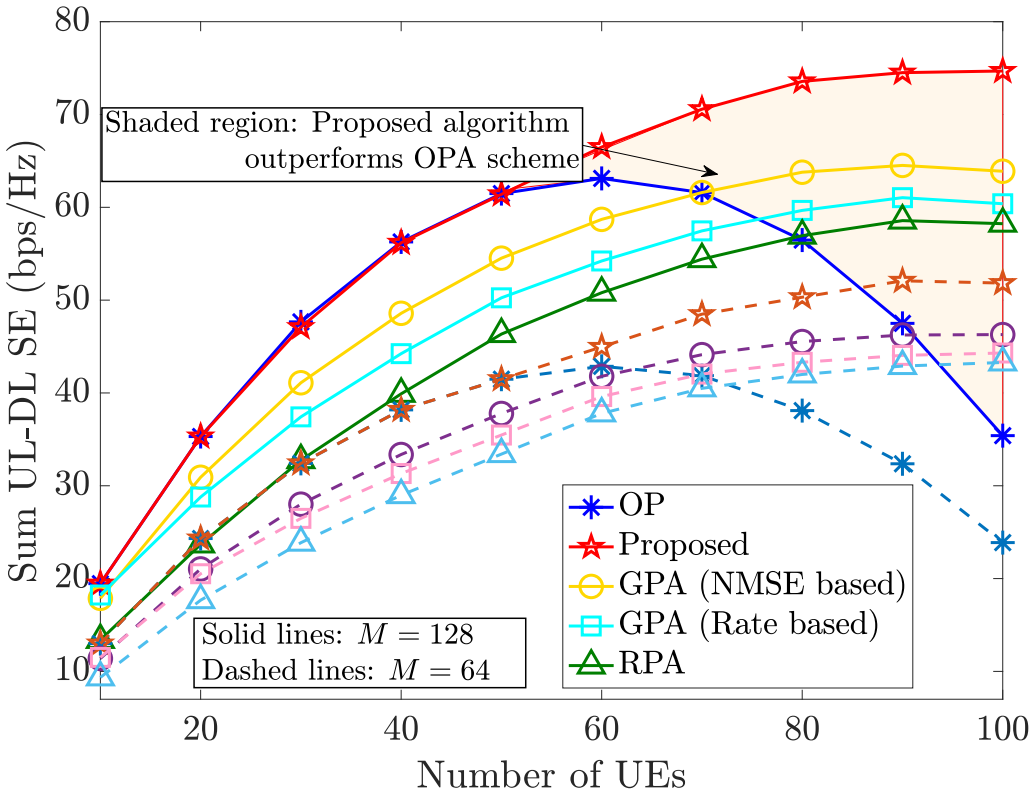

Figure 2.18: Sum UL-DL SE vs. the number of UEs. Our proposed algorithm outperforms (see the shaded region for $M = 128$) the use of orthogonal pilots as the number of UEs increases. The acronyms are: OP: orthogonal pilots across UEs, Proposed: our proposed algorithm, RPA: Random pilot assignment. Normalized MSE based greedy assignment corresponds to Algorithm 3 [33], and rate-based greedy assignment corresponds to [19, 48].

---

is considerably higher than the SE under orthogonal pilots. This underlines the utility of pilot reuse in a CF-MIMO system. Further, in Fig. 2.19, we plot the CDFs achieved via different pilot allocations and observe that our proposed algorithm uniformly outperforms existing iterative and greedy methods [31, 46, 49].

Remark 2.9. *As the graph coloring-based algorithm procures the best results compared to the previous algorithms, we use it in the subsequent chapters for pilot allocation.*

2.5 Chapter Summary

The benefits of CF-mMIMO rely heavily on the locally available CSI quality at the APs.

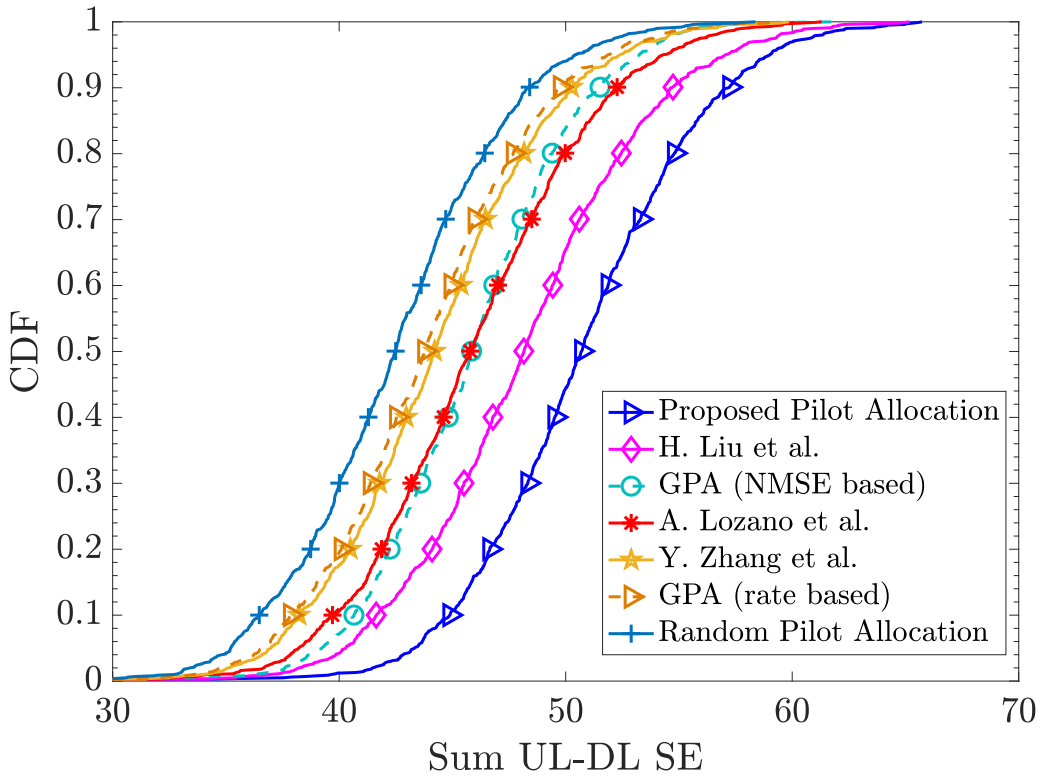

Figure 2.19: CDF of the sum UL-DL SE with $K = 80$ and $M = 64$ under different pilot allocation schemes. This experiment illustrates the superiority of the proposed scheme over several existing methods. Here, the legends H. Liu et al., A. Lozano et al., and Y. Zhang et al. correspond to the methods proposed by the authors in [46], [49], and [31], respectively.

$$\mathsf{SINR}_{\mathsf{u},k} = \frac{(N-\tau_p)\mathcal{E}_{\mathsf{u},k}\left(\sum_{m=1}^{M}\alpha_{mk}^2\right)^2}{\left(\begin{array}{c}\sum_{k'=1}^{K}\mathcal{E}_{\mathsf{u},k'}\sum_{m=1}^{M}\alpha_{mk}^2(\beta_{mk'}-\alpha_{mk'}^2) \\ +(N-\tau_p)\sum_{i\in\mathcal{P}_{l(k)}\setminus k}\mathcal{E}_{\mathsf{u},i}\left(\sum_{m=1}^{M}\alpha_{mi}^2\right)^2 + N_0\sum_{m=1}^{M}\alpha_{mk}^2\end{array}\right)}. \tag{2.19}$$

This chapter explored three separate approaches towards the issue of channel estimation and pilot allocation for CF-mMIMO systems. We first tackled the CSI-acquisition problem via quasi-orthonormal pilots and UE clustering in Section 2.2. We demonstrated that, in CF-mMIMO systems, pilots from MUOB codebooks minimize coherent interference among

the set of quasi-orthogonal pilot sequences. Next, we pointed out that ZC-sequences could be adopted to construct MUOB pilot matrices that comply with the 5G-NR standard. Additionally, we developed an AP-centric clustering algorithm for the pilot assignment. Our numerical findings illustrated that, in comparison to OPR, MUOB-based pilots procured superior throughput and fairness.

Next, we developed an iterative pilot allocation algorithm (see Algorithm 3) that obviated the need for initial AP-centric clustering. We have numerically illustrated the performance of the proposed algorithm in comparison with OPR and other comparable schemes.

Finally, we observed that the above two methods and also the existing works on channel estimations in CF-mMIMO literature focus on pilot design or pilot allocation given a predetermined length for the pilot sequences. Hence, in Section 2.4, we minimized the number of pilots required to ensure orthogonality among the UEs in close proximity via formulating an equivalent graph coloring problem, with the constraint that connected vertices (i.e., the UEs that are connected to a common AP) are allotted distinct colors (orthogonal pilots). Although the problem is NP-hard in general, it can be optimally solved for bipartite graphs (as is the case in our problem) via a low complexity greedy algorithm (see Algorithm 4), thereby minimizing the number of colors (i.e., the pilot length). We empirically showed that Algorithm 4 substantially improves the NMSE of the estimated channels compared to existing methods. Also, clustering aids in reducing the pilot length, keeping a balance between the data duration and pilot contamination.

3 Dynamic TDD with Cell-Free: Virtual Full-Duplex

Chapter Highlights

In this chapter, we examine the sum UL-DL SE performance of a CF-mMIMO system, where each AP can operate either in the UL or DL mode in each slot, corresponding to DTDD across the APs. We derive the sum UL-DL SE of the system considering equal weighting as well as an optimal weighted combining of the signals received at the CPU. Our analyses start with a simple case where the perfect CSI is available at the APs and the CPU and then extend to a more practical scenario where statistical or trained CSI is used to derive the sum UL-DL SE. We show that the sum SE is a sub-modular function of the subset of active APs under weighted combining at the CPU, and the results hold true for perfect, statistical, and trained CSI. We exploit this to develop a novel, low-complexity, greedy algorithm for choosing the mode of operation of the APs, which is guaranteed to achieve within $(1 - 1/e)$ of the sum UL-DL SE attained via a full-complexity brute-force search. We numerically illustrate the efficacy of the greedy algorithm and benchmark the performance of DTDD-enabled CF-mMIMO against TDD-based CF systems where all APs simultaneously operate in the UL or DL modes. Our results show that DTDD with greedy AP mode selection can nearly *double* the sum SE compared to a TDD-based CF-mMIMO system where all APs operate in the UL or DL modes simultaneously. This is because *DTDD offers additional degrees of freedom in terms of the APs' UL and DL mode selection based on the local traffic load* in the system. Thus, it is a promising duplexing scheme for beyond 5G communications.

3.1 Introduction: What is DTDD?

DTDD refers to a duplexing scheme where the UL reception and DL transmission modes of the HD APs in a geographical area can be dynamically scheduled based on the local UL and DL traffic load around each or a subset of APs. This is in contrast with the traditional static TDD systems, where all the APs operate either in UL or in DL in any given slot, and thus the UL/DL frame structures are fixed across all APs. Now, the traffic load in a wireless system is inherently asymmetric and heterogeneous in the sense that not every UE requires an equal amount of UL and DL data (asymmetric); and neither do all UEs demand UL or DL data at the same time (heterogeneous). In such a scenario, adaptive and flexible UL and DL frame allocation across APs leads to better and more efficient resource utilization. Further, it has been argued in the literature that traffic-adaptive UL/DL frame scheduling reduces latency compared to the static TDD case [54]. Extensive field measurements have revealed the superiority of DTDD over static TDD for cellular use cases. Hence, it has been included in the LTE standard, where it is referred to as enhanced interference mitigation and traffic adaptation (eIMTA) for LTE-Advanced (LTE-A) in Release 12 [55]. Like LTE, 5G NR supports DTDD [56, 57].

However, DTDD introduces two additional interferences: interference between a DL-scheduled AP to a UL-scheduled AP, i.e., InAI, and interference from UL UEs to the DL UEs, i.e., InUI. InAI and InUI are commonly referred to as CLI[1], and the performance improvement by DTDD is heavily dependent on satisfactory CLI mitigations. Now, we note that the current DTDD standards and studies are for cellular MMO systems, where CLI mitigation often demands cooperation and information exchange among the BSs, which incurs additional signal processing overhead. Further, the algorithms involved in small-cell BS clustering for joint beamforming and resource allocation across cells are prohibitively complex. An excellent survey of CLI mitigation algorithms can be found in [58]. Also, it

[1]Here, we recapitulate that acronyms InAI, InUI, and CLI stand for inter-AP interference, inter-UE interference, and cross-link interference, respectively.

is important to note that irrespective of how sophisticated the interference management techniques are, cellular deployments inevitably suffer from multi-cell interference. Thus, a fundamentally novel aspect that we would like to explore in this chapter is the combination of flexible duplexing in conjunction with CF mMIMO operation. This offers the best of both worlds, allowing the system to manage interference effectively via joint processing at the CPU while meeting diverse and asymmetric UL and DL data requirements from the UEs. Further, we note that cellular DTDD does not fully cater to heterogeneous data demands within the cells. That is, a UE with UL data demand will still have to wait for a slot where its serving BS is operating in the UL mode in order to complete its transmission; similarly for a UE with DL data demand. On the other hand, in a CF-mMIMO system, since the UEs are not associated with a particular AP, if the APs can dynamically select the slots where they operate in UL and DL modes, any UE with a specific data demand can find some nearby APs operating in the corresponding mode in the same slot.

3.1.a DTDD-Enabled CF: Virtual FD

In a DTDD-enabled CF system, the subset of HD APs operates in UL, and its complementary subset operates in DL. The sizes of the UL and DL scheduled AP sets depend on the UL and DL data traffic in the given geographical area. How to schedule an AP in UL or DL will be discussed in detail in the succeeding sections. Now, given a set of UL and DL AP schedules, we illustrate the system in Figure 3.1 indicating InAI and InUI. We observe from Figure 3.1 that in CF DTDD, any UL (or DL) UE can always be served by a subset of nearby UL (or DL) scheduled APs. This is in contrast with the cellular DTDD system, where in a given slot, if a BS is scheduled in UL(/DL), the DL(/UL) UEs in that cell cannot be served by the same BS at that slot. Thus, DTDD-enabled cellular systems, although they offer superior performance compared to TDD, cannot serve both UL and DL UEs in a cell simultaneously, only with HD BSs. However, as evident from Figure 3.1, the DTDD-enabled CF can serve *all* the UL and DL UEs simultaneously with HD APs;

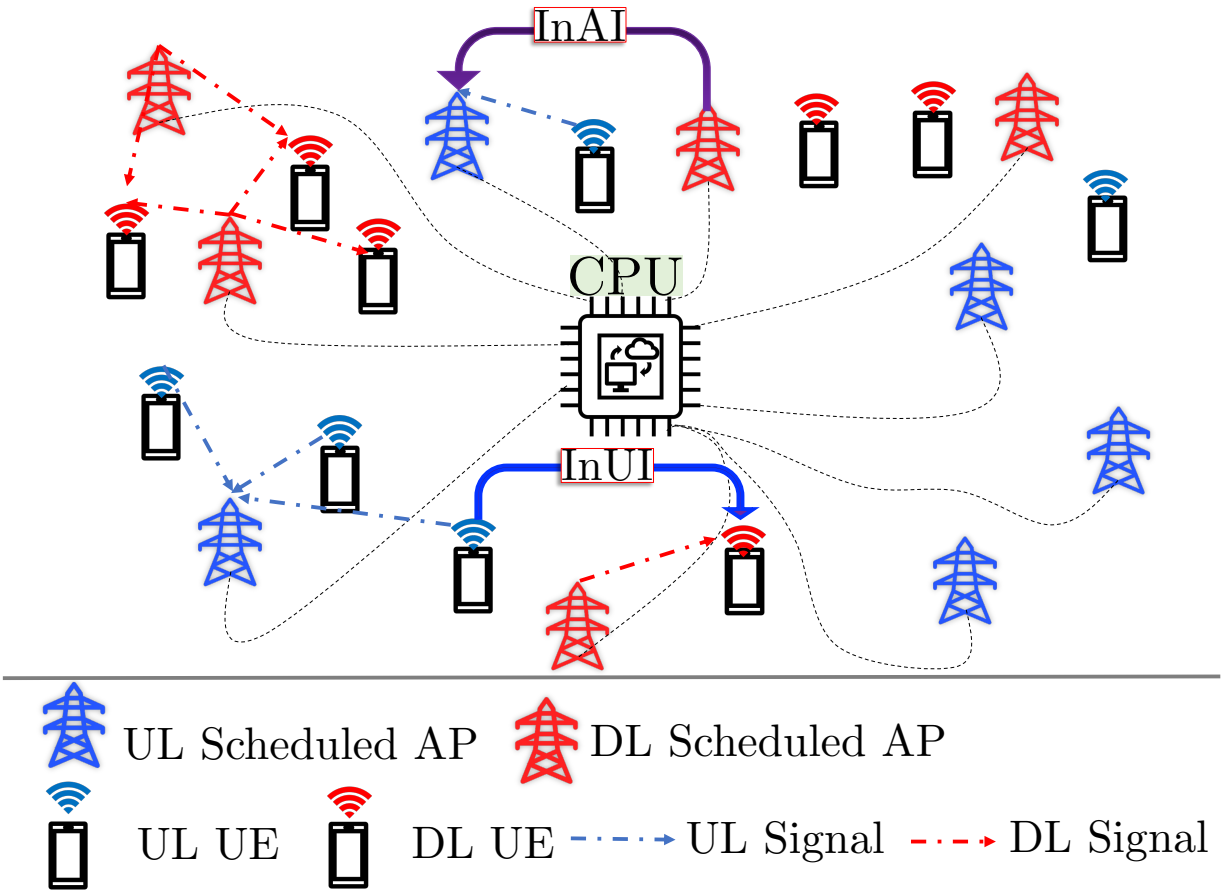

Figure 3.1: DTDD-enabled CF system.

hence, we call DTDD-enabled CF a virtual FD system. We emphasize that all APs in DTDD-enabled CF are HD; therefore, SI cancelation is completely avoided, which is a serious challenge for an FD-enabled system. Additionally, in a DTDD-enabled CF system, the amount of InAI can potentially be less compared to the conventional FD CF system. This is because only a subset of APs scheduled in DL contribute to InAI, whereas in the FD CF system, all the APs contribute to InAI. The effect of CLI on the system performance and a comparative study of DTDD versus FD cellular and CF systems will be presented in later chapters. This chapter provides an initial exposure to the SE analysis of DTDD-enabled CF with equal combining at the CPU Section 3.2. Subsequently, we develop SINR-optimal combining at the CPU and an AP-scheduling algorithm Section 3.3 with optimality guarantees. Throughout this chapter, we consider either perfect CSI or

orthogonal pilots and perfect InAI cancelation. Later, in Chapter 4, we relax these constraints and present theoretical results considering pilot contamination and imperfect InAI cancelation. In summary, the major contributions of this chapter are:

1. We first derive the UL and DL rates achievable by a DTDD-enabled CF-mMIMO system with MRC and MFP. We consider equal weighting at the CPU for UL and equal power allocation for the DL. We show that the overall sum UL-DL SE across UEs depends on the underlying UL/DL AP schedule.

2. Following this, we present a greedy algorithm for scheduling the modes of operations of the APs to maximize the achievable sum SE. Each iteration of this algorithm adds a single AP to the schedule, allotting it either UL or DL mode of operation. The choice of the AP and its corresponding mode of operation depends on the incremental sum rate achieved. This is presented in Algorithm 5.

3. We next argue that an equal weighting-based scheme is sub-optimal for a CF system, and the performance of DTDD can be further improved via optimal combining at the CPU. We analyze the UL/DL SINRs and SE under an SINR-maximizing weighted combining scheme at the CPU. We then prove that, under a weighted precoding/combining scheme introduced in this work, UL and the DL SINRs are monotonically non-decreasing *modular* functions of the activated AP set, and the sum UL-DL SE is a *sub-modular* function of the activated AP set. The analysis in this paper holds for perfect, statistical, as well as trained CSI.

4. We leverage the sub-modularity property to obtain optimality guarantees from an iterative algorithm presented as Algorithm 5 in the sequel.

5. We empirically show that DTDD enabled CF-mMIMO almost *doubles the sum UL-DL SE* compared to a canonical TDD-based system. Essentially, DTDD-enabled CF-mMIMO exploits both the joint signal processing of a CF system and the adaptive

UL-DL slot selection at the APs based on local traffic demands.

This leads us to conclude that DTDD, in conjunction with the CF-mMIMO system with appropriately scheduled APs, is a promising solution to meet heterogeneous traffic demands in next-generation wireless communication systems.

3.2 DTDD-enabled CF: SE Analysis with Equal Weighting at the CPU

We consider a CF-mMIMO system with M HD-APs jointly and coherently serving K single-antenna UEs. Each AP is equipped with N antennas and is connected to a CPU via an ideal back-haul link. The channel from kth UE to the mth AP is modeled as $\mathbf{f}_{mk} = \sqrt{\beta_{mk}}\mathbf{h}_{mk} \in \mathbb{C}^N$, where β_{mk} is the path loss coefficient and $\mathbf{h}_{mk} \overset{\text{i.i.d.}}{\sim} \mathcal{CN}(\mathbf{0}, \mathbf{I}_N)$ is the fast fading component. Note that β_{mk} remains unchanged over several coherence intervals and is assumed to be known to the APs and the CPU. Also, under a quasi-static fading model, $\mathbf{h}_{mk}$ remains constant over one coherence interval and takes independent values from the same distribution in subsequent coherence intervals.

The simultaneous UL and DL traffic results in inter-AP and inter-UE CLIs, in addition to the multi-user interference. The inter-AP channels are typically slowly varying and can be assumed to remain unchanged over several coherence intervals. Additionally, the transmitted DL data vectors are known at the CPU. Therefore, the known data vectors can be used to estimate the inter-AP channels accurately, and the InAI can be eliminated at the CPU. In Chapter 4, we consider imperfect estimates of inter-AP channels and analyze their effect on the system performance and AP scheduling. In order to capture the inter-UE CLIs, we model the channel between nth UL UE and the kth DL UE as $\mathsf{g}_{nk} \sim \mathcal{CN}(0, \epsilon_{nk})$, and is independent across all UE pairs.

3.2.a Problem Statement

Let $\mathcal{U}_{\mathsf{u}}$ and $\mathcal{U}_{\mathsf{d}}$ be the index sets containing the UE indices demanding UL and DL access,

respectively. Let $\mathcal{A}$ be the set of AP indices, with $M = |\mathcal{A}|$. Let the indices of the APs scheduled in UL and DL modes be contained in the index sets $\mathcal{A}_{\mathsf{u}}$ and $\mathcal{A}_{\mathsf{d}}$, respectively. Then, for each distinct choice of $\mathcal{A}_{\mathsf{u}}$ and $\mathcal{A}_{\mathsf{d}}$, we obtain a distinct value of the sum UL-DL SE, denoted by $\mathcal{R}_{\mathrm{s}}(\mathcal{A}_{\mathsf{u}}, \mathcal{A}_{\mathsf{d}})$. Therefore, the CPU needs to suitably schedule the APs to maximize $\mathcal{R}_{\mathrm{s}}(\mathcal{A}_{\mathsf{u}}, \mathcal{A}_{\mathsf{d}})$ over all possible choices of $\mathcal{A}_{\mathsf{u}}$ and $\mathcal{A}_{\mathsf{d}}$, i.e.,

$$\begin{aligned} &\max_{\mathcal{A}_{\mathsf{u}}, \mathcal{A}_{\mathsf{d}}} \quad \mathcal{R}_{\mathrm{s}}(\mathcal{A}_{\mathsf{u}}, \mathcal{A}_{\mathsf{d}}) \\ &\text{s.t.} \quad \mathcal{A}_{\mathsf{u}}, \mathcal{A}_{\mathsf{d}} \subseteq \mathcal{A}, \quad \mathcal{A}_{\mathsf{u}} \cap \mathcal{A}_{\mathsf{d}} = \emptyset, \quad \mathcal{A}_{\mathsf{u}} \cup \mathcal{A}_{\mathsf{d}} = \mathcal{A}. \end{aligned} \tag{3.1}$$

We observe from (3.1) that searching over all possible UL/DL configurations requires the evaluation of the sum SE corresponding to 2^M choices, making exhaustive search computationally expensive. This motivates us to develop a low complexity AP-scheduling algorithm that can solve (3.1) in polynomial time. To this end, we first derive an analytical expression for $\mathcal{R}_{\mathrm{s}}$ in the next section.

3.2.b Performance Analysis

We assume that out of the total τ channel uses per coherence interval, the first K are reserved for UL channel estimation. During these K channel uses, all the UEs transmit mutually orthogonal pilot sequences to the APs. The APs use the received pilot sequences and obtain local estimates of the AP to UE channels. Let the pilot sequence of the kth UE be denoted as $\boldsymbol{\phi}_k$ and $\mathcal{E}_{p,k}$ be the corresponding pilot power. Then using the theory developed in Section 2.3.a, we can easily show that the MMSE estimate of $\mathbf{f}_{mk}$, $\hat{\mathbf{f}}_{mk} \sim \mathcal{CN}(\mathbf{0}, \alpha_{mk}^2 \mathbf{I}_N)$, with $\alpha_{mk}^2 = \dfrac{\tau_p \mathcal{E}_{p,k} \beta_{mk}^2}{\tau_p \mathcal{E}_{p,k} \beta_{mk} + N_0}$. Let the estimation error, orthogonal to $\hat{\mathbf{f}}_{mk}$, be denoted by $\tilde{\mathbf{f}}_{mk}$, such that $\tilde{\mathbf{f}}_{mk} \sim \mathcal{CN}(\mathbf{0}, \bar{\alpha}_{mk}^2 \mathbf{I}_N)$, with $\bar{\alpha}_{mk} = \sqrt{\beta_{mk} - \alpha_{mk}^2}$.

Let the kth UE transmit the symbol $s_{\mathsf{u},k}$ in the UL. The data symbols transmitted by each UE are assumed to be zero mean, unit variance, and uncorrelated with the symbols sent by the other UEs. Then, the UL signal received at the mth AP ($m \in \mathcal{A}_{\mathsf{u}}$) can be

expressed as

$$\mathbf{y}_{\mathsf{u},m} = \sqrt{\mathcal{E}_{\mathsf{u},k}}\mathbf{f}_{mk}s_{\mathsf{u},k} + \sum_{n\in\mathcal{U}_{\mathsf{u}}\setminus k}\sqrt{\mathcal{E}_{\mathsf{u},n}}\mathbf{f}_{mn}s_{\mathsf{u},n} + \mathbf{w}_{\mathsf{u},m},$$

where $\mathcal{E}_{\mathsf{u},n}$ is the UL energy associated with the nth UE, and $\mathbf{w}_{\mathsf{u},m} \sim \mathcal{CN}(\mathbf{0}, N_0\mathbf{I}_N)$. Now, considering the maximal ratio combining (MRC) at the AP, the kth stream of the UL combined signal at the CPU can be expressed as

$$r_{\mathsf{u},k} = \sqrt{\mathcal{E}_{\mathsf{u},k}}\mathbb{E}\left[\sum_{m\in\mathcal{A}_{\mathsf{u}}}\hat{\mathbf{f}}_{mk}^H\mathbf{f}_{mk}\right]s_{\mathsf{u},k} + z_{\mathsf{u},k}, \tag{3.2}$$

with the effective noise $z_{\mathsf{u},k}$ given by

$$\begin{aligned} z_{\mathsf{u},k} = &\sqrt{\mathcal{E}_{\mathsf{u},k}}\left(\sum_{m\in\mathcal{A}_{\mathsf{u}}}\hat{\mathbf{f}}_{mk}^H\mathbf{f}_{mk} - \mathbb{E}\left[\sum_{m\in\mathcal{A}_{\mathsf{u}}}\hat{\mathbf{f}}_{mk}^H\mathbf{f}_{mk}\right]\right)s_{\mathsf{u},k} \\ &+ \sum_{m\in\mathcal{A}_{\mathsf{u}}}\sum_{n\in\mathcal{U}_{\mathsf{u}}\setminus k}\sqrt{\mathcal{E}_{\mathsf{u},n}}\hat{\mathbf{f}}_{mk}^H\mathbf{f}_{mn}s_{\mathsf{u},n} + \sum_{m\in\mathcal{A}_{\mathsf{u}}}\hat{\mathbf{f}}_{mk}^H\mathbf{w}_{\mathsf{u},mk}. \end{aligned}$$

It is easy to show that

$$\begin{aligned} \mathbb{E}\left[|z_{\mathsf{u},k}|^2\right] &= \mathcal{E}_{\mathsf{u},k}\mathtt{var}\left(\sum\nolimits_{m\in\mathcal{A}_{\mathsf{u}}}\hat{\mathbf{f}}_{mk}^H\mathbf{f}_{mk}\right) \\ &+ \sum_{m\in\mathcal{A}_{\mathsf{u}}}\sum_{n\in\mathcal{U}_{\mathsf{u}}\setminus k}\mathcal{E}_{\mathsf{u},n}\mathbb{E}\left[\left|\hat{\mathbf{f}}_{mk}^H\mathbf{f}_{mn}\right|^2\right] + \sum_{m\in\mathcal{A}_{\mathsf{u}}}\mathbb{E}\left[\left|\hat{\mathbf{f}}_{mk}^H\mathbf{w}_{\mathsf{u},mk}\right|^2\right] \\ &= N\sum_{n\in\mathcal{U}_{\mathsf{u}}}\mathcal{E}_{\mathsf{u},n}\sum_{m\in\mathcal{A}_{\mathsf{u}}}\alpha_{mk}^2\beta_{mn} + NN_0\sum_{m\in\mathcal{A}_{\mathsf{u}}}\alpha_{mk}^2. \end{aligned}$$

Next, considering the jth DL AP, let $\mathcal{E}_{\mathsf{d},j}$ be the total radiated DL power and κ_{jn} be the fraction of power dedicated by the jth AP to the nth DL UE ($n \in \mathcal{U}_{\mathsf{d}}$). Then, under the assumption of perfect channel reciprocity, the signal received by the nth ($n \in \mathcal{U}_{\mathsf{d}}$) DL UE can be expressed as

$$r_{\mathsf{d},n} = \sum\nolimits_{j\in\mathcal{A}_{\mathsf{d}}}\kappa_{jn}\sqrt{\mathcal{E}_{\mathsf{d},j}}\mathbb{E}\left[\mathbf{f}_{jn}^T\mathbf{f}_{jn}^*\right]s_{\mathsf{d},n} + z_{\mathsf{d},n}, \tag{3.3}$$

with $z_{\mathsf{d},k}$ being the effective DL noise and interference with

$$z_{\mathsf{d},n} = \sum_{j\in\mathcal{A}_\mathsf{d}} \kappa_{jn}\sqrt{\mathcal{E}_{\mathsf{d},j}}\left(\mathbf{f}_{jn}^T\mathbf{f}_{jn}^* - \mathbb{E}\left[\mathbf{f}_{jn}^T\mathbf{f}_{jn}^*\right]\right) s_{\mathsf{d},n} + \sum_{k\in\mathcal{U}_\mathsf{u}} \sqrt{\mathcal{E}_{\mathsf{u},k}}\mathbf{g}_{nk}s_{\mathsf{u},k} + \sum_{j\in\mathcal{A}_\mathsf{d}}\sum_{q\in\mathcal{U}_\mathsf{d}\setminus n} \kappa_{jq}\sqrt{\mathcal{E}_{\mathsf{d},j}}\mathbf{f}_{jn}^T\mathbf{f}_{jq}^* s_{\mathsf{d},q} + w_{\mathsf{d},n},$$

where $w_{\mathsf{d},n} \sim \mathcal{CN}(0, N_0)$ is the additive noise at the nth DL UE. We can show that

$$\mathbb{E}\left[|z_{\mathsf{d},n}|^2\right] = N\sum_{q\in\mathcal{U}_\mathsf{d}}\sum_{j\in\mathcal{A}_\mathsf{d}} \mathcal{E}_{\mathsf{d},j}\kappa_{jq}^2\beta_{jn}\alpha_{jq}^2 + \sum_{k\in\mathcal{U}_\mathsf{u}} \mathcal{E}_{\mathsf{u},k}\epsilon_{nk} + N_0.$$

We can now evaluate the achievable UL and the DL SEs, and hence the sum throughput of the network.

Theorem 3.1. *The sum SE of the system is given by*[2]

$$\mathcal{R}_\mathsf{s}(\mathcal{A}_\mathsf{u}, \mathcal{A}_\mathsf{d}) = \frac{\tau - \tau_p}{\tau}\left[\sum_{k\in\mathcal{U}_\mathsf{u}} \mathcal{R}_{\mathsf{u},k}(\mathcal{A}_\mathsf{u}) + \sum_{n\in\mathcal{U}_\mathsf{d}} \mathcal{R}_{\mathsf{d},n}(\mathcal{A}_\mathsf{u})\right]. \tag{3.4}$$

Here, the achievable UL SE for the kth UE is $\mathcal{R}_{\mathsf{u},k} = \log(1+\eta_{\mathsf{u},k}(\mathcal{A}_\mathsf{u}))$, where $\eta_{\mathsf{u},k}(\mathcal{A}_\mathsf{u})$ is the UL SINR, which equals

$$\frac{N\mathcal{E}_{\mathsf{u},k}\left(\sum_{m\in\mathcal{A}_\mathsf{u}}\alpha_{mk}^2\right)^2}{\sum_{n\in\mathcal{U}_\mathsf{u}}\mathcal{E}_{\mathsf{u},n}\sum_{m\in\mathcal{A}_\mathsf{u}}\alpha_{mk}^2\beta_{mn} + N_0\sum_{m\in\mathcal{A}_\mathsf{u}}\alpha_{mk}^2}.$$

The achievable DL SE for the nth UE is $\mathcal{R}_{\mathsf{d},n}(\mathcal{A}_\mathsf{d}) = \log(1+\eta_{\mathsf{d},n}(\mathcal{A}_\mathsf{d}))$, where $\eta_{\mathsf{d},n}(\mathcal{A}_\mathsf{d})$ is the DL SINR, which equals

$$\frac{N^2\left(\sum_{j\in\mathcal{A}_\mathsf{d}}\kappa_{jn}\sqrt{\mathcal{E}_{\mathsf{d},j}}\alpha_{jn}^2\right)^2}{N\sum_{q\in\mathcal{U}_\mathsf{d}}\sum_{j\in\mathcal{A}_\mathsf{d}}\mathcal{E}_{\mathsf{d},j}\kappa_{jq}^2\beta_{jn}\alpha_{jq}^2 + \sum_{k\in\mathcal{U}_\mathsf{u}}\mathcal{E}_{\mathsf{u},k}\epsilon_{nk} + N_0}.$$

Proof. The result is easily derived by applying techniques described in [19]. ■

[2]In fact, the theorem presents a lower bound on the ergodic sum UL-DL SE of the system. The tightness and efficacy of such a bound have been well established in the CF literature [19].

Algorithm 5: Greedy AP-scheduling

Input: $\mathcal{A}$: the set of all AP indices

Initialization: $\mathcal{A}_{\mathsf{u}} = \mathcal{A}_{\mathsf{d}} = \emptyset$, $\mathcal{A}_{\text{greedy}} = \mathcal{A}_{\mathsf{u}} \cup \mathcal{A}_{\mathsf{d}}$, $\mathcal{A}'_{\text{greedy}} = \mathcal{A}$

[1]: **while** $\mathcal{A}'_{\text{greedy}} \neq \emptyset$ **do**

[2]: $\quad i^{\star}_{\mathsf{u}} = \arg \max_{i \in \mathcal{A}'_{\text{greedy}}} \mathcal{R}_{\text{s}}(\mathcal{A}_{\mathsf{u}} \cup \{i\})$

[3]: $\quad i^{\star}_{\mathsf{d}} = \arg \max_{i \in \mathcal{A}'_{\text{greedy}}} \mathcal{R}_{\text{s}}(\mathcal{A}_{\mathsf{d}} \cup \{i\})$

[4]: $\quad$ **if** $\mathcal{R}_{\text{s}}(\mathcal{A}_{\mathsf{u}} \cup \{i^{\star}_{\mathsf{u}}\}) \geq \mathcal{R}_{\text{s}}(\mathcal{A}_{\mathsf{d}} \cup \{i^{\star}_{\mathsf{d}}\})$ **then**

[5]: $\quad\quad$ **Update** $\mathcal{A}_{\mathsf{u}} = \mathcal{A}_{\mathsf{u}} \cup \{i^{\star}_{\mathsf{u}}\}$

[6]: $\quad\quad$ **else**

[7]: $\quad\quad\quad$ **Update** $\mathcal{A}_{\mathsf{d}} = \mathcal{A}_{\mathsf{d}} \cup \{i^{\star}_{\mathsf{d}}\}$;

[8]: $\quad\quad$ **end**

[9]: $\quad$ **end**

[10]: $\quad \mathcal{A}_{\text{greedy}} = \mathcal{A}_{\mathsf{u}} \cup \mathcal{A}_{\mathsf{d}}$

[11]: $\quad \mathcal{A}'_{\text{greedy}} = \mathcal{A} \backslash \{i\}$; $\quad$ % `Update the unscheduled AP index set`

[12]: **end**

[13]: **Return** $\mathcal{A}_{\text{greedy}}$

Based on the above, we can develop a greedy algorithm for AP scheduling, summarized as Algorithm 5. Here, in each iteration, we evaluate the incremental gain on the sum UL-DL SE when one AP is scheduled in either UL or DL mode. Following this, we schedule the AP and the mode that results in maximal incremental gain. We repeat this process until all the APs have been scheduled.

3.2.c DTDD versus TDD: Numerical Experiments

For numerical experiments, the UE locations are deployed uniformly at random over a square 1 km^2 area, and we consider Monte Carlo simulations over 10^4 such UE locations and channel instantiations. The UEs are randomly assigned to carry UL or DL traffic based on the UL and DL traffic demand. For the CF-DTDD system, M N-antenna HD-APs are scheduled via Algorithm 5 and are deployed on a uniform grid to ensure equitable coverage. The path loss exponent and the reference distance from each AP are assumed to be -3.76 and 10 m, respectively [19]. The UL SNR is set by fixing the noise variance

N_0 to unity and varying the UL powers $\mathcal{E}_{\mathrm{u},k}$ such that $\mathcal{E}_{\mathrm{u},k}/N_0$ equals the desired value. In the DL, we set $\kappa_{jn} = (N\sum_{k'\in\mathcal{U}_\mathrm{d}}\alpha_{jk'}^2)^{-1}$ [14,47]. The coherence interval (τ) is taken as 600 symbols, and we set $\tau_p = K$. The carrier frequency is 1.9 GHz and the signal bandwidth is 20 MHz.

We benchmark the performance of a DTDD-enabled CF-mMIMO against the existing HD TDD-based CF-mMIMO [19]. The HD TDD-based CF-mMIMO system follows similar parameters (i.e., path loss exponent, power control coefficients, AP locations, etc.) as above, except that all the APs simultaneously operate either in UL or in DL. A detailed discussion of HD TDD-based CF-mMIMO can be found in [19].

In Figure 3.2, we verify the efficacy of the greedy algorithm by plotting the per UE UL-DL SE against the number of antennas per AP. We see that the SE attained via the greedy algorithm matches with that of attained via a brute force search over all possible UL and DL AP schedules. Based on this, we employ the greedy algorithm for AP scheduling for the subsequent plots in this section.

Next, in Figure 3.3, we plot the 95%-likely sum UL-DL SE vs. UL and DL data SNR to validate the theoretical expressions of SE derived in Theorem 3.1. The theoretical curve is obtained by averaging the 95%-likely sum UL-DL SE obtained from (3.4) over the UE locations. The simulation results corroborate well with our theoretical results, verifying the accuracy of the expression for $\mathcal{R}_\mathrm{s}$ presented in Theorem 3.1.

In Figure 3.4, we investigate the performance improvement offered by DTDD-enabled CF-mMIMO over canonical TDD-based CF-mMIMO systems. We see that the use of DTDD facilitates a more efficient time resource utilization compared to TDD as the UL/DL reception/transmission mode of each AP is scheduled based on the localized traffic demand in the system, therefore, which in turn leads to better sum UL-DL SE. The cumulative distribution functions (CDFs) of the SE achieved under DTDD against TDD, as presented in Figure 3.4 is in agreement with this. For instance, under the availability of perfect CSI (solid curves in Figure 3.4), we observe that the median of the sum UL-DL SE with

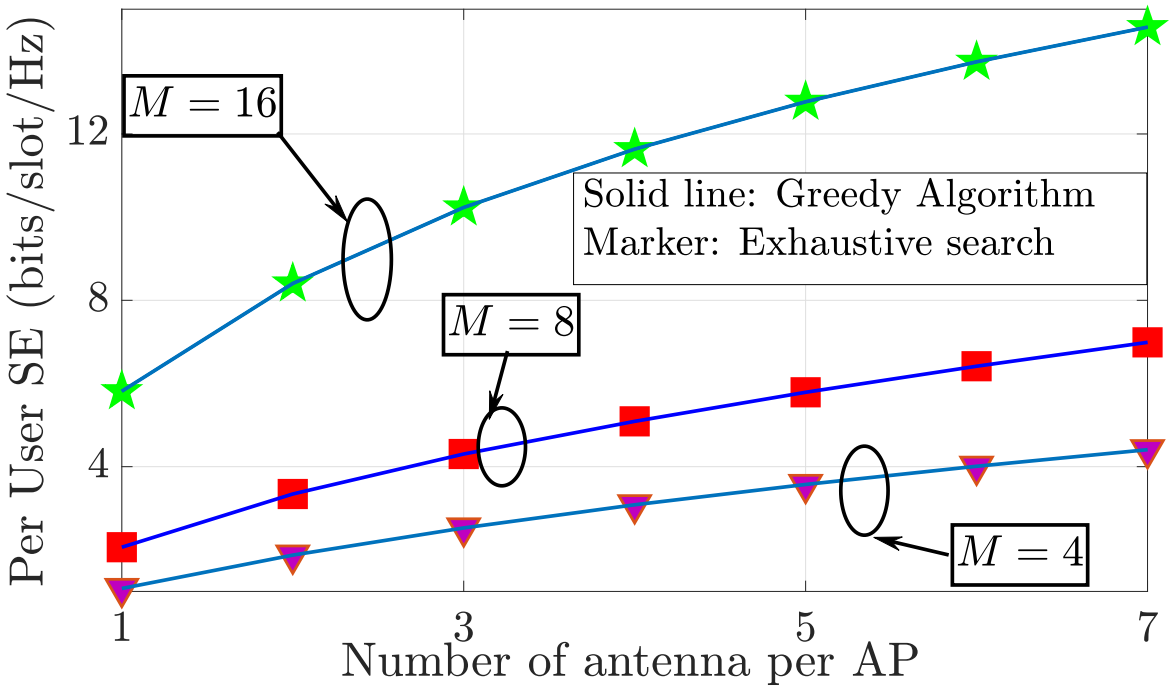

Figure 3.2: The accuracy of the greedy algorithm for AP scheduling considering $K = 40$ data and pilot SNRs 10 dB.

DTDD is more than 25 bps/slot/Hz with $M = 128$. Under similar settings, TDD can only achieve a median sum UL-DL SE of around 15 bps/slot/Hz.

In Figure 3.5, we plot the 95%-likely UL sum SE against the 95%-likely DL sum SE obtained AP/ antenna configurations. For each of these cases, we use Algorithm 5 to determine the mode of operation across the APs. We observe in Figure 3.5 that the rate regions attained using DTDD uniformly outperform the rate region attained using CF-TDD for similar antenna densities and with similar configurations, indicating the superiority of the DTDD-based scheme.

Finally, in Figure 3.6, we plot the rate regions of DTDD-enabled CF mMIMO against the canonical TDD-based cellular system. We observe that a DTDD-based CF system with ($M = 32$) substantially outperforms a cellular TDD system with ($L = 64$) with similar antenna density, revealing the advantage of joint signal processing at the CPU in a CF-based system.

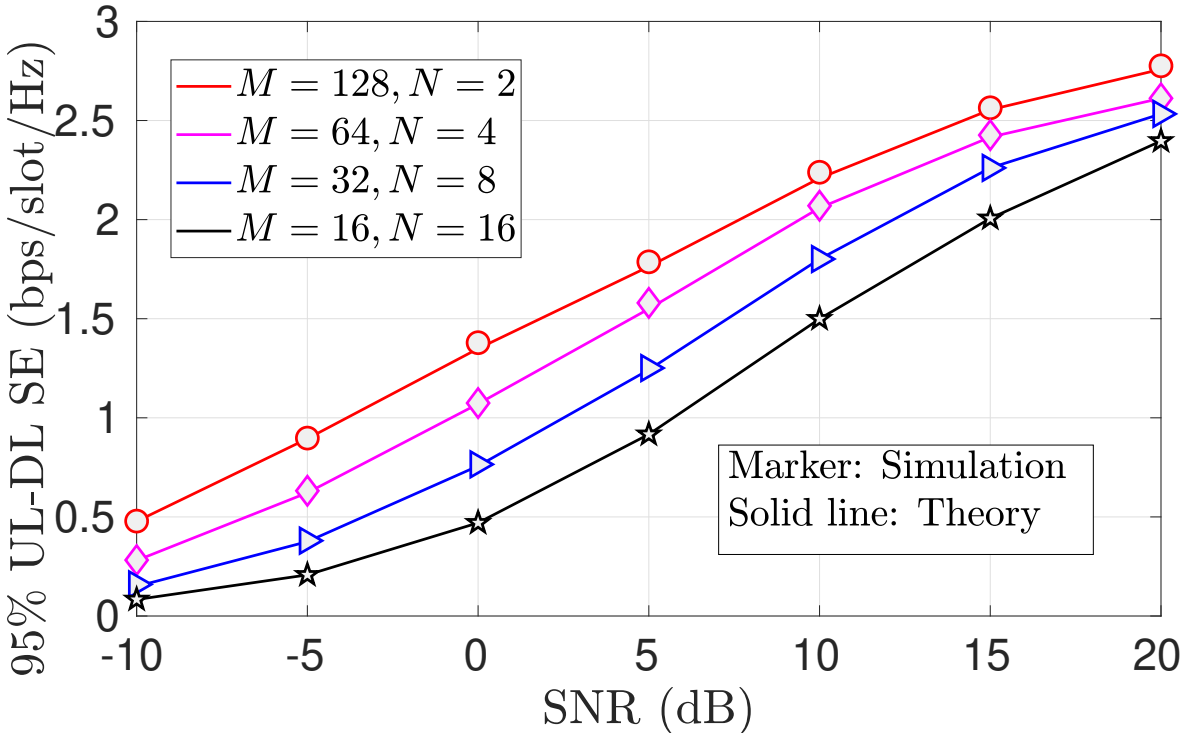

Figure 3.3: Validation of the derived sum UL-DL SE. We observe that the sum UL-DL SE derived in Theorem 3.1 closely matches with the simulation.

In summary, our numerical experiments showed that a DTDD-enabled CF-mMIMO system substantially improves the sum UL-DL SE compared to TDD CF and TDD cellular mMIMO systems. Essentially, DTDD CF-mMIMO exploits the joint signal processing of a DAA system coupled with the adaptive scheduling of UL-DL slots based on the localized traffic demands at the APs. However, the AP-scheduling algorithm is heuristic, and to develop guarantees related to the optimality of such an iterative algorithm, we next present SINR optimal combining and precoding schemes, and analyze the system performance compared to the equal weighting-based scheme discussed in Section 3.2.b

3.3 Weighted Combing and Optimality Guarantee

For ease of understanding, in this section, we first analyze the sum SE when perfect CSI (PCSI) is available at the APs and CPU. The kth stream of the received signal

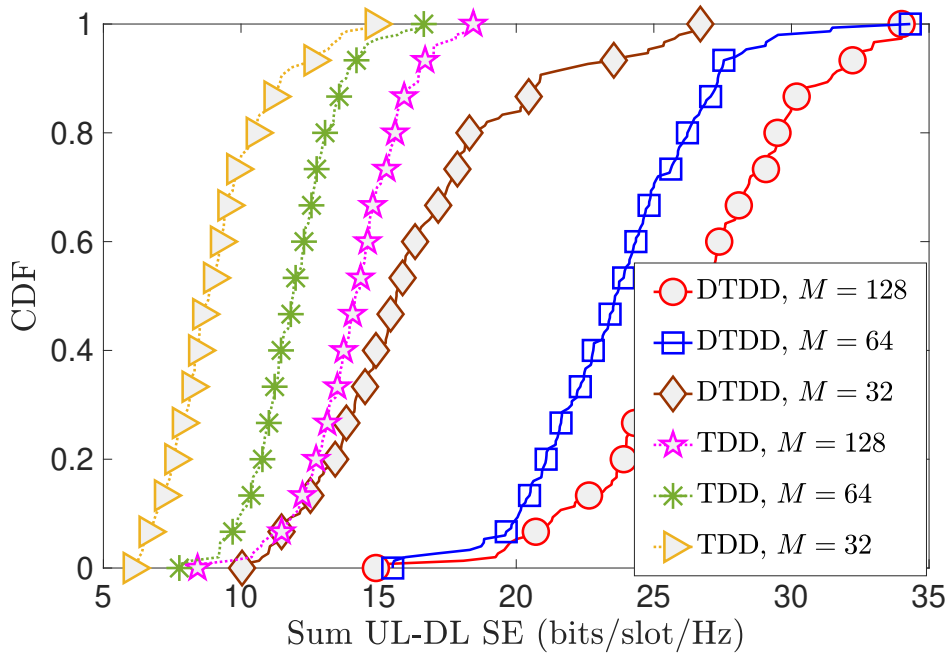

Figure 3.4: Performance of DTDD based CF-mMIMO and canonical TDD CF-mMIMO, with $K = 40$, and $MN = 512$. DTDD considerably outperforms the TDD protocol.

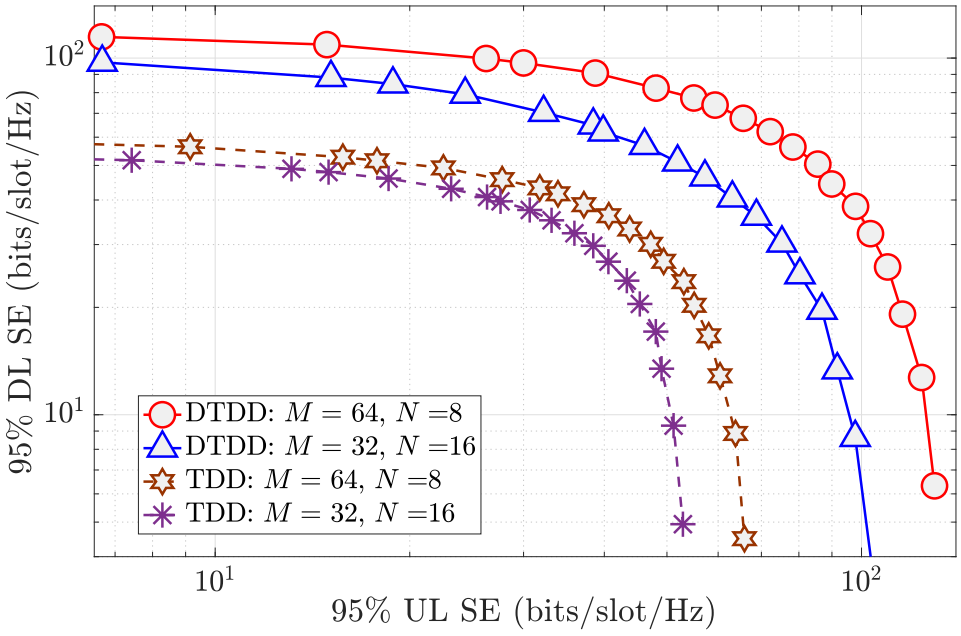

Figure 3.5: Rate region comparison of DTDD against TDD in CF-mMIMO system with $K = 80$.

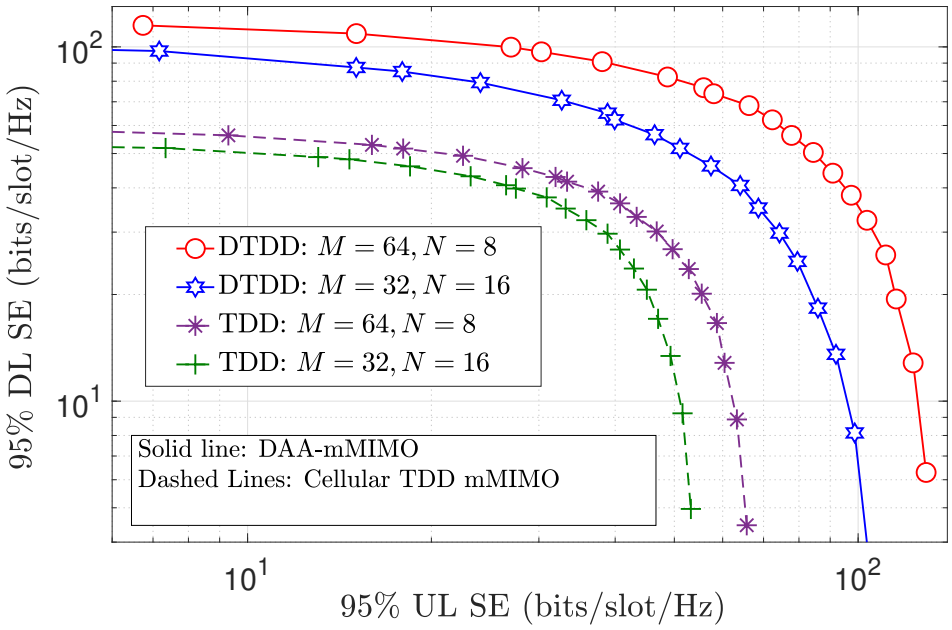

Figure 3.6: Rate region comparison of DTDD enabled CF-mMIMO system against TDD based canonical cellular system.

(corresponding to the signal transmitted by the kth UL UE) at the mth UL AP ($m \in \mathcal{A}_{\mathsf{u}}$) is given by

$$r_{\mathsf{u},mk} = \sqrt{\mathcal{E}_{\mathsf{u},k}}\mathbf{v}_{mk}^H \mathbf{f}_{mk} s_{\mathsf{u},k} + \sum_{k' \in \mathcal{U}_{\mathsf{u}} \setminus k} \mathbf{v}_{mk}^H \sqrt{\mathcal{E}_{\mathsf{u},k'}} \mathbf{f}_{mk'} s_{\mathsf{u},k'} + \sqrt{N_0}\mathbf{v}_{mk}^H \mathbf{n}_m,$$

where $s_{\mathsf{u},k}$ is the signal transmitted by kth UL UE with power $\mathcal{E}_{\mathsf{u},k}$, $\mathbf{v}_{mk} \in \mathbb{C}^N$ is the combiner vector at mth UL AP for kth UL UE, and $\mathbf{n}_m \sim \mathcal{CN}(\mathbf{0}, \mathbf{I}_N)$ is the additive noise.

Now, since the SINR of the kth UE is different at the different APs, the signals forwarded by the APs to the CPU need to be appropriately scaled so as to maximize the SINR of the combined signal at the CPU. This can be accomplished by scaling $r_{\mathsf{u},mk}$ by a weight $w_{mk} \in \mathbb{R}^+$. Then, for the kth UE, the accumulated signal at the CPU can be expressed as

$$r_{\mathsf{u},k} = \sum\nolimits_{m \in \mathcal{A}_{\mathsf{u}}} w_{mk} \Big(\sqrt{\mathcal{E}_{\mathsf{u},k}} \mathbf{v}_{mk}^H \mathbf{f}_{mk} s_{\mathsf{u},k} + \sum\nolimits_{k' \in \mathcal{U}_{\mathsf{u}} \setminus k} \mathbf{v}_{mk}^H \sqrt{\mathcal{E}_{\mathsf{u},k'}} \mathbf{f}_{mk'} s_{\mathsf{u},k'} + \sqrt{N_0} \mathbf{v}_{mk}^H \mathbf{n}_m \Big), \quad (3.5)$$

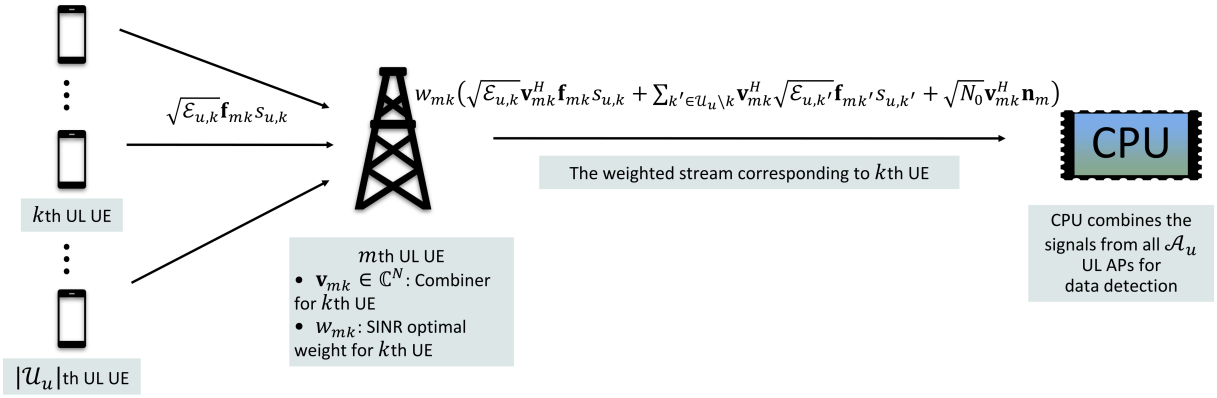

Figure 3.7: Signal flow in the UL of a CF-mMIMO system. The APs are connected to the CPU via error-free backhaul links.

---

where w_{mk} is computed as [59][3]

$$w_{mk} \triangleq \frac{\sqrt{\mathcal{E}_{\mathsf{u},k}}\mathbb{E}\left[\mathbf{v}_{mk}^H\mathbf{f}_{mk}\right]}{\mathbb{E}\left[\left|\sum\limits_{k'\in\mathcal{U}_\mathsf{u}\setminus k}\mathtt{I}_{\mathsf{u},mkk'} + \sqrt{N_0}\mathbf{v}_{mk}^H\mathbf{n}_m\right|^2\right]}, \tag{3.6}$$

with $\mathtt{I}_{\mathsf{u},mkk'} \triangleq \mathbf{v}_{mk}^H\sqrt{\mathcal{E}_{\mathsf{u},k'}}\mathbf{f}_{mk'}s_{\mathsf{u},k'}$. We illustrate the UL signal flow in Figure 3.7.

Next, considering MRC in the UL, i.e., $\mathbf{v}_{mk} = \mathbf{f}_{mk}$, we get

$$w_{mk} = \frac{\sqrt{\mathcal{E}_{\mathsf{u},k}}N\beta_{mk}}{N\sum_{k'\in\mathcal{U}_\mathsf{u}\setminus k}\mathcal{E}_{\mathsf{u},k'}\beta_{mk}\beta_{mk'} + NN_0\beta_{mk}} = \frac{\sqrt{\mathcal{E}_{\mathsf{u},k}}N\beta_{mk}}{\bar{\mathtt{I}}_{\mathsf{u},mk}},$$

with

$$\bar{\mathtt{I}}_{\mathsf{u},mk} = N\sum_{k'\in\mathcal{U}_\mathsf{u}\setminus k}\mathcal{E}_{\mathsf{u},k'}\beta_{mk}\beta_{mk'} + NN_0\beta_{mk}.$$

Then, the kth stream of the processed signal at the CPU becomes

$$\bar{r}_{\mathsf{u},k} = \sum_{m\in\mathcal{A}_\mathsf{u}} w_{mk}r_{\mathsf{u},mk} = \sum_{m\in\mathcal{A}_\mathsf{u}} w_{mk}\sqrt{\mathcal{E}_{\mathsf{u},k}}\mathbf{f}_{mk}^H\mathbf{f}_{mk}s_{\mathsf{u},k} + \sum_{m\in\mathcal{A}_\mathsf{u}} w_{mk}\left(\sum_{k'\in\mathcal{U}_\mathsf{u}\setminus k}\mathbf{f}_{mk}^H\sqrt{\mathcal{E}_{\mathsf{u},k'}}\mathbf{f}_{mk'}s_{\mathsf{u},k'} + \sqrt{N_0}\mathbf{f}_{mk}^H\mathbf{n}_m\right). \tag{3.7}$$

[3]We note that $\mathcal{R}_\mathsf{s}$ in (3.1) is the sum of each UE's achievable SE, and hence the SINR maximizing weights also maximize $\mathcal{R}_\mathsf{s}$.

We present the UL sum SE in the following Theorem.

Theorem 3.2. *The UL sum SE, denoted by* $\mathcal{R}_{\mathsf{u}}(\mathcal{A}_{\mathsf{u}})$*, can be expressed as* $\mathcal{R}_{\mathsf{u}}(\mathcal{A}_{\mathsf{u}}) = \sum_{k\in\mathcal{U}_{\mathsf{u}}} \log\left[1+\eta_{\mathsf{u},k}(\mathcal{A}_{\mathsf{u}})\right]$*, with kth UL UE's SINR being*

$$\eta_{\mathsf{u},k}(\mathcal{A}_{\mathsf{u}}) = \sum_{m\in\mathcal{A}_{\mathsf{u}}} \frac{N\mathcal{E}_{\mathsf{u},k}\beta_{mk}^2}{\sum_{k'\in\mathcal{U}_{\mathsf{u}}\setminus k}\mathcal{E}_{\mathsf{u},k'}\beta_{mk}\beta_{mk'}+N_0\beta_{mk}}. \tag{3.8}$$

Proof. The result is easily derived by applying techniques described in [19] and [3]. ■

Remark 3.1. *Typically, the APs design the combiners/precoders based on the locally available channel information and statistics [19], and relay the combined signals to the CPU for the joint data decoding. However, in our work, the APs relay a weighted version of the post-combined received signals to the CPU. The weights are chosen to maximize the SINR of the combined signal at the CPU. This weighted combination is key to establishing the modularity of the UL and DL SINRs. For example, the sum of the combined signals across the APs does not satisfy the modularity property.*

Next, we present the DL SE analysis. Assuming channel reciprocity, since the jth DL AP has knowledge of the downlink channel $\mathbf{f}_{jn}$ to the nth DL UE, the precoded signal transmitted by the jth DL AP, $j\in\mathcal{A}_{\mathsf{d}}$, can be written as

$$\mathbf{r}_{\mathsf{d},j} = \kappa_{jn}\sqrt{\mathcal{E}_{\mathsf{d},j}}\mathbf{f}_{jn}^{*}s_{\mathsf{d},n} + \sum\nolimits_{q\in\mathcal{U}_{\mathsf{d}}\setminus n}\kappa_{jq}\sqrt{\mathcal{E}_{\mathsf{d},j}}\mathbf{f}_{jq}^{*}s_{\mathsf{d},q}, \tag{3.9}$$

where $\mathcal{E}_{\mathsf{d},j}$ is the total DL power budget of the jth AP, κ_{jn} is the power control coefficient for the nth DL UE, and $s_{\mathsf{d},n}$ is the DL transmitted symbol intended for nth DL UE with $\mathbb{E}[|s_{\mathsf{d},n}|^2]=1$, and $\mathbb{E}[s_{\mathsf{d},n}s_{\mathsf{d},q}^{*}]=0, \forall q\neq n$. Then, the signal received at the nth DL UE prior to adding noise is given by

$$\tilde{r}_{\mathsf{d},jn} = \kappa_{jn}\sqrt{\mathcal{E}_{\mathsf{d},j}}\mathbf{f}_{jn}^{T}\mathbf{f}_{jn}^{*}s_{\mathsf{d},n} + \sum\nolimits_{q\in\mathcal{U}_{\mathsf{d}}\setminus n}\kappa_{jq}\sqrt{\mathcal{E}_{\mathsf{d},j}}\mathbf{f}_{jn}^{T}\mathbf{f}_{jq}^{*}s_{\mathsf{d},q}.$$

Similar to the UL case, let w_{jn} be a weighting coefficient designed by jth DL AP for the nth DL UE. Let $\mathtt{I}_{\mathsf{d},jnq} \triangleq \kappa_{jq}\sqrt{\mathcal{E}_{\mathsf{d},j}}\mathbf{f}_{jn}^{T}\mathbf{f}_{jq}^{*}s_{\mathsf{d},q}$. The SINR maximizing $w_{jn} = \dfrac{\kappa_{jn}\sqrt{\mathcal{E}_{\mathsf{d},j}}\mathbb{E}[\mathbf{f}_{jn}^{T}\mathbf{f}_{jn}^{*}]}{\mathbb{E}[|\sum_{q\in\mathcal{U}_{\mathsf{d}}\setminus n}\mathtt{I}_{\mathsf{d},jnq}|^2]}$

[59], which reduces to

$$w_{jn} = \frac{\kappa_{jn}\sqrt{\mathcal{E}_{\mathsf{d},j}}\beta_{jn}}{\left(\sum_{q\in\mathcal{U}_{\mathsf{d}}\setminus n}\kappa_{jq}^2\mathcal{E}_{\mathsf{d},j}\beta_{jn}\beta_{jq}\right)}. \tag{3.10}$$

Including the weighting, the signal received at the nth UE is

$$r_{\mathsf{d},n} = \sum_{j\in\mathcal{A}_{\mathsf{d}}} w_{jn}\kappa_{jn}\sqrt{\mathcal{E}_{\mathsf{d},j}}\mathbf{f}_{jn}^T\mathbf{f}_{jn}^* s_{\mathsf{d},n} + \sum_{k\in\mathcal{U}_{\mathsf{u}}}\mathcal{E}_{\mathsf{u},k}\mathbb{E}\left|\mathsf{g}_{nk}\right|^2 + \sum_{j\in\mathcal{A}_{\mathsf{d}}} w_{jn}\mathbf{f}_{jn}^T\sum_{q\in\mathcal{U}_{\mathsf{d}}\setminus n}\kappa_{jq}\sqrt{\mathcal{E}_{\mathsf{d},j}}\mathbf{f}_{jq}^* s_{\mathsf{d},q} + \sqrt{N_0}n_n, \tag{3.11}$$

with $n_n \sim \mathcal{CN}(0,1)$ is the receiver noise at nth DL UE. We have the following theorem regarding the DL sum SE.

Theorem 3.3. *The DL sum SE, denoted by $\mathcal{R}_{\mathsf{d}}(\mathcal{A}_{\mathsf{d}})$, can be expressed as $\mathcal{R}_{\mathsf{d}}(\mathcal{A}_{\mathsf{d}}) = \sum_{n\in\mathcal{U}_{\mathsf{d}}}\log\left[1+\eta_{\mathsf{d},n}(\mathcal{A}_{\mathsf{d}})\right]$, with the DL SINR of the nth DL UE being*

$$\begin{aligned}\eta_{\mathsf{d},n}(\mathcal{A}_{\mathsf{d}}) &= N^2\left(\sum_{j\in\mathcal{A}_{\mathsf{d}}}\frac{\mathcal{E}_{\mathsf{d},j}\kappa_{jn}^2\beta_{jn}^2}{\sum_{q\in\mathcal{U}_{\mathsf{d}}\setminus n}\mathcal{E}_{\mathsf{d},q}\kappa_{jq}\beta_{jn}\beta_{jq}}\right)^2 \\ &\quad\times\left(\sum_{j\in\mathcal{A}_{\mathsf{d}}}\frac{N\mathcal{E}_{\mathsf{d},j}\kappa_{jn}^2\beta_{jn}^2}{\sum_{q\in\mathcal{U}_{\mathsf{d}}\setminus n}\mathcal{E}_{\mathsf{d},j}\kappa_{jq}\beta_{jn}\beta_{jq}} + \sum_{k\in\mathcal{U}_{\mathsf{u}}}\mathcal{E}_{\mathsf{u},k}\epsilon_{nk} + N_0\right)^{-1} \\ &\approx \sum_{j\in\mathcal{A}_{\mathsf{d}}}\frac{N\mathcal{E}_{\mathsf{d},j}\kappa_{jn}^2\beta_{jn}^2}{\sum_{q\in\mathcal{U}_{\mathsf{d}}\setminus n}\mathcal{E}_{\mathsf{d},j}\kappa_{jq}\beta_{jn}\beta_{jq}}.\end{aligned} \tag{3.12}$$

Proof. We omit the proof as it is straightforward. ■

Remark 3.2. *We observe from (3.11) that the InUI power and the DL noise component do not scale with N, while the desired signal strength and multi-DL UE interference power scale with N^2 and N, respectively. Therefore, we approximate the DL SINR, considering only the effect of multi-DL UE interference. However, we later numerically validate the robustness of our AP-mode selection algorithm considering both inter-UE CLI and noise and provide experimental justification for the approximation presented in (3.12).*

We can now write the sum UL-DL SE as

$$\mathcal{R}_{\mathsf{s}}(\mathcal{A}_s) = \mathcal{R}_{\mathsf{u}}(\mathcal{A}_{\mathsf{u}}) + \mathcal{R}_{\mathsf{d}}(\mathcal{A}_{\mathsf{d}}), \tag{3.13}$$

where $\mathcal{A}_s \triangleq (\mathcal{A}_{\mathsf{u}}, \mathcal{A}_{\mathsf{d}})$ is a generic set which constitutes of both the UL and DL AP-indices. Note that, as the APs are HD, $\mathcal{A}_{\mathsf{d}}$ and $\mathcal{A}_{\mathsf{d}}$ are mutually exclusive sets of AP indices.

3.3.a Statistical CSI

In deriving the UL SINR in the Theorem 3.2, we used the fact that $\mathbf{f}_{mk}^H \mathbf{f}_{mk} \approx N\beta_{mk}$. In fact, $\mathbb{E}\left[\mathbf{f}_{mk}^H \mathbf{f}_{mk}\right] = N\beta_{mk}$, and thus, the error due to this approximation, i.e., $\mathtt{var}\left(\mathbf{f}_{mk}^H \mathbf{f}_{mk} - \mathbb{E}\left[\mathbf{f}_{mk}^H \mathbf{f}_{mk}\right]\right)$, known as beamforming uncertainty [19], can also be incorporated in the analysis. The UL received signal becomes

$$\begin{aligned} r_{\mathsf{u},mk} = &\sqrt{\mathcal{E}_{\mathsf{u},k}} \left(\mathbb{E}\left[\mathbf{f}_{mk}^H \mathbf{f}_{mk}\right] + \left(\mathbf{f}_{mk}^H \mathbf{f}_{mk} - \mathbb{E}\left[\mathbf{f}_{mk}^H \mathbf{f}_{mk}\right]\right)\right) s_{\mathsf{u},k} \\ &+ \sum\nolimits_{k' \in \mathcal{U}_{\mathsf{u}} \setminus k} \mathbf{f}_{mk}^H \sqrt{\mathcal{E}_{\mathsf{u},k'}} \mathbf{f}_{mk'} s_{\mathsf{u},k'} + \sqrt{N_0} \mathbf{f}_{mk}^H \mathbf{n}_m. \end{aligned} \tag{3.14}$$

It is easy to show that the SINR-optimal combining coefficient w_{mk} is $N\sqrt{\mathcal{E}_{\mathsf{u},k}}\beta_{mk}/\bar{\mathtt{I}}_{\mathsf{u},mk}$, with $\bar{\mathtt{I}}_{\mathsf{u},mk} = N\sum_{k' \in \mathcal{U}_{\mathsf{u}}} \mathcal{E}_{\mathsf{u},k'}\beta_{mk}\beta_{mk'} + NN_0\beta_{mk}$, which now includes the error due to kth UE's beamforming uncertainty. A similar analysis also follows in the case of the DL SINR. We present the modified UL and DL SINRs in the following corollary.

Corollary 3.1. *The UL and DL SINR of the kth UL UE and the nth DL UE can be expressed as*

$$\eta_{\mathsf{u},k}(\mathcal{A}_{\mathsf{u}}) = \sum\nolimits_{m \in \mathcal{A}_{\mathsf{u}}} \frac{N\mathcal{E}_{\mathsf{u},k}\beta_{mk}^2}{\sum_{k' \in \mathcal{U}_{\mathsf{u}}} \mathcal{E}_{\mathsf{u},k'}\beta_{mk}\beta_{mk'} + N_0\beta_{mk}}, \tag{3.15a}$$

$$\eta_{\mathsf{d},n}(\mathcal{A}_{\mathsf{d}}) \approx \sum\nolimits_{j \in \mathcal{A}_{\mathsf{d}}} \frac{N\mathcal{E}_{\mathsf{d},n}\kappa_{jn}^2\beta_{jn}^2}{\sum_{q \in \mathcal{U}_{\mathsf{d}}} \mathcal{E}_{\mathsf{d},q}\kappa_{jq}\beta_{jn}\beta_{jq}}, \tag{3.15b}$$

respectively, with the sum UL-DL SE being evaluated as (3.13).

3.3.b Trained CSI (TCSI)

Until now, we have considered the availability of accurate CSI at the APs. Although this is a good simplifying assumption to analyze the system behavior, it is impractical in practice. Therefore, we next consider the system performance under trained CSI.

We consider that out of the total τ channel uses per coherence interval, the first $\tau_p \geq K$ are reserved for UL channel estimation. During these τ_p channel uses, all the UEs synchronously transmit τ_p-length orthonormal pilots to the APs, which are then used by the APs to obtain local estimates of the UE-AP channels. Let $\mathcal{E}_{p,k}$ be the pilot power of kth UE's transmitted pilot sequence. It is easy to show that the MMSE estimate of $\mathbf{f}_{mk}$, denoted by $\hat{\mathbf{f}}_{mk}$, is distributed as $\mathcal{CN}(\mathbf{0}, \alpha_{mk}^2 \mathbf{I}_N)$, with $\alpha_{mk}^2 = \dfrac{\tau_p \mathcal{E}_{p,k} \beta_{mk}^2}{\tau_p \mathcal{E}_{p,k} \beta_{mk} + N_0}$. Let the estimation error, orthogonal to $\hat{\mathbf{f}}_{mk}$, be denoted by $\tilde{\mathbf{f}}_{mk}$, such that $\tilde{\mathbf{f}}_{mk} \sim \mathcal{CN}(\mathbf{0}, \bar{\alpha}_{mk}^2 \mathbf{I}_N)$, with $\bar{\alpha}_{mk} = \sqrt{\beta_{mk} - \alpha_{mk}^2}$.

In this case, the signal received at the mth UL AP becomes

$$\begin{aligned} r_{\mathsf{u},mk} &= \sum\nolimits_{k' \in \mathcal{U}_\mathsf{u}} \hat{\mathbf{f}}_{mk}^H \left(\sqrt{\mathcal{E}_{\mathsf{u},k'}} \mathbf{f}_{mk'} s_{\mathsf{u},k'} + \sqrt{N_0} \mathbf{n}_{mk} \right) \\ &= \sqrt{\mathcal{E}_{\mathsf{u},k}} \hat{\mathbf{f}}_{mk}^H \hat{\mathbf{f}}_{mk} s_{\mathsf{u},k} + \sqrt{\mathcal{E}_{\mathsf{u},k}} \hat{\mathbf{f}}_{mk}^H \tilde{\mathbf{f}}_{mk} s_{\mathsf{u},k} \\ &+ \sum_{k' \in \mathcal{U}_\mathsf{u} \setminus k} \sqrt{\mathcal{E}_{\mathsf{u},k'}} \hat{\mathbf{f}}_{mk}^H \mathbf{f}_{mk'} s_{\mathsf{u},k'} + \sqrt{N_0} \hat{\mathbf{f}}_{mk}^H \mathbf{n}_m, \end{aligned}$$

Now, as derived in (3.6), under trained CSI, $w_{mk} = N \sqrt{\mathcal{E}_{\mathsf{u},k}} \alpha_{mk}^2 / \bar{\mathtt{I}}_{\mathsf{u},mk}$, with $\bar{\mathtt{I}}_{\mathsf{u},mk} = N \mathcal{E}_{\mathsf{u},mk} \alpha_{mk}^2 \bar{\alpha}_{mk}^2 + N \sum_{k' \in \mathcal{U}_\mathsf{u} \setminus k} \mathcal{E}_{\mathsf{u},k'} \alpha_{mk}^2 \beta_{mk'} + N N_0 \alpha_{mk}^2$. Thus, the kth stream of the accumulated signal received at the CPU becomes $\bar{r}_{\mathsf{u},k} = \sum_{m \in \mathcal{A}_\mathsf{u}} w_{mk} r_{\mathsf{u},mk}$, which can be expanded as

$$\begin{aligned} \bar{r}_{\mathsf{u},k} &= \sum_{m \in \mathcal{A}_\mathsf{u}} \sqrt{\mathcal{E}_{\mathsf{u},k}} w_{mk} \hat{\mathbf{f}}_{mk}^H (\hat{\mathbf{f}}_{mk} + \tilde{\mathbf{f}}_{mk}) s_{\mathsf{u},k} \\ &+ \sum\nolimits_{m \in \mathcal{A}_\mathsf{u}} w_{mk} \hat{\mathbf{f}}_{mk}^H \left(\sum_{k' \in \mathcal{U}_\mathsf{u} \setminus k} \sqrt{\mathcal{E}_{\mathsf{u},k'}} \mathbf{f}_{mk'} s_{\mathsf{u},k'} + \sqrt{N_0} \mathbf{n}_m \right). \end{aligned}$$

The UL SINR under trained CSI can be derived following similar arguments as discussed

in Theorem 3.2, as follows.

Lemma 3.1. *Under trained CSI, the UL sum SE can be expressed as*

$$\mathcal{R}_{\mathsf{u}}(\mathcal{A}_{\mathsf{u}}) = \frac{\tau - \tau_p}{\tau} \sum_{k \in \mathcal{U}_{\mathsf{u}}} \log[1 + \eta_{\mathsf{u},k}(\mathcal{A}_{\mathsf{u}})],$$

with the UL SINR of the kth UL UE, denoted as $\eta_{\mathsf{u},k}(\mathcal{A}_{\mathsf{u}})$*, being*

$$\eta_{\mathsf{u},k}(\mathcal{A}_{\mathsf{u}}) = \sum_{m \in \mathcal{A}_{\mathsf{u}}} \frac{N \mathcal{E}_{\mathsf{u},k} \alpha_{mk}^4}{\mathcal{E}_{\mathsf{u},k} \alpha_{mk}^2 \bar{\alpha}_{mk}^2 + \sum\limits_{k' \in \mathcal{U}_{\mathsf{u}} \setminus k} \mathcal{E}_{\mathsf{u},k'} \alpha_{mk}^2 \beta_{mk'} + N_0 \alpha_{mk}^2}. \tag{3.16}$$

Similarly, considering matched filter precoding, the DL received signal at the nth UE can be written as

$$\begin{aligned} r_{\mathsf{d},n} =& \sum\nolimits_{j \in \mathcal{A}_{\mathsf{d}}} w_{jn} \kappa_{jn} \sqrt{\mathcal{E}_{\mathsf{d},j}} (\hat{\mathbf{f}}_{jn} + \tilde{\mathbf{f}}_{jn})^T \hat{\mathbf{f}}_{jn}^* s_{\mathsf{d},n} + \sum\nolimits_{j \in \mathcal{A}_{\mathsf{d}}} w_{jn} \mathbf{f}_{jn}^T \sum\nolimits_{q \in \mathcal{U}_{\mathsf{d}} \setminus n} \kappa_{jq} \sqrt{\mathcal{E}_{\mathsf{d},j}} \hat{\mathbf{f}}_{jq}^* s_{\mathsf{d},q} \\ &+ \sum\nolimits_{k \in \mathcal{U}_{\mathsf{u}}} \mathcal{E}_{\mathsf{u},k} \mathbb{E}\left|\mathsf{g}_{nk}\right|^2 + \sqrt{N_0} n_n, \end{aligned} \tag{3.17}$$

where $w_{jn} = \kappa_{jn} \sqrt{\mathcal{E}_{\mathsf{d},j}} \alpha_{jn}^2 / (\sum_{q \in \mathcal{U}_{\mathsf{d}} \setminus n} \kappa_{jq}^2 \mathcal{E}_{\mathsf{d},q} \alpha_{jn}^2 \beta_{jq} + \kappa_{jn}^2 \mathcal{E}_{\mathsf{d},j} \bar{\alpha}_{jn}^2)$, evaluated similarly as (3.10).

Lemma 3.2. *Under trained CSI, the DL sum SE can be expressed as*

$$\mathcal{R}_{\mathsf{d}}(\mathcal{A}_{\mathsf{d}}) = \frac{\tau - \tau_p}{\tau} \sum\nolimits_{n \in \mathcal{U}_{\mathsf{d}}} \log\left[1 + \eta_{\mathsf{d},n}(\mathcal{A}_{\mathsf{d}})\right],$$

with the DL SINR of the nth DL UE being $\eta_{\mathsf{d},n}(\mathcal{A}_{\mathsf{d}}) \approx \sum\limits_{j \in \mathcal{A}_{\mathsf{d}}} \dfrac{N \mathcal{E}_{\mathsf{d},j} \kappa_{jn}^2 \alpha_{jn}^4}{\sum\limits_{q \in \mathcal{U}_{\mathsf{d}} \setminus n} \kappa_{jq}^2 \mathcal{E}_{\mathsf{d},j} \alpha_{jn}^2 \beta_{jq} + \kappa_{jn}^2 \mathcal{E}_{\mathsf{d},j} \bar{\alpha}_{jn}^2}$.

We next discuss the greedy AP scheduling technique leveraging the sub-modularity of the sum UL-DL SE.

3.4 Greedy AP Mode (UL/DL) Selection

In this section, we establish the modularity of the UL and DL SINRs and the sub-modularity [60] of the sum UL-DL SE.

Theorem 3.4. *The UL SINR of the kth UE, $\forall k \in \mathcal{U}_{\mathsf{u}}$, is a monotonically non-decreasing modular function of the activated AP set, i.e., given $\mathcal{A}_s$ and $\mathcal{A}_t$, where, $\mathcal{A}_s \subseteq \mathcal{A}_t \subseteq \mathcal{A}$, and for any $\{j\} \notin \mathcal{A}_t$, we have $\eta_{\mathsf{u},k}(\mathcal{A}_s) \leq \eta_{\mathsf{u},k}(\mathcal{A}_t)$, and*

$$\eta_{\mathsf{u},k}(\mathcal{A}_s \cup \{j\}) - \eta_{\mathsf{u},k}(\mathcal{A}_s) = \eta_{\mathsf{u},k}(\mathcal{A}_t \cup \{j\}) - \eta_{\mathsf{u},k}(\mathcal{A}_t),$$

where $\eta_{\mathsf{u},k}$ is evaluated as (3.8), (3.15a), and (3.16) for perfect CSI, statistical CSI, and trained CSI, respectively.

Proof. See Appendix B.1. ■

Similarly, we can show that DL SINR is a monotonic, non-decreasing modular function of the activated AP set.

Theorem 3.5. *The sum UL-DL SE, under perfect and trained CSI, is a monotonically non-decreasing sub-modular function of the activated AP set, i.e., given $\mathcal{A}_s$ and $\mathcal{A}_t$, with, $\mathcal{A}_s \subseteq \mathcal{A}_t \subseteq \mathcal{A}$, and for any $\{j\} \notin \mathcal{A}_t$, $\mathcal{R}_s(\mathcal{A}_s) \leq \mathcal{R}_s(\mathcal{A}_t)$, and*

$$\mathcal{R}_s(\mathcal{A}_s \cup \{j\}) - \mathcal{R}_s(\mathcal{A}_s) \geq \mathcal{R}_s(\mathcal{A}_t \cup \{j\}) - \mathcal{R}_s(\mathcal{A}_t), \tag{3.18}$$

where $\mathcal{R}_s(.)$ is evaluated using (3.13) with the UL and DL SEs obtained via Theorem 3.2 and Theorem 3.3 under perfect CSI; and Lemma 3.1 and Lemma 3.2 under trained CSI.

Proof. See Appendix B.2. ■

We can exploit the sub-modular nature of sum UL-DL SE to schedule the APs via the greedy algorithm presented Algorithm 5. Recall that, in each iteration of the algorithm; we activate an AP and its corresponding mode of operation such that the incremental gain in $\mathcal{R}_{\mathrm{s}}$ as evaluated by (3.13) is maximized, and repeat the procedure until the last AP is activated. Due to the sub-modular nature of $\mathcal{R}_{\mathrm{s}}$, the sum UL-DL SE achieved by the solution obtained via the greedy algorithm is guaranteed to be within a $(1 - \frac{1}{e})$-fraction of its global optimal value [60] obtained via exhaustive search. We note that the complexity

of the exhaustive search is $O(2^M)$. However, the complexity of greedy is $\mathcal{O}(M)$. Hence, whenever there is a change in the data demand, we only need to perform M iterations of the algorithm, which substantially reduces the complexity.

3.5 Benefits of SINR Optimal Weighting: Numerical Validations

The simulation setup is the same as described in Section 3.2.c. We consider 50% of the UEs demand UL data per time slot.[4] The acronyms used in the plots are as follows:

(i) **PCSI (TCSI)**: perfect (trained) CSI.

(ii) **PCSI+Intf. (TCSI+Intf.)**: perfect (trained) CSI, including InAI as well as InUI in the sum UL-DL SE evaluation.

Figure 3.8 illustrates the near-optimality of greedy AP scheduling by comparing it with exhaustive search-based AP scheduling. The sum UL-DL SE attained via exhaustive search matches with the greedy algorithm under both perfect and trained CSI. This holds true even in the presence of inter-UE and inter-AP CLIs.[5] Also, the difference in the sum SEs with and without the CLIs is marginal, which justifies the approximations in Theorem 3.3.

Next, in Figure 3.9, we plot the average 90%-sum UL-DL SE versus the data SNR. Although the APs are HD in both TDD and DTDD CF-mMIMO schemes, DTDD allows simultaneous UL/DL transmission, which greatly enhances the sum UL-DL SE compared to the TDD case.

In Figure 3.10, we compare weighted combining/precoding with the approach in Section 3.2, where the APs are activated based on the sub-modularity of the product SINRs

[4]Since the UE locations are random, the UL/DL traffic load at each AP is different, and for each instantiation, the APs are activated using Algorithm 5.

[5]For the plots corresponding to (PCSI+Intf.) and (TCSI+Intf.), we include inter-AP CLI in UL SINR to illustrate the robustness of the greedy algorithm. Specifically, we have considered imperfect InAI cancelation and modeled residual DL AP to UL AP interference as in [61].

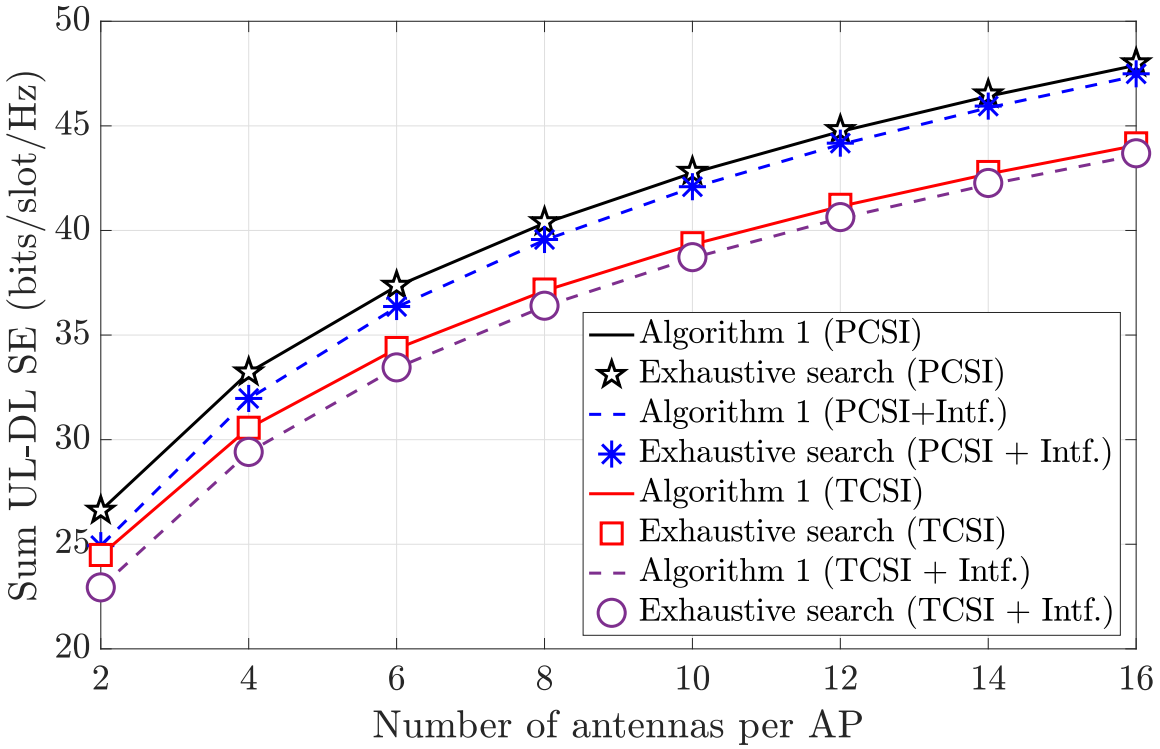

Figure 3.8: Validation of the greedy algorithm with $(M = 8, K = 16, N = 8)$.

and the CPU only obtains the sum of the combined signals from the APs. To ensure that weighting does not alter the radiated power at each AP, we consider a scaled version of w_{jn}, denoted by $\dot{w}_{jn} = \sqrt{\mu_j} w_{jn}$, which ensures equal radiated power for both weighted and unweighted scheme. It is easy to show that $\mu_j = \dfrac{\sum_{q \in \mathcal{U}_\mathrm{d}} \beta_{jq}}{\sum_{n \in \mathcal{U}_\mathrm{d}} w_{jn}^2 \beta_{jn}}$ normalizes the weights correctly. The 90%-likely SE achieved via the weighted scheme with $(M = 64)$ is more than double that can be attained via the unweighted scheme, which underlines the utility of weighted combining over the conventional unweighted scheme.

3.6 Chapter Summary

In this paper, we analyzed the performance of DTDD in a CF-mMIMO system. We formulated a sum UL-DL SE maximization problem for scheduling the UL/DL mode of the APs based on the local UL/DL traffic demands of the UEs. We proved that the sum UL-DL SE is a sub-modular function of the underlying AP set and then employed

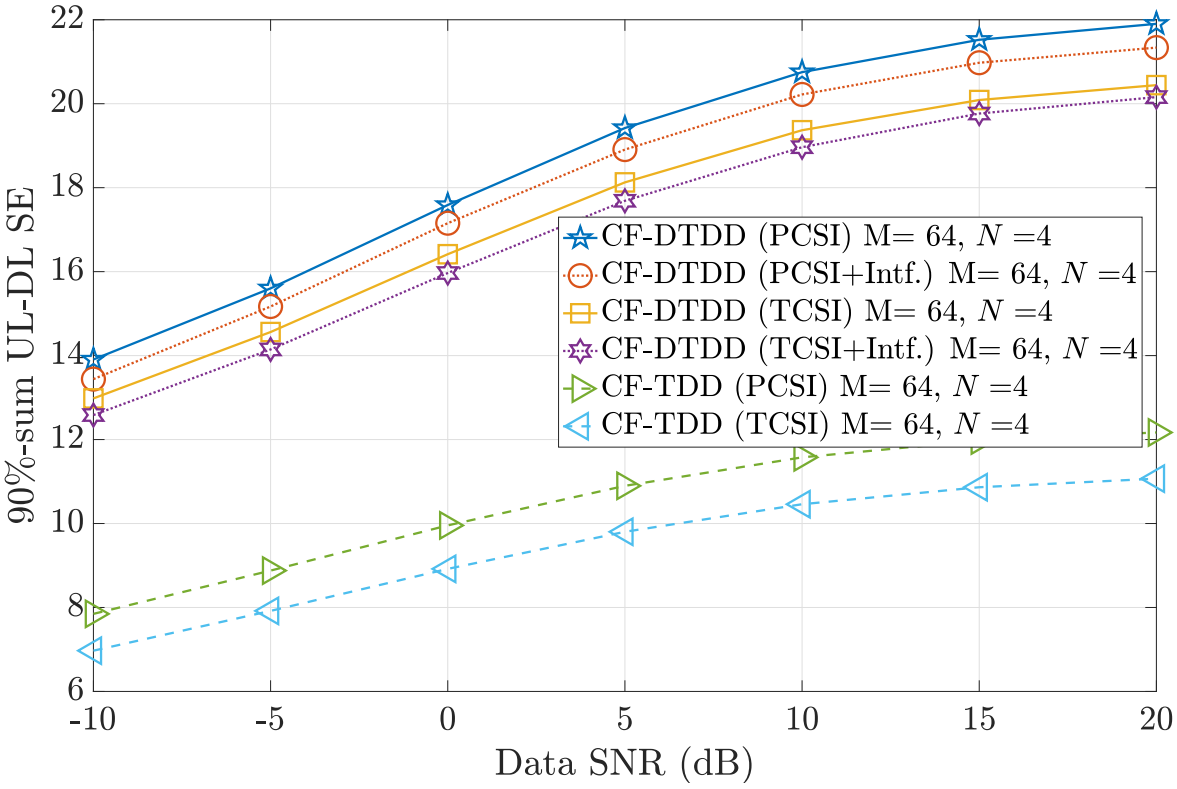

Figure 3.9: 90%-sum UL-DL SE with $(M = 64, N = 4, K = 40)$.

a greedy algorithm to activate the APs in polynomial time. Our numerical experiments revealed that DTDD-enabled CF-mMIMO substantially improves the sum SE compared to conventional TDD-based CF systems.

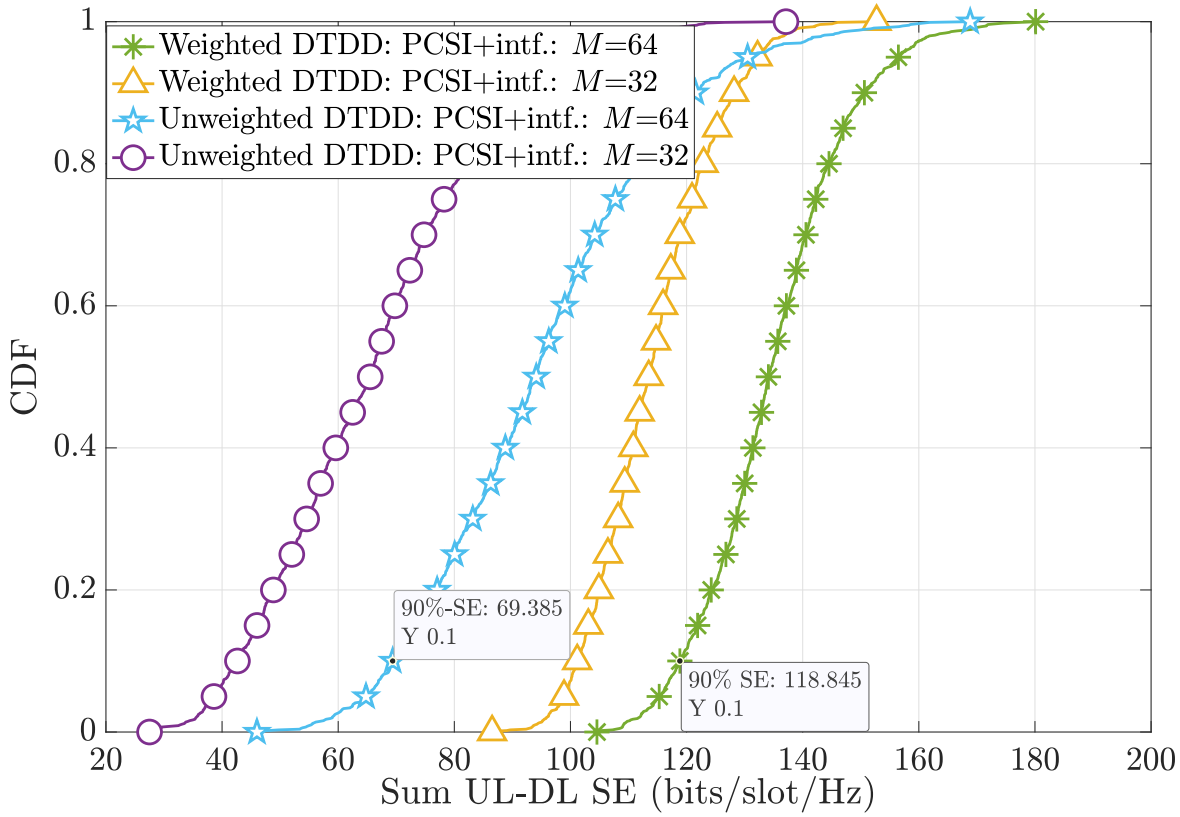

Figure 3.10: Comparison of the weighted combiner/precoder with [19], with $K = \tau_p = 40$.

4 Can DTDD Cell-Free Outperform Full-Duplex Cellular?

Chapter Highlights

This chapter overcomes two shortcomings of the previous chapter, i.e., orthogonal pilots and perfect InAI cancelation. We first derive the sum of UL-DL SEs for the DTDD CF system considering MRC in the UL and MFP in the DL, incorporating the effects of pilot contamination and imperfect CLI cancelation. Then, we develop a new, low-complexity, greedy algorithm for the combinatorial AP scheduling problem, with an optimality guarantee theoretically established by showing that a lower bound of the sum UL-DL SE is sub-modular. We compare the performance of our solutions, both theoretically and via simulations, against an FD multi-cell mMIMO system. Our results show that, due to the joint processing of the signals at the CPU, CF-mMIMO with dynamic HD AP-scheduling significantly outperforms cellular FD-mMIMO in terms of the sum SE and 90% likely SE. We see that an FD-system with 4 BSs having 128 transmit and receive antennas each offers a 90% sum UL-DL SE of 13.2 bits/slot/Hz, whereas the CF-DTDD based system with $(M = 64, N = 8)$ offers 27 bits/slot/Hz, a more than 100% improvement. Further, we observe that the UL-DL rate region procured by enabling DTDD in a CF-mMIMO system overwhelms the UL-DL rate region procured by a multi-cell FD mMIMO system. Our experiments lead us to conclude that *DTDD-enabled HD CF-mMIMO, which enjoys the benefits of both worlds (i.e., DTDD and CF), is a promising alternative to cellular FD-mMIMO without incurring the hardware cost for SI suppression.*

4.1 Introduction

In a CF-mMIMO system, APs coherently and simultaneously serve a number of UEs distributed over a large geographical area [15, 16, 19, 47]. Recently, CF-mMIMO has emerged as a promising candidate technology for the physical layer of next-generation wireless communication systems [62]. It has been shown that under appropriate conditions [15], CF-mMIMO inherits many of the advantages offered by cellular massive MIMO, such as channel hardening and favorable propagation. However, in their current form, CF-mMIMO systems are designed to work in the TDD mode, hence serving either only UL or only DL traffic at any given point in time. While enabling FD capabilities at the APs can simultaneously cater to the UL and DL data demands, the performance of such systems is limited by the residual SI power at each AP [63].

4.1.a Motivation

In the context of cellular mMIMO, DTDD has recently been explored to cater to heterogeneous UL-DL data demands from the UEs. This technique entails adaptive and independent splitting of the transmission frame into UL and DL slots by the different BSs according to the UL-DL traffic demands from the UEs in each cell [64]. While this improves the overall spectral and time resource utilization across cells, it does not fully cater to heterogeneous data demands within the cells. That is, a UE with UL data demand will still have to wait for a slot where its serving BS is operating in the UL mode in order to complete its transmission, and similarly for a UE with DL data demand. On the other hand, in a CF-mMIMO system, since the UEs are not associated with a particular AP, if the APs can dynamically select the slots where they operate in UL and DL modes, any UE with a specific data demand can find some nearby APs operating in the corresponding mode in the same slot. Further, the joint processing of the signals at the CPU can mitigate the CLIs that arise in a CF DTDD system. Due to this, a CF-mMIMO system with

DTDD can potentially match or even exceed the performance of an FD-capable cellular system while using HD hardware at the APs. Therefore, the use of DTDD in conjunction with CF-mMIMO is the focus of this work.

4.1.b Related Work

DTDD is a well accepted technique; it has been included in cellular communication standards such as 3GPP LTE Release 12 [55] and 5G NR [56,65] to accommodate heterogeneous traffic loads. Traffic-dependent UL-DL slot adaptation schemes have been shown to reduce the overall system latency [66] and improve the SE [67,68] compared to TDD-based conventional cellular and CF mMIMO systems. However, the performance of DTDD is limited by two types of CLI, namely, the interference from the DL BSs to the UL BSs and from the UL UEs to the DL UEs. The CLI can be mitigated via intra-cell cooperation, power control and beamforming design, UE scheduling, etc. An excellent survey on the methods for CLI mitigation in cellular mMIMO can be found in [58].

On the other hand, FD technology can also serve UL and DL UEs simultaneously and has the potential to double the system capacity. Note that, in a cellular FD mMIMO system, similar CLIs exist as in DTDD based systems. However, in addition, each BS suffers from its own residual SI. In fact, the transmit RF-chain noise, oscillator phase noise, and related device imperfections get amplified while propagating through the SI channel and limit the FD system performance [63]. Also, the benefits of an FD cellular system considerably degrade under asymmetric traffic load [69]. In contrast, DTDD obviates the need for expensive and potentially power-hungry hardware as well as digital signal processing costs associated with SI mitigation. Numerical experiments have shown that the throughput of the cellular FD-system degrades relative to cellular DTDD as the UL-DL traffic asymmetry increases [70].

The current deployments of cellular DTDD require inter-cell cooperation, i.e., the neighboring cells need to exchange information (such as the estimated channel statistics or the

per-cell traffic load) for optimal UL-DL slot scheduling or interference mitigation. Although such techniques are attractive in theory, the sub-problems of BS/UE scheduling, power control, cell clustering [71], and joint beamformer design [72] are prohibitively complex for practical implementation. Moreover, the performance loss of the cell-edge UEs due to out-of-cell interference and CLI is a serious issue in cellular systems.

In contrast to cellular mMIMO, in a CF system, all the UEs in a given geographical area are served by all the available APs by jointly processing the signals to/from the UEs at a CPU. At the cost of a larger front-haul bandwidth, the CPU can utilize the knowledge of locally estimated channels from each AP to suppress the CLIs without inter-AP cooperation or extra signaling overhead [61]. Due to this, the QoS delivered is nearly uniform across all the UEs [16]. The advantages offered by DTDD along with the inherent benefits of the CF-architecture can be exploited to further enhance the system throughput under asymmetric traffic load. We not only dispense with the SI cancellation hardware at each AP; the computational burden and signaling overhead involved in CLI mitigation of a cellular mMIMO system is also considerably reduced at the CPU.

In the context of DTDD-enabled CF-mMIMO systems, the authors in [61] presented a UE scheduling algorithm to alleviate the CLI from UL UEs to DL UEs. Recently, in [73], the authors proposed a so-called beamforming training-based scheme, where the estimates of the effective DL channels are exploited to reduce inter-AP CLI. All the previous works assume a fixed UL and DL configuration across the APs, and focus primarily on CLI mitigation methods. However, unless the transmission and reception mode of each AP is dynamically adapted based on the traffic demands of the UEs, the benefits of DTDD cannot be fully exploited. Therefore, to enable DTDD, we need to split the time resources optimally at each of the APs. However, scheduling the APs via an exhaustive search over all possible AP configurations is prohibitively complex. Motivated by this, we formulate the problem of optimally scheduling APs in the UL or DL modes to maximize the sum UL-DL SE in a DTDD-enabled CF-mMIMO system and propose a scalable solution by

exploiting a sub-modularity property of the sum UL-DL SE.

4.1.c Contributions

In this chapter, we investigate how to facilitate DTDD in a CF-mMIMO system with HD-APs. DTDD allows us to partition the time slots at each AP into UL and DL slots according to the UL and the DL traffic demands at the UEs. The scheduling of APs based on the data demands and analyzing the resulting network throughput performance is the main goal of this work. For example, if the UL traffic demand of the UEs in the vicinity of one or a group of APs is high, those APs should be scheduled to receive UL data in most of the slots. We note that the achievable sum UL-DL SE depends on which APs are scheduled to operate in UL and which in DL. This motivates the need to develop a data demand-based AP-scheduling algorithm in order to improve/maximize the achievable sum UL-DL SE.

Our main contributions are as follows:

1. We derive the closed-form expressions of the achievable uplink and DL SEs, accounting for the effects of pilot contamination, imperfect inter-AP interference cancellation, and inter-UE interferences. Our derived results also capture the interdependence of the achievable SEs and the traffic load of the system.

2. We formulate the AP-scheduling problem as one of maximizing the sum UL-DL SE given the traffic demands from the UEs and considering MFP in the DL and MRC in the UL based on the locally estimated channels. This problem turns out to be NP-hard, and hence, the computational complexity of a brute-force search-based solution grows exponentially with the number of APs. We first argue that the achievable sum UL-DL SE is a monotonic nondecreasing function of the set of scheduled APs. Then, we observe that the dependence of the sum UL-DL SE on the scheduled AP-set is non-linear in nature and, therefore, proving sub-modularity becomes mathematically intractable. To circumvent that, we derive the following results:

   (a) We lower bound the sum UL-DL SE and prove that problem of maximizing the lower bound is equivalent to the problem of maximizing product of the SINRs.

   (b) We prove that the product of the SINRs of all UEs is a sub-modular set function of the APs scheduled in the system.

3. This allows us to develop a greedy algorithm for dynamic AP scheduling, where, at each step, the transmission mode of the AP that maximizes the incremental SE is added to the already scheduled AP-subset. The lower bound on the sum UL-DL SE achieved by the solution obtained via the greedy algorithm is guaranteed to be within a $\left(1 - \frac{1}{e}\right)$-fraction or 65% of its global optimal value. We note that the computational complexity of the greedy algorithm is linear in the number of APs.

4. We also analyze the UL and DL SE considering an MMSE-based combiner in the UL and RZF precoder in the DL and demonstrate the performance improvement obtained compared to MRC and MFP.

Our experimental results show that the greedy algorithm procures a sum UL-DL SE that matches with exhaustive search-based AP scheduling and that the algorithm is robust to both inter-UE and inter-AP CLI. Furthermore, DTDD CF-mMIMO substantially enhances the system performance compared to static TDD based CF as well as cellular systems. Interestingly, the DTDD-based CF-system outperforms an FD cellular mMIMO system under both MRC & MFP as well as MMSE & RZF combiner and precoder employed at the APs/BSs. For example, a CF-DTDD system with $(M = 16, N = 64)$ even outperforms the cellular FD-system having twice the antenna density, i.e., $(L = 16, N_t = N_r = 64)$. If we increase the number of APs with half the antenna density compared to the FD (see the curve corresponding to $(M = 64, N = 16)$ in Figure 4.7), the sum UL-DL SE offered by HD CF-DTDD improves, significantly outperforming the cellular FD system.

We conclude that, due to the benefits offered by joint signal processing at the CPU, HD CF-mMIMO with dynamic AP-scheduling offers improved sum SE as well as 90%-likely

SE compared to static TDD-based CF systems and even the cellular FD mMIMO system. Therefore, DTDD-enabled CF-mMIMO with appropriately scheduled APs is a promising solution to meet the heterogeneous traffic loads in next-generation wireless systems.

4.2 System Model and Problem Statement

We consider a CF-mMIMO system with M HD-APs jointly and coherently serving K single-antenna UEs. Each AP is equipped with N antennas and is connected to the CPU via an infinite capacity front-haul link. Time is divided into slots, and in any given slot, each AP can operate either in the UL mode or in the DL mode. We assume that the UL/DL traffic demands of the UEs are known at the CPU; its task is to decide the mode of operation of each AP based on the traffic demands in its vicinity.

The channel from kth UE to the mth AP is modeled as $\mathbf{f}_{mk} = \sqrt{\beta_{mk}}\mathbf{h}_{mk} \in \mathbb{C}^N$, where $\beta_{mk} > 0$ denotes the large scale fading and path loss coefficient, and are known to the APs and the CPU. Note that β_{mk} remains unchanged over several channel coherence intervals [16,19,47]. The fast fading components, $\mathbf{h}_{mk} \sim \mathcal{CN}(\mathbf{0}, \mathbf{I}_N) \in \mathbb{C}^N$, are independent and identically distributed (i.i.d.) and are estimated at the APs (and the CPU) using pilot signals. Under a quasi-static fading model, $\mathbf{h}_{mk}$ remains constant over one coherence interval and takes independent values from the same distribution in subsequent coherence intervals [16,19,20,47]. While the foregoing analysis can be extended to the case of spatially correlated channels with some effort, the equations become cumbersome and do not offer significant additional insights.

Due to simultaneous UL and DL data transmissions, the APs transmitting in the DL cause interference to the APs receiving the UL data, which is the source of inter-AP interference. However, since the CSI of the inter-AP channels available at the CPU may be erroneous, residual inter-AP interference exists even after interference cancellation. In the literature, the residual interference is modeled as Gaussian distributed additive noise [24, 53, 61, 74, 75]; we use the same approach. We model the residual interference

Symbol	Definition
τ_p	Length of the pilot sequence.
$\{\boldsymbol{\phi}_1, \boldsymbol{\phi}_2, \ldots, \boldsymbol{\phi}_{\tau_p}\}$	Set of orthonormal pilot symbols.
$\mathcal{I}_p$	Number of UEs using pth pilot sequence. Hence, the cardinality of $\mathcal{I}_p$ indicates the repetition factor of the pth pilot sequence, such that $\sum_{p=1}^{\tau_p} \lvert\mathcal{I}_p\rvert = K$.
$\mathcal{E}_{p,k}$	The power of the pilot signal by the kth UE
$\hat{\mathbf{f}}_{mk}$	MMSE estimate of the channel between the mth AP and the kth UE.
$\tilde{\mathbf{f}}_{mk}$	MMSE estimation error of the channel $\mathbf{f}_{mk} \in \mathbb{C}^N$
α^2_{mk}	Defined as $\frac{1}{N}\mathtt{tr}\left(\mathbb{E}\left[\hat{\mathbf{f}}_{mk}\hat{\mathbf{f}}^H_{mk}\right]\right)$, and evaluated as $\alpha^2_{mk} = c_{mk}\tau_p\mathcal{E}_{p,k}\beta^2_{mk}$ (2.12).
c_{mk}	Indicates the effects of pilot contamination on channel estimates, and evaluated as $c_{mk} = \left(\tau_p\mathcal{E}_{p,k}\beta_{mk} + \tau_p \sum_{n\in\mathcal{I}_p\setminus k} \mathcal{E}_{p,n}\beta_{mn} + N_0\right)^{-1}$ (2.13).
$\bar{\alpha}_{mk}$	$\sqrt{\beta_{mk} - \alpha^2_{mk}}$

Table 4.1: Symbols related to MMSE channel estimation.

channel between jth DL AP and the mth UL AP by $\mathbf{G}_{mj} \in \mathbb{C}^{N\times N}$, with its elements being i.i.d. $\mathcal{CN}(0, \zeta_{mj})$, where ζ_{mj} depends on the inter AP path loss and channel estimation error variance. Similarly, we let g_{nk} denote the channel between nth UL UE and the kth DL UE, and we model $\mathsf{g}_{nk} \sim \mathcal{CN}(0, \epsilon_{nk})$ and independent across all UEs [53, 74].

4.2.a Problem Statement

In this work, we investigate DTDD in a CF mMIMO system with HD APs. Let $\mathcal{A}$ be the set of AP indices, with $M = |\mathcal{A}|$. Let the indices of the APs scheduled in the UL and DL modes be contained in the index sets $\mathcal{A}_{\mathsf{u}}$ and $\mathcal{A}_{\mathsf{d}}$, respectively. We aim to maximize the achievable sum UL-DL SE $R_{\text{sum}}(\mathcal{A}_{\mathsf{u}} \cup \mathcal{A}_{\mathsf{d}})$ over all possible choices of $\mathcal{A}_{\mathsf{u}}$ and $\mathcal{A}_{\mathsf{d}}$ by solving:

$$\begin{aligned} &\max_{\mathcal{A}_{\mathsf{u}},\mathcal{A}_{\mathsf{d}}} \quad R_{\text{sum}}(\mathcal{A}_{\mathsf{u}} \cup \mathcal{A}_{\mathsf{d}}) \\ &\text{s.t.} \quad \mathcal{A}_{\mathsf{u}}, \mathcal{A}_{\mathsf{d}} \subset \mathcal{A}, \quad \mathcal{A}_{\mathsf{u}} \cap \mathcal{A}_{\mathsf{d}} = \emptyset, \quad \mathcal{A}_{\mathsf{u}} \cup \mathcal{A}_{\mathsf{d}} = \mathcal{A}. \end{aligned} \tag{4.1}$$

Here, the condition $\mathcal{A}_{\mathsf{u}} \cap \mathcal{A}_{\mathsf{d}} = \emptyset$ arises because of the half-duplex constraint at the APs.

Evidently, an exhaustive search can be performed across all 2^M possible configurations, but this becomes computationally expensive as M gets large. We later develop a low complexity AP scheduling algorithm in Section 4.4. We observed that the overarching problem of investigation is similar to that described in Section 3.2.a. However, unlike Chapter 3, here we consider the effects of pilot contamination and also imperfect CLI cancelation, which considerably change the way $R_{\text{sum}}(\mathcal{A}_{\mathsf{u}} \cup \mathcal{A}_{\mathsf{d}})$ depends on the underlying optimization variables; which in turn entails more involved theoretical developments.

We next discuss the CF-mMIMO signal model within each slot, which is our point of departure in this work. For channel estimation, the readers are referred to Section 2.3.a, which we avoid repeating here. For the reader's immediate reference, we provide the notations and corresponding definitions related to the MMSE channel estimation in Table 4.1. These notations will be used in the succeeding sections.

4.2.b Signaling Model: UL and DL Data Transmissions

Let $\mathcal{U}_{\mathsf{u}}, \mathcal{U}_{\mathsf{d}}, \mathcal{A}_{\mathsf{u}}$, and $\mathcal{A}_{\mathsf{d}}$ denote the sets containing the indices of UL UEs, DL UEs, UL APs, and DL APs, respectively. Now, let the kth UL UE send the symbol $s_{u,k}$ with power $\mathcal{E}_{u,k}$. The data symbol of each UE is assumed to be zero mean, unit variance, and independent of the data symbols sent by the other UEs. Then, the UL signal received at the mth AP ($m \in \mathcal{A}_{\mathsf{u}}$) can be expressed as

$$\mathbf{y}_{u,m} = \sqrt{\mathcal{E}_{u,k}}\mathbf{f}_{mk}s_{u,k} + \sum_{n \in \mathcal{U}_{\mathsf{u}} \setminus k} \sqrt{\mathcal{E}_{u,n}}\mathbf{f}_{mn}s_{u,n} + \sum_{j \in \mathcal{A}_{\mathsf{d}}} \mathbf{G}_{mj}\mathbf{x}_{d,j} + \mathbf{w}_{u,m} \in \mathbb{C}^N, \tag{4.2}$$

where $\mathbf{w}_{u,m} \sim \mathcal{CN}(\mathbf{0}, N_0\mathbf{I}_N)$ is the additive noise, and $\mathbf{x}_{d,j} = \sqrt{\mathcal{E}_{d,j}}\mathbf{P}_j\mathsf{diag}(\boldsymbol{\kappa}_j)\mathbf{s}_{\mathsf{d}}$ is the transmitted DL data vector, with $\mathcal{E}_{d,j}$ being the total power, $\mathbf{P}_j \in \mathbb{C}^{N \times K_{\mathsf{d}}}$ being the precoding matrix, and $\boldsymbol{\kappa}_j$ being the vector of power control coefficients, all at the jth DL AP. Note that κ_{jn}, i.e., the nth element of $\boldsymbol{\kappa}_j$, indicates the fraction of power dedicated by the jth AP to the the nth DL UE ($n \in \mathcal{U}_{\mathsf{d}}$). Typically, κ_{jn} is designed such that

$\mathbb{E}\left[\|\mathbf{x}_{d,j}\|^2\right] \leq \mathcal{E}_{d,j} \Rightarrow \sum_{n\in\mathcal{U}_\mathsf{d}} \kappa_{jn}\mathbb{E}\|\mathbf{p}_{jn}\|^2 \leq 1$ [19].

Let $\mathbf{v}_{mk}$ denote the locally available combining vector at the mth AP for the kth UE's UL data stream. The kth component of the accumulated signal received at the CPU, $r_{u,k} \triangleq \sum_{m\in\mathcal{A}_\mathsf{u}} \mathbf{v}_{mk}^H \mathbf{y}_{u,m}$, can be expanded as

$$\begin{aligned} r_{u,k} = & \sum_{m\in\mathcal{A}_\mathsf{u}} \sqrt{\mathcal{E}_{u,k}}\mathbf{v}_{mk}^H \mathbf{f}_{mk} s_{u,k} + \sum_{m\in\mathcal{A}_\mathsf{u}} \sum_{n\in\mathcal{U}_\mathsf{u}\setminus k} \sqrt{\mathcal{E}_{u,n}}\mathbf{v}_{mk}^H \mathbf{f}_{mn} s_{u,n} \\ & + \sum_{j\in\mathcal{A}_\mathsf{d}} \sqrt{\mathcal{E}_{d,j}} \sum_{n\in\mathcal{U}_\mathsf{d}} \kappa_{jn} \sum_{m\in\mathcal{A}_\mathsf{u}} \mathbf{v}_{mk}^H \mathbf{G}_{mj} \mathbf{p}_{jn} s_{d,n} + \sum_{m\in\mathcal{A}_\mathsf{u}} \mathbf{v}_{mk}^H \mathbf{w}_{u,mk}, \end{aligned} \tag{4.3}$$

where $\mathbf{p}_{jn}$ is the nth column of $\mathbf{P}_j$. Similarly, assuming perfect channel reciprocity, the signal received by the nth ($n \in \mathcal{U}_\mathsf{d}$) DL UE can be expressed as

$$r_{d,n} = \sum_{j\in\mathcal{A}_\mathsf{d}} \kappa_{jn}\sqrt{\mathcal{E}_{d,j}}\mathbf{f}_{jn}^T \mathbf{p}_{jn} s_{d,n} + \sum_{k\in\mathcal{U}_\mathsf{u}} \sqrt{\mathcal{E}_{u,n}}\mathbf{g}_{nk} s_{u,k} + \sum_{j\in\mathcal{A}_\mathsf{d}} \sum_{q\in\mathcal{U}_\mathsf{d}\setminus n} \kappa_{jq}\sqrt{\mathcal{E}_{d,j}}\mathbf{f}_{jn}^T \mathbf{p}_{jq} s_{d,q} + w_{d,n}, \tag{4.4}$$

where $w_{d,n} \sim \mathcal{CN}(0, N_0)$ is the AWGN at the nth DL UE.

We illustrate the frame structure described above, and contrast it with the frame structure in a TDD-based CF system, in Figure 4.1. We can now derive the achievable UL and DL SEs for the DTDD-enabled CF-mMIMO system.

4.3 Spectral Efficiency Analysis: MRC & MFP

In this section, we derive the achievable SEs considering MFP in the DL and MRC in the UL. Here, we first consider MFP and MRC for ease of exposition, and also because it suffices to elucidate the main point of this work, namely, the benefits obtainable by enabling DTDD in a CF-mMIMO system. In several other works, for example, in [19, 21, 76], MRC and MFP have been extensively used for the tractable and interpretable analysis. For deriving the UL and DL SE, we employ the *use-and-then-forget* capacity bounding

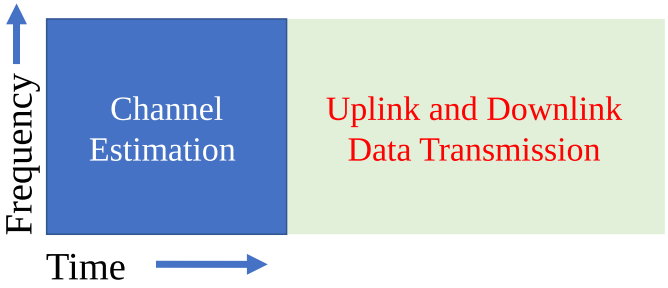

(a) Frame structure of DTDD based CF system.

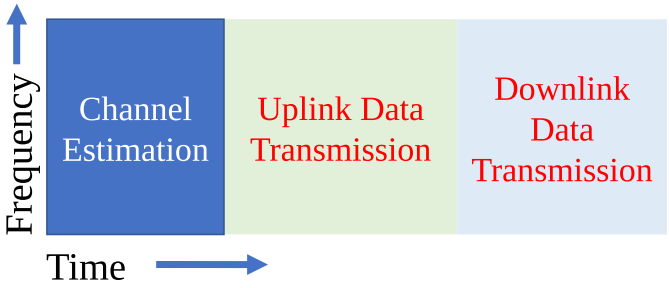

(b) Frame structure of TDD based CF system.

Figure 4.1: DTDD utilizes the same time-frequency resources for simultaneous UL and DL data transmission by different HD UEs/APs, unlike TDD, where time is partitioned between the UL and DL UEs.

technique whose effectiveness in CF-mMIMO systems has been well established [16,19,76].

Now, with $\mathbf{v}_{mk} = \hat{\mathbf{f}}_{mk}$ in (4.3), the kth UE's of the combined signal at the CPU becomes

$$\begin{aligned} r_{u,k} = & \sqrt{\mathcal{E}_{u,k}}\mathbb{E}\Big[\sum_{m\in\mathcal{A}_\mathsf{u}} \hat{\mathbf{f}}_{mk}^H \mathbf{f}_{mk}\Big] s_{u,k} + \sqrt{\mathcal{E}_{u,k}}\Big\{\sum_{m\in\mathcal{A}_\mathsf{u}} \hat{\mathbf{f}}_{mk}^H \mathbf{f}_{mk} - \mathbb{E}\Big[\sum_{m\in\mathcal{A}_\mathsf{u}} \hat{\mathbf{f}}_{mk}^H \mathbf{f}_{mk}\Big]\Big\} s_{u,k} \\ & + \sum_{m\in\mathcal{A}_\mathsf{u}} \hat{\mathbf{f}}_{mk}^H \Big\{\sum_{n\in\mathcal{I}_p\setminus k} \sqrt{\mathcal{E}_{u,n}}\mathbf{f}_{mn} s_{u,n} + \sum_{q\in\mathcal{U}_u\setminus\mathcal{I}_p} \sqrt{\mathcal{E}_{u,q}}\mathbf{f}_{mq} s_{u,q}\Big\} \\ & + \sum_{m\in\mathcal{A}_\mathsf{u}} \sum_{j\in\mathcal{A}_\mathsf{d}} \sum_{n\in\mathcal{U}_\mathsf{d}} \kappa_{jn}\sqrt{\mathcal{E}_{d,j}} \hat{\mathbf{f}}_{mk}^H \mathbf{G}_{mj} \hat{\mathbf{f}}_{jn}^* s_{d,n} + \sum_{m\in\mathcal{A}_\mathsf{u}} \hat{\mathbf{f}}_{mk}^H \mathbf{w}_{u,mk}. \end{aligned} \tag{4.5}$$

The first and second terms of (4.5) respectively represent the expected effective array gain and UL beamforming uncertainty, and are uncorrelated with each other. Similarly, the first term is uncorrelated with all the other terms of (4.5). Invoking the worst case noise theorem [39], the effective SINR of the kth UE's data stream, denoted by $\eta_{u,k}$, can be written as

$$\begin{aligned} \eta_{u,k} = \mathcal{E}_{u,k} & \left[\left|\mathbb{E}\left[\sum_{m\in\mathcal{A}_\mathsf{u}} \hat{\mathbf{f}}_{mk}^H \mathbf{f}_{mk}\right]\right|^2\right] \times \left(\mathcal{E}_{u,k}\mathtt{var}\left\{\sum_{m\in\mathcal{A}_\mathsf{u}} \hat{\mathbf{f}}_{mk}^H \mathbf{f}_{mk}\right\}\right. \\ & + \sum_{n\in\mathcal{I}_p\setminus k} \mathcal{E}_{u,n}\mathbb{E}\left[\left|\sum_{m\in\mathcal{A}_\mathsf{u}} \hat{\mathbf{f}}_{mk}^H \mathbf{f}_{mn}\right|^2\right] + \sum_{q\in\mathcal{U}_u\setminus\mathcal{I}_p} \mathcal{E}_{u,n}\mathbb{E}\left[\left|\sum_{m\in\mathcal{A}_\mathsf{u}} \hat{\mathbf{f}}_{mk}^H \mathbf{f}_{mq}\right|^2\right] \\ & \left. + \sum_{n\in\mathcal{U}_\mathsf{d}} \mathbb{E}\left[\left|\sum_{m\in\mathcal{A}_\mathsf{u}}\sum_{j\in\mathcal{A}_\mathsf{u}} \sqrt{\mathcal{E}_{d,j}}\kappa_{jn}\hat{\mathbf{f}}_{mk}^H \mathbf{G}_{mj}\hat{\mathbf{f}}_{jn}^*\right|^2\right] + N_0 \sum_{m\in\mathcal{A}_\mathsf{u}} \mathbb{E}\big\|\hat{\mathbf{f}}_{mk}^H\big\|^2\right)^{-1}. \end{aligned} \tag{4.6}$$

We simplify the above expression in the following theorem.

Theorem 4.1. *The achievable UL SE for the kth UE can be expressed as $\mathcal{R}_{u,k} = \log_2(1+\eta_{u,k})$, where $\eta_{u,k}$ is the UL SINR which is given by*

$$\eta_{u,k} = \frac{N\mathcal{E}_{u,k}\left(\sum_{m\in\mathcal{A}_\mathsf{u}} \alpha_{mk}^2\right)^2}{\mathtt{NCoh}_{u,k} + \mathtt{Coh}_{u,k} + \mathtt{IAP}_{u,k} + N_0 \sum_{m\in\mathcal{A}_\mathsf{u}} \alpha_{mk}^2}, \tag{4.7}$$

where α_{mk}^2 is defined in (2.12), $\mathtt{NCoh}_{u,k}$ represents the non-coherent inter UE interference, $\mathtt{Coh}_{u,k}$ represents the coherent inter UE interference due to pilot contamination, $\mathtt{IAP}_{u,k}$

represents the inter AP interference, and $N_0 \sum_{m\in\mathcal{A}_\mathsf{u}} \alpha_{mk}^2$ *corresponds to the effect of AWGN in the UL. These are expressed as*

$$\mathtt{NCoh}_{u,k} = \sum_{n\in\mathcal{U}_\mathsf{u}} \mathcal{E}_{u,n} \sum_{m\in\mathcal{A}_\mathsf{u}} \alpha_{mk}^2 \beta_{mn}, \tag{4.8a}$$

$$\mathtt{Coh}_{u,k} = N \sum_{n\in\mathcal{I}_p\setminus k} \mathcal{E}_{u,n} \left(\sum_{m\in\mathcal{A}_\mathsf{u}} \alpha_{mk}^2 \sqrt{\frac{\mathcal{E}_{p,n}}{\mathcal{E}_{p,k}}} \frac{\beta_{mn}}{\beta_{mk}} \right)^2, \tag{4.8b}$$

$$\mathtt{IAP}_{u,k} = N \sum_{m\in\mathcal{A}_\mathsf{u}} \sum_{j\in\mathcal{A}_\mathsf{d}} \sum_{n\in\mathcal{U}_\mathsf{d}} \kappa_{jn}^2 \zeta_{mj} \alpha_{mk}^2 \alpha_{jn}^2 \mathcal{E}_{d,j}. \tag{4.8c}$$

Proof. See Appendix C.1. ■

We now consider the DL case. Letting $\mathbf{p}_{jn} = \hat{\mathbf{f}}_{jn}^*$, the signal received by the nth ($n \in \mathcal{U}_\mathsf{d}$) DL UE can be expressed as

$$\begin{aligned} r_{d,n} = {} & \sum_{j\in\mathcal{A}_\mathsf{d}} \kappa_{jn} \sqrt{\mathcal{E}_{d,j}} \mathbb{E}\left[\mathbf{f}_{jn}^T \hat{\mathbf{f}}_{jn}^*\right] s_{d,n} + \sum_{j\in\mathcal{A}_\mathsf{d}} \kappa_{jn} \sqrt{\mathcal{E}_{d,j}} \left\{ \mathbf{f}_{jn}^T \hat{\mathbf{f}}_{jn}^* - \mathbb{E}\left[\mathbf{f}_{jn}^T \hat{\mathbf{f}}_{jn}^*\right] \right\} s_{d,n} \\ & + \sum_{j\in\mathcal{A}_\mathsf{d}} \left\{ \sum_{q\in\mathcal{I}_p\setminus n} \sqrt{\mathcal{E}_{d,j}} \kappa_{jq} \mathbf{f}_{jn}^T \hat{\mathbf{f}}_{jq}^* s_{d,q} + \sum_{q\in\mathcal{U}_d\setminus\mathcal{I}_p} \sqrt{\mathcal{E}_{d,j}} \kappa_{jq} \mathbf{f}_{jn}^T \hat{\mathbf{f}}_{jq}^* s_{d,q} \right\} \\ & + \sum_{k\in\mathcal{U}_\mathsf{u}} \sqrt{\mathcal{E}_{u,n}} \mathbf{g}_{nk} s_{u,k} + w_{d,n}. \end{aligned} \tag{4.9}$$

We present the DL SE in the following theorem.

Theorem 4.2. *The achievable DL SE for the nth UE can be expressed as* $\mathcal{R}_{d,n} = \log_2(1+\eta_{d,n})$*, with DL SINR of the nth UE,* $\eta_{d,n}$*, expressed as*

$$\eta_{d,n} = \frac{N^2 \left(\sum_{j\in\mathcal{A}_\mathsf{d}} \kappa_{jn} \sqrt{\mathcal{E}_{d,j}} \alpha_{jn}^2 \right)^2}{\mathtt{NCoh}_{d,n} + \mathtt{Coh}_{d,n} + \mathtt{IU}_{d,n} + N_0}, \tag{4.10}$$

where α_{jn}^2 *is defined in* (2.12)*,* $\mathtt{NCoh}_{d,n}$*,* $\mathtt{Coh}_{d,n}$*, and* $\mathtt{IU}_{d,n}$ *represent the DL non-coherent interference, coherent interference, and the UE to UE CLI, respectively, and given by*

$$\mathtt{NCoh}_{d,n} = N \sum_{q\in\mathcal{U}_\mathsf{d}} \sum_{j\in\mathcal{A}_\mathsf{d}} \mathcal{E}_{d,j} \kappa_{jq}^2 \beta_{jn} \alpha_{jq}^2, \tag{4.11a}$$

$$\mathtt{Coh}_{d,n} = N^2 \sum_{q \in \mathcal{I}_p \setminus n} \left(\sum_{j \in \mathcal{A}_\mathsf{d}} \sqrt{\mathcal{E}_{d,j}} \kappa_{jq} \alpha_{jq}^2 \sqrt{\frac{\mathcal{E}_{p,n}}{\mathcal{E}_{p,q}}} \frac{\beta_{jn}}{\beta_{jq}} \right)^2, \tag{4.11b}$$

$$\mathtt{IU}_{d,n} = \sum_{k \in \mathcal{U}_\mathsf{u}} \mathcal{E}_{u,n} \epsilon_{nk}. \tag{4.11c}$$

Proof. See Appendix C.2. ■

Now, the overall sum UL-DL SE of the system can be expressed as

$$\mathcal{R}_{\text{sum}} = \frac{\tau - \tau_p}{\tau} \left[\sum_{k \in \mathcal{U}_\mathsf{u}} \mathcal{R}_{u,k} + \sum_{n \in \mathcal{U}_\mathsf{d}} \mathcal{R}_{d,n} \right]. \tag{4.12}$$

We note that, from Theorem 4.1 and Theorem 4.2, the gain and various interference terms involved in $\mathcal{R}_{u,k}$ and $\mathcal{R}_{d,k}$ are dependent on $\mathcal{A}_\mathsf{u}$ and $\mathcal{A}_\mathsf{d}$. Therefore, we obtain different values of $\mathcal{R}_{\text{sum}}$ for different choices of $\mathcal{A}_\mathsf{u}$ and $\mathcal{A}_\mathsf{d}$. To characterize this dependence, from this point onward, we write the achievable sum UL-DL SE as $\mathcal{R}_{\text{sum}}(\mathcal{A}_x)$, where $\mathcal{A}_x \triangleq (\mathcal{A}_\mathsf{u}, \mathcal{A}_\mathsf{d})$. Note that, as $\mathcal{U}_u$ and $\mathcal{U}_\mathsf{d}$ are given, we omit their dependence on $\mathcal{R}_{\text{sum}}$. Now, the brute-force approach of listing out all the $2^{|\mathcal{A}_\mathsf{u} \cup \mathcal{A}_\mathsf{d}|}$ possible AP schedules and computing their achievable sum UL-DL SE using (4.12) makes the complexity of finding an optimal AP schedule exponential in the number of APs. We present a low-complexity solution in the next section.

4.4 Sum Rate Optimization

We recall that the problem of finding the optimal AP schedule, namely, determining which APs should operate in the UL and which APs should operate in the DL, based on the local data demands from the UEs, is a combinatorially complex optimization problem. In this section, we circumvent this by developing a greedy AP-scheduling scheme based on sub-modularity. At each step of the procedure, we select which AP to schedule and whether the scheduled AP should operate in the UL or DL mode, such that the incremental gain in $\mathcal{R}_{\text{sum}}$ is maximized. This process is repeated until the last AP is scheduled, thereby solving the problem in polynomial time. Such a greedy approach to SE maximization has

been previously proposed in the antenna selection literature, based on the monotonicity of the cost function [77]. However, to provide concrete guarantees on the performance of the greedy search, we need to show that the cost function is a sub-modular set function of the scheduled APs. In this case, the greedy algorithm is guaranteed to yield a solution that achieves at least $(1-1/e)$-fraction of the optimal value of the cost function. For the sake of completeness, we formally define the monotonicity and sub-modularity properties as follows.

Definition 4.1. *[60] Let $\mathcal{S}$ be a finite set, and let $2^{\mathcal{S}}$ denote its power set. A function $f: 2^{\mathcal{S}} \to \mathbb{R}$, with $f(\emptyset)=0$, is said to be **monotone nondecreasing** if for every $\mathcal{A} \subseteq \mathcal{B} \subseteq \mathcal{S}$, $f(\mathcal{A}) \leq f(\mathcal{B})$, and is said to be **sub-modular** if for every $\{j\} \in \mathcal{S} \backslash \mathcal{B}$,*

$$f(\mathcal{A} \cup \{j\}) - f(\mathcal{A}) \geq f(\mathcal{B} \cup \{j\}) - f(\mathcal{B}).$$

We first focus on the monotonicity of the sum UL-DL SE. Let $\mathcal{A}$ be the indices of the APs in the network, where each AP (i.e., each index) can be scheduled either in the UL or DL. Further, let $\mathcal{A}_s = \mathcal{A}_u \cup \mathcal{A}_d$ denote the index set of the APs that have been previously scheduled, and $\mathcal{A}'_s = \mathcal{A} \backslash \mathcal{A}_s$ be the index set of unscheduled APs. We need to show that adding an element from $\mathcal{A}'_s$ to $\mathcal{A}_s$ does not decrease $\mathcal{R}_{\text{sum}}$. Now, for any AP $m \in \mathcal{A}'_s$, let $\mathcal{A}_t \triangleq \mathcal{A}_s \cup \{m\}$. We note that when the mth AP is added to the set of UL APs, $\mathcal{A}_u$, it does not introduce any new interference, and hence the sum rate can only improve. However, if the mth AP is added to $\mathcal{A}_d$, then it has the option to transmit with zero power. If it chooses to transmit at zero power, it is as if the AP was not added at all, so the sum rate obtained is the same as that obtained without it. However, if the AP optimally chooses a nonzero transmit power in order to maximize the sum rate, the sum rate can be potentially improved. Hence, the sum rate with the new AP added can only be greater than or equal to the sum rate obtained without the AP, and $\mathcal{R}_{\text{sum}}(\mathcal{A}_s) \leq \mathcal{R}_{\text{sum}}(\mathcal{A}_t)$ with $\mathcal{A}_s \subseteq \mathcal{A}_t$. This shows that the sum rate is a monotone nondecreasing set function.

We now focus on the proof of sub-modularity. First, we observe that due to pilot contamination and CLIs, $\mathcal{R}_{\text{sum}}$ is a non-separable function of the scheduled AP sets $\mathcal{A}_{\mathsf{u}}$ and $\mathcal{A}_{\mathsf{d}}$. For example, if the jth AP, $\{j\} \notin \mathcal{A}_{\mathsf{u}} \cup \mathcal{A}_{\mathsf{d}}$, is scheduled in the UL mode, we can write the gain and the coherent interference terms in (4.7) and (4.8b) as

$$\left(\sum_{m\in\mathcal{A}_{\mathsf{u}}\cup\{j\}} \alpha_{mk}^2\right)^2 = \left(\sum_{m\in\mathcal{A}_{\mathsf{u}}} \alpha_{mk}^2\right)^2 + \alpha_{jk}^4 + 2\alpha_{jk}^2 \sum_{m\in\mathcal{A}_{\mathsf{u}}} \alpha_{mk}^2, \tag{4.13a}$$

$$\sum_{n\in\mathcal{I}_p\setminus k} \mathcal{E}_{u,n} \left(\sum_{m\in\mathcal{A}_{\mathsf{u}}\cup\{j\}} \alpha_{mk}^2 \sqrt{\frac{\mathcal{E}_{p,n}}{\mathcal{E}_{p,k}}} \frac{\beta_{mn}}{\beta_{mk}}\right)^2 = \sum_{n\in\mathcal{I}_p\setminus k} \mathcal{E}_{u,n} \Bigg[\left(\sum_{m\in\mathcal{A}_{\mathsf{u}}} \alpha_{mk}^2 \sqrt{\frac{\mathcal{E}_{p,n}}{\mathcal{E}_{p,k}}} \frac{\beta_{mn}}{\beta_{mk}}\right)^2 + \alpha_{jk}^4 \frac{\mathcal{E}_{p,n}}{\mathcal{E}_{p,k}} \frac{\beta_{jn}^2}{\beta_{jk}^2} + 2\alpha_{jk}^2 \sqrt{\frac{\mathcal{E}_{p,n}}{\mathcal{E}_{p,k}}} \frac{\beta_{jn}}{\beta_{jk}} \sum_{m\in\mathcal{A}_{\mathsf{u}}} \alpha_{mk}^2 \sqrt{\frac{\mathcal{E}_{p,n}}{\mathcal{E}_{p,k}}} \frac{\beta_{mn}}{\beta_{mk}} \Bigg], \tag{4.13b}$$

respectively. We note that in (4.13a) and (4.13b), the first two terms in the right-hand side correspond to the gain and coherent interferences due to set $\mathcal{A}_{\mathsf{u}}$ and scheduled $\{j\}$th UL AP, respectively. However, due to the nonlinearity and the cross terms, the UL SINR is not a separable function of the set of scheduled APs. Thus, $\eta_{u,k}(\mathcal{A}_{\mathsf{u}} \cup \{j\}) \neq \eta_{u,k}(\mathcal{A}_{\mathsf{u}}) + \eta_{u,k}(\{j\})$. Similar observations hold in DL. Furthermore, in our system, the UL SINRs and the DL SINRs are coupled with the DL-transmitted signals via the AP-to-AP CLI and UL-transmitted signals via UE-to-UE CLI, respectively, which makes the SINRs dependent on the power control coefficients. Therefore, our problem becomes challenging compared to previous works in antenna selection and UE scheduling literature, which have considered either linear cost functions with respect to the maximization sets [78] or perfect CSI at the APs [79].

In several studies, the authors rely on approximations such as high SNR [80], or the SE under asymptotic antenna density [78], which lead to tractable analytical expressions. Such approximate cost function-based analysis is known as *sub-modular relaxation* [80]. In this work, we note that as the number of antennas at each AP, N, goes to infinity, the non-coherent interferences become negligible compared to the gain and coherent interferences as observed in Theorem 4.1 and Theorem 4.2. Also, in a CF system, the CPU can potentially

cancel the AP-AP CLI with the global knowledge of the DL data streams. Therefore, to make the analysis tractable, we bound both the UL and DL rates and formulate an equivalent optimization problem based on the product SINR. Note that, as $N \to \infty$, we can show that

$$\begin{aligned}\mathcal{R}_{u,k} &\geq \log_2 \frac{\mathcal{E}_{u,k}\left(\sum\limits_{m\in\mathcal{A}_\mathsf{u}} \alpha_{mk}^2\right)^2}{\sum\limits_{n\in\mathcal{I}_p\setminus k} \mathcal{E}_{u,n}\left(\sum\limits_{m\in\mathcal{A}_\mathsf{u}} \alpha_{mk}^2 \sqrt{\frac{\mathcal{E}_{p,n}}{\mathcal{E}_{p,k}}}\frac{\beta_{mn}}{\beta_{mk}}\right)^2} \\ &\geq \log_2 \frac{\left(\sqrt{\mathcal{E}_{u,k}}\sum\limits_{m\in\mathcal{A}_\mathsf{u}} \alpha_{mk}^2\right)^2}{\left(\sum\limits_{n\in\mathcal{I}_p\setminus k} \sqrt{\mathcal{E}_{u,n}}\sum\limits_{m\in\mathcal{A}_\mathsf{u}} \alpha_{mk}^2 \sqrt{\frac{\mathcal{E}_{p,n}}{\mathcal{E}_{p,k}}}\frac{\beta_{mn}}{\beta_{mk}}\right)^2}, \end{aligned} \tag{4.14}$$

$$\begin{aligned}\mathcal{R}_{d,n} &\geq \log_2 \frac{\left(\sum\limits_{j\in\mathcal{A}_\mathsf{d}} \kappa_{jn}\sqrt{\mathcal{E}_{j,n}}\alpha_{jn}^2\right)^2}{\sum\limits_{q\in\mathcal{I}_p\setminus n}\left(\sum\limits_{j\in\mathcal{A}_\mathsf{d}} \sqrt{\mathcal{E}_{d,j}}\kappa_{jq}\alpha_{jq}^2 \sqrt{\frac{\mathcal{E}_{p,n}}{\mathcal{E}_{p,q}}}\frac{\beta_{jn}}{\beta_{jq}}\right)^2} \\ &\geq \log_2 \frac{\left(\sum\limits_{j\in\mathcal{A}_\mathsf{d}} \kappa_{jn}\sqrt{\mathcal{E}_{j,n}}\alpha_{jn}^2\right)^2}{\left(\sum\limits_{q\in\mathcal{I}_p\setminus n}\sum\limits_{j\in\mathcal{A}_\mathsf{d}} \sqrt{\mathcal{E}_{d,j}}\kappa_{jq}\alpha_{jq}^2 \sqrt{\frac{\mathcal{E}_{p,n}}{\mathcal{E}_{p,q}}}\frac{\beta_{jn}}{\beta_{jq}}\right)^2}. \end{aligned} \tag{4.15}$$

The latter lower bounds in (4.14) and (4.15) follow as we have only added more interference terms in the denominators. Let

$$\mathcal{R}'_{u,k} = \log_2 \frac{(\sqrt{\mathcal{E}_{u,k}}\sum\limits_{m\in\mathcal{A}_\mathsf{u}} \alpha_{mk}^2)^2}{(\sum\limits_{n\in\mathcal{I}_p\setminus k} \sqrt{\mathcal{E}_{u,n}}\sum\limits_{m\in\mathcal{A}_\mathsf{u}} \alpha_{mk}^2 \sqrt{\frac{\mathcal{E}_{p,n}}{\mathcal{E}_{p,k}}}\frac{\beta_{mn}}{\beta_{mk}})^2} = 2\log_2 \frac{\sum\limits_{m\in\mathcal{A}_\mathsf{u}} \mathtt{G}_{u,mk}}{\sum\limits_{m\in\mathcal{A}_\mathsf{u}} \mathtt{I}_{u,mk}}, \tag{4.16}$$

and

$$\mathcal{R}'_{d,n} = \log_2 \frac{(\sum\limits_{j\in\mathcal{A}_\mathsf{d}} \kappa_{jn}\sqrt{\mathcal{E}_{j,n}}\alpha_{jn}^2)^2}{(\sum\limits_{q\in\mathcal{I}_p\setminus n}\sum\limits_{j\in\mathcal{A}_\mathsf{d}} \sqrt{\mathcal{E}_{d,j}}\kappa_{jq}\alpha_{jq}^2 \sqrt{\frac{\mathcal{E}_{p,n}}{\mathcal{E}_{p,q}}}\frac{\beta_{jn}}{\beta_{jq}})^2} = 2\log_2 \frac{\sum\limits_{j\in\mathcal{A}_\mathsf{d}} \mathtt{G}_{d,jn}}{\sum\limits_{j\in\mathcal{A}_\mathsf{d}} \mathtt{I}_{d,jn}}, \tag{4.17}$$

with the respective terms being defined as

$$\mathtt{G}_{u,mk} \triangleq \sqrt{\mathcal{E}_{u,k}}\alpha_{mk}^2, \tag{4.18a}$$

$$\mathtt{I}_{u,mk} \triangleq \sum_{n\in\mathcal{I}_p\setminus k} \sqrt{\mathcal{E}_{u,n}}\alpha_{mk}^2\sqrt{\frac{\mathcal{E}_{p,n}}{\mathcal{E}_{p,k}}}\frac{\beta_{mn}}{\beta_{mk}}, \tag{4.18b}$$

$$\mathtt{G}_{d,jn} \triangleq \kappa_{jn}\sqrt{\mathcal{E}_{j,n}}\alpha_{jn}^2, \tag{4.18c}$$

$$\mathtt{I}_{d,jn} \triangleq \sum_{q\in\mathcal{I}_p\setminus n} \sqrt{\mathcal{E}_{d,j}}\kappa_{jq}\alpha_{jq}^2\sqrt{\frac{\mathcal{E}_{p,n}}{\mathcal{E}_{p,q}}}\frac{\beta_{jn}}{\beta_{jq}}. \tag{4.18d}$$

Now, given the set of APs $\mathcal{A}_s$, our problem is to optimally decide the partition $\mathcal{A}_\mathtt{u}$ and $\mathcal{A}_\mathtt{d}$ such that the sum UL-DL SE, i.e. $\mathcal{R}'_{\text{sum}} \triangleq \left[\sum_{k\in\mathcal{U}_\mathtt{u}} \mathcal{R}'_{u,k} + \sum_{n\in\mathcal{U}_\mathtt{d}} \mathcal{R}'_{d,n}\right]$, is maximized. For notational simplicity, we rewrite our problem as follows

$$\begin{aligned}\max_{\mathcal{A}_s} \mathcal{R}'_{\text{sum}} &= \max_{\mathcal{A}_s} \sum_{k=1}^{K} 2\log_2 \frac{\sum\limits_{m\in\mathcal{A}_s} \mathtt{G}_{mk}(\mathcal{A}_s)}{\sum\limits_{m\in\mathcal{A}_s} \mathtt{I}_{mk}(\mathcal{A}_s)} \\ &\overset{(a)}{\equiv} \max_{\mathcal{A}_s} \prod_{k=1}^{K} \frac{\sum\limits_{m\in\mathcal{A}_s} \mathtt{G}_{mk}(\mathcal{A}_s)}{\sum\limits_{m\in\mathcal{A}_s} \mathtt{I}_{mk}(\mathcal{A}_s)},\end{aligned} \tag{4.19}$$

where the kth UE can be either UL or DL, and mth AP is either scheduled in UL or in the DL. Here, we explicitly write the gain and interferences as a function of $\mathcal{A}_s$. The equivalence in (a) follows from the monotonicity of $\log_2(.)$.

Theorem 4.3. *The product SINR, $f_{mk}(\mathcal{A}_x) = \prod_{k=1}^{K} \frac{\sum_{m\in\mathcal{A}_x} \mathtt{G}_{mk}(\mathcal{A}_x)}{\sum_{m\in\mathcal{A}_x} \mathtt{I}_{mk}(\mathcal{A}_x)}$, is a sub-modular function of the number of scheduled APs in the system. That is, if $\mathcal{A}_s$ and $\mathcal{A}_t$ are index sets of active APs, with $\mathcal{A}_s \subseteq \mathcal{A}_t$, and if $\{j\} \notin \mathcal{A}_t$, then*

$$f_{mk}(\mathcal{A}_s \cup \{j\}) - f_{mk}(\mathcal{A}_s) \geq f_{mk}(\mathcal{A}_t \cup \{j\}) - f_{mk}(\mathcal{A}_t).$$

Proof. See Appendix C.3. ■

Now, exploiting the sub-modularity of $\mathcal{R}'_{\text{sum}}$, we can develop a greedy algorithm similar

Algorithm 6: Greedy algorithm for AP scheduling

Input: $\mathcal{A}$: the set of all AP indices

Initialization: $\mathcal{A}_u = \mathcal{A}_d = \emptyset$, $\mathcal{A}_s = \mathcal{A}_u \cup \mathcal{A}_d$

[1]: **while** $\mathcal{A}'_s \neq \emptyset$ **do**

[2]: `Find the AP and the associated mode (UL/ DL) that give maximum incremental gain in the product SINR in` (4.19)

$$i^{\star}_{\mathsf{u}} = \arg\max_{i \in \mathcal{A}'_s} \prod_{k \in \mathcal{U}_{\mathsf{u}} \cup \mathcal{U}_{\mathsf{d}}} \frac{\sum\limits_{m \in \mathcal{A}_s} \mathtt{G}_{mk}(\mathcal{A}_s \cup \{i\})}{\sum\limits_{m \in \mathcal{A}_s} \mathtt{I}_{mk}(\mathcal{A}_s \cup \{i\})} \tag{4.20}$$

$$i^{\star}_{\mathsf{d}} = \arg\max_{i \in \mathcal{A}'_s} \prod_{k \in \mathcal{U}_{\mathsf{u}} \cup \mathcal{U}_{\mathsf{d}}} \frac{\sum\limits_{m \in \mathcal{A}_s} \mathtt{G}_{mk}(\mathcal{A}_s \cup \{i\})}{\sum\limits_{m \in \mathcal{A}_s} \mathtt{I}_{mk}(\mathcal{A}_s \cup \{i\})} \tag{4.21}$$

[3]: **if** $i^{\star}_{\mathsf{u}} \geq i^{\star}_{\mathsf{d}}$ **then**

[4]: **Update:** $\mathcal{A}_{\mathsf{u}} = \mathcal{A}_{\mathsf{u}} \cup \{i^{\star}_u\}$ % `Schedule` i`th AP in UL`

[5]: **else**

[6]: **Update:** $\mathcal{A}_d = \mathcal{A}_d \cup \{i^{\star}_d\}$ % `Schedule` i`th AP in DL`

[7]: **end**

[8]: **end**

[9]: **Update the scheduled AP set:** $\mathcal{A}_s = \mathcal{A}_u \cup \mathcal{A}_d$

[10]: **end**

[11]: **Return:** $\mathcal{A}_u$ and $\mathcal{A}_d$

to Algorithm 5 for scheduling the APs.[1] For completeness and the reader's immediate reference, we describe the recipe in Algorithm 6. It follows that $\mathcal{R}'_{\text{sum}}(\dot{\mathcal{A}}) \geq \left(1 - \frac{1}{e}\right) \mathcal{R}'_{\text{sum}}(\mathcal{A}^{\star})$, where $\mathcal{A}^{\star}$ is the index set containing the optimal AP configuration that maximizes the cost function $\mathcal{R}'_{\text{sum}}$, and $\dot{\mathcal{A}}$ denotes the AP configuration returned by Algorithm 6. We validate the effectiveness of the greedy algorithm via numerical simulations in Figure 4.2.

[1]Recall that Algorithm 5 uses $\mathcal{R}_{\text{s}}$ for AP scheduling which is the sum UL-DL SE without pilot contamination and perfect InAI cancelation. However, here, $\mathcal{R}'_{\text{sum}}$ is the product of UL-DL SINRs that capture the effects of pilot contamination. Thus, although the structure of the greedy algorithm is the same, due to the underlying sub-modularity, the utility metrics being optimized are different.

The simulation parameters are detailed in Section 4.7. For the brute force-based search, we have considered our original cost function $\mathcal{R}_{\text{sum}}$ as expressed in (4.12) over all possible AP-schedules to find the optimal SE. We also use the AP schedule generated by Algorithm 6 and evaluate $\mathcal{R}_{\text{sum}}$ using (4.12). We observe that the sum UL-DL SE obtained via exhaustive search over all 2^M UL-DL AP-configurations and considering the effects of CLIs matches closely with that obtained via Algorithm 6 based on sub-modularity of the lower-bounded cost function.

In Figure 4.3, we plot the 90%-likely sum UL-DL SE vs. UL and DL data SNR to validate the theoretical expressions of SE derived in Theorem 4.1 and Theorem 4.2. For the simulation, we consider $10,000$ Monte Carlo channel instantiations and UE locations; the other parameters used can be found in Section 4.7. The theoretical curve is obtained by averaging the 90% likely sum SE obtained from (4.12). The simulation corroborates well with our derived results, verifying the accuracy of the expression for $\mathcal{R}_{\text{sum}}$ derived above.

4.5 Performance Analysis: MMSE & RZF

It is known that the performance of CF-mMIMO can be improved with centralized MMSE combining in the UL and RZF precoding in the DL [20, 61]. In this section, we briefly analyze the performance of our system model under these combining and precoding schemes.

Let $\mathcal{A}_{\mathsf{u}}(m)$ and $\mathcal{U}_{\mathsf{u}}(k)$ denote the mth UL AP and the kth UL UE in $\mathcal{A}_{\mathsf{u}}$ and $\mathcal{U}_{\mathsf{u}}$, respectively. Let $\mathcal{A}_{\mathsf{d}}(j)$ and $\mathcal{U}_{\mathsf{d}}(n)$ denote the jth DL AP and the nth DL UE in $\mathcal{A}_{\mathsf{d}}$ and $\mathcal{U}_{\mathsf{d}}$, respectively. Let $\hat{\mathbf{f}}_{u,k} \in \mathbb{C}^{N|\mathcal{A}_{\mathsf{u}}|}$ denote the estimated channel matrix of the kth UL UE to all the UL APs, i.e., $\hat{\mathbf{f}}_{u,k} = \left[\hat{\mathbf{f}}^T_{\mathcal{A}_{\mathsf{u}}(1)k}, \ldots, \hat{\mathbf{f}}^T_{\mathcal{A}_{\mathsf{u}}(|\mathcal{A}_{\mathsf{u}}|)k}\right]^T, \forall k \in \mathcal{U}_{\mathsf{u}}$, and let the estimated UL channel matrix available at the CPU be denoted by $\hat{\mathbf{F}}_{\mathsf{u}} \triangleq \left[\hat{\mathbf{f}}_{u,\mathcal{U}_{\mathsf{u}}(1)}, \ldots, \hat{\mathbf{f}}_{u,\mathcal{U}_{\mathsf{u}}(|\mathcal{U}_{\mathsf{u}}|)}\right] \in \mathbb{C}^{N|\mathcal{A}_{\mathsf{u}}|\times|\mathcal{U}_{\mathsf{u}}|}$. Similarly, we can express the estimated channel of the DL UEs as $\hat{\mathbf{F}}_{\mathsf{d}} \triangleq \left[\hat{\mathbf{f}}_{d,\mathcal{U}_{\mathsf{d}}(1)}, \ldots, \hat{\mathbf{f}}_{d,\mathcal{U}_{\mathsf{d}}(|\mathcal{U}_{\mathsf{d}}|)}\right] \in \mathbb{C}^{N|\mathcal{A}_{\mathsf{d}}|\times|\mathcal{U}_{\mathsf{d}}|}$ with $\hat{\mathbf{f}}_{d,n} = \left[\hat{\mathbf{f}}^T_{\mathcal{A}_{\mathsf{d}}(1)n}, \ldots, \hat{\mathbf{f}}^T_{\mathcal{A}_{\mathsf{d}}(|\mathcal{A}_{\mathsf{d}}|)n}\right]^T \in \mathbb{C}^{N|\mathcal{A}_{\mathsf{d}}|}, \forall n \in \mathcal{U}_{\mathsf{d}}$. Now, the concatenated

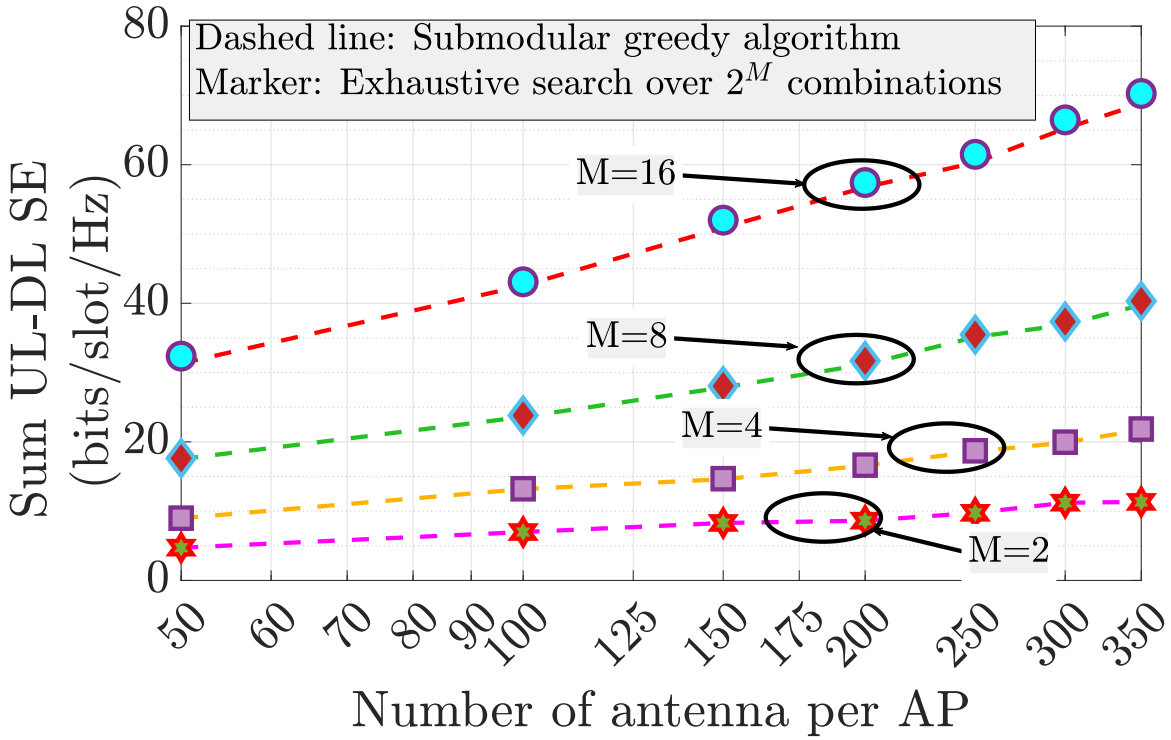

Figure 4.2: Sum UL-DL SE (bits/slot/Hz) vs number of AP-antennas for different numbers of APs. This plot shows the effectiveness of the sub-modular algorithm.

UL signal received at the CPU becomes

$$\mathbf{y}_{\mathsf{u}} = \sum_{k \in \mathcal{U}_{\mathsf{u}}} \sqrt{\mathcal{E}_{u,k}} \left(\hat{\mathbf{f}}_{u,k} + \tilde{\mathbf{f}}_{u,k} \right) s_{u,k} + \sum_{n \in \mathcal{U}_{\mathsf{d}}} \mathbf{G} \mathbf{p}_n s_{d,n} + \mathbf{w}_{ul}, \tag{4.22}$$

where $\mathbf{G} \in \mathbb{C}^{N|\mathcal{A}_{\mathsf{u}}| \times N|\mathcal{A}_{\mathsf{d}}|}$ denotes the residual interference channel between DL APs and UL APs, and $\mathbf{p}_n \in \mathbb{C}^{N|\mathcal{A}_{\mathsf{d}}|}$ is the nth column of the DL precoder $\mathbf{P} = \left[\mathbf{p}_{\mathcal{U}_{\mathsf{d}}(1)}, \ldots, \mathbf{p}_{\mathcal{U}_{\mathsf{d}}(|\mathcal{U}_{\mathsf{d}}|)} \right] \in \mathbb{C}^{N|\mathcal{A}_{\mathsf{d}}| \times |\mathcal{U}_{\mathsf{d}}|}$. With a slight abuse of notation, let $\mathbf{P}_j \in \mathbb{C}^{N \times |\mathcal{U}_{\mathsf{d}}|}$ denote the precoding matrix for the jth DL AP, and let $\mathcal{E}_{d,j}$ denote the power budget per antenna at the jth DL AP, so that the power constraint becomes $\mathtt{tr}(\mathbf{P}_j \mathbf{P}_j^H) \leq N \mathcal{E}_{d,j}$ [61]. Finally, $\mathbf{w}_{ul} \sim \mathcal{CN}(\mathbf{0}, N_0 \mathbf{I}_{N|\mathcal{A}_{\mathsf{u}}|})$ is the additive noise. Then, $\mathbf{V} = \mathbf{Q}_{\mathsf{u}}^{-1} \hat{\mathbf{F}}_{\mathsf{u}} \in \mathbb{C}^{N|\mathcal{A}_{\mathsf{u}}| \times |\mathcal{U}_{\mathsf{u}}|}$ is the joint MMSE combiner, with $\mathbf{Q}_{\mathsf{u}} = \left(\sum_{k \in \mathcal{U}_{\mathsf{u}}} \mathcal{E}_{u,k} \hat{\mathbf{f}}_{u,k} \hat{\mathbf{f}}_{u,k}^H + \mathbf{R}_{\mathsf{u}} + N_0 \mathbf{I}_{N|\mathcal{A}_{\mathsf{u}}|} \right)$, where

$$\mathbf{R}_{\mathsf{u}} = \left(\sum_{k \in \mathcal{U}_{\mathsf{u}}} \mathcal{E}_{u,k} \mathbb{E}\left[\tilde{\mathbf{f}}_{u,k} \tilde{\mathbf{f}}_{u,k}^H \right] + \sum_{i \in \mathcal{U}_{\mathsf{d}}} \mathbb{E}\left[\mathbf{G} \mathbf{p}_n \mathbf{p}_n^H \mathbf{G}^H \right] \right). \tag{4.23}$$

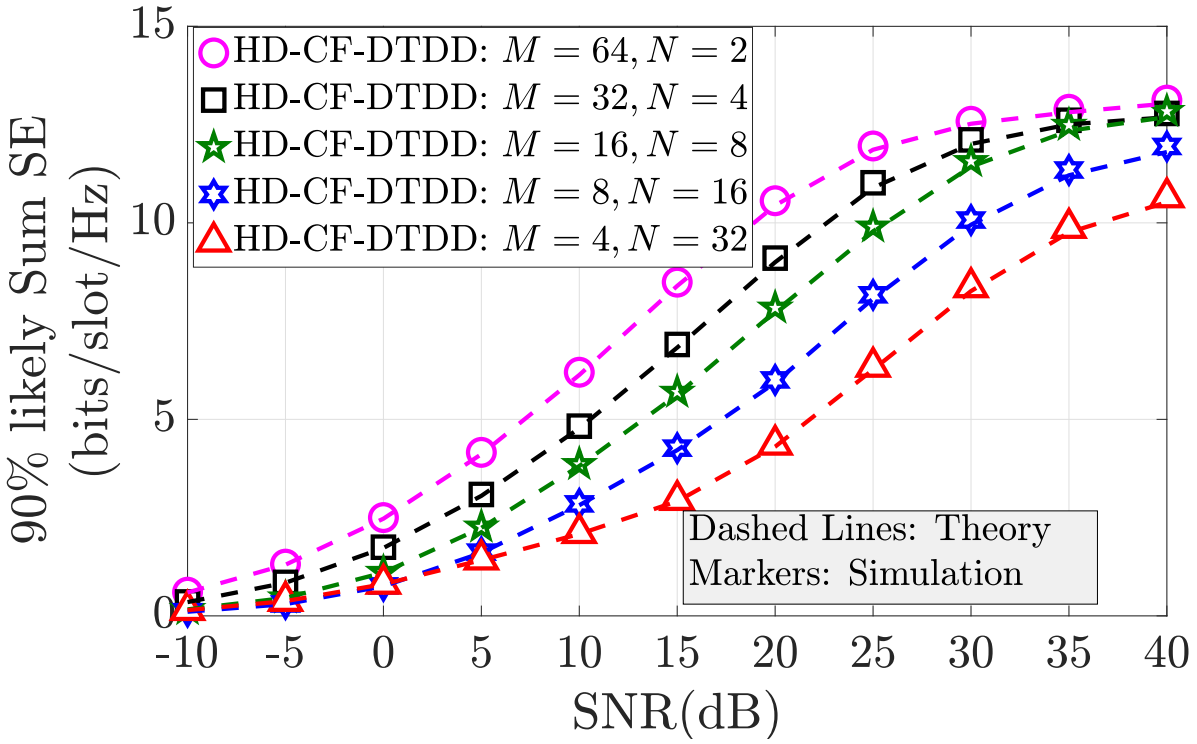

Figure 4.3: The 90%-likely sum UL-DL SE vs. data SNR with $K = 100$. This figure validates the derived theoretical expressions of the sum SE with Monte Carlo simulations.

$$\eta_{u,k} = \frac{\mathcal{E}_{u,k} \left| \hat{\mathbf{f}}_{u,k}^H \mathbf{Q}_{\mathsf{u}}^{-1} \hat{\mathbf{f}}_{u,k} \right|^2}{\sum\limits_{k' \in \mathcal{U}_{\mathsf{u}} \setminus k} \mathcal{E}_{u,k'} \left| \hat{\mathbf{f}}_{u,k}^H \mathbf{Q}_{\mathsf{u}}^{-1} \hat{\mathbf{f}}_{u,k'} \right|^2 + \hat{\mathbf{f}}_{u,k}^H \mathbf{Q}_{\mathsf{u}}^{-1} \left(\mathbf{R}_{\mathsf{u}} + N_0 \mathbf{I}_{N|\mathcal{A}_{\mathsf{u}}|} \right) \mathbf{Q}_{\mathsf{u}}^{-1} \hat{\mathbf{f}}_{u,k}}. \tag{4.24}$$

Then, the UL sum SE becomes [20] $\mathcal{R}_{\mathsf{u}} = \sum\limits_{k \in \mathcal{U}_{\mathsf{u}}} \mathbb{E}\left[\log_2\left(1 + \eta_{u,k}\right)\right]$, where $\eta_{u,k}$ is expressed in (4.24), with the expectation being taken over the channel realizations. The MMSE combiner presented here maximizes the kth UL UE's instantaneous SINR [20, 39].

In the DL, the RZF precoder is a commonly used linear precoding scheme to control inter-UE interference [61]. It is designed as $\mathbf{P} = \kappa \mathbf{Q}_{\mathsf{d}}^{-1} \hat{\mathbf{F}}_{\mathsf{d}}$, where $\mathbf{Q}_{\mathsf{d}} = \left(\hat{\mathbf{F}}_{\mathsf{d}} \hat{\mathbf{F}}_{\mathsf{d}}^H + \xi \mathbf{I}_{N|\mathcal{A}_{\mathsf{d}}|} \right)$, κ is the power normalization factor, and $\xi > 0$ is a regularization parameter [81, 82]. The DL sum SE can be increased by appropriately selecting ξ [81], and the DL power control parameter κ is evaluated at the CPU based on the estimated channel statistics.

$$\eta_{d,n} = \frac{\kappa^2 \left| \mathbb{E}\left[\mathbf{f}_n^H \mathbf{Q}_{\mathtt{d}}^{-1} \hat{\mathbf{f}}_n \right] \right|^2}{\kappa^2 \sum\limits_{n' \in \mathcal{U}_{\mathtt{d}} \setminus n} \mathbb{E}\left[\left| \mathbf{f}_n^H \mathbf{Q}_{\mathtt{d}}^{-1} \hat{\mathbf{f}}_{n'} \right|^2 \right] + \mathtt{var}\left(\mathbf{f}_n^H \mathbf{Q}_{\mathtt{d}}^{-1} \hat{\mathbf{f}}_n \right) + \sum\limits_{k \in \mathcal{U}_{\mathtt{u}}} \mathcal{E}_{u,k} \mathbb{E}\left| \mathrm{g}_{nk} \right|^2 + N_0} \tag{4.25}$$

Considering an equal power budget at each DL AP, i.e., $\mathcal{E}_{d,j} = \mathcal{E}_{\mathtt{d}}$, it is easy to show $\kappa_j^2 = N\mathcal{E}_{\mathtt{d}} / \mathtt{tr}(\mathbf{P}_j \mathbf{P}_j^H)$ satisfies the DL power constraint. We set $\kappa^2 = \min_j \kappa_j^2$, for all $j \in \mathcal{A}_{\mathtt{d}}$, an approach previously used in [83]. We consider that the DL UEs know the mean of the precoded signal, and therefore, applying the use-and-then forget bound, we can write the DL SE as $\mathcal{R}_{\mathtt{d}} = \sum\limits_{n \in \mathcal{U}_{\mathtt{d}}} \log_2(1 + \eta_{d,n})$, with $\eta_{d,n}$ (expressed in (4.25)) being the DL SINR of the nth UE, where the expectations are taken over the channel realizations.

With the above UL and DL SE expressions in hand, we can compare MRC/MFP based combiner/precoding with the MMSE-type combining/precoding. The APs are scheduled according to Algorithm 6, with the sum rate computed using the UL and DL SINRs evaluated according to (4.24) and (4.25), respectively. In Figure 4.4, we see that, with $(M = 64, N = 4)$, the 90%-sum UL-DL SE achieved via MMSE/RZF is double the sum UL-DL SE achieved via MRC/MFP under similar settings. This shows the interference suppression capability of MMSE-based combiner and precoder, as well as the benefits of the centralized MMSE-processing scheme. However, the complexity of these schemes increases significantly with system dimension, i.e., number of UEs and number of APs. Also, when we increase the number of APs from 8 to 64, we observe a substantial performance improvement irrespective of the processing scheme. There are two contributing factors to this improvement: First, as we increase the number of APs, the flexibility to schedule the APs either in UL or in DL mode also increases, and therefore, the sum UL-DL SE improves considerably. Second, with more APs, the probability that an UE finds an AP (or APs) in its proximity also increases, and which in turn improves the rate achieved by that UE, leading to an improvement in sum UL-DL SE.

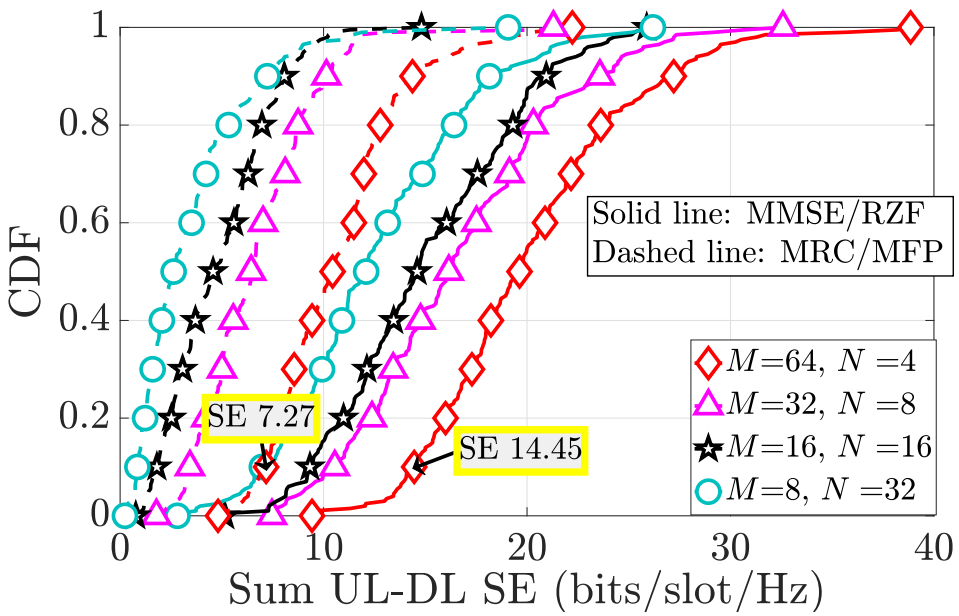

Figure 4.4: Performance comparison of MMSE-type precoder/combiner with MRC/MFP with $K = 32$.

4.6 Full-Duplex Multi-cell Systems

In this section, we briefly present the sum UL-DL SE achieved by an FD-enabled multi-cell mMIMO system, based on [53], to enable fair comparison with the DTDD-based CF-mMIMO system. We assume that each cell has one FD BS with N_t transmit and N_r receive antennas. To maintain the consistency with our previous analysis, we assume that the total number of UEs across all cells is same as the total number of UEs (K) in the CF system. Let $\mathcal{U}_{l,u}$ and $\mathcal{U}_{l,d}$ denote the index sets of HD UL and DL UEs within the lth cell, such that $\sum_{l=1}^{L}(|\mathcal{U}_{l,u}| + |\mathcal{U}_{l,d}|) = K$. We also assume that each FD BS can perfectly cancel out its self-interference. However, we do not assume any inter-BS cooperation for interference management. Therefore, each BS experiences interference from neighboring cells. Let the UL channel from kth UE of lth cell to the jth BS be denoted by $\mathbf{f}_{u,jlk} = \sqrt{\beta_{jlk}}\mathbf{h}_{u,jlk} \in \mathbb{C}^{N_r \times 1}$, with β_{jlk} being the slow fading component that includes the path loss, and $\mathbf{h}_{u,jlk} \sim \mathcal{CN}(0, \mathbf{I}_{N_r})$ being the fast fading component. Similarly, the DL channel from the jth BS to the nth DL UE of the lth cell can be modeled as $\mathbf{f}_{d,jln} = \sqrt{\beta_{jln}}\mathbf{h}_{d,jln} \in \mathbb{C}^{N_t \times 1}$.

The channel matrix from the DL antenna array of the jth BS to the UL antenna array of the lth BS is denoted by $\mathbf{T}_{jl} \in \mathbb{C}^{N_r \times N_t}$, with each element modeled as $\mathcal{CN}(0, \rho_{ij})$. We model the channel between the kth UL UE of the lth cell and the nth DL UE of l'th cell as $\mathbf{g}_{lk,l'n} \sim \mathcal{CN}(0, \epsilon_{lk,l'n})$.In the channel estimation phase, we assume that all the UL and DL UEs synchronously transmit orthogonal pilots for channel estimation [53, 74]. The UL and the DL estimated channels $\hat{\mathbf{f}}_{u,jlk}$ and $\hat{\mathbf{f}}_{d,jlk}$ of $\mathbf{f}_{u,jlk}$ and $\mathbf{f}_{d,jlk}$, respectively, can be expressed as $\mathbf{f}_{x,jlk} = \hat{\mathbf{f}}_{x,jlk} + \tilde{\mathbf{f}}_{x,jlk}$, $x \in u, d$, with $\tilde{\mathbf{f}}_{x,jlk}$ being the estimation error vector, consisting of i.i.d. entries such that $\tilde{\mathbf{f}}_{x,jlk} \sim \mathcal{CN}(0, (\beta_{jlk} - \sigma^2_{jlk})\mathbf{I})$ with $\sigma_{jlk} = \sqrt{\dfrac{\tau_p \mathcal{E}_{p,lk} \beta^2_{jlk}}{\tau_p \sum\limits_{l'} \tau_p \mathcal{E}_{p,l'k} \beta_{jl'k} + N_0}}$. Here, the UEs are numbered such that identically indexed UEs across different cells share the same pilot sequence.

Following this, the UEs and the BSs simultaneously transmit their data. Let $\hat{\mathbf{v}}_{u,jk} \in \mathbb{C}^N$ be the UL combiner kth column of the UL combiner vector designed at the jth BS. Similarly, let $\hat{\mathbf{v}}_{d,jn} \in \mathbb{C}^N$ be the DL precoder designed at the jth BS and is intended for the nth DL UE. Let the kth UL UE of the jth cell transmit its symbol $s_{u,jk}$ with power $\mathcal{E}_{u,jk}$, and the jth BS transmit the precoded DL data $\mathbf{v}_{d,jn} s_{u,jn}$. The total power expended by the jth BS is denoted by $\mathcal{E}_{d,j}$ and the power control coefficient for the corresponding nth UE is denoted by κ_{jn}. We present the sum UL-DL SE for a cellular FD-mMIMO system with MRC (i.e. $\mathbf{v}_{u,lk} = \hat{\mathbf{f}}_{u,llk}$) in the UL and MFP (i.e. $\mathbf{v}_{d,ln} = \hat{\mathbf{f}}^*_{d,lln}$) in the DL in the following Lemma based on [53]:

Lemma 4.1. *The achievable sum UL-DL SE of a cellular FD-mMIMO system with MRC/MFP is*

$$\mathcal{R}^{FD}_{sum} = \frac{\tau - \tau_p}{\tau} \sum_{l=1}^{L} \left\{ \sum_{k \in \mathcal{U}_u} \log_2 \left(1 + \eta^{FD}_{u,lk}\right) + \sum_{n \in \mathcal{U}_d} \log_2 \left(1 + \eta^{FD}_{d,ln}\right) \right\}, \tag{4.26}$$

with the UL and DL SINRs being

$$\eta^{FD}_{u,lk} = \frac{N_r \sigma^2_{llk} \mathcal{E}_{u,lk}}{\mathtt{IBS}_{jk} + \mathtt{MUI}_{u,jk} + N_0}, \tag{4.27}$$

and

$$\eta_{d,ln}^{FD} = \frac{N_t^2 \kappa_{ln}^2 \mathcal{E}_{d,l} \sigma_{lln}^4}{\mathtt{IUI}_{ln} + \mathtt{MUI}_{d,ln} + N_0}, \tag{4.28}$$

respectively, with inter-BS interference ($\mathtt{IBS}_{jk}$), UL multi-user interference ($\mathtt{MUI}_{u,jk}$), inter-UE interference ($\mathtt{MUI}_{u,jk}$), and DL multi-user interference ($\mathtt{MUI}_{d,ln}$) being

$$\mathtt{IBS}_{jk} \triangleq N_t \sum_{j=1, j\neq l}^{L} \sum_{n \in \mathcal{U}_{j,d}} \kappa_{jn}^2 \mathcal{E}_{d,j} \rho_{lj} + N_t \sum_{n \in \mathcal{U}_{l,d}} \kappa_{ln}^2 \mathcal{E}_{d,l} \rho_{ll}, \tag{4.29a}$$

$$\mathtt{MUI}_{u,jk} \triangleq N_r \sum_{j=1, j\neq l}^{L} \sigma_{ljk}^2 \mathcal{E}_{u,jk} + \sum_{j=1}^{L} \sum_{k' \in \mathcal{U}_{j,u}} \beta_{ljk'} \mathcal{E}_{u,jk'} \tag{4.29b}$$

$$\mathtt{IUI}_{ln} \triangleq \sum_{j=1}^{L} \sum_{k' \in \mathcal{U}_{j,u}} \mathcal{E}_{u,lk'} \epsilon_{jk',ln} \tag{4.29c}$$

$$\mathtt{MUI}_{d,ln} \triangleq N_t^2 \sum_{j=1, j\neq l}^{L} \sigma_{jln}^2 \sigma_{lln}^2 \mathcal{E}_{d,j} \kappa_{jn}^2 + N_t \sum_{j=1}^{L} \sum_{k' \in \mathcal{U}_{j,d}} \beta_{jln} \sigma_{jjk'}^2 \mathcal{E}_{d,j} \kappa_{jk'}^2, \tag{4.29d}$$

respectively.

4.7 Numerical Results

In this section, we present numerical insights into the performance of DTDD-enabled HD-CF mMIMO systems. The UEs are dropped uniformly at random locations over a 1 km $\times$ 1 km area and are served by M HD-APs, depending on the AP-schedules obtained via Algorithm 6. The APs are arranged in a grid for fair comparison and maximal coverage [16, 20]. The path loss exponent and the reference distance from each AP are assumed to be -3.76 and 10 m, respectively [19]. The UL SNR is set by fixing the noise variance N_0 to unity and varying the UL powers $\mathcal{E}_{u,k}$ such that $\mathcal{E}_{u,k}/N_0$ equals the desired value. In the DL, we set $\kappa_{jn} = (N \sum_{k' \in \mathcal{U}_d} \alpha_{jk'}^2)^{-1}$ in (4.9), as in [19, 47]. For the cellular system, we partition the area into L equal-sized cells with an FD-mMIMO BS deployed at each of the cell centers, and each UE is served by its nearest BS. The results are obtained by averaging over 10^4 random UE location and channel instantiations.

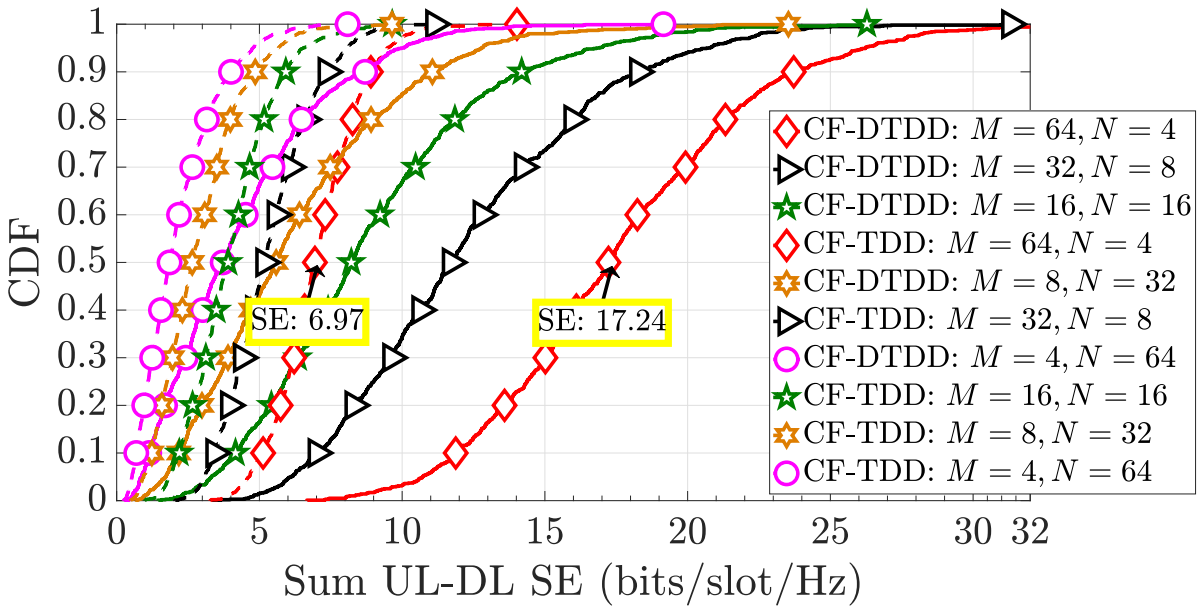

Figure 4.5: CDF of the sum UL-DL SE of DTDD CF-mMIMO and TDD CF-mMIMO with different AP/antenna configurations.

4.7.a Performance comparison with MRC & MFP:

In Figure 4.5 and Figure 4.6, we compare the performance of DTDD CF-mMIMO with TDD-based HD cellular and CF mMIMO, via the CDFs of the sum UL-DL SE. We consider $K = 32$ UEs with 50% of the UEs having UL data demand in each time slot. For each instantiation of UE positions, the APs are scheduled using the proposed greedy algorithm. In the cellular case, we consider $L = 8$, with the BS in each cell equipped with N antennas. For the HD TDD-CF and DTDD-enabled CF, we consider multiple combinations M and N. From Figure 4.5, we see that the DTDD-enabled CF-mMIMO system considerably improves the sum UL-DL SE compared to the other schemes. For example, CF-DTDD with $(M = 64, N = 4)$ offers a median sum UL-DL SE of 17 bits/slot/Hz, whereas TDD CF offers only 7 bits/slot/Hz. Next, in Figure 4.6, we compare DTDD CF-mMIMO with cellular TDD mMIMO. Cellular TDD with $(L = 8, N = 256)$ performs similar to DTDD CF-mMIMO with $(M = 16, N = 16)$; note that the antenna density in the cellular system is 8 times the antenna density of the CF system. DTDD schedules the APs based on the

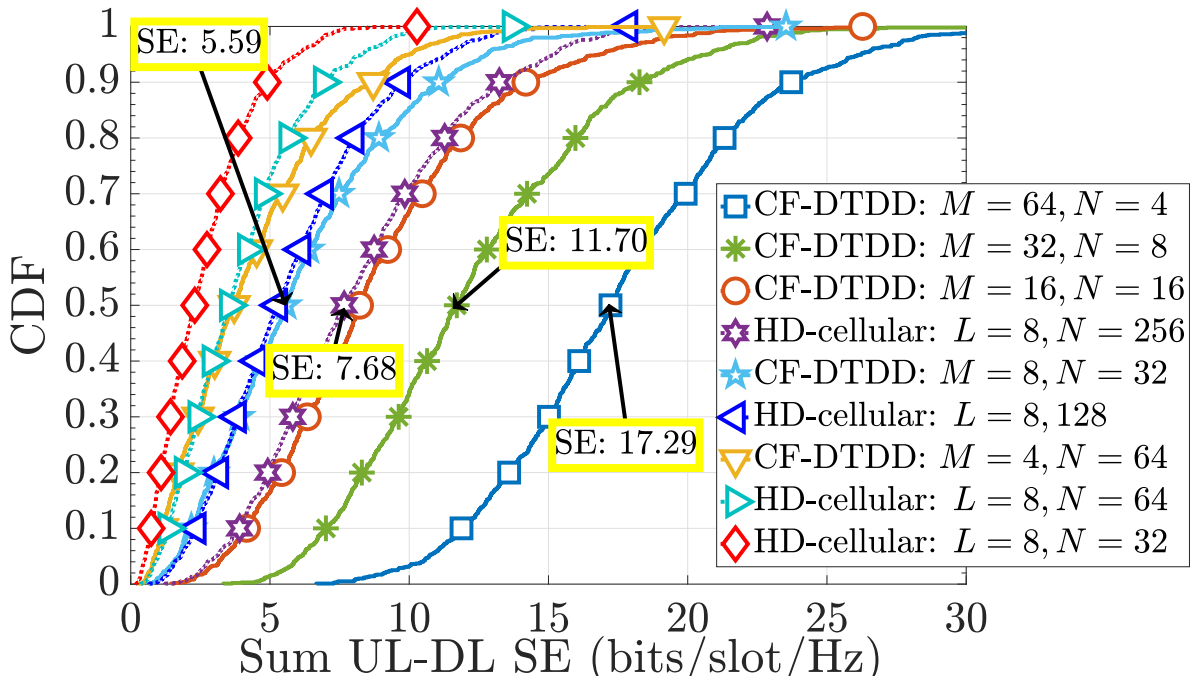

Figure 4.6: CDF of the sum UL-DL SE of DTDD CF-mMIMO and TDD enabled cellular mMIMO.

localized traffic demand, and the UL-DL transmissions occur simultaneously, which results in the dramatic improvement in the system sum UL-DL SE compared to cellular TDD.

Next, in Figure 4.7, we compare DTDD CF-mMIMO with an FD cellular system. CF-DTDD with HD APs and $(M = 16, N = 64)$ outperforms the cellular FD-system with double the antenna density, i.e., $(L = 16, N_t = N_r = 64)$. Increasing the number of APs, but still with half the antenna density compared to the FD (see the curve corresponding to $(M = 64, N = 16)$), results in significantly better sum UL-DL SE in HD CF-DTDD compared to the cellular FD system. Thus, although each BS in cellular system is equipped with simultaneous transmit and receive capability, the HD-APs with dynamic scheduling and the joint processing benefits of DTDD CF-mMIMO results in better sum UL-DL SE.

Next, we illustrate the dependence of the sum UL-DL SE on the data SNR. In Figure 4.8, we plot the average 90%-likely sum UL-DL SE as a function of the UL and DL data SNR. We observe that at low data SNR regime (-10 to 10 dB), an FD-cellular system with

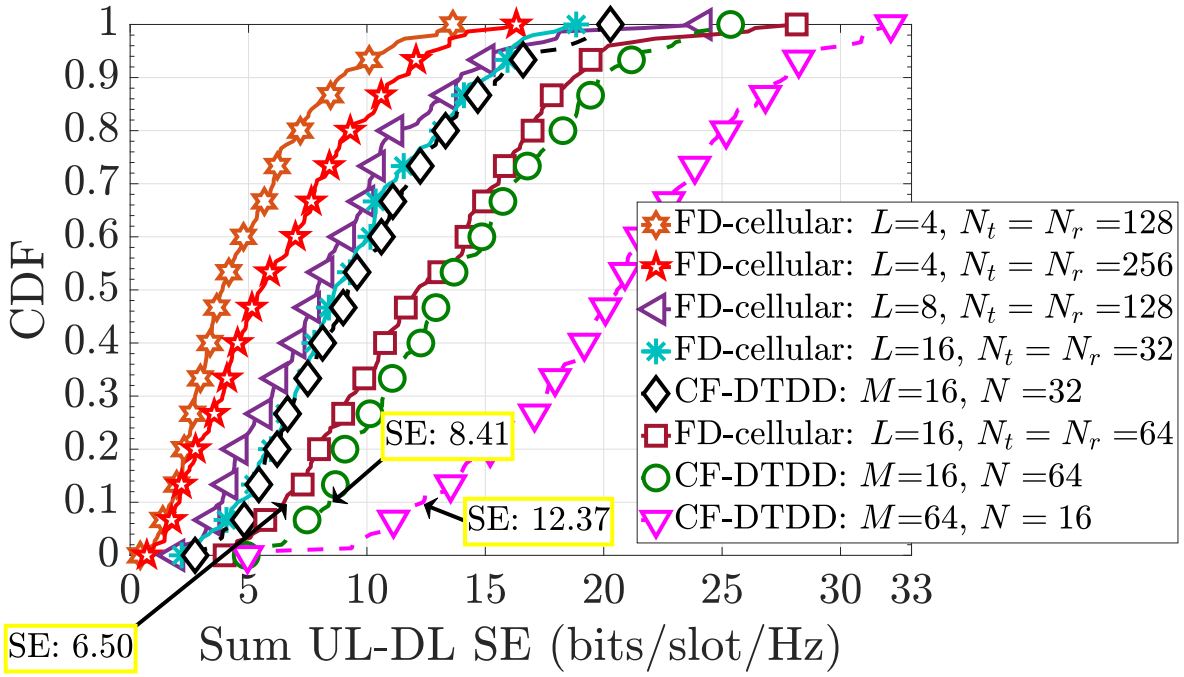

Figure 4.7: CDF of the sum UL-DL SE of a DTDD CF-mMIMO and a cellular FD-mMIMO system with $K = 32$ UEs.

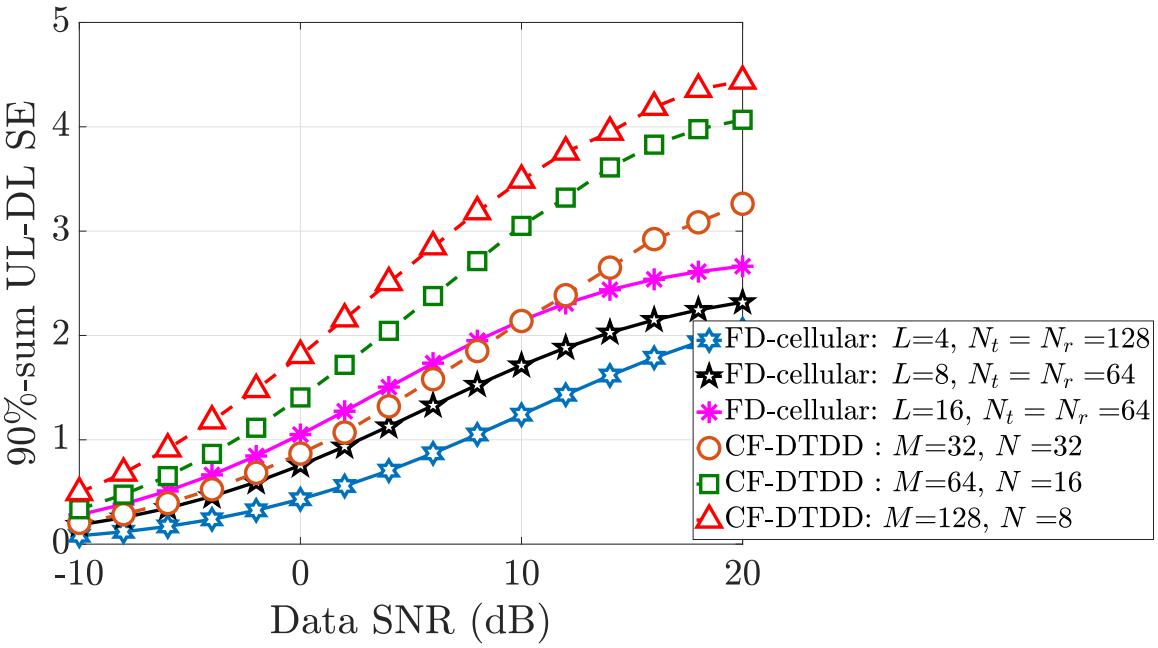

Figure 4.8: 90%-likely sum UL-DL SE vs. UL and DL data SNR, with $K = 60$ UEs.

$(L = 16, N_t = N_r = 64)$ offers similar 90%-likely UL-DL SE compared to the CF-DTDD system with half the antenna density $(M = 32, N = 32)$. Moreover, if we increase the number of APs deployed, for example, $(M = 64, N = 16), (M = 128, N = 8)$, CF-DTDD offers better performance throughout the entire range of data SNR. In both cases, for a given antenna density, having a larger number of BS/APs is better: the beamforming gains are insufficient to offset the path loss and interference.

In Figure 4.9 and Figure 4.10, we show the trade-off between the pilot length and the available data duration via plotting the 90%-likely sum UL-DL SE as a function of the ratio of the number of active UEs to the coherence interval. We consider two cases: (i) $\tau_p = 30$ irrespective of the number of UEs in the system (Figure 4.9), (ii) $\tau_p = K$, i.e., the pilot length is scaled linearly with the UE load (Figure 4.10). We consider the overall fractional UL-DL data demands to be the same across the number of UEs. In case (i), the sum UL-DL SE increases monotonically, even though there is pilot contamination in the system. This shows the effectiveness of the iterative pilot allocation algorithm presented in Section 2.3. However, in case (ii), the duration available for data transmission reduces, leading to a decrease in the SE as the number of UEs increases. For instance, in Figure 4.10, with $(M = 64, N = 2)$, the sum UL-DL SE decreases sharply when the UE load goes beyond 55% of the coherence interval. Thus, as the UE load increases, it is better to repeat shorter length pilots, along with a suitable algorithm to ensure minimal pilot contamination, to balance the errors introduced by pilot contamination with the data transmission duration.

Next in Figure 4.11, we investigate the effect of AP-AP and inter-BS CLI on the UL sum SE in CF and cellular mMIMO systems, respectively. Here, we fix the DL SNR to 10 dB for all UEs. We observe that in a cellular FD system, the UL sum SE reduces dramatically when the inter-BS CLI exceeds -40 dB. In contrast, in the DTDD-enabled HD CF-mMIMO system, as the AP-AP CLI increases, the greedy algorithm ensures an AP-schedule that balances the UL and DL SE to maximize the overall sum SE. For instance, with $(M = 32, N = 4)$, as CLI increases from -70 dB to -60 dB, we observe a decrease

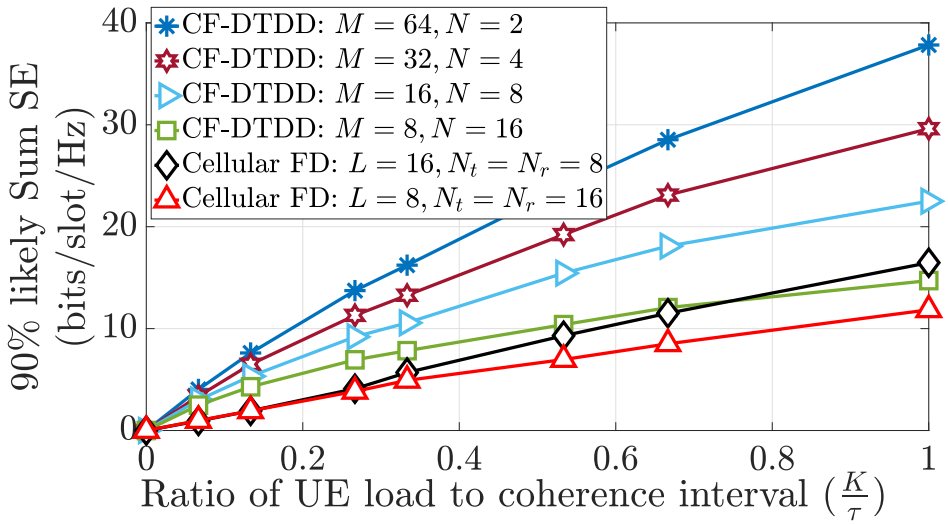

Figure 4.9: The 90%-likely sum UL-DL SE vs. the number of UEs, with $\tau_p = 30$, $\tau = 200$.

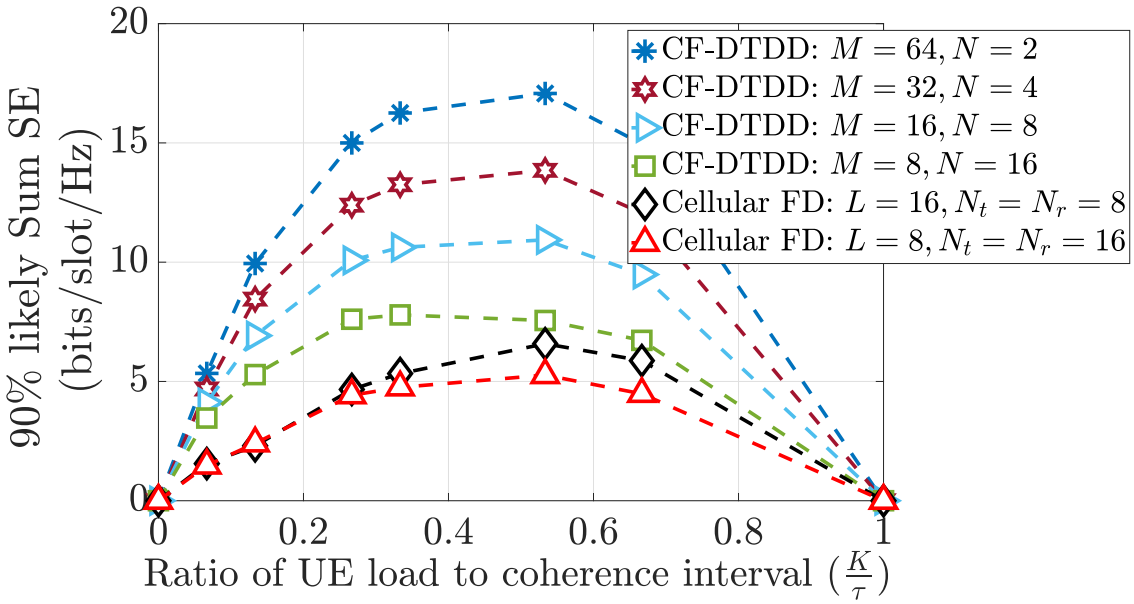

Figure 4.10: The 90%-likely sum UL-DL SE vs. the number of UEs, with $\tau_p = K$, $\tau = 200$.

in the UL SE, and beyond -20 dB, it saturates to about 5 bits/slot/Hz. In contrast, in an FD cellular system with $(L = 8, N_t = N_r = 16)$ the UL SE reduces to nearly 0 bits/slot/Hz at -20 dB of inter-BS CLI. Thus, HD-APs with DTDD are more resilient to SI cancellation errors. Also, the performance of the cellular FD-mMIMO in Figure 4.11 is

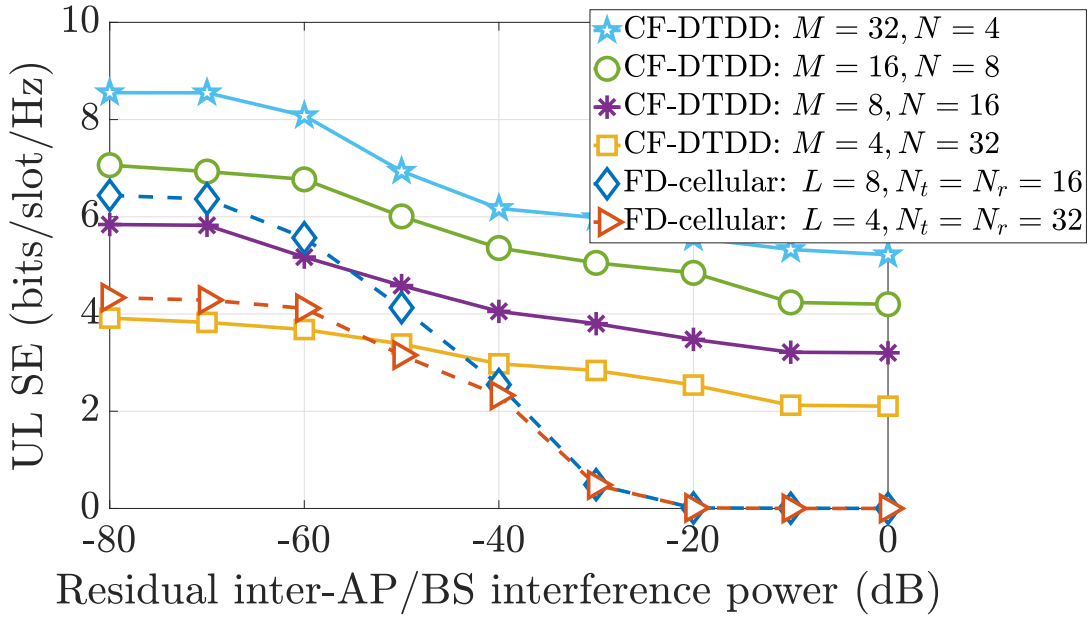

Figure 4.11: The average UL sum SE vs residual BS-BS/AP-AP CLI power. CF-mMIMO system with HD APs and DTDD is more resilient to CLI.

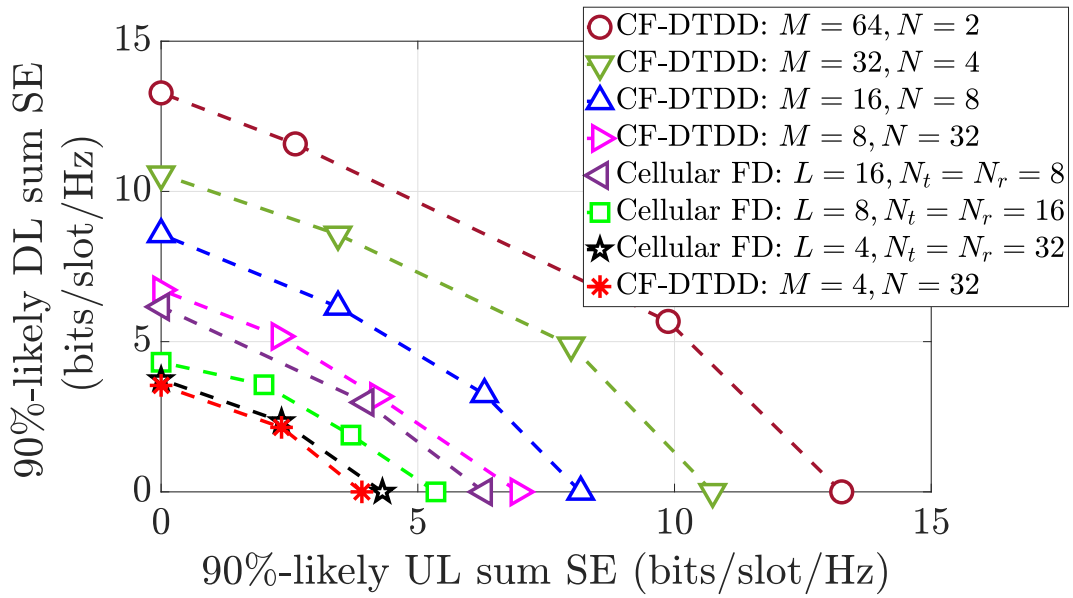

Figure 4.12: Rate region between 90%-likely UL sum SE vs. 90%-likely DL sum SE. We observe that more APs with smaller antennas provides larger rate regions compared to cellular FD systems.

an upper bound, since we consider perfect SI cancelation at the BSs.

In Figure 4.12, to illustrate the effect of the traffic demand on the UL and DL SE, we vary the fraction of UEs demanding UL data from 0 to 1, and plot the 90%-likely UL sum SE against the 90%-likely DL sum SE obtained for each fractional UL-data demand. At each fractional UL-data demand, we use Algorithm 6 to determine the mode of operation across the APs. We observe that the rate region attained by HD CF-DTDD is significantly larger than that of the cellular FD system, e.g., the HD CF-DTDD curve with $(M = 16, N = 8)$ and the FD-cellular curve with $(L = 16, N_t = N_r = 8)$. In fact, even with 100% UL data demand (the points along the x-axis) or 100% DL data demand (the points on the y-axis), HD CF-DTDD outperforms FD-cellular by more than 2 bits/slot/Hz. This is because the FD-cellular system has to contend with inter-cell interference, even if the SI cancelation is perfect. The joint data processing at the CPU and dynamic AP scheduling based on the UE data demands results in the larger rate region of the HD CF-DTDD mMIMO system.

4.7.b Performance comparison with MMSE & RZF:

In Figure 4.13, we compare the TDD-based canonical CF-mMIMO system with our proposed DTDD-enabled CF-mMIMO system. For both schemes, we consider a centralized MMSE combiner in the UL and RZF in the DL. DTDD CF-mMIMO with $(M = 64, N = 2)$ procures a sum UL-DL SE of 14.63 bits/slot/Hz, while in similar settings, the TDD-based CF-system only obtains 9.83 bits/slot/Hz. Thus, although MMSE-type combiners and precoders improve the SE of both TDD and DTDD-based systems, the simultaneous UL-DL data traffic handling capabilities of DTDD-based systems help further enhance the achievable sum UL-DL SE.

Next, we compare the performance of an FD-enabled cellular mMIMO system with the CF DTDD-based system. For the cellular case, we consider the multi-cell MMSE (M-MMSE) combiner and precoder [39]. From Figure 4.14, we observe that an FD cellular system with $(L = 16, N_t = N_r = 32)$ and a CF-DTDD system with $(M = 16, N = 32)$ have a similar CDF of the sum UL-DL SE, in spite of the CF-system having half the antenna

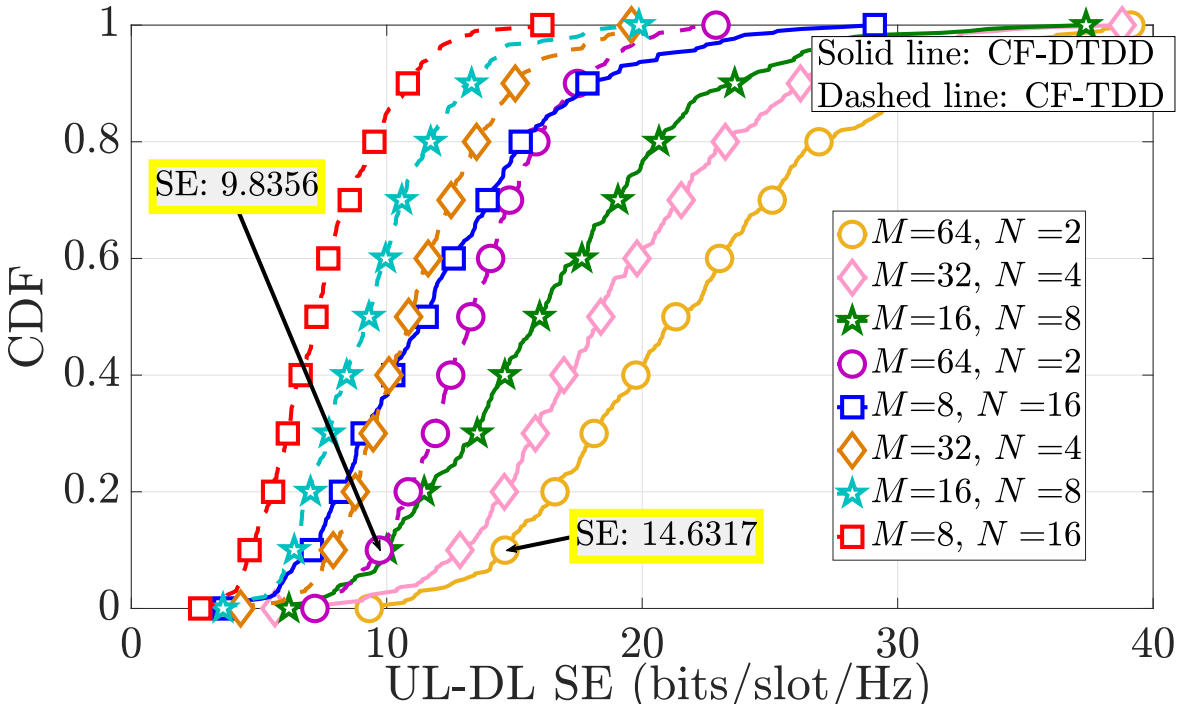

Figure 4.13: Comparison of DTDD CF-mMIMO and TDD based CF-mMIMO.

density as the FD system. Also, in the CF system, since the APs are HD, only a subset of the 16 APs serve the UL UEs, and its complement serves the DL APs. In contrast, all the 16 FD BS can simultaneously serve both UL and DL UEs in their respective cells. We further see that an FD-system with 4 BSs having 128 transmit and receive antennas each offers a 90% sum UL-DL SE of 13.2 bits/slot/Hz, whereas the CF-DTDD based system with $(M = 64, N = 8)$ offers 27 bits/slot/Hz, a more than 100% improvement. Although both FD cellular and CF-DTDD systems support simultaneous UL and DL traffic load, the joint signal processing capability at the CPU in the CF architecture helps to improve the sum UL-DL SE substantially.

4.8 Chapter Summary

In this chapter, we analyzed the performance of a CF-mMIMO system under DTDD, where the transmission mode at each HD AP is scheduled so that the sum UL-DL SE

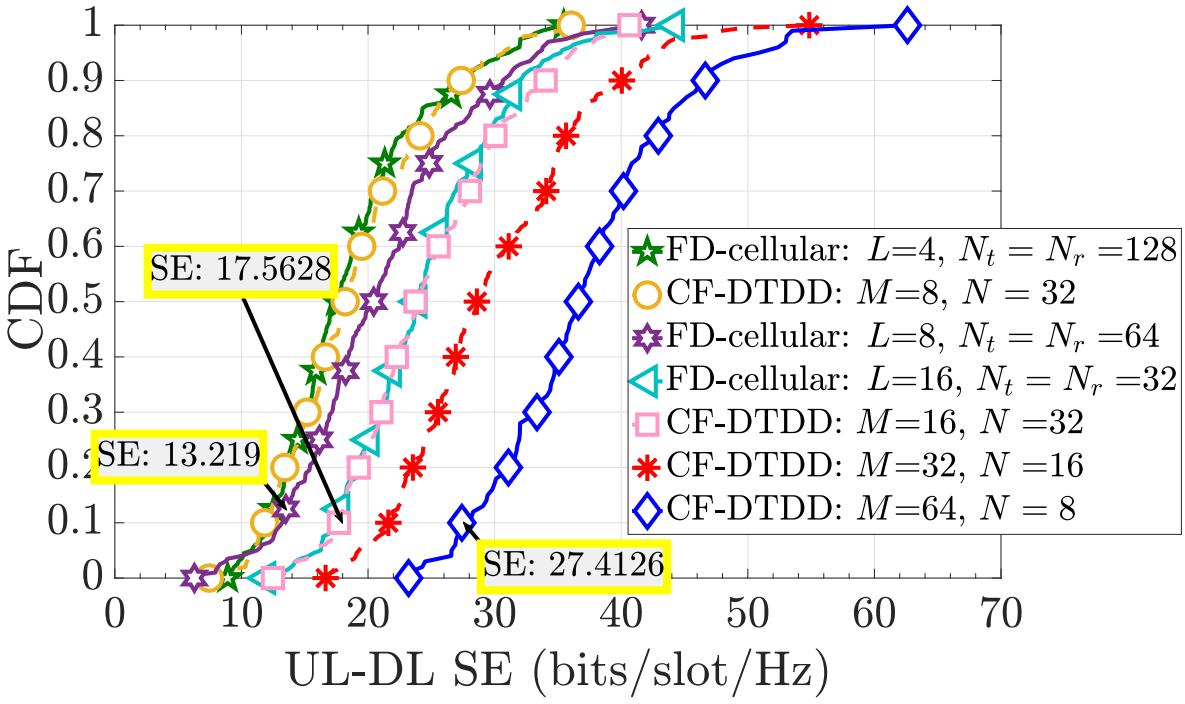

Figure 4.14: CDF of the sum UL-DL SE achieved via DTDD CF-MIMO and FD mMIMO systems.

is maximized. The complexity of the brute-force search increases exponentially with the number of APs. To tackle this problem, we developed a sub-modularity based greedy algorithm with associated optimality guarantees. Our numerical experiments revealed that a DTDD-enabled CF-mMIMO system substantially improves the sum UL-DL SE compared to HD TDD CF and HD TDD cellular mMIMO systems. The key reason for the performance improvement in DTDD compared to TDD-based systems is that the former duplexing scheme can simultaneously serve the UL and the DL UEs in the system. Furthermore, the HD DTDD CF-mMIMO can even outperform an FD-cellular mMIMO system. We numerically illustrated the sum SE improvement of DTDD CF-mMIMO over the cellular FD system under different antenna densities, number of UEs, and fractional UL/DL data demands. We considered the MRC/MFP-based scheme as well as the centralized MMSE/RZF-based scheme in both cellular and CF systems. Under all these different system settings, we showed that CF-DTDD with a large number of APs can

improve the sum UL-DL SE compared to an FD cellular system under similar antenna densities. Essentially, DTDD CF-mMIMO exploits the joint signal processing of a CF system coupled with the adaptive scheduling of UL-DL slots based on the localized traffic demands at the APs. A key advantage of DTDD-enabled CF over FD cellular is that we no longer need additional hardware at each AP to cancel the SI. The system performance can be further improved by incorporating UL-to-DL UE interference cancellation techniques or power control strategies, which will be addressed in the next chapter.

5 Can DTDD Cell-Free Outperform Full-Duplex Cell-Free?

Chapter Highlights

The previous two chapters analyzed DTDD CF systems considering maximal ratio (MR)-based comber & precoder and with fixed/equal UL-DL power allocation and then benchmarked the performance with TDD CF & cellular and FD cellular systems. In this chapter, we present a rigorous comparative study of HD APs with DTDD and FD APs in CF systems, considering different choices of combiners & precoders and UL-DL power control. DTDD and FD CF systems both support concurrent DL transmission and UL reception capability; but the sum UL-DL SE is limited by various CLIs, viz. InUI, InAI for both DTDD and FD systems, and, additionally, IrAI for an FD system. We derive the sum UL-DL SE in closed form, considering zero-forcing (ZF) combining and precoding along with the SINR optimal weighting at the CPU. Our derived UL/DL SEs reveal the effects of CLIs and power control coefficients on the overall system performance. We then present a provably convergent algorithm for joint UL-DL power allocation and UL/DL mode scheduling of the APs (for DTDD) to maximize the sum UL-DL SE. Further, we show that the proposed algorithms are precoder and combiner agnostic and come with closed-form update equations for the UL/DL power control coefficients. Our numerical results illustrate *the superiority of the proposed power control algorithms over several benchmark schemes and show that the sum UL-DL SE with DTDD can outperform an FD CF system with similar antenna density.* We also observe that with UL-DL power control, optimal weighting in the UL, and ZF combining & precoding, the sum UL-DL SE of the DTDD CF system can be substantially improved compared to the case when either equal power allocation is employed, or only apply weighted combining in the UL, considering MR-based combining & precoding (which was the case with previous two chapters). We conclude that DTDD combined with CF is a promising alternative to FD that attains the same performance using HD APs, thereby obviating the burden of IrAI cancellation.

5.1 Introduction

Wireless systems for 5G and beyond are required to serve an increasingly large number of UEs while supporting uniformly good QoS and high SE requirements. With this in mind, two potential physical layer solutions have been envisioned: (*i*) the capability to serve both UL and the DL UEs using the same time-frequency resources, thereby potentially doubling the sum UL-DL SE over conventional time/frequency division duplexing (T/FDD) systems, and (*ii*) distributed deployments of the remote radio units or APs for ubiquitous connectivity and high macro-diversity as opposed to a centralized MIMO cellular system. The key enablers of the above are: (*i*) the use of FD APs [53] or the use of DTDD with HD APs [33, 58, 84]; and (*ii*) CF-MIMO [16, 20, 85, 86]; respectively. This chapter presents a comparative performance analysis of FD and DTDD CF-MIMO[1] systems.

We note that, in CF systems, both FD and DTDD can enable simultaneous transmission (reception) to (from) HD UEs over the same time-frequency resources. However, CLIs, i.e., the InAI and InUI, limit the achievable SE in both systems. Additionally, in the FD system, the received signal at each AP is contaminated by its own transmitted signal, called *SI* [53], which we refer to as IrAI in the sequel. The cancellation of IrAI demands power-hungry and expensive hardware in addition to baseband signal processing overheads. However, if IrAI can be effectively canceled, in an FD-CF system, *all* the APs in the vicinity can assist in a given UE's transmission/reception, while in the DTDD system, only the subset of APs operating in UL (DL) can assist in decoding (precoding) the UE's data signal. On the other hand, as we will see, InAI is higher in an FD system, as *all* the APs interfere with the received signal at any AP. However, with DTDD, only the subset of APs operating in DL mode cause InAI at the APs operating in UL mode. Thus, which duplexing scheme is better and under what conditions is not clear. Answering this question via a careful theoretical analysis is the main aim of this chapter.

[1] DTDD CF and FD CF are also referred to as network-assisted full-duplex (NAFD) CF MIMO in the literature [87, 88].

5.1.a Literature review

CF, DTDD, and FD are all technologies that have received intense research attention over the past few years. The focus of this literature review is on studies that consider either DTDD or FD systems in the CF architecture. The analysis of the sum SE of a DTDD CF system with fully centralized processing was presented in [89]; however, with a pre-scheduled set of UL and DL APs. Further, in [87, 90], the authors addressed the AP-mode selection for DTDD-based CF-systems to maximize the UL/DL SEs, with power constraints at the UEs and APs. In [91], the authors considered a hybrid-duplex (both FD and HD APs) architecture, where antenna mode assignment at each multi-antenna AP is solved under the goal of secrecy SE maximization. Here, we note that [87,90,91] assume the availability of perfect CSI *at the CPU,* rather than the statistical/estimated CSI. Therefore, all resource allocation needs to be executed in the time scale of fast-fading coefficients. Moreover, the authors assumed a fully centralized CPU-based CF system. Thus, the APs must send the full channel state information to the CPU, incurring high front-haul overhead, especially when the numbers of APs and UEs are large, which is not scalable [17, 20]. In contrast, consideration of distributed processing, where precoding/combining is performed locally at the APs, is critical for scalable CF systems.

In [33], we presented a distributed processing-based sum UL-DL SE analysis with a low complexity algorithm for AP scheduling and fixed UL and DL power allocation, and this was the theme of the previous chapter. The contents of this chapter significantly extend the results presented in the previous chapter by considering MMSE/ZF precoding and combining at the APs and SINR-optimal combining at the CPU, joint UL-DL power allocation for sum UL-DL SE maximization, and comparing the performance against an FD system. A detailed comparison is presented in Table 5.1. Recently, the authors in [92] investigated the joint power UL-DL power allocation problem, assuming perfect CSI, in a DTDD CF system. The power allocation policy of [92] is derived for MRC and MFP, with equal weighting-based combining of the APs' signals at the CPU in the UL, which is

Chapters	Channel Estimation	Combiner & Precoder	UL & DL Power Control
Chapter 3	1. Perferect CSI 2. Orthogonal Pilots	MRC & MFP	Fixed or equal power allocation
Chapter 4	Pilot Contamination	1. MRC & MFP 2. MMSE/RZF (only via simulation)	Fixed or equal power allocation
Chapter 5	Pilot Contamination	1. MMSE Combiner & RZF Precoder 2. ZF Combiner & Precoder	UL and DL power control algorithms with FP and ADMM
Chapters	**Optimal Combining at the CPU**	**Comments on Algorithms**	**Key Message(s)**
Chapter 3	Only for the special case of perfect CSI and orthogonal pilots.	Sum SE is submodular with perfect InAI cancellation and optimal combining without pilot contamination.	DTDD CF outperforms TDD CF systems.
Chapter 4	Not considered (This chapter mainly focuses on the effects of pilot contamination and imperfect InAI cancellation.)	Product SINR is submodular after accounting for the effects of pilot contamination and InAI.	DTDD CF outperforms cellular FD systems.
Chapter 5	Considered	1. Sub-problems of UL and DL power controls are proven to converge. 2. Numerical validation of the convergence of overall alternating optimization.	1. DTDD CF outperforms FD CF system. 2. Power control coupled with optimal weighting at the CPU substantially improves compared to equal/fixed power allocation and equal weighting or optimal weighting.

Table 5.1: Comparative view of the results presented in this thesis.

suboptimal for CF [20]. Recently, the authors extended their work in [92] incorporating LSFD for the UL combining at the CPU [93]. However, the analyses in [93] assume the availability of orthogonal pilots for channel estimation and MRC/MFP for UL and DL data detection. Former can lead to inordinately high pilot overhead, and MRC/MFP are suboptimal choices for CF-system [20]. Thus, it is essential to consider ZF or MMSE-type combiners and precoders that are more robust to interference, which we address in this work.

On the other hand, the performance improvement achieved by FD APs over conventional TDD CF systems has been investigated in [24,94,95]. We conducted an expository study on the interplay of the CLIs and IrAI on the achievable SEs under DTDD and FD in [96], and this will be discussed later in this chapter as a special case. However, the results obtained were based on fixed power allocation and under the availability of perfect CSI. Now, finding a pilot allocation scheme in a CF system is challenging because multiple APs jointly serve the UEs in the area. Specifically, in contrast to a cellular system where only the serving AP

requires CSI from a given UE, in CF, accurate CSI is required at all the APs in the vicinity of the UE. The works that account for pilot allocation in DTDD CF systems consider either complex iterative algorithm [33], random allocation of pilots [89], or assume orthogonal pilots across all UEs [92]. Recent works on FD CF systems have also considered orthogonal pilots [24, 88, 97] or have analyzed the effect of pilot contamination by abstracting it as an additive channel error term in the channel estimate [95], which does not explicitly account for the pilot length, design or allocation across the UEs. Previously, in Section 2.4, in contrast to pilot allocation with predetermined pilot length [19, 22, 29, 31–33, 46, 49, 96], we optimized the pilot length and developed a low-complexity solution that incurs little signal processing overhead and is applicable in both DTDD and FD settings. Now, in this chapter, we analyze the effects of pilot contamination[2] on the sum UL-DL SE of the DTDD-enabled CF MIMO system and, subsequently, on the UL-DL power allocation strategies.

5.1.b Contributions

To the best of our knowledge, a comprehensive study of these two duplexing schemes accounting for practical issues such as pilot length optimization, optimal weighting at the CPU, interference canceling precoder and combiner design, AP scheduling, and UL/DL power allocation is not available in the literature. It is essential to account for these aspects because the critical bottleneck, namely, the CLIs of DTDD and FD, is heavily dependent on and can be controlled by these factors. In this regard, our analysis accounts for pilot contamination and, consequently, includes the effects of coherent interference on the optimal weights and sum UL-DL SE, which was missing in previous work [93]. Further, we provide closed-form expressions for the SE with ZF combiner and precoder

[2]Here, we note that the pilot allocation algorithm developed in Section 2.4, applies not only to TDD-based CF MIMO system but also to DTDD and FD CF systems. Convinced by the superior performance of the proposed pilot allocation algorithm, we will use the same method for channel estimation for this chapter.

and, subsequently, closed-form updates for all the power allocation algorithms developed. Our algorithms need to be executed only in the time scale of large-scale fading, which remains constant for several channel coherence intervals, in contrast to instantaneous CSI-based approaches in [87, 90, 91].

Our key contributions are:

1. We analyze the sum UL-DL SE considering MMSE combiners and regularized ZF (RZF) precoders. We also derive closed-form expressions for the sum UL-DL SE with ZF combiners and precoders (see Lemma 5.3 and Lemma 5.4). These expressions uncover the effects of InAI, IrAI, and InUI on the UL-DL SEs, and how power control and UL/DL scheduling of the APs (for DTDD) dictate the strengths of these CLIs. Also, in the UL, we present an SINR optimal weighting scheme, which ensures that the received SINR at the CPU is maximized (see Lemma 5.2).

2. Next, we focus on the sum UL-DL SE maximization with set constraints on the UL/DL APs and transmit power constraints on the APs and UEs. This problem of joint AP scheduling and power control is non-convex and NP-hard. We decouple it into two sub-problems.

   (a) We optimize the UL and DL power control coefficients for a given AP schedule. We solve this non-convex problem using fractional programming (FP)[3] that employs a series of equivalent convex reformulations. Further, closed-form solutions for the power allocation coefficients and associated auxiliary variables are derived using the alternating direction method of multipliers (ADMM)[4] in the case of DL and using an augmented Lagrange multiplier in the case of UL. Also,

[3]FP convexifies the non-convex cost function such that the optimal solution of the surrogate cost function and the original cost function is the same [98]. This is in contrast with the approach adopted in [92, 94], where the convex cost function is typically a lower bound of the original cost function and the algorithms optimize the lower bound.

[4]ADMM is an effective approach for reducing the computational cost in large dimensional problems compared to interior-point methods or general purpose solvers such as CVX or MOSEK [99].

in the UL, we observe considerable improvement in the proposed SINR optimal combining coupled with UL power control compared to existing benchmarks and when either of these two schemes is applied individually (see Figure 5.4). The resulting algorithms for each sub-problem are shown to converge to local optima (see Proposition 5.2 and Proposition 5.3). Finally, our proposed FP-based algorithms are precoder/combiner scheme agnostic, unlike [92, 93], and require fewer auxiliary variables, which makes our solutions widely applicable and scalable for large distributed systems.

(b) For AP scheduling, we develop a greedy AP mode (UL/DL) selection algorithm, where, at each iteration, we select the AP and the corresponding mode such that the incremental gain in the sum UL-DL SE is maximum. This pragmatic low-complexity approach solves an otherwise exponentially complex scheduling algorithm in polynomial time.

We perform extensive numerical experiments that reveal the superiority of the proposed pilot length optimization and pilot allocation scheme, the UL/DL power control algorithms, and the AP-scheduling algorithm over several existing schemes (see Figure 5.4 and Figure 5.5). Surprisingly, our results show that for the same number of APs and antenna density, DTDD procures a better sum UL-DL SE compared to an FD-enabled CF system. Specifically, the 90%-likely sum UL-DL SE of the DTDD CF system is 21% higher than that of the FD system under similar system parameters (see Figure 5.6). Further, we observe that even with double the antenna density, the performance of the FD system can be limited by InAI and IrAI, while DTDD is more resilient to InAI (see Figure 5.9). Thus, we can obtain the benefits of FD via DTDD itself, obviating the need for IrAI suppression at the APs.

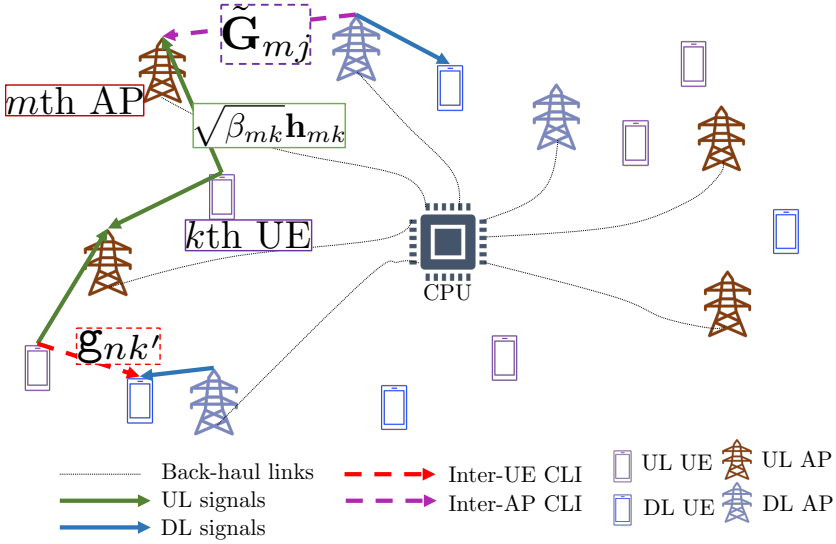

Figure 5.1: DTDD CF MIMO system: the overall system can serve UL and DL UEs simultaneously, forming a *virtual* FD system.

5.2 System Model

In the DTDD CF setup, M HD-APs, each equipped with N antennas, jointly and coherently serve a total of K single antenna UL and DL UEs using the same time-frequency resources. Let the sets $\mathcal{U}_{\mathsf{u}}$ and $\mathcal{U}_{\mathsf{d}}$ contain the indices of UL UEs and DL UEs, respectively, with $\mathcal{U}_{\mathsf{u}} \cap \mathcal{U}_{\mathsf{d}} = \emptyset$, $\mathcal{U}_{\mathsf{u}} \cup \mathcal{U}_{\mathsf{d}} = \mathcal{U}$, and $|\mathcal{U}| = K$. The UL channel from the kth UE to the mth AP is modeled as $\mathbf{f}_{mk} = \sqrt{\beta_{mk}}\mathbf{h}_{mk} \in \mathbb{C}^N$, where $\beta_{mk} > 0$ captures the effect of large scale fading and path-loss which remain unchanged over several channel coherence intervals and are known to the APs and the CPU [20]. The fast fading component, $\mathbf{h}_{mk} \sim \mathcal{CN}(\mathbf{0}_N, \mathbf{I}_N) \in \mathbb{C}^N$, is independent and identically distributed (i.i.d.) and is estimated at the APs using pilot signals at the beginning of each coherence block.

In the FD system, each AP is equipped with N_{tx} transmit and N_{rx} receive antennas. Let $\mathbf{f}_{\mathsf{u},mk} = \sqrt{\beta_{\mathsf{u},mk}}\mathbf{h}_{\mathsf{u},mk} \in \mathbb{C}^{N_{\mathsf{rx}}}$ and $\mathbf{f}_{\mathsf{d},mn} = \sqrt{\beta_{\mathsf{d},mn}}\mathbf{h}_{\mathsf{d},mn} \in \mathbb{C}^{N_{\mathsf{tx}}}$ be the UL channel between the receive antenna array of the mth AP to kth UL UE and the DL channel between the transmit antenna array of the mth AP to the nth DL UE, respectively. Here, $\beta_{\mathsf{i},mk}$ and $\mathbf{h}_{\mathsf{i},mk}$, $\mathsf{i} = \{\mathsf{u}, \mathsf{d}\}$, corresponds to the fast and slow fading components of the UL and the

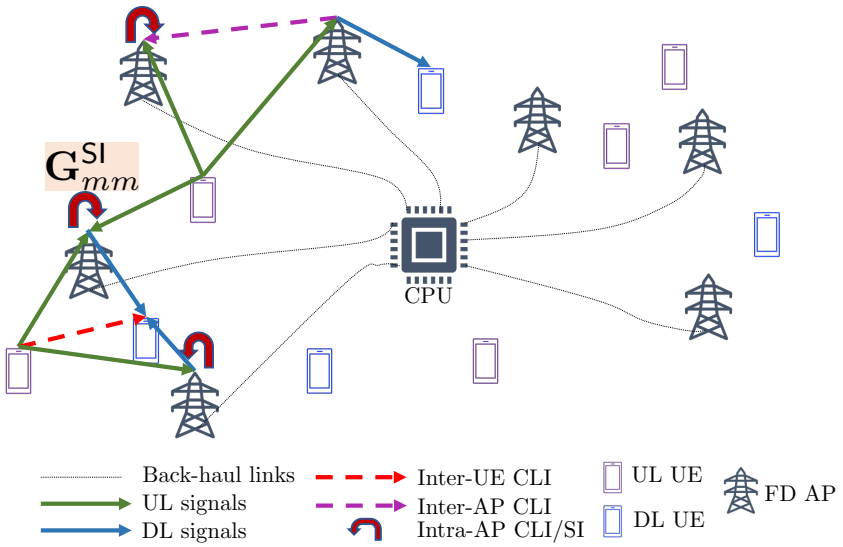

Figure 5.2: FD-enabled CF system: each AP can serve both UL and DL UEs; however, the APs suffer from IrAI.

DL channels, respectively, and follow similar statistical modeling as in the DTDD system.

The inter-AP channels remain constant for several coherence intervals and are mostly line-of-sight (LoS), whose CSI can be made available to the CPU before the pilot and data transmission phase. Thus, the overhead of inter-AP channel estimation does not affect the available data transmission duration. However, the inter-AP CSI at the CPU may be erroneous, which we model using Gaussian distributed additive noise as per [24, 33, 53]. Specifically, the inter-AP channel from the jth DL AP to the mth UL AP is denoted by $\tilde{\mathbf{G}}_{mj} \in \mathbb{C}^{N \times N}$ whose elements are i.i.d. $\mathcal{CN}(0, \zeta^{\mathsf{InAI}}_{mj})$. Here $\zeta^{\mathsf{InAI}}_{mj}$ captures the effects of both the large scale fading and the power of the residual InAI.

For FD CF, IrAI at each AP can be suppressed via active SI cancelation and antenna isolation. It has been argued that the residual IrAI follows the Rayleigh distribution [100]. Following this, we model mth AP's residual IrAI channel between the transmit and the receive antenna links as $\mathbf{G}^{\mathsf{SI}}_{mm} \sim \mathcal{CN}(0, \zeta^{\mathsf{SI}}_{mm})$, where the residual IrAI ζ^{SI}_{mm} depends on the interference suppression capability of the hardware [95, 97].

Finally, let g_{nk} denote the channel between kth UL UE and the nth DL UE, modeled as $\mathcal{CN}(0, \epsilon_{nk})$, and is independent across all UEs [33, 53]. The channel modeling discussed

above is illustrated in Figure 5.1 and Figure 5.2.

5.2.a Problem Statement

Having described the system model, we now present the key problems considered in this chapter. As illustrated in Figure 5.1 and Figure 5.2, the performance of both DTDD and FD is affected by CLIs, viz. InAI, IrAI (for FD), and InUI. Now, the strengths of these CLIs, as we shall see in Section 5.3, depend on the estimated UL/DL channel statistics, choice of precoder and combiners, and, most critically, on the UL and DL power allocation strategies. Further, in DTDD, we get the additional flexibility to schedule the APs' UL/DL modes, which can reduce InAI. Keeping these in mind, our goal is to maximize the achievable sum UL-DL SE under these two duplexing schemes.[5] In this regard, we pose and address the following problems: (*i*) Allocation of pilot signals that can ensure no contamination in the APs in the vicinity of every UE while using a minimum number of orthogonal pilots; (*ii*) design of combiners and precoders at the APs and the CPU to reduce interference; (*iii*) AP scheduling in the UL/DL modes for DTDD; and (*iv*) UL/DL power allocation policies for DTDD and FD to maximize the sum UL-DL SE. We begin with channel estimation and pilot allocation in the next section.

Remark 5.1. *Typically, the CPU consists of multiple cores with a multi-threaded software architecture capable of processing UL and DL data simultaneously for DTDD and FD. Essentially, the DL threads are run on a subset of the cores at the CPU, and the UL threads are run using a different set of cores.*

5.2.b Channel Estimation and Pilot Allocation

The UL channel estimation has been discussed in detail in Chapter 2. Here, we briefly recapitulate the same in the context of DTDD and FD CF-mMIMO systems. This will

[5] In [16], the authors point out that since a distributed CF system is inherently fair, additionally requiring fairness degrades the sum SE without an appreciable improvement in the fairness criterion. Thus, we consider the sum UL-DL SE as the metric to be maximized.

also help us follow the latter contents.

5.2.b.i DTDD CF

During the channel estimation phase, the UL and DL UEs synchronously send UL pilot sequences to the APs. The APs use the received pilot signals to estimate the channels between the UEs and the APs. Now, allocating orthogonal pilot sequences to all the UEs can incur inordinately high channel estimation overhead. Therefore, we consider that pilot length is constrained to be τ_p, where $\tau_p \leq K$, and these pilot sequences are reused among the UEs. Let $\mathcal{P} = \{\boldsymbol{\varphi}_1, \boldsymbol{\varphi}_2, \ldots, \boldsymbol{\varphi}_{\tau_p}\}$ be the set of orthonormal pilot sequences, where $\boldsymbol{\varphi}_l \in \mathbb{C}^{\tau_p}$. Let $l(k)$ denote the index of the pilot used by the kth UE and $\mathcal{P}_{l(k)}$ denote the set of UE indices, including the kth UE, that use $\boldsymbol{\varphi}_{l(k)}$. Therefore, $\langle \boldsymbol{\varphi}_{l(k)}, \boldsymbol{\varphi}_{l(k')} \rangle = 1$, if $k' \in \mathcal{P}_{l(k)}$, and equals to 0 if $k' \notin \mathcal{P}_{l(k)}$. Let $\mathcal{E}_{p,k}$ be the power of the pilot signal of the kth UE. We can show that the MMSE estimate of the channel $\mathbf{f}_{mk}$, denoted by $\hat{\mathbf{f}}_{mk}$ [101, see Chapter 12], is distributed as $\hat{\mathbf{f}}_{mk} = \sqrt{\tau_p \mathcal{E}_{p,k}} \beta_{mk} c_{mk} \mathbf{y}_{p,m}$, with $c_{mk} \triangleq (\tau_p \mathcal{E}_{p,k} \beta_{mk} + \tau_p \sum_{n \in \mathcal{P}_{l(k)} \setminus k} \mathcal{E}_{p,n} \beta_{mn} + N_0)^{-1}$. Further, $\hat{\mathbf{f}}_{mk} \sim \mathcal{CN}(\mathbf{0}_N, \alpha_{mk}^2 \mathbf{I}_N)$, with $\alpha_{mk}^2 = c_{mk} \tau_p \mathcal{E}_{p,k} \beta_{mk}^2$. The estimation error, denoted by $\tilde{\mathbf{f}}_{mk} \triangleq \mathbf{f}_{mk} - \hat{\mathbf{f}}_{mk}$, is distributed as $\mathcal{CN}(\mathbf{0}_N, \bar{\alpha}_{mk}^2 \mathbf{I}_N)$, with $\bar{\alpha}_{mk} \triangleq \sqrt{\beta_{mk} - \alpha_{mk}^2}$, and $\tilde{\mathbf{f}}_{mk}$ is uncorrelated with $\hat{\mathbf{f}}_{mk}$ due to orthogonality principle.

5.2.b.ii FD CF

For the FD system, all UEs transmit pilots in the UL direction, and we estimate the channels between the UEs and every AP's *transmit* and *receive* antennas using these UL pilots. The DL precoders are later designed using channel reciprocity, which obviates the need for separate DL training [24, 53, 97]. Similar to the DTDD case, the estimated UL channel $\hat{\mathbf{f}}_{\mathsf{u},mk}$ follows $\mathcal{CN}(\mathbf{0}, \alpha_{\mathsf{u},mk}^2 \mathbf{I}_N)$, with $\alpha_{\mathsf{u},mk}^2 = \tau_p \mathcal{E}_{p,k} \beta_{\mathsf{u},mk}^2 c_{\mathsf{u},mk}$ and

$$c_{\mathsf{u},mk}^{-1} = \tau_p \mathcal{E}_{p,k} \beta_{\mathsf{u},mk} + \tau_p \sum_{n \in \mathcal{P}_{l(k)} \setminus k} \mathcal{E}_{p,n} \beta_{\mathsf{u},mn} + N_0.$$

The estimated DL channel $\hat{\mathbf{f}}_{\mathsf{d},mn}$ follows $\mathcal{CN}(\mathbf{0}_N, \alpha^2_{\mathsf{d},mn}\mathbf{I}_N)$, with $\alpha^2_{\mathsf{d},mn} = \tau_p \mathcal{E}_{p,n} \beta^2_{\mathsf{d},mn} c_{\mathsf{d},mn}$ and

$$c^{-1}_{\mathsf{d},mn} = \tau_p \mathcal{E}_{p,n} \beta_{\mathsf{d},mn} + \tau_p \sum_{n' \in \mathcal{P}_{l(n)} \setminus n} \mathcal{E}_{p,n'} \beta_{\mathsf{d},mn'} + N_0.$$

The UL/DL channel estimation error $\tilde{\mathbf{f}}_{\mathsf{i},mn}$ follows $\mathcal{CN}(\mathbf{0}_N, \bar{\alpha}^2_{\mathsf{i},mn}\mathbf{I}_N)$, with

$$\bar{\alpha}_{\mathsf{i},mn} \triangleq \sqrt{\beta_{\mathsf{i},mn} - \alpha^2_{\mathsf{i},mn}},$$

where $\mathsf{i} \in \{\mathsf{u}, \mathsf{d}\}$.

We illustrated the frame structure for channel estimation in FD and DTDD systems in Figure 4.1a. For pilot allocation, the readers are referred to Section 2.4. This chapter focuses on the effect of pilot allocation policy on the sum UL-DL SE of DTDD and FD CF-MIMO system.

5.3 Spectral Efficiency Analysis: CF DTDD

This section presents the UL and DL signaling model and derives closed-form expressions for the sum UL-DL SE, which we further use for AP scheduling and power allocation. Let the sets $\mathcal{A}_\mathsf{u}$ and $\mathcal{A}_\mathsf{d}$ contain the indices of the APs scheduled in the UL and DL, respectively. In a DTDD system, the APs are HD. Thus, $\mathcal{A}_\mathsf{u} \cap \mathcal{A}_\mathsf{d} = \emptyset$. Also, let $\mathcal{A}_\mathsf{s} \triangleq \mathcal{A}_\mathsf{u} \cup \mathcal{A}_\mathsf{d} \subseteq \mathcal{A}$.

5.3.a Analysis with MMSE combiner & RZF precoder

In the UL, the kth UE ($k \in \mathcal{U}_\mathsf{u}$) sends the symbol $s_{\mathsf{u},k}$ with power $\mathcal{E}_{\mathsf{u},k}$. The data symbol of each UE is modeled as zero mean, unit variance, and $\mathbb{E}[s_{\mathsf{u},k} s^*_{\mathsf{u},k'}] = 0, k' \neq k, \forall k, k' \in \mathcal{U}_\mathsf{u}$. The signal received at the mth UL AP can be expressed as

$$\mathbf{y}_{\mathsf{u},m} = \sum_{n \in \mathcal{U}_\mathsf{u}} \sqrt{\mathcal{E}_{\mathsf{u},n}} \mathbf{f}_{mn} s_{\mathsf{u},n} + \sum_{j \in \mathcal{A}_\mathsf{d}} \tilde{\mathbf{G}}_{mj} \mathbf{x}_{\mathsf{d},j} + \mathbf{w}_{\mathsf{u},m} \in \mathbb{C}^N, \tag{5.1}$$

where $\mathbf{x}_{\mathsf{d},j} = \sqrt{\mathcal{E}_\mathsf{d}} \mathbf{P}_j \mathsf{diag}(\boldsymbol{\kappa}_j) \mathbf{s}_\mathsf{d} = \sqrt{\mathcal{E}_\mathsf{d}} \left[\mathbf{p}_{j1}, \ldots, \mathbf{p}_{j|\mathcal{U}_\mathsf{d}|}\right] \mathsf{diag}(\boldsymbol{\kappa}_j) \mathbf{s}_\mathsf{d}$ is the transmitted DL data vector with $\mathcal{E}_\mathsf{d}$ being the total radiated power, $\mathbf{p}_{jn} = [\mathbf{P}_j]_{:,n} \in \mathbb{C}^N$ being the precoding

matrix for the nth DL UE, and $\boldsymbol{\kappa}_j \triangleq [\kappa_{j1}, \kappa_{j2}, \ldots, \kappa_{j|\mathcal{U}_\mathsf{d}|}]^T$ being the vector of power control coefficients, all at the jth DL AP. Here, κ_{jn}, i.e., the nth element of $\boldsymbol{\kappa}_j$, indicates the fraction of power dedicated by the jth AP to the nth DL UE ($n \in \mathcal{U}_\mathsf{d}$). The DL signal vector $\mathbf{s}_\mathsf{d} = \left[s_{\mathsf{d},1}, \ldots, s_{\mathsf{d},|\mathcal{U}_\mathsf{d}|}\right]^T$ follows $\mathbb{E}\left[\mathbf{s}_\mathsf{d}\mathbf{s}_\mathsf{d}^H\right] = \mathbf{I}_{|\mathcal{U}_\mathsf{d}|}$. Finally, $\mathbf{w}_{\mathsf{u},m} \sim \mathcal{CN}(\mathbf{0}_N, N_0\mathbf{I}_N)$ is the additive noise. Each AP pre-processes the received signals using local combiners and sends them to the CPU for joint decoding, which is important for the scalability of the overall system [20]. Let $\mathbf{v}_{mk} \in \mathbb{C}^N$ be the local combining vector at the mth AP for kth UE's UL data stream. Then, the local estimate of the kth UE's signal at the mth AP becomes

$$\hat{s}_{\mathsf{u},mk} = \sqrt{\mathcal{E}_{\mathsf{u},k}}\mathbf{v}_{mk}^H\mathbf{f}_{mk}s_{\mathsf{u},k} + \sum_{n\in\mathcal{U}_\mathsf{u}\setminus k}\sqrt{\mathcal{E}_{\mathsf{u},n}}\mathbf{v}_{mk}^H\mathbf{f}_{mn}s_{\mathsf{u},n} + \sqrt{\mathcal{E}_\mathsf{d}}\sum_{j\in\mathcal{A}_\mathsf{d}}\sum_{n\in\mathcal{U}_\mathsf{d}}\kappa_{jn}\mathbf{v}_{mk}^H\tilde{\mathbf{G}}_{mj}\mathbf{p}_{jn}s_{\mathsf{d},n} + \mathbf{v}_{mk}^H\mathbf{w}_{\mathsf{u},mk}. \quad (5.2)$$

To design $\mathbf{v}_{mk}$, the AP utilizes the knowledge of $\hat{\mathbf{f}}_{mk}, \forall k \in \mathcal{U}_\mathsf{u}$, so that the MSE of the locally estimated signal is minimized, i.e., $\mathbf{v}_{mk}^{\mathsf{opt.}} = \min_{\mathbf{v}_{mk}\in\mathbb{C}^N} \mathbb{E}\left[|s_{\mathsf{u},k} - \mathbf{v}_{mk}^H\mathbf{y}_{\mathsf{u},m}|^2|\hat{\mathbf{f}}_{mk}\right]$. Thus, the optimal combiner is $\mathbf{v}_{mk}^{\mathsf{opt.}} = \mathbf{R}_{mk}^{-1}\hat{\mathbf{f}}_{mk}$, where

$$\mathbf{R}_{mk} = \Big(\sum_{k\in\mathcal{U}_\mathsf{u}}\mathcal{E}_{\mathsf{u},k}\hat{\mathbf{f}}_{mk}\hat{\mathbf{f}}_{mk}^H + \sum_{k\in\mathcal{U}_\mathsf{u}}\mathcal{E}_{\mathsf{u},k}\mathbb{E}[\tilde{\mathbf{f}}_{mk}\tilde{\mathbf{f}}_{mk}^H] + \mathcal{E}_\mathsf{d}\sum_{j\in\mathcal{A}_\mathsf{d}}\sum_{n\in\mathcal{U}_\mathsf{d}}\kappa_{jn}^2\mathbb{E}[\tilde{\mathbf{G}}_{mj}\mathbf{p}_{jn}\mathbf{p}_{jn}^H\tilde{\mathbf{G}}_{mj}^H] + N_0\mathbf{I}_N\Big). \quad (5.3)$$

Next, these locally estimated signals relayed from the APs are linearly combined at the CPU with combining weights being $\omega_{mk}, \forall m \in \mathcal{A}_\mathsf{u}, \forall k \in \mathcal{U}_\mathsf{u}$ so that the received SINR at the CPU for each UE is maximized. This is illustrated in Figure 5.3. Thus, the kth stream of the received signal at the CPU is

$$\hat{s}_{\mathsf{u},k} = \sqrt{\mathcal{E}_{\mathsf{u},k}}\sum_{m\in\mathcal{A}_\mathsf{u}}\omega_{mk}^*\mathbf{v}_{mk}^H\mathbf{f}_{mk}s_{\mathsf{u},k} + \sum_{n\in\mathcal{U}_\mathsf{u}\setminus k}\sqrt{\mathcal{E}_{\mathsf{u},n}}\sum_{m\in\mathcal{A}_\mathsf{u}}\omega_{mk}^*\mathbf{v}_{mk}^H\mathbf{f}_{mn}s_{\mathsf{u},n} + \sum_{m\in\mathcal{A}_\mathsf{u}}\omega_{mk}^*\sum_{j\in\mathcal{A}_\mathsf{d}}\sqrt{\mathcal{E}_\mathsf{d}}\sum_{n\in\mathcal{U}_\mathsf{d}}\kappa_{jn}\mathbf{v}_{mk}^H\tilde{\mathbf{G}}_{mj}\mathbf{p}_{jn}s_{\mathsf{d},n} + \sum_{m\in\mathcal{A}_\mathsf{u}}\omega_{mk}^*\mathbf{v}_{mk}^H\mathbf{w}_{\mathsf{u},mk}. \quad (5.4)$$

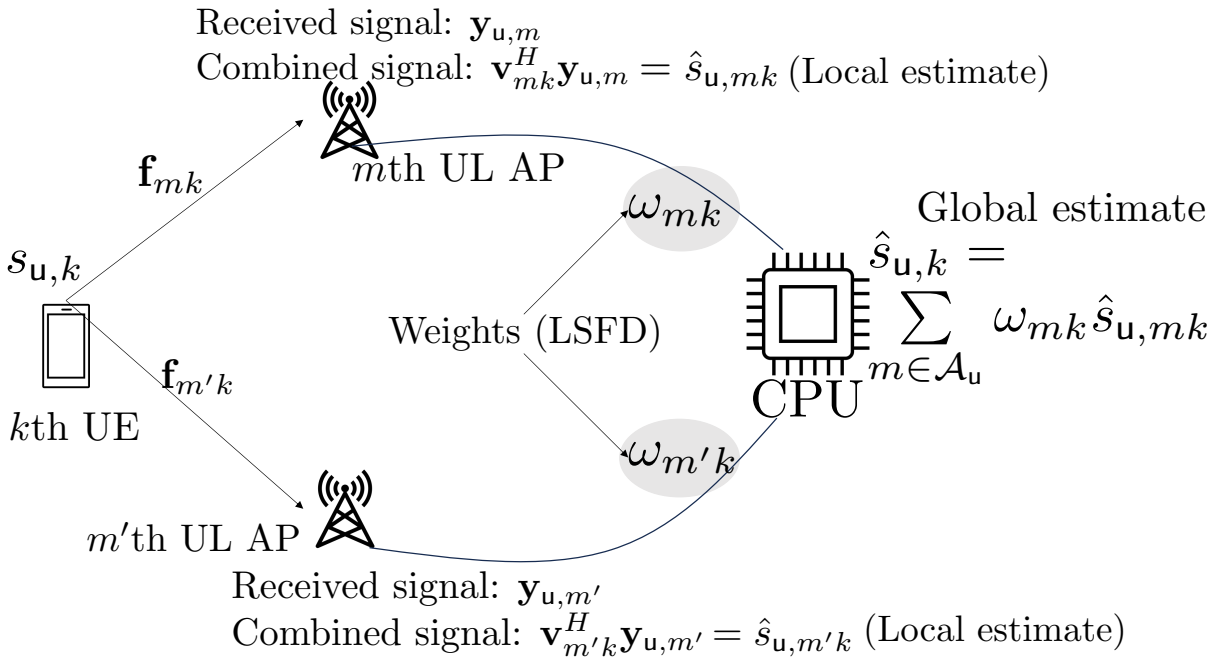

Figure 5.3: Optimal weighting at the CPU.

Then the UL SINR of the kth UE, denoted by $\eta_{\mathsf{u},k}$, at the CPU is equal to [20]

$$\frac{\mathcal{E}_{\mathsf{u},k} |\boldsymbol{\omega_k}^H \mathbb{E}[\mathbf{u}_{kk}]|^2}{\boldsymbol{\omega_k}^H \left(\sum\limits_{i \in \mathcal{U}_\mathsf{u}} \mathcal{E}_{\mathsf{u},i} \mathbb{E}[\mathbf{u}_{ki} \mathbf{u}_{ki}^H] - \mathcal{E}_{\mathsf{u},k} \mathbb{E}[\mathbf{u}_{kk}] \mathbb{E}[\mathbf{u}_{kk}^H] + \sum\limits_{n \in \mathcal{U}_\mathsf{d}} \mathbb{E}[\mathbf{a}_{kn} \mathbf{a}_{kn}^H] + \mathbf{N}_{\mathsf{eff.}} \right) \boldsymbol{\omega_k}}, \tag{5.5}$$

where $\boldsymbol{\omega_k} \triangleq [\omega_{1k}, \omega_{2k}, \ldots, \omega_{|\mathcal{A}_\mathsf{u}|k}]^T \in \mathbb{C}^{|\mathcal{A}_\mathsf{u}|}$, $\mathbf{u}_{ki} \triangleq [\mathbf{v}_{1k}^H \mathbf{f}_{1i}, \mathbf{v}_{2k}^H \mathbf{f}_{2i}, \ldots, \mathbf{v}_{|\mathcal{A}_\mathsf{u}|k}^H \mathbf{f}_{|\mathcal{A}_\mathsf{u}|i}]^T \in \mathbb{C}^{|\mathcal{A}_\mathsf{u}|}$, $[\mathbf{a}_{kn}]_m = \sum\limits_{j \in \mathcal{A}_\mathsf{d}} \sqrt{\mathcal{E}_\mathsf{d}} \kappa_{jn} \mathbf{v}_{mk}^H \tilde{\mathbf{G}}_{mj} \mathbf{p}_{jn}$, and $\mathbf{N}_{\mathsf{eff.}} = N_0 \mathtt{diag}(\mathbb{E}[\|\mathbf{v}_{1k}\|^2], \ldots, \mathbb{E}[\|\mathbf{v}_{|\mathcal{A}_\mathsf{u}|k}\|^2]) \in \mathbb{C}^{|\mathcal{A}_\mathsf{u}| \times |\mathcal{A}_\mathsf{u}|}$. We evaluate the optimal weights using the following lemma.

Lemma 5.1. *The SINR of the kth ($k \in \mathcal{U}_\mathsf{u}$) UE is maximized by* $\boldsymbol{\omega}_k^{\mathsf{opt.}} = \mathsf{c}_k \sqrt{\mathcal{E}_{\mathsf{u},k}} \mathbf{R}_{\omega,k}^{-1} \mathbb{E}[\mathbf{u}_{kk}]$, *where*[6]

$$\mathbf{R}_{\omega,k} \triangleq \left(\sum_{i \in \mathcal{U}_\mathsf{u}} \mathcal{E}_{\mathsf{u},i} \mathbb{E}[\mathbf{u}_{ki} \mathbf{u}_{ki}^H] - \mathcal{E}_{\mathsf{u},k} \mathbb{E}[\mathbf{u}_{kk}] \mathbb{E}[\mathbf{u}_{kk}^H] + \sum_{n \in \mathcal{U}_\mathsf{d}} \mathbb{E}[\mathbf{a}_{kn} \mathbf{a}_{kn}^H] + \mathbf{N}_{\mathsf{eff.}} \right), \tag{5.6}$$

[6] *We use the fact that for any given vector* $\mathbf{x} \in \mathbb{C}^N$ *and a positive definite matrix* $\mathbf{A}$, $\max_{\mathbf{y} \in \mathbb{C}^N} [|\mathbf{y}^H \mathbf{x}|^2 / (\mathbf{y}^H \mathbf{A} \mathbf{y})] = \mathbf{x}^H \mathbf{A} \mathbf{x}$, *and* $\mathbf{y}^{\mathsf{opt.}} = \mathbf{A}^{-1} \mathbf{x}$.

and c_k *is a scaling constant and can be taken as* $\sqrt{\mathcal{E}_{\mathsf{u},k}}$ *to make the weights dimensionless. Also, the maximum SINR is* $\mathcal{E}_{\mathsf{u},k}\mathbb{E}[\mathbf{u}_{kk}^H]\mathbf{R}_{\omega,k}^{-1}\mathbb{E}[\mathbf{u}_{kk}]$.

In the DL, the counterpart of the MMSE combiner is the RZF precoder, which is

$$\mathbf{p}_{jn} = \mathcal{E}_{\mathsf{d},n}\left(\sum_{n'\in\mathcal{U}_\mathsf{d}} \mathcal{E}_{\mathsf{d},n'}\hat{\mathbf{f}}_{jn'}\hat{\mathbf{f}}_{jn'}^H + \sum_{n'\in\mathcal{U}_\mathsf{d}} \mathcal{E}_{\mathsf{d},n'}\mathbb{E}\left[\tilde{\mathbf{f}}_{jn'}\tilde{\mathbf{f}}_{jn'}^H\right] + N_0\mathbf{I}_N\right)^{-1}\hat{\mathbf{f}}_{jn}. \tag{5.7}$$

Assuming channel reciprocity, the signal received at the nth ($n \in \mathcal{U}_\mathsf{d}$) DL UE can be written as

$$r_{\mathsf{d},n} = \sum_{j\in\mathcal{A}_\mathsf{d}} \kappa_{jn}\sqrt{\mathcal{E}_\mathsf{d}}\mathbf{f}_{jn}^T\mathbf{p}_{jn}s_{\mathsf{d},n} + \sum_{k\in\mathcal{U}_\mathsf{u}} \sqrt{\mathcal{E}_{\mathsf{u},k}}\mathsf{g}_{nk}s_{\mathsf{u},k} + \sum_{j\in\mathcal{A}_\mathsf{d}}\sum_{q\in\mathcal{U}_\mathsf{d}\setminus n} \kappa_{jq}\sqrt{\mathcal{E}_\mathsf{d}}\mathbf{f}_{jn}^T\mathbf{p}_{jq}s_{\mathsf{d},q} + w_{\mathsf{d},n}. \tag{5.8}$$

The AWGN $w_{\mathsf{d},n}$ follows $\mathcal{CN}(0, N_0)$. Now, the corresponding DL SINR, denoted by $\eta_{\mathsf{d},n}$, becomes

$$\eta_{\mathsf{d},n} = \frac{\mathcal{E}_\mathsf{d}|\boldsymbol{\kappa}_n^T\mathbb{E}[\mathbf{d}_{nn}]|^2}{\left(\begin{array}{c}\mathcal{E}_\mathsf{d}\mathtt{var}\{\boldsymbol{\kappa}_n^T\mathbf{d}_{nn}\} + \mathcal{E}_\mathsf{d}\sum\limits_{q\in\mathcal{U}_\mathsf{d}\setminus n}\mathbb{E}[|\boldsymbol{\kappa}_q^T\mathbf{d}_{nq}|^2] \\ + \sum\limits_{k\in\mathcal{U}_\mathsf{u}}\mathcal{E}_{\mathsf{u},k}\mathbb{E}|\mathsf{g}_{nk}|^2 + N_0\end{array}\right)}, \tag{5.9}$$

where $\boldsymbol{\kappa}_n \triangleq [\kappa_{1n}, \kappa_{2n}, \ldots, \kappa_{|\mathcal{A}_\mathsf{d}|n}]^T$ and $\mathbf{d}_{nq} \triangleq [\mathbf{f}_{1n}^T\mathbf{p}_{1q}, \mathbf{f}_{2n}^T\mathbf{p}_{2q}, \ldots, \mathbf{f}_{|\mathcal{A}_\mathsf{d}|n}^T\mathbf{p}_{|\mathcal{A}_\mathsf{d}|q}]^T$. The DL power control coefficients, $\boldsymbol{\kappa}_n$, are the weights assigned to the signal transmitted to each UE from every AP, which can be controlled to maximize the sum SE.

We use results from random matrix theory to derive closed-form expressions for the SINRs. Often such formulae involve computations of iterative inverses from which it is difficult to derive intuitive understandings. We present the expressions for the case of ZF precoders and combiners. Our analysis includes not only the effects of CLIs but also coherent interference, unlike [93], where MRC and MFP are considered without accounting for the effects of pilot contamination.

5.3.b Analysis with ZF combiner & precoder

We first construct the ZF combining and precoding matrices. As $\tau_p < K$, the concatenated estimated channel matrix at mth UL AP, denoted by $\hat{\mathbf{F}}_{\mathsf{u},m} = [\hat{\mathbf{f}}_{m1}, \ldots, \hat{\mathbf{f}}_{m|\mathcal{U}_\mathsf{u}|}] \in \mathbb{C}^{N \times |\mathcal{U}_\mathsf{u}|}$, may not have full column rank, i.e., $\hat{\mathbf{F}}_{\mathsf{u},m}^H \hat{\mathbf{F}}_{\mathsf{u},m}$ may not be invertible. Thus, we construct a full rank matrix as $\mathbf{Z}_{\mathsf{u},m} \triangleq \mathbf{Y}_{p,m}\boldsymbol{\Phi} \in \mathbb{C}^{N \times \tau_p}$, where $\boldsymbol{\Phi}$ is the pilot matrix with its lth column being $\boldsymbol{\varphi}_l$ and $\mathbf{Y}_{p,m}$. We observe that we can compute $\hat{\mathbf{f}}_{mk}$ from $\mathbf{Z}_{\mathsf{u},m}$ using the relation $\hat{\mathbf{f}}_{mk} = c_{mk}\sqrt{\tau_p \mathcal{E}_{p,k}}\beta_{mk}\mathbf{Z}_{\mathsf{u},m}\mathbf{e}_{l(k)}$, where $\mathbf{e}_{l(k)} \in \mathbb{C}^{\tau_p}$ is the standard basis with $l(k)$th coordinate being 1.[7] Then, the ZF combining vector intended for the kth UE at the mth AP becomes $\mathbf{v}_{mk} = \gamma_{mk}\mathbf{Z}_{\mathsf{u},m}(\mathbf{Z}_{\mathsf{u},m}^H \mathbf{Z}_{\mathsf{u},m})^{-1}\mathbf{e}_{l(k)}$, where we set $\gamma_{mk} = \sqrt{\tau_p \mathcal{E}_{p,k}}\beta_{mk}$ to ensure that $\mathbb{E}[\mathbf{v}_{mk}^H \hat{\mathbf{f}}_{mk}] = \alpha_{mk}^2$. In the DL, we again construct a full rank matrix $\mathbf{Z}_{\mathsf{d},j} = \mathbf{Y}_{p,j}\boldsymbol{\Phi} \in \mathbb{C}^{N \times \tau_p}$, $\forall j \in \mathcal{A}_\mathsf{d}$. We can obtain $\hat{\mathbf{f}}_{jn}$ from $\mathbf{Z}_{\mathsf{d},j}$ as $\hat{\mathbf{f}}_{jn} = c_{jn}\sqrt{\tau_p \mathcal{E}_{p,j}}\beta_{jn}\mathbf{Z}_{\mathsf{d},j}\mathbf{e}_{l(n)}$. Next, the ZF precoding vector (unit normalized) intended for the nth DL UE at the jth AP is $\mathbf{p}_{jn} = \dfrac{\mathbf{Z}_{\mathsf{d},j}\left(\mathbf{Z}_{\mathsf{d},j}^H \mathbf{Z}_{\mathsf{d},j}\right)^{-1}\mathbf{e}_{l(n)}}{\sqrt{\mathbb{E}\left[\|\mathbf{Z}_{\mathsf{d},j}\left(\mathbf{Z}_{\mathsf{d},j}^H \mathbf{Z}_{\mathsf{d},j}\right)^{-1}\mathbf{e}_{l(n)}\|^2\right]}}$. Using [102, Lemma 6], we can show that $\mathbb{E}\left[\|\mathbf{Z}_{\mathsf{d},j}(\mathbf{Z}_{\mathsf{d},j}^H \mathbf{Z}_{\mathsf{d},j})^{-1}\mathbf{e}_{l(n)}\|^2\right] = \dfrac{c_{jn}}{N - \tau_p}$.[8] Next, we present closed-form expressions for the optimal weights and UL-DL SINRs with ZF combiners and precoders.

Lemma 5.2. *The optimal weights for the kth UE's data stream at the CPU for $|\mathcal{A}_\mathsf{u}|$ UL APs is $\boldsymbol{\omega}_k^{\mathsf{opt}} = \mathcal{E}_{\mathsf{u},k}\mathbf{R}_{\omega,k}^{-1}\bar{\mathbf{u}}_k$, with $\bar{\mathbf{u}}_k = \left[\alpha_{1k}^2, \alpha_{2k}^2, \ldots, \alpha_{|\mathcal{A}_\mathsf{u}|k}^2\right]^T$ and*

$$\mathbf{R}_{\omega,k} = \sum_{k' \in \mathcal{P}_{l(k)} \setminus k} \mathcal{E}_{\mathsf{u},k'}\bar{\mathbf{u}}_{k'}\bar{\mathbf{u}}_{k'}^H + \frac{1}{N - \tau_p}\dot{\mathbf{R}}_{\omega,k} + \frac{\mathcal{E}_\mathsf{d}}{N - \tau_p}\ddot{\mathbf{R}}_{\omega,k}, \tag{5.10}$$

[7] Here, we recapitulate that kth UE uses the pilot sequence $\boldsymbol{\varphi}_{l(k)}$, and the set $\mathcal{P}_{l(k)}$ contains all the UE indices, including the kth UE, which use the pilot sequence $\boldsymbol{\varphi}_{l(k)}$. Thus, multiplying $\mathbf{Z}_{\mathsf{u},m}$ by $\mathbf{e}_{l(k)}$, we obtain a common estimate for the channels of all UEs which use the pilot sequence $\boldsymbol{\varphi}_{l(k)}$.

[8] Thus, the condition $N \geq (\tau_p + 1)$ has to be satisfied. Each AP has τ_p combining and precoding vectors, and the same vector is utilized for all UEs sharing the same pilot sequence.

where $\dot{\mathbf{R}}_{\omega,k}$ *and* $\ddot{\mathbf{R}}_{\omega,k} \in \mathbb{C}^{|\mathcal{A}_\mathsf{u}|\times|\mathcal{A}_\mathsf{u}|}$ *are two diagonal matrices with* m*th diagonal entries*

$$\left[\dot{\mathbf{R}}_{\omega,k}\right]_m = \sum_{k'\in\mathcal{U}_\mathsf{u}} \mathcal{E}_{\mathsf{u},k'}\alpha_{mk}^2(\beta_{mk'} - \alpha_{mk'}^2) + N_0\alpha_{mk}^2, \tag{5.11}$$

and

$$\left[\ddot{\mathbf{R}}_{\omega,k}\right]_m = \sum_{j\in\mathcal{A}_\mathsf{d}} N\kappa_{jn}^2\zeta_{mj}^{\mathsf{InAI}}\alpha_{mk}^2, \tag{5.12}$$

respectively.

Proof. See Appendix D.1. ■

Later, in Figure 5.4, we illustrate the correctness of the above lemma by matching the UL SE obtained using the weights computed from the above lemma with the sum UL SE obtained from Lemma 5.1 by averaging the expectations over channel realizations. We next provide an explicit closed-form expression for the UL SE, applicable for any choice of weights.

Lemma 5.3. *The UL SINR of the* k*th UE with ZF-combining can be written as*

$$\eta_{\mathsf{u},k} = \frac{(N-\tau_p)\mathcal{E}_{\mathsf{u},k}\left(\sum_{m\in\mathcal{A}_\mathsf{u}}\omega_{mk}^*\alpha_{mk}^2\right)^2}{\mathtt{EST}_{\mathsf{u},k} + \mathtt{MUI}_{\mathsf{u},k} + \mathtt{IAP}_k + N_0\sum_{m\in\mathcal{A}_\mathsf{u}}|\omega_{mk}^*|^2\alpha_{mk}^2}, \tag{5.13}$$

where $\mathtt{EST}_{\mathsf{u},k}$, $\mathtt{MUI}_{\mathsf{u},k}$ *and* $\mathtt{IAP}_k$ *capture the error due to channel estimation, multi-UE interference from the pilot sharing UEs, and inter-AP CLI. These are respectively evaluated as*

$$\mathtt{EST}_{\mathsf{u},k} = \sum_{k'\in\mathcal{U}_\mathsf{u}}\mathcal{E}_{\mathsf{u},k'}\sum_{m\in\mathcal{A}_\mathsf{u}}|\omega_{mk}^*|^2\alpha_{mk}^2(\beta_{mk'} - \alpha_{mk'}^2), \tag{5.14a}$$

$$\mathtt{MUI}_{\mathsf{u},k} = (N-\tau_p)\sum_{i\in\mathcal{P}_{l(k)}\setminus k}\mathcal{E}_{\mathsf{u},i}\left(\sum_{m\in\mathcal{A}_\mathsf{u}}\omega_{mk}^*\alpha_{mi}^2\right)^2, \tag{5.14b}$$

$$\mathtt{IAP}_k = N\sum_{n\in\mathcal{U}_\mathsf{d}}\sum_{m\in\mathcal{A}_\mathsf{u}}\sum_{j\in\mathcal{A}_\mathsf{d}}\mathcal{E}_\mathsf{d}\kappa_{jn}^2\zeta_{mj}^{\mathsf{InAI}}|\omega_{mk}^*|^2\alpha_{mk}^2. \tag{5.14c}$$

Proof. Follows by using similar techniques as the proof of Lemma 5.2. ■

Note that the above result is also valid when equal weights are applied at the CPU, i.e., $\omega_{mk} = \frac{1}{|\mathcal{A}_{\mathsf{u}}|}, \forall k, \forall m$. However, as will be shown in Figure 5.4, optimal weighting yields significantly improved sum SE compared to equal weighting. Next, we present the DL SINR with ZF precoding.

Lemma 5.4. *The DL SINR of the nth UE with ZF precoding is*

$$\eta_{\mathsf{d},n} = \frac{(N-\tau_p)\mathcal{E}_{\mathsf{d}} \left(\sum\limits_{j \in \mathcal{A}_{\mathsf{d}}} \alpha_{jn} \kappa_{jn} \right)^2}{\mathtt{EST}_{\mathsf{d},n} + \mathtt{MUI}_{\mathsf{d},n} + \mathtt{IUE}_n + N_0}, \tag{5.15}$$

where $\mathtt{EST}_{\mathsf{d},n}$, $\mathtt{MUI}_{\mathsf{d},n}$, *and* $\mathtt{IUE}_n$ *capture the interference due to channel estimation error, the DL multi-UE interference from pilot sharing UEs, and the UL UE to DL UE CLI. These are respectively evaluated as*

$$\mathtt{EST}_{\mathsf{d},n} = \sum_{q \in \mathcal{U}_{\mathsf{d}}} \sum_{j \in \mathcal{A}_{\mathsf{d}}} \mathcal{E}_{\mathsf{d}} \kappa_{jq}^2 (\beta_{jn} - \alpha_{jn}^2), \tag{5.16a}$$

$$\mathtt{MUI}_{\mathsf{d},n} = (N-\tau_p)\mathcal{E}_{\mathsf{d}} \sum_{q \in \mathcal{P}_{l(n)} \setminus n} \left(\sum_{j \in \mathcal{A}_{\mathsf{d}}} \kappa_{jq} \alpha_{jn} \right)^2, \tag{5.16b}$$

$$\mathtt{IUE}_n = \sum_{k \in \mathcal{U}_{\mathsf{u}}} \mathcal{E}_{\mathsf{u},k} \epsilon_{nk}. \tag{5.16c}$$

Proof. See Appendix D.2. ■

Lemma 5.3 and Lemma 5.4 explicitly capture the dependence of the SINRs on the UL-DL power control coefficients and underlying UL-DL AP sets. Thus, the sum UL-DL SE, given by (5.17) below, too, depends on the choice of these parameters.

$$\mathcal{R}_{\mathsf{s}}(\mathcal{A}_{\mathsf{s}}, \boldsymbol{\kappa}, \boldsymbol{\mathcal{E}}_{\mathsf{u}}) = \frac{\tau - \tau_p}{\tau} \left[\sum_{k \in \mathcal{U}_{\mathsf{u}}} \log[1 + \eta_{\mathsf{u},k}] + \sum_{n \in \mathcal{U}_{\mathsf{d}}} \log[1 + \eta_{\mathsf{d},n}] \right], \tag{5.17}$$

where $\boldsymbol{\kappa} \triangleq [\boldsymbol{\kappa}_1^T, \ldots, \boldsymbol{\kappa}_n^T, \ldots, \boldsymbol{\kappa}_{|\mathcal{U}|_{\mathsf{d}}}^T]^T \in \mathbb{C}^{|\mathcal{U}_{\mathsf{d}}||\mathcal{A}_{\mathsf{d}}|}$ (recall $\boldsymbol{\kappa}_n = [\kappa_{1n}, \kappa_{2n}, \ldots, \kappa_{|\mathcal{A}_{\mathsf{d}}|n}]^T$), $\boldsymbol{\mathcal{E}}_{\mathsf{u}} \triangleq [\mathcal{E}_{\mathsf{u},1}, \ldots, \mathcal{E}_{\mathsf{u},|\mathcal{U}_{\mathsf{u}}|}] \in \mathbb{C}^{|\mathcal{U}_{\mathsf{u}}|}$, and $\mathcal{A}_{\mathsf{s}} = \mathcal{A}_{\mathsf{u}} \cup \mathcal{A}_{\mathsf{d}} \subseteq \mathcal{A}$. Next, we optimize $\boldsymbol{\kappa}$, $\boldsymbol{\mathcal{E}}_{\mathsf{u}}$, and find a

schedule for UL/DL APs in $\mathcal{A}_{\mathsf{s}}$ to maximize $\mathcal{R}_{\mathsf{s}}(.)$.

5.4 Joint Scheduling and Power Control

Here, we aim to solve the following problem:

$$\max_{\{\mathcal{A}_{\mathsf{s}},\kappa_{jn},\mathcal{E}_{\mathsf{u},k}\}} \quad \mathcal{R}_{\mathsf{s}}\left(\mathcal{A}_{\mathsf{s}},\boldsymbol{\kappa},\boldsymbol{\mathcal{E}}_{\mathsf{u}}\right) \tag{5.18a}$$

$$\text{subject to} \quad \mathcal{A}_{\mathsf{u}} \cup \mathcal{A}_{\mathsf{d}} = \mathcal{A}_{\mathsf{s}} \subseteq \mathcal{A}; \mathcal{A}_{\mathsf{u}} \cap \mathcal{A}_{\mathsf{d}} = \emptyset; \tag{5.18b}$$

$$0 \leq \mathcal{E}_{\mathsf{u},k} \leq \mathcal{E}_{\mathsf{u}}, \forall k \in \mathcal{U}_{\mathsf{u}}; \tag{5.18c}$$

$$\sum_{q \in \mathcal{U}_{\mathsf{d}}} \kappa_{jq}^2 \leq 1, \forall j \in \mathcal{A}_{\mathsf{d}}. \tag{5.18d}$$

With $\mathcal{R}_{\mathsf{s}}(\cdot)$ given by (5.17), the above problem is non-convex and NP-hard. We next present our solution.

5.4.a AP-scheduling

Let us define $\overline{\mathcal{R}}_{\mathsf{s}}\left(\mathcal{A}_{\mathsf{s}}\right) = \max\limits_{\kappa_{jn},\mathcal{E}_{\mathsf{u},k}} \quad \mathcal{R}_{\mathsf{s}}\left(\mathcal{A}_{\mathsf{s}},\boldsymbol{\kappa},\boldsymbol{\mathcal{E}}_{\mathsf{u}}\right)$ as the sum UL-DL SE attained via optimizing the power allocation coefficients when the underlying set of APs is $\mathcal{A}_{\mathsf{s}} = \mathcal{A}_{\mathsf{u}} \cup \mathcal{A}_{\mathsf{d}}$. Now, the UL and DL power control coefficients for a sub-set of APs, $\mathcal{A}_{\mathsf{s}}$, may not be optimal when we add one more AP in either UL or DL, say $\{j_{\mathsf{mode}}\}, \mathsf{mode} \in \{\mathsf{u},\mathsf{d}\}$, to $\mathcal{A}_{\mathsf{s}}$. Thus, we need to reoptimize the power control coefficients for $\mathcal{A}_{\mathsf{s}} \cup \{j_{\mathsf{mode}}\}$. The following proposition holds when we optimize the power control coefficients for both $\mathcal{A}_{\mathsf{s}}$ and $\mathcal{A}_{\mathsf{s}} \cup \{j_{\mathsf{mode}}\}$.

Proposition 5.1. *For two sets of scheduled UL and DL APs, $\mathcal{A}_{\mathsf{s}}$ and $\mathcal{A}_{\mathsf{t}}$, where $\mathcal{A}_{\mathsf{s}} \subseteq \mathcal{A}_{\mathsf{t}}$, $\overline{\mathcal{R}}_{\mathsf{s}}\left(\mathcal{A}_{\mathsf{s}}\right) \leq \overline{\mathcal{R}}_{\mathsf{s}}\left(\mathcal{A}_{\mathsf{t}}\right)$, where, for both $\mathcal{A}_{\mathsf{s}}$ and $\mathcal{A}_{\mathsf{t}}$, the UL and DL power control coefficients are optimized to maximize the sum UL-DL SE.*

Thus, $\overline{\mathcal{R}}_{\mathsf{s}}\left(\mathcal{A}_{\mathsf{s}}\right)$ is a monotonically non-decreasing function of the underlying scheduled AP set. Motivated by this, we schedule APs one-by-one, where, at each iteration, we schedule

an AP and its associated mode such that incremental gain in the (optimized) sum UL-DL SE is maximized. Thus, we can apply Algorithm 5 in this case, with a caveat that now we optimize the power control coefficients in each iteration. Our algorithm procures the AP schedule in polynomial time ($\mathcal{O}(M)$), whereas exhaustive search-based AP scheduling requires optimization of the sum UL-DL SEs over all 2^M AP configurations, which is not a scalable approach. Such greedy approaches have been previously used in the antenna selection literature [77] exploiting the monotonicity of the utility metric.

We next address the power control problem given an AP schedule $\mathcal{A}_{\mathsf{s}}$. Now, as the UL power control coefficients affect the DL SE via inter-UE CLI and the DL power control coefficients affect the UL SE via inter-AP CLI, the joint optimization of UL-DL sum SE is still a non-convex and prohibitively complex task. In the next subsections, we present an alternating optimization approach, where we optimize the DL power control coefficients to maximize the DL sum SE given the UL power control coefficients and vice-versa until convergence.

5.4.b Uplink power control

First, we note that the UL power control coefficients influence the sum UL-DL SE predominantly via the sum UL SE. This is because, although the InUE term in the sum DL SE depends on UL transmit powers $\mathcal{E}_{\mathsf{u},k}, \forall k \in \mathcal{U}_{\mathsf{u}}$, it does not scale with the number of antennas (see (5.16c)). Thus, the DL multi-UE and DL coherent interference terms dominate the InUE term in the sum DL SE. Hence, for mathematical tractability, we consider the sum UL SE maximization to optimize $\mathcal{E}_{\mathsf{u},k}, \forall k \in \mathcal{U}_{\mathsf{u}}$. This simplifies the joint UL-DL SE maximization and comes with closed-form update equations as well as convergence guarantees for the sum UL SE maximization sub-problem. We use a similar approach for DL power control, by maximizing the DL SE.

Second, we note that, with SINR-optimal weighting at the CPU, since the weights maximize the received SINR at the CPU for each UE, they also maximize the sum UL SE.

However, UEs' transmit powers can be optimized to improve the sum UL SE. Also, the recipe for power control presented here can be applied to any choice of weights at the CPU.

For convenience, we rewrite the problem as follows:

$$\max_{\boldsymbol{\mathcal{E}}_{\mathsf{u}}} \quad \sum_{k \in \mathcal{U}_{\mathsf{u}}} \log\left(1 + \frac{\mathsf{G}_{\mathsf{u},k}\left(\boldsymbol{\mathcal{E}}_{\mathsf{u}}\right)}{\mathsf{I}_{\mathsf{u},k}\left(\boldsymbol{\mathcal{E}}_{\mathsf{u}}\right)}\right), \tag{5.19a}$$

$$\text{subject to} \quad 0 \leq \mathcal{E}_{\mathsf{u},k} \leq \mathcal{E}_{\mathsf{u}}, \forall k \in \mathcal{U}_{\mathsf{u}}, \tag{5.19b}$$

where, with the help of Lemma 5.3, we define $\mathsf{G}_{\mathsf{u},k}(\boldsymbol{\mathcal{E}}_{\mathsf{u}}) = (N - \tau_p)\mathcal{E}_{\mathsf{u},k}\left(\sum_{m \in \mathcal{A}_{\mathsf{u}}} \omega^*_{mk}\alpha^2_{mk}\right)^2$ and $\mathsf{I}_{\mathsf{u},k}(\boldsymbol{\mathcal{E}}_{\mathsf{u}}) = \mathtt{EST}_{\mathsf{u},k} + \mathtt{MUI}_{\mathsf{u},k} + \sigma^2_{\mathsf{eff.},\mathsf{u},k}$, with $\sigma^2_{\mathsf{eff.},\mathsf{u},k} \triangleq \left(\mathtt{IAP}_k + N_0 \sum_{m \in \mathcal{A}_{\mathsf{u}}} |\omega^*_{mk}|^2 \alpha^2_{mk}\right)$ being the effective noise that is independent of the UL transmit powers. Now, we recognize that (5.19a) is a sum of the logarithm of ratios which can be converted into a convex problem via FP using a few auxiliary variables that can be iteratively solved in closed form. Further, FP guarantees that the optimal value of the objective and the variables that attain the optimum are the same for both the original objective function and the transformed surrogate objective function. This makes FP an excellent choice for the problem at hand. We next present the recipe in the context of our work.

To this end, we first introduce a set of auxiliary variables $\boldsymbol{\varpi}_{\mathsf{u}} \triangleq \left\{\varpi_{\mathsf{u},1}, \ldots, \varpi_{\mathsf{u},|\mathcal{U}_{\mathsf{u}}|}\right\}$, and formulate an *equivalent* problem of $\max_{\boldsymbol{\mathcal{E}}_{\mathsf{u}}, \boldsymbol{\varpi}_{\mathsf{u}}} \quad f\left(\boldsymbol{\mathcal{E}}_{\mathsf{u}}, \boldsymbol{\varpi}_{\mathsf{u}}\right)$, with

$$\begin{aligned} f\left(\boldsymbol{\mathcal{E}}_{\mathsf{u}}, \boldsymbol{\varpi}_{\mathsf{u}}\right) \triangleq & \sum_{k \in \mathcal{U}_{\mathsf{u}}} \ln\left(1 + \varpi_{\mathsf{u},k}\right) - \sum_{k \in \mathcal{U}_{\mathsf{u}}} \varpi_{\mathsf{u},k} \\ & + \sum_{k \in \mathcal{U}_{\mathsf{u}}} \frac{(1 + \varpi_{\mathsf{u},k})\mathsf{G}_{\mathsf{u},k}\left(\boldsymbol{\mathcal{E}}_{\mathsf{u}}\right)}{\mathsf{G}_{\mathsf{u},k}\left(\boldsymbol{\mathcal{E}}_{\mathsf{u}}\right) + \mathsf{I}_{\mathsf{u},k}\left(\boldsymbol{\mathcal{E}}_{\mathsf{u}}\right)}. \end{aligned} \tag{5.20}$$

and the same constraints are same as in (5.19a). Using results available in [98], we can show that the above two problems are equivalent in the sense that $\mathcal{E}_{\mathsf{u},k}, \forall k$, are the solution to (5.19) if and only if they are also the solution to (5.20), and further, the maximum value

of the objective in (5.20) and (5.19a) are the same. Now, to maximize $f\left(\boldsymbol{\mathcal{E}}_{\mathsf{u}}, \boldsymbol{\varpi}_{\mathsf{u}}\right)$, alternately optimize $\boldsymbol{\mathcal{E}}_{\mathsf{u}}$ and $\boldsymbol{\varpi}_{\mathsf{u}}$, while keeping the other variable constant. We observe that $f\left(\boldsymbol{\mathcal{E}}_{\mathsf{u}}, \boldsymbol{\varpi}_{\mathsf{u}}\right)$ is a concave differentiable function over $\boldsymbol{\varpi}_{\mathsf{u}}$ when $\boldsymbol{\mathcal{E}}_{\mathsf{u}}$ is fixed, say $\boldsymbol{\mathcal{E}}_{\mathsf{u}}^{\mathtt{iter}}$. Thus, $\boldsymbol{\varpi}_{\mathsf{u}}^{\mathtt{iter}+1} = \arg\max_{\boldsymbol{\varpi}_{\mathsf{u}}} f\left(\boldsymbol{\mathcal{E}}_{\mathsf{u}}^{\mathtt{iter}}, \boldsymbol{\varpi}_{\mathsf{u}}\right)$ can be optimally determined by setting $\dfrac{\partial f\left(\boldsymbol{\mathcal{E}}_{\mathsf{u}}, \boldsymbol{\varpi}_{\mathsf{u}}\right)}{\partial \varpi_{\mathsf{u},k}} = 0$ for each $\varpi_{\mathsf{u},k}$. This yields $\varpi_{\mathsf{u},k}^{\mathtt{iter}+1} = \dfrac{\mathsf{G}_{\mathsf{u},k}\left(\boldsymbol{\mathcal{E}}_{\mathsf{u}}^{\mathtt{iter}}\right)}{\mathsf{I}_{\mathsf{u},k}\left(\boldsymbol{\mathcal{E}}_{\mathsf{u}}^{\mathtt{iter}}\right)}, \forall k \in \mathcal{U}_{\mathsf{u}}$. Now, for fixed $\boldsymbol{\varpi}_{\mathsf{u}}$, the first and the second term of (5.20) are constants. The third term, i.e., $\sum\limits_{k\in\mathcal{U}_{\mathsf{u}}} \dfrac{(1+\varpi_{\mathsf{u},k})\mathsf{G}_{\mathsf{u},k}\left(\boldsymbol{\mathcal{E}}_{\mathsf{u}}\right)}{\mathsf{G}_{\mathsf{u},k}\left(\boldsymbol{\mathcal{E}}_{\mathsf{u}}\right)+\mathsf{I}_{\mathsf{u},k}\left(\boldsymbol{\mathcal{E}}_{\mathsf{u}}\right)}$, is in the sum of ratios form, which can be reformulated using a quadratic transform as $\max_{\boldsymbol{\mathcal{E}}_{\mathsf{u}}, \tilde{\boldsymbol{\varpi}}} f(\boldsymbol{\mathcal{E}}_{\mathsf{u}}, \tilde{\boldsymbol{\varpi}}_{\mathsf{u}})$, where

$$
\begin{aligned}
f(\boldsymbol{\mathcal{E}}_{\mathsf{u}}, \tilde{\boldsymbol{\varpi}}_{\mathsf{u}}) \triangleq & \sum_{k\in\mathcal{U}_{\mathsf{u}}} 2\tilde{\varpi}_{\mathsf{u},k}\sqrt{(1+\varpi_{\mathsf{u},k})\mathsf{G}_{\mathsf{u},k}\left(\boldsymbol{\mathcal{E}}_{\mathsf{u}}\right)} \\
& - \sum_{k\in\mathcal{U}_{\mathsf{u}}} \tilde{\varpi}_{\mathsf{u},k}^{2}\left(\mathsf{G}_{\mathsf{u},k}\left(\boldsymbol{\mathcal{E}}_{\mathsf{u}}\right)+\mathsf{I}_{\mathsf{u},k}\left(\boldsymbol{\mathcal{E}}_{\mathsf{u}}\right)\right) + \mathsf{c}_{\boldsymbol{\varpi}_{\mathsf{u}}},
\end{aligned} \tag{5.21}
$$

and $\tilde{\boldsymbol{\varpi}}_{\mathsf{u}} \triangleq \left\{\tilde{\varpi}_{\mathsf{u},1}, \ldots, \tilde{\varpi}_{\mathsf{u},|\mathcal{U}_{\mathsf{u}}|}\right\}$ being a new set of auxiliary variables and $\mathsf{c}_{\boldsymbol{\varpi}_{\mathsf{u}}}$ is a constant dependent only on $\boldsymbol{\varpi}_{\mathsf{u}}$. We can solve for $\tilde{\varpi}_{\mathsf{u},k}$ and $\boldsymbol{\mathcal{E}}_{\mathsf{u}}$ via partial differentiation of (5.21), for fixed $\varpi_{\mathsf{u},k}$. We summarize the overall recipe in Algorithm 7. The derivation of updates for $\tilde{\varpi}_{\mathsf{u},k}^{\mathtt{iter}+1}$ and $\mathcal{E}_{\mathsf{u},k}^{\mathtt{iter}in+1}$ (5.22) use simple algebraic manipulations.

Proposition 5.2. *The UL power control Algorithm 7 is convergent in the objective since $f\left(\boldsymbol{\mathcal{E}}_{\mathsf{u}}, \boldsymbol{\varpi}_{\mathsf{u}}\right)$ in (5.20) is bounded above and monotonically non-decreasing after each iteration.*

Proof. See Appendix D.3 ■

Remark 5.2. *Once the UL transmit powers of all the UEs are decided, the CPU can use this information to refine the SINR optimal weights. Specifically, the CPU initially finds $\boldsymbol{\omega}_{k}^{\mathsf{opt.}}$ considering equal power allocation. Once the UL transmit powers are optimized, CPU can reoptimize $\boldsymbol{\omega}_{k}^{\mathsf{opt.}}$ based on the received SINRs with $\mathcal{E}_{\mathsf{u},k}$ given by Algorithm 7. This process can be repeated until convergence of the sum UL SE.*

Remark 5.3. *We observe that lines 2, 3, and 4 in Algorithm 7 are independent of the*

Algorithm 7: Uplink Power Control

Input: $\kappa_{jn}, \forall j \in \mathcal{A}_{\mathsf{d}}, n \in \mathcal{U}_{\mathsf{d}}$

Initialization: $\boldsymbol{\mathcal{E}}_{\mathsf{u}}^{0}$, $\texttt{iter} = 0$

[1]: **while** $|f\left(\boldsymbol{\mathcal{E}}_{\mathsf{u}}, \boldsymbol{\varpi}_{\mathsf{u}}\right)^{\texttt{iter}+1} - f\left(\boldsymbol{\mathcal{E}}_{\mathsf{u}}, \boldsymbol{\varpi}_{\mathsf{u}}\right)^{\texttt{iter}}| \geq \delta_{\mathsf{u}}$ **do**

[2]: Evaluate: $\varpi_{\mathsf{u},k}^{\texttt{iter}+1} = \dfrac{\mathsf{G}_{\mathsf{u},k}\left(\boldsymbol{\mathcal{E}}_{\mathsf{u}}\right)}{\mathsf{I}_{\mathsf{u},k}\left(\boldsymbol{\mathcal{E}}_{\mathsf{u}}\right)}|_{\boldsymbol{\mathcal{E}}_{\mathsf{u}}=\boldsymbol{\mathcal{E}}_{\mathsf{u}}^{\texttt{iter}}}$

[3]: Evaluate: $\left.\dfrac{\partial f(\boldsymbol{\mathcal{E}}_{\mathsf{u}}, \tilde{\boldsymbol{\varpi}}_{\mathsf{u}})}{\partial \tilde{\varpi}_{\mathsf{u},k}}\right|_{\substack{\boldsymbol{\mathcal{E}}_{\mathsf{u}}=\boldsymbol{\mathcal{E}}_{\mathsf{u}}^{\texttt{iter}}, \\ \varpi_{\mathsf{u},k}=\varpi_{\mathsf{u},k}^{\texttt{iter}+1}, \forall k \in \mathcal{U}_{\mathsf{u}}}} = 0 \Rightarrow$

$$\tilde{\varpi}_{\mathsf{u},k}^{\texttt{iter}+1} = \frac{\sqrt{\left(1+\varpi_{\mathsf{u},k}^{\texttt{iter}+1}\right)\mathsf{G}_{\mathsf{u},k}\left(\boldsymbol{\mathcal{E}}_{\mathsf{u}}^{\texttt{iter}}\right)}}{\mathsf{G}_{\mathsf{u},k}\left(\boldsymbol{\mathcal{E}}_{\mathsf{u}}^{\texttt{iter}}\right)+\mathsf{I}_{\mathsf{u},k}\left(\boldsymbol{\mathcal{E}}_{\mathsf{u}}^{\texttt{iter}}\right)}$$

[4]: Set: $\left.\dfrac{\partial f(\boldsymbol{\mathcal{E}}_{\mathsf{u}}, \tilde{\boldsymbol{\varpi}}_{\mathsf{u}})}{\partial \mathcal{E}_{\mathsf{u},k}}\right|_{\substack{\varpi_{\mathsf{u},k}=\varpi_{\mathsf{u},k}^{\texttt{iter}+1}, \\ \tilde{\varpi}_{\mathsf{u},k}=\tilde{\varpi}_{\mathsf{u},k}^{\texttt{iter}+1}}} = 0$ to obtain (5.22)

[5]: Update: $\mathcal{E}_{\mathsf{u},k}^{\texttt{iter}+1} = \min\left\{(5.22), \mathcal{E}_{\mathsf{u}}\right\}, \forall k \in \mathcal{U}_{\mathsf{u}}$

[6]: Update: $\texttt{iter} = \texttt{iter} + 1$

[7]: **end**

$$\mathcal{E}_{\mathsf{u},k}^{\texttt{iter}+1} = \frac{\left(\tilde{\varpi}_{\mathsf{u},k}^{\texttt{iter}+1}\sqrt{\left(1+\varpi_{\mathsf{u},k}^{\texttt{iter}+1}\right)}\right)^2 (N-\tau_p)\left(\sum\limits_{m\in\mathcal{A}_{\mathsf{u}}}\omega_{mk}^{*}\alpha_{mk}^{2}\right)^2}{\left(\begin{array}{c}\sum\limits_{n\in\mathcal{U}_{\mathsf{u}}}(\tilde{\varpi}_{\mathsf{u},n}^{\texttt{iter}+1})^2\left\{(N-\tau_p)\left(\sum\limits_{m\in\mathcal{A}_{\mathsf{u}}}\omega_{mn}^{*}\alpha_{mk}^{2}\right)^2\right. \\ \left. + \sum\limits_{m\in\mathcal{A}_{\mathsf{u}}}|\omega_{mn}^{*}|^2\alpha_{mn}^{2}(\beta_{mk}-\alpha_{mk}^{2})\right\}\end{array}\right)^2}, \forall k \in \mathcal{U}_{\mathsf{u}}. \tag{5.22}$$

combining scheme, and are applicable even under maximal ratio combining, unlike [92] where the power control algorithm is tied to the specific combining scheme used. More importantly, the FP approach guarantees that the maximum objective of the surrogate and original objective functions are the same, unlike the lower-bound surrogate-based optimization in [92].

5.4.c Downlink power control

Now, in DL also, we can apply FP to optimize the DL power control coefficients. To this end, we first introduce some useful mathematical notation. Let

$$\mathbf{g}_{\mathsf{d},n} \triangleq \left[\mathbb{E}\left[\mathbf{f}_{1n}^T\mathbf{p}_{1n}\right], \mathbb{E}\left[\mathbf{f}_{2n}^T\mathbf{p}_{2n}\right], \ldots, \mathbb{E}\left[\mathbf{f}_{|\mathcal{A}_\mathsf{d}|n}^T\mathbf{p}_{|\mathcal{A}_\mathsf{d}|n}\right]\right]^T, \tag{5.23}$$

which equals $(N-\tau_p)\left[\alpha_{1n}, \alpha_{2n}, \ldots, \alpha_{|\mathcal{A}_\mathsf{d}|n}\right]^T$ under ZF precoding. Also, let $[\mathbf{I}_{nq}]_{jj'} \triangleq \mathbb{E}\left[\mathbf{f}_{jn}^T\mathbf{p}_{jq}\mathbf{p}_{j'q}^H\mathbf{f}_{j'n}^*\right], \forall j, j' \in \mathcal{A}_\mathsf{d}$. With ZF precoding, $\mathbf{I}_{nq}$ has the following structure:

$$[\mathbf{I}_{nq}]_{jj'} = \begin{cases} (N-\tau_p)\alpha_{jn}^2|\langle\boldsymbol{\varphi}_{l(n)}, \boldsymbol{\varphi}_{l(q)}\rangle|^2 + (\beta_{jn}-\alpha_{jn}^2), \text{if } j = j' \\ (N-\tau_p)\alpha_{j'n}\alpha_{jn}|\langle\boldsymbol{\varphi}_{l(n)}, \boldsymbol{\varphi}_{l(q)}\rangle|^2, \text{otherwise.} \end{cases} \tag{5.24}$$

Then, $\mathbb{E}\left[\left|\sum_{j\in\mathcal{A}_\mathsf{d}} \kappa_{jq}\mathbf{f}_{jn}^T\mathbf{p}_{jq}\right|^2\right]$ can be expressed as

$$\sum_{j\in\mathcal{A}_\mathsf{d}}\sum_{j'\in\mathcal{A}_\mathsf{d}} \kappa_{jq}\mathbb{E}\left[\mathbf{f}_{jn}^T\mathbf{p}_{jq}\mathbf{p}_{j'q}^H\mathbf{f}_{j'n}^*\right]\kappa_{j'q} = \boldsymbol{\kappa}_q^T\mathbf{I}_{nq}\boldsymbol{\kappa}_q.$$

The effective DL noise, independent of DL power control coefficients, is defined as $\sigma_{\mathsf{eff.},\mathsf{d},n}^2 = \mathtt{IUE}_n + N_0$. Thus DL SINR becomes $\eta_{\mathsf{d},n}(\mathcal{A}_\mathsf{s}) = \dfrac{\mathsf{G}_{\mathsf{d},n}(\boldsymbol{\kappa})}{\mathsf{I}_{\mathsf{d},n}(\boldsymbol{\kappa})}$, with $\mathsf{G}_{\mathsf{d},n}(\boldsymbol{\kappa}) = \left(\boldsymbol{\kappa}_n^T\mathbf{g}_{\mathsf{d},n}\right)^2$ and $\mathsf{I}_{\mathsf{d},n}(\boldsymbol{\kappa}) \triangleq \sum\limits_{q\in\mathcal{U}_\mathsf{d}} \boldsymbol{\kappa}_q^T\mathbf{I}_{nq}\boldsymbol{\kappa}_q - \left(\boldsymbol{\kappa}_q^T\mathbf{g}_{\mathsf{d},n}\right)^2 + \dfrac{1}{\mathcal{E}_\mathsf{d}}\sigma_{\mathsf{eff.},\mathsf{d},n}^2$. Observe that, substituting $\mathbf{g}_{\mathsf{d},n}$ and (5.24), we obtain Lemma 5.4. Now, the sum DL SE maximization problem becomes:

$$\max_{\kappa_{jn}} \quad \sum_{n\in\mathcal{U}_\mathsf{d}} \log\left(1 + \frac{\mathsf{G}_{\mathsf{d},n}(\boldsymbol{\kappa})}{\mathsf{I}_{\mathsf{d},n}(\boldsymbol{\kappa})}\right) \tag{5.25a}$$

$$\text{subject to} \quad \sum_{q\in\mathcal{U}_\mathsf{d}} \kappa_{jq}^2 \leq 1, \forall j \in \mathcal{A}_\mathsf{d}. \tag{5.25b}$$

We apply the Lagrange-dual transform [98] with auxiliary variables

$$\boldsymbol{\varpi}_\mathsf{d} = \left[\varpi_{\mathsf{d},1}, \varpi_{\mathsf{d},2}, \ldots, \varpi_{\mathsf{d},|\mathcal{U}_\mathsf{d}|}\right],$$

to obtain:

$$\max_{\kappa_{jn},\boldsymbol{\varpi}_{\mathsf{d}}} f(\boldsymbol{\kappa},\boldsymbol{\varpi}_{\mathsf{d}}) \triangleq \sum_{n\in\mathcal{U}_{\mathsf{d}}} \ln\left(1+\varpi_{\mathsf{d},n}\right) - \sum_{n\in\mathcal{U}_{\mathsf{d}}} \varpi_{\mathsf{d},n} + \sum_{n\in\mathcal{U}_{\mathsf{d}}} \frac{(1+\varpi_{\mathsf{d},n})\mathsf{G}_{\mathsf{d},n}\left(\boldsymbol{\kappa}\right)}{\mathsf{G}_{\mathsf{d},n}\left(\boldsymbol{\kappa}\right)+\mathsf{I}_{\mathsf{d},n}\left(\boldsymbol{\kappa}\right)} \tag{5.26a}$$

$$\text{subject to} \quad \sum_{q\in\mathcal{U}_{\mathsf{d}}} \kappa_{jq}^2 \leq 1; \forall j \in \mathcal{A}_{\mathsf{d}}. \tag{5.26b}$$

The problems in (5.25a) and in (5.26a) are equivalent in the sense that $\boldsymbol{\kappa}$ is a solution of (5.25a) if and only if it is the solution of (5.26a) [98]. We now alternately optimize $\boldsymbol{\kappa}$ and $\boldsymbol{\varpi}_{\mathsf{d}}$. For fixed $\boldsymbol{\kappa}$, $f(\boldsymbol{\kappa},\boldsymbol{\varpi}_{\mathsf{d}})$ is a concave differentiable function over $\boldsymbol{\varpi}_{\mathsf{d}}$. Thus, $\frac{\partial f(\boldsymbol{\kappa},\boldsymbol{\varpi}_{\mathsf{d}})}{\partial \varpi_{\mathsf{d},n}} = 0$ yields $\varpi_{\mathsf{d},n}^{\text{opt.}} = \frac{\mathsf{G}_{\mathsf{d},n}\left(\boldsymbol{\kappa}\right)}{\mathsf{I}_{\mathsf{d},n}\left(\boldsymbol{\kappa}\right)}$. For fixed $\boldsymbol{\varpi}_{\mathsf{d}}$, the first and the second terms of $f(\boldsymbol{\kappa},\boldsymbol{\varpi}_{\mathsf{d}})$ are constants. Hence, to optimize $\boldsymbol{\kappa}$, we need to solve $\max_{\boldsymbol{\kappa}} \sum_{n\in\mathcal{U}_{\mathsf{d}}} \frac{(1+\varpi_{\mathsf{d},n})\mathsf{G}_{\mathsf{d},n}\left(\boldsymbol{\kappa}\right)}{\mathsf{G}_{\mathsf{d},n}\left(\boldsymbol{\kappa}\right)+\mathsf{I}_{\mathsf{d},n}\left(\boldsymbol{\kappa}\right)}$, for which we use FP. To do so, we define $\bar{\mathsf{G}}_{\mathsf{d},n}\left(\boldsymbol{\kappa}\right) \triangleq (1+\varpi_{\mathsf{d},n})\mathsf{G}_{\mathsf{d},n}\left(\boldsymbol{\kappa}\right)$, and $\bar{\mathsf{I}}_{\mathsf{d},n}\left(\boldsymbol{\kappa}\right) \triangleq \mathsf{G}_{\mathsf{d},n}\left(\boldsymbol{\kappa}\right)+\mathsf{I}_{\mathsf{d},n}\left(\boldsymbol{\kappa}\right)$. Then, the equivalent problem is to maximize $\sum_{n\in\mathcal{U}_{\mathsf{d}}} \frac{\bar{\mathsf{G}}_{\mathsf{d},n}\left(\boldsymbol{\kappa}\right)}{\bar{\mathsf{I}}_{\mathsf{d},n}\left(\boldsymbol{\kappa}\right)}$ subject to $\sum_{q\in\mathcal{U}_{\mathsf{d}}} \kappa_{jq}^2 \leq 1$. Now, the dual of $\sum_{n\in\mathcal{U}_{\mathsf{d}}} \frac{\bar{\mathsf{G}}_{\mathsf{d},n}\left(\boldsymbol{\kappa}\right)}{\bar{\mathsf{I}}_{\mathsf{d},n}(\boldsymbol{\kappa})}$ is $\sum_{n\in\mathcal{U}_{\mathsf{d}}} (2\tilde{\varpi}_{\mathsf{d},n}\sqrt{\bar{\mathsf{G}}_{\mathsf{d},n}(\boldsymbol{\kappa})} - \tilde{\varpi}_{\mathsf{d},n}^2\bar{\mathsf{I}}_{\mathsf{d},n}(\boldsymbol{\kappa}))$ with new auxiliary variables $\tilde{\boldsymbol{\varpi}}_{\mathsf{d}} = \left[\tilde{\varpi}_{\mathsf{d},1},\tilde{\varpi}_{\mathsf{d},2},\ldots,\tilde{\varpi}_{\mathsf{d},|\mathcal{U}_{\mathsf{d}}|}\right]^T$ [98, Corollary 1]. Substituting, we obtain

$$\max_{\boldsymbol{\kappa},\tilde{\boldsymbol{\varpi}}_{\mathsf{d}}} f(\boldsymbol{\kappa},\tilde{\boldsymbol{\varpi}}_{\mathsf{d}}) \triangleq \sum_{n\in\mathcal{U}_{\mathsf{d}}} \Bigg(2\tilde{\varpi}_{\mathsf{d},n}\sqrt{(1+\varpi_{\mathsf{d},n})\left(\boldsymbol{\kappa}_q^T\mathbf{g}_{\mathsf{d},n}\right)^2} - \tilde{\varpi}_{\mathsf{d},n}^2\left(\sum_{q\in\mathcal{U}_{\mathsf{d}}} \boldsymbol{\kappa}_q^T\mathbf{I}_{nq}\boldsymbol{\kappa}_q + \sigma_{\text{eff.},\mathsf{d},n}^2\right)\Bigg), \tag{5.27a}$$

$$\text{subject to} \quad \sum_{q\in\mathcal{U}_{\mathsf{d}}} \kappa_{jq}^2 \leq 1, \forall j \in \mathcal{A}_{\mathsf{d}}. \tag{5.27b}$$

Observe that $\boldsymbol{\varpi}_{\mathsf{d}}$ is already fixed. Then, for fixed $\boldsymbol{\kappa}$, $f(\boldsymbol{\kappa},\tilde{\boldsymbol{\varpi}}_{\mathsf{d}})$ is strongly concave with respect to $\tilde{\boldsymbol{\varpi}}_{\mathsf{d}}$ and thus, we can set $\frac{\partial f(\boldsymbol{\kappa},\tilde{\boldsymbol{\varpi}}_{\mathsf{d}})}{\partial \tilde{\varpi}_{\mathsf{d},n}} = 0$, leading to $\tilde{\varpi}_{\mathsf{d},n}^{\text{opt.}} = \frac{\sqrt{1+\varpi_{\mathsf{d},n}}\mathbf{g}_{\mathsf{d},n}^T\boldsymbol{\kappa}_n}{\sum_{q\in\mathcal{U}_{\mathsf{d}}} \boldsymbol{\kappa}_q^T\mathbf{I}_{nq}\boldsymbol{\kappa}_q + \sigma_{\text{eff.},\mathsf{d},n}^2}$; $\forall n \in \mathcal{U}_{\mathsf{d}}$. Finally, we obtain $\boldsymbol{\kappa}^{\text{opt.}}$ given $\boldsymbol{\varpi}_{\mathsf{d}}$ and $\tilde{\boldsymbol{\varpi}}_{\mathsf{d}}$ by solving

$$\max_{\boldsymbol{\kappa},\tilde{\boldsymbol{\varpi}}_{\mathsf{d}}} \quad \sum_{n\in\mathcal{U}_{\mathsf{d}}} \Bigg(2\tilde{\varpi}_{\mathsf{d},n}\sqrt{(1+\varpi_{\mathsf{d},n})\left(\boldsymbol{\kappa}_n^T\mathbf{g}_{\mathsf{d},n}\right)^2}$$

$$-\tilde{\varpi}_{\mathsf{d},n}^2\left(\sum_{q\in\mathcal{U}_\mathsf{d}}\boldsymbol{\kappa}_q^T\mathbf{I}_{nq}\boldsymbol{\kappa}_q+\sigma_{\mathsf{eff.},\mathsf{d},n}^2\right)\Bigg), \tag{5.28a}$$

$$\text{subject to}\quad \sum_{q\in\mathcal{U}_\mathsf{d}}\kappa_{jq}^2\leq 1,\forall j\in\mathcal{A}_\mathsf{d}. \tag{5.28b}$$

We observe that matrix $\mathbf{I}_{nq}$ is positive semi-definite. Hence, $f(\boldsymbol{\kappa})$, as given below,

$$f(\boldsymbol{\kappa})\triangleq\sum_{n\in\mathcal{U}_\mathsf{d}}\left(2\tilde{\varpi}_{\mathsf{d},n}\sqrt{\left(1+\varpi_{\mathsf{d},n}\right)\left(\boldsymbol{\kappa}_n^T\mathbf{g}_{\mathsf{d},n}\right)^2}-\tilde{\varpi}_{\mathsf{d},n}^2\left(\sum_{q\in\mathcal{U}_\mathsf{d}}\boldsymbol{\kappa}_q^T\mathbf{I}_{nq}\boldsymbol{\kappa}_q+\sigma_{\mathsf{eff.}}^2\right)\right), \tag{5.29}$$

is concave with respect to $\boldsymbol{\kappa}$. The above problem is a QCQP, which can be *optimally* solved via ADMM (see [99, Chapter 5]), yielding a closed form update for κ_{jn}, which is also known to be efficient in terms of convergence for large dimensional problems compared to using off-the-shelf convex solvers. This is presented next.

We reformulate (5.28a) with the help of new auxiliary variables $\boldsymbol{\pi}=[\pi_{jn}]_{j\in\mathcal{A}_d,n\in\mathcal{U}_d}$ as

$$\min_{\boldsymbol{\kappa},\boldsymbol{\pi}}\quad \mathbb{1}_{\boldsymbol{\kappa}}(\boldsymbol{\pi})-f(\boldsymbol{\kappa}), \tag{5.30a}$$

$$\text{subject to}\quad \kappa_{jn}=\pi_{jn},\forall j\in\mathcal{A}_\mathsf{d},n\in\mathcal{U}_\mathsf{d}, \tag{5.30b}$$

where $\mathbb{1}_{\boldsymbol{\kappa}}(\boldsymbol{\pi})$ is defined as

$$\mathbb{1}_{\boldsymbol{\kappa}}(\boldsymbol{\pi})=\begin{cases}0, & \text{if}\quad \|\boldsymbol{\pi}_{j,:}\|^2\leq 1,\forall j\in\mathcal{A}_\mathsf{d}\\ \infty, & \text{otherwise,}\end{cases} \tag{5.31}$$

where $\boldsymbol{\pi}_{j,:}\triangleq\left[\pi_{j1},\pi_{j2},\ldots,\pi_{j|\mathcal{U}_\mathsf{d}|}\right]^T$. Here, $\mathbb{1}_{\boldsymbol{\kappa}}(\boldsymbol{\pi})$ is an indicator whether the auxiliary variables satisfy the feasibility constraint $\|\boldsymbol{\pi}_{j,:}\|^2\leq 1$ corresponding to $\boldsymbol{\kappa}$. Essentially, $\boldsymbol{\pi}$ is a copy of the main optimization variable $\boldsymbol{\kappa}$ and should satisfy the same constraint. Let $\bar{\pi}_{jn}$ denote the scaled dual variables[9] corresponding to the equality constraints $\pi_{jn}=\kappa_{jn},\forall j\in\mathcal{A}_\mathsf{d},n\in\mathcal{U}_\mathsf{d}$. Then, the augmented Lagrangian can be written as $\mathcal{L}\left(\boldsymbol{\kappa},\boldsymbol{\pi},\bar{\boldsymbol{\pi}}\right)=\mathbb{1}_{\boldsymbol{\kappa}}(\boldsymbol{\pi})-f(\boldsymbol{\kappa})+\frac{\delta_\mathsf{p}}{2}\sum_{n\in\mathcal{U}_\mathsf{d}}\sum_{j\in\mathcal{A}_\mathsf{d}}\left(\pi_{jn}-\kappa_{jn}+\bar{\pi}_{jn}\right)^2$, where δ_p is a penalty parameter. We now

[9] In the ADMM terminology, the variables $\boldsymbol{\kappa}$ and $\boldsymbol{\pi}$ can be considered as the first and second blocks of primal variables, respectively. In ADMM, a set of dual variables are introduced for the equality constraint in (5.30a), and they are to be updated in each iteration with the primal variables.

$$\arg\min_{\boldsymbol{\kappa}} \left(\sum_{n\in\mathcal{U}_{\mathsf{d}}} \boldsymbol{\kappa}_n^T \left(\sum_{q\in\mathcal{U}_{\mathsf{d}}} \tilde{\varpi}_{\mathsf{d},n}^2 \mathbf{I}_{nq} + \frac{\delta_{\mathsf{p}}}{2} \mathbf{I}_{|\mathcal{A}_{\mathsf{d}}|} \right) \right) \boldsymbol{\kappa}_n$$
$$- 2 \sum_{n\in\mathcal{U}_{\mathsf{d}}} \left(\tilde{\varpi}_{\mathsf{d},n} \sqrt{(1+\varpi_{\mathsf{d},n})} \mathbf{g}_{\mathsf{d},n} + \frac{\delta_{\mathsf{p}}}{2} \left(\boldsymbol{\pi}_{:,n} + \bar{\boldsymbol{\pi}}_{:,n} \right) \right)^T \boldsymbol{\kappa}_{\boldsymbol{n}}. \tag{5.33}$$

$$\boldsymbol{\kappa}_n^{\mathsf{opt.}} = \left(\sum_{q\in\mathcal{U}_{\mathsf{d}}} \tilde{\varpi}_{\mathsf{d},n}^2 \mathbf{I}_{nq} + \frac{\delta_{\mathsf{p}}}{2} \mathbf{I}_{|\mathcal{A}_{\mathsf{d}}|} \right)^{-1}$$
$$\times \left(\tilde{\varpi}_{\mathsf{d},n} \sqrt{(1+\varpi_{\mathsf{d},n})} \mathbf{g}_{\mathsf{d},n} + \frac{\delta_{\mathsf{p}}}{2} \left(\boldsymbol{\pi}_{:,n} + \bar{\boldsymbol{\pi}}_{:,n} \right) \right) \in \mathbb{C}^{|\mathcal{A}_{\mathsf{d}}|\times 1}, \forall n \in \mathcal{U}_{\mathsf{d}}. \tag{5.34}$$

---

update $\boldsymbol{\kappa}_n, \forall n \in \mathcal{U}_{\mathsf{d}}$, as the solution of

$$\arg\min_{\boldsymbol{\kappa}} -f(\boldsymbol{\kappa}) + \frac{\delta_{\mathsf{p}}}{2} \sum_{n\in\mathcal{U}_{\mathsf{d}}} \sum_{j\in\mathcal{A}_{\mathsf{d}}} \left(\pi_{jn} - \kappa_{jn} + \bar{\pi}_{jn} \right)^2. \tag{5.32}$$

Upon substituting for $f(\boldsymbol{\kappa})$ in (5.32), we get (5.33), from which we obtain $\boldsymbol{\kappa}_n^{\mathsf{opt.}}$ as given in (5.34). Here, $\boldsymbol{\pi}_{:,n} \triangleq \left[\pi_{1,n}, \pi_{2,n}, \ldots, \pi_{|\mathcal{A}_{\mathsf{d}|,n}} \right]^T$ and $\bar{\boldsymbol{\pi}}_{:,n} \triangleq \left[\bar{\pi}_{1,n}, \bar{\pi}_{2,n}, \ldots, \bar{\pi}_{|\mathcal{A}_{\mathsf{d}|,n}} \right]^T$. Next, we can find the optimal update of the second block of primal variables as

$$\arg\min_{\boldsymbol{\pi}} \mathbb{1}_{\boldsymbol{\kappa}}(\boldsymbol{\pi}) + \frac{\delta_{\mathsf{p}}}{2} \sum_{n\in\mathcal{U}_{\mathsf{d}}} \sum_{j\in\mathcal{A}_{\mathsf{d}}} \left(\pi_{jn} - \kappa_{jn} + \bar{\pi}_{jn} \right)^2.$$

Equivalently, $\pi_{jn}^{\mathsf{opt.}}$ is the solution of

$$\arg\min_{\pi_{jn}} \quad \frac{\delta_{\mathsf{p}}}{2} \sum_{n\in\mathcal{U}_{\mathsf{d}}} \sum_{j\in\mathcal{A}_{\mathsf{d}}} \left(\pi_{jn} - \kappa_{jn} + \bar{\pi}_{jn} \right)^2, \tag{5.35a}$$

$$\text{subject to} \quad \sum_{n\in\mathcal{U}_{\mathsf{d}}} \pi_{jn}^2 \leq 1, \forall j \in \mathcal{A}_{\mathsf{d}}. \tag{5.35b}$$

$$\tilde{\varpi}_{\mathsf{d},n}^{\mathtt{iter}+1} = \frac{\sqrt{1+\varpi_{\mathsf{d},n}^{\mathtt{iter}+1}}\sqrt{(N-\tau_p)}\sqrt{\mathcal{E}_{\mathsf{d}}}\left(\sum\limits_{j\in\mathcal{A}_{\mathsf{d}}}\alpha_{jn}\kappa_{jn}^{\mathtt{iter}}\right)}{\left(\begin{array}{c}\sum\limits_{q\in\mathcal{U}_{\mathsf{d}}}\sum\limits_{j\in\mathcal{A}_{\mathsf{d}}}\mathcal{E}_{\mathsf{d}}(\kappa_{jq}^{\mathtt{iter}})^2(\beta_{jn}-\alpha_{jn}^2) \\ +(N-\tau_p)\sum\limits_{q\in\mathcal{U}_{\mathsf{d}}}\mathcal{E}_{\mathsf{d}}\left(\sum\limits_{j\in\mathcal{A}_{\mathsf{d}}}\kappa_{jq}^{\mathtt{iter}}\alpha_{jn}\right)^2|\langle\boldsymbol{\varphi}_{l(n)},\boldsymbol{\varphi}_{l(q)}\rangle|^2+\sigma_{\mathsf{eff.},\mathsf{d},n}^2\end{array}\right)}. \tag{5.38}$$

Now, (5.35a) can be solved independently for each AP index by evaluating

$$\arg\min_{\pi_{jn}} \quad \frac{\delta_{\mathsf{p}}}{2}\sum_{n\in\mathcal{U}_{\mathsf{d}}}\left(\pi_{jn}-\kappa_{jn}+\bar{\pi}_{jn}\right)^2, \tag{5.36}$$

for each $j \in \mathcal{A}_{\mathsf{d}}$ subject to the per-AP power constraint $\sum_{n\in\mathcal{U}_{\mathsf{d}}}\pi_{jn}^2 \leq 1$. Using the KKT condition, we can show that the optimal solution corresponding to the jth DL AP, $\boldsymbol{\pi}_j^{\mathsf{opt.}}$, is

$$\boldsymbol{\pi}_j^{\mathsf{opt.}} = \min\left\{1, \sqrt{\frac{1}{\|\dot{\boldsymbol{\pi}}_j\|^2}}\right\}\dot{\boldsymbol{\pi}}_j, \forall j \in \mathcal{A}_{\mathsf{d}}, \tag{5.37}$$

with $\dot{\boldsymbol{\pi}}_j \triangleq \left[(\kappa_{j1}-\bar{\pi}_{j1}),(\kappa_{j2}-\bar{\pi}_{j2}),\ldots,(\kappa_{j|\mathcal{U}_{\mathsf{d}}|}-\bar{\pi}_{j|\mathcal{U}_{\mathsf{d}}|})\right]^T$. We summarize the iterative recipe for solving our original problem (5.28a) via ADMM approach in Algorithm 8. We note that the $\{\kappa_{jn}\}$ yielded by Algorithm 8 are *globally optimal*. We present the overall DL power control recipe in Algorithm 9. The stopping criterion of the algorithm is decided by the threshold δ_{d}. Also, with ZF precoding, the closed-form update equation for $\tilde{\varpi}_n^{\mathtt{iter}+1}$ is presented in (5.38). To update $\boldsymbol{\kappa}$, $\mathbf{I}_{nq}$ needs to be substituted in (5.34) from (5.24).

Proposition 5.3. *The DL power allocation algorithm is convergent in objective since* $f(\boldsymbol{\kappa},\boldsymbol{\varpi}_{\mathsf{d}})$ *is bounded above and monotonically non-decreasing after each iteration.*

We now highlight the key benefits of our DL power control scheme. First of all, the DL power allocation algorithm is precoder and combiner agnostic (lines 2, 3 in Algorithm 9

Algorithm 8: Solving (5.28a) via ADMM

Input: $\pi^0_{jn}, \forall j \in \mathcal{A}_{\mathsf{d}}, n \in \mathcal{U}_{\mathsf{d}}$, $\delta_{\mathsf{ADMM}} > 0$

Initialization: $\bar{\pi}^0_{jn} = 0, \forall j \in \mathcal{A}_{\mathsf{d}}, n \in \mathcal{U}_{\mathsf{d}}$, $\mathtt{iter} = 0$

[1]: **while** $\|\boldsymbol{\kappa_n} - \boldsymbol{\pi}_{:,n}\| \geq \delta_{\mathsf{ADMM}}$ **do**

[2]: Evaluate: $\boldsymbol{\kappa}_n^{\mathtt{iter}+1}$ using (5.34) with $\boldsymbol{\pi}_{:,n}^{\mathtt{iter}}$ and $\bar{\boldsymbol{\pi}}_{:,n}^{\mathtt{iter}}$

[3]: Evaluate: $\boldsymbol{\pi}_{:,n}^{\mathtt{iter}+1}$ using (5.37) with

$$\dot{\boldsymbol{\pi}}_j \triangleq \left[(\kappa_{j1}^{\mathtt{iter}+1} - \bar{\pi}_{j1}^{\mathtt{iter}}), \ldots, (\kappa_{j|\mathcal{U}_{\mathsf{d}}|}^{\mathtt{iter}+1} - \bar{\pi}_{j|\mathcal{U}_{\mathsf{d}}|}^{\mathtt{iter}})\right]^T$$

[4]: Update: $\bar{\pi}_{jn}^{\mathtt{iter}+1} = \pi_{jn}^{\mathtt{iter}} - \kappa_{jn}^{\mathtt{iter}+1} + \bar{\pi}_{jn}^{\mathtt{iter}}$

[5]: Update: $\mathtt{iter} = \mathtt{iter} + 1$

[6]: **end**

Algorithm 9: Downlink Power Control

Input: $\mathcal{E}_{\mathsf{u},k}, \forall k \in \mathcal{U}_{\mathsf{u}}$

Initialization: $\kappa^0_{jn}, \forall j \in \mathcal{A}_{\mathsf{d}}, n \in \mathcal{U}_{\mathsf{d}}$, $\mathtt{iter} = 0$

[1]: **while** $|f(\boldsymbol{\kappa}, \boldsymbol{\varpi}_{\mathsf{d}})^{\mathtt{iter}+1} - f(\boldsymbol{\kappa}, \boldsymbol{\varpi}_{\mathsf{d}})^{\mathtt{iter}}| \geq \delta_{\mathsf{d}}$ **do**

[2]: Evaluate:
$$\varpi_{\mathsf{d},n}^{\mathtt{iter}+1} = \frac{\left((\boldsymbol{\kappa}_q^{\mathtt{iter}})^T \mathbf{g}_{\mathsf{d},n}\right)^2}{\sum\limits_{q \in \mathcal{U}_{\mathsf{d}}} (\boldsymbol{\kappa}_q^{\mathtt{iter}})^T \mathbf{I}_{nq} \boldsymbol{\kappa}_q^{\mathtt{iter}} - \left((\boldsymbol{\kappa}_q^{\mathtt{iter}})^T \mathbf{g}_{\mathsf{d},n}\right)^2 + \sigma^2_{\text{eff.}}}$$

[3]: Evaluate:
$$\tilde{\varpi}_n^{\mathtt{iter}+1} = \frac{\sqrt{1 + \varpi_{\mathsf{d},n}^{\mathtt{iter}+1}}\, \mathbf{g}_{\mathsf{d},n}^T \boldsymbol{\kappa}_n^{\mathtt{iter}}}{\sum\limits_{q \in \mathcal{U}_{\mathsf{d}}} (\boldsymbol{\kappa}_q^{\mathtt{iter}})^T \mathbf{I}_{nq} \boldsymbol{\kappa}_q^{\mathtt{iter}} + \sigma^2_{\text{eff.}}}$$

[4]: Evaluate: $\boldsymbol{\kappa}_q^{\mathtt{iter}+1}$ via solving (5.28a) with $\varpi_{\mathsf{d},n} = \varpi_{\mathsf{d},n}^{\mathtt{iter}+1}$ and $\tilde{\varpi}_{\mathsf{d},n} = \tilde{\varpi}_{\mathsf{d},n}^{\mathtt{iter}+1}$

[5]: Update: $\mathtt{iter} = \mathtt{iter} + 1$

[6]: **end**

and lines 2, 3, and 4 in Algorithm 8 apply to any choice of precoder), similar to our UL power allocation algorithm. This makes our algorithms more widely applicable compared to [92]. Also, as mentioned for UL, most of the works in literature lower bound the original cost function (e.g., the sum SE optimization in [92], [88]) by a series of surrogate convex functions and use available general-purpose convex solvers. In contrast, we provide closed-form update equations for all the auxiliary variables, and, thanks to FP, our algorithm directly optimizes the original cost function. Finally, interested readers can refer to Appendix D.5 for detailed numerical simulations related to the convergence properties of the

subproblems as well as the overall alternating optimization.

5.4.d Complexity Analysis

We now present the order complexity of the UL and DL power control algorithms. FP admits closed-form updates for the power control coefficients and auxiliary variables. In the case of UL, we need to compute three such parameters via simple arithmetic operations at each iteration. Thus, the overall complexity of the UL power control is $\mathcal{O}(|\mathcal{U}_u|)$. In contrast, the algorithms for power control that use sequential convex programming and numerical solvers for sum SE maximization, such as [103], are of a complexity $\mathcal{O}(|\mathcal{U}_u|^4)$. Hence, FP-based UL power allocation is substantially less complex compared to the existing comparative approaches. Similarly, the main burden of the DL FP algorithm is the inner ADMM algorithm, which involves a matrix inversion. It can be argued that the overall FP and ADMM have a complexity of $\mathcal{O}(|\mathcal{U}_d||\mathcal{A}_d|^3)$. However, solving the QCQP with interior point programming leads to the complexity of $\mathcal{O}(|\mathcal{U}_d|^3|\mathcal{A}_d|^3)$; which is much larger, especially when the number of UEs in the system is high. This leads us to conclude that having closed-form updates help to reduce the complexity of the power control algorithms compared to existing tools.

Remark 5.4. *One can generalize* (5.18)*, for example, to include user priority or fairness guarantees, by considering weighted sum UL-DL SE. The technical development, algorithms, and update equations directly extend to weighted sum UL-DL SE maximization, thanks to the FP-based approach [98], at the cost of additional notational bookkeeping. Hence, for simplicity, we do not include it in this chapter.*

5.5 FD CF MIMO System

We now present the SE analysis and power control for an FD-enabled CF MIMO system. The analysis for the FD system is similar to that of the DTDD system presented in Section 5.3, except that all the APs are now capable of concurrent transmission and

reception. Hence, $\mathcal{A}_{\mathsf{u}} = \mathcal{A}_{\mathsf{d}} = \mathcal{A}$ with $|\mathcal{A}| = M$. Also, each AP suffers from IrAI. We can express the kth stream of the UL received signal (after local combining using $\mathbf{v}_{mk} \in \mathbb{C}^{N_{\mathrm{rx}}}$) at the mth FD AP as

$$\begin{aligned}\hat{s}_{\mathsf{u},mk} = \sqrt{\mathcal{E}_{\mathsf{u},k}}\mathbf{v}_{mk}^H\mathbf{f}_{mk}s_{\mathsf{u},k} + \sum_{n\in\mathcal{U}_{\mathsf{u}}\setminus k}\sqrt{\mathcal{E}_{\mathsf{u},n}}\mathbf{v}_{mk}^H\mathbf{f}_{mn}s_{\mathsf{u},n} \\ \underbrace{+\sqrt{\mathcal{E}_{\mathsf{d}}}\sum_{\substack{j\neq m,\\ j=1}}^{M}\sum_{n\in\mathcal{U}_{\mathsf{d}}}\kappa_{jn}\mathbf{v}_{mk}^H\tilde{\mathbf{G}}_{mj}\mathbf{p}_{jn}s_{\mathsf{d},n}}_{\text{InAI from all APs except the } m\text{th AP}} \\ \underbrace{+\sqrt{\mathcal{E}_{\mathsf{d}}}\sum_{n\in\mathcal{U}_{\mathsf{d}}}\kappa_{mn}\mathbf{v}_{mk}^H\mathbf{G}_m^{\mathsf{SI}}\mathbf{p}_{mn}s_{\mathsf{d},n}}_{\text{IrAI of } m\text{th AP}} + \mathbf{v}_{mk}^H\mathbf{w}_{\mathsf{u},mk}.\end{aligned} \tag{5.39}$$

In (5.39), the third and fourth terms correspond to the InAI and IrAI, as indicated. We see that DL signals from all the APs interfere with the UL signal received at any AP, unlike DTDD, where only the APs scheduled in DL interfere with signals received at the APs scheduled in UL. Then, the weighted received signal from the kth UL UE at the CPU becomes

$$\begin{aligned}\hat{s}_{\mathsf{u},k} = \sum_{m=1}^{M}\omega_{mk}^*\hat{s}_{\mathsf{u},mk} = \sqrt{\mathcal{E}_{\mathsf{u},k}}\sum_{m=1}^{M}\omega_{mk}^*\mathbf{v}_{mk}^H\mathbf{f}_{mk}s_{\mathsf{u},k} + \sum_{n\in\mathcal{U}_{\mathsf{u}}\setminus k}\sqrt{\mathcal{E}_{\mathsf{u},n}}\sum_{m=1}^{M}\omega_{mk}^*\mathbf{v}_{mk}^H\mathbf{f}_{mn}s_{\mathsf{u},n} \\ + \sqrt{\mathcal{E}_{\mathsf{d}}}\sum_{m=1}^{M}\omega_{mk}^*\sum_{\substack{j\neq m,\\ j=1}}^{M}\sum_{n\in\mathcal{U}_{\mathsf{d}}}\kappa_{jn}\mathbf{v}_{mk}^H\tilde{\mathbf{G}}_{mj}\mathbf{p}_{jn}s_{\mathsf{d},n} \\ + \sqrt{\mathcal{E}_{\mathsf{d}}}\sum_{m=1}^{M}\omega_{mk}^*\sum_{n\in\mathcal{U}_{\mathsf{d}}}\kappa_{mn}\mathbf{v}_{mk}^H\mathbf{G}_m^{\mathsf{SI}}\mathbf{p}_{mn}s_{\mathsf{d},n} + \sum_{m=1}^{M}\omega_{mk}^*\mathbf{v}_{mk}^H\mathbf{w}_{\mathsf{u},mk}.\end{aligned} \tag{5.40}$$

Hence, we can write the UL SINR of the kth UE for the FD system as follows:

$$\frac{\mathcal{E}_{\mathsf{u},k}|\boldsymbol{\omega_k}^H\mathbb{E}[\mathbf{u}_{kk}]|^2}{\boldsymbol{\omega_k}^H\left(\begin{array}{c}\sum\limits_{i\in\mathcal{U}_{\mathsf{u}}}\mathcal{E}_{\mathsf{u},i}\mathbb{E}[\mathbf{u}_{ki}\mathbf{u}_{ki}^H] - \mathcal{E}_{\mathsf{u},k}\mathbb{E}\left[\mathbf{u}_{kk}\right]\mathbb{E}[\mathbf{u}_{kk}^H] \\ + \sum\limits_{n\in\mathcal{U}_{\mathsf{d}}}\mathbb{E}[\mathbf{a}_{kn}\mathbf{a}_{kn}^H] + \mathbf{N}_{\mathsf{eff.}}\end{array}\right)\boldsymbol{\omega_k}},$$

where $\boldsymbol{\omega_k} \triangleq [\omega_{1k}, \omega_{2k}, \ldots, \omega_{Mk}]^T \in \mathbb{C}^M$, $\mathbf{u}_{ki} \triangleq [\mathbf{v}_{1k}^H\mathbf{f}_{1i}, \mathbf{v}_{2k}^H\mathbf{f}_{2i}, \ldots, \mathbf{v}_{Mk}^H\mathbf{f}_{Mi}]^T \in \mathbb{C}^M$, $[\mathbf{a}_{kn}]_m =$

$\sum_{\substack{j=1,\\ j\neq m}}^{M} \sqrt{\mathcal{E}_{\mathsf{d}}}\kappa_{jn}\mathbf{v}_{mk}^H\tilde{\mathbf{G}}_{mj}\mathbf{p}_{jn} + \sqrt{\mathcal{E}_{\mathsf{d}}}\kappa_{mn}\mathbf{v}_{mk}^H\mathbf{G}_m^{\mathsf{SI}}\mathbf{p}_{mn}$, and

$$\mathbf{N}_{\mathsf{eff.}} = N_0\mathtt{diag}\left(\mathbb{E}\left[\|\mathbf{v}_{1k}\|^2\right],\ldots,\mathbb{E}\left[\|\mathbf{v}_{Mk}\|^2\right]\right) \in \mathbb{C}^{M\times M}.$$

We note that the FD-SINR expression is similar to the DTDD case (see ((5.5)) except that we have set $\mathcal{A}_{\mathsf{u}} = M$ since all the APs are capable of UL reception, and the addition of IrAI in $[\mathbf{a}_{kn}]_m$. Hence, to avoid repetition, we present the final results related to the optimal CPU combining weights, the UL and DL SE expressions, and the power control algorithms for the FD system without detailed proofs.[10]

Corollary 5.1. *The optimal weighting vector for the kth UL UE at the CPU is* $\boldsymbol{\alpha}_k^{\mathsf{opt.}} = \mathcal{E}_{\mathsf{u},k}\mathbf{R}_\alpha^{-1}\bar{\mathbf{u}}_k$, *with* $\bar{\mathbf{u}}_k = [\alpha_{\mathsf{u},1k}^2, \alpha_{\mathsf{u},2k}^2,\ldots,\alpha_{\mathsf{u},Mk}^2]^T$ *and* $\mathbf{R}_\alpha = \sum_{k'\in\mathcal{P}_{l(k)\setminus k}} \mathcal{E}_{\mathsf{u},k'}\bar{\mathbf{u}}_{k'}\bar{\mathbf{u}}_{k'}^H + \frac{1}{N_{\mathsf{rx}}-\tau_p}\dot{\mathbf{R}}_\alpha + \frac{\mathcal{E}_{\mathsf{d}}}{N_{\mathsf{rx}}-\tau_p}\ddot{\mathbf{R}}_\alpha$, *where* $\dot{\mathbf{R}}_\alpha$ *and* $\ddot{\mathbf{R}}_\alpha$ *are diagonal matrices with mth diagonal entry being*

$$[\dot{\mathbf{R}}_\alpha]_m = \sum_{k'\in\mathcal{U}_{\mathsf{u}}} \mathcal{E}_{\mathsf{u},k'}\alpha_{\mathsf{u},mk}^2(\beta_{\mathsf{u},mk'} - \alpha_{\mathsf{u},mk'}^2) + N_0\alpha_{\mathsf{u},mk'}^2,$$
$$[\ddot{\mathbf{R}}_\alpha]_m = \sum_{j=1,j\neq m}^{M} N_{\mathsf{tx}}\kappa_{jn}^2\zeta_{mj}^{\mathsf{InAI}}\alpha_{\mathsf{u},mk}^2 + N_{\mathsf{tx}}\kappa_{mn}^2\alpha_{\mathsf{u},mk}^2\zeta_{mm}^{\mathsf{SI}},$$

respectively, for $m = 1,2,\ldots,M$.

Corollary 5.2. *The UL and DL SINRs of the FD CF MIMO system are, respectively,*

$$\eta_{\mathsf{u},k}(\boldsymbol{\kappa},\boldsymbol{\mathcal{E}}_{\mathsf{u}}) = \frac{(N_{\mathsf{rx}}-\tau_p)\mathcal{E}_{\mathsf{u},k}(\sum_{m=1}^{M}\omega_{mk}^*\alpha_{\mathsf{u},mk}^2)^2}{\left(\begin{array}{c}\mathtt{EST}_{\mathsf{u},k} + \mathtt{MUI}_{\mathsf{u},k}\\ +\mathtt{IAP}_k + N_0\sum_{m=1}^{M}|\omega_{mk}^*|^2\alpha_{\mathsf{u},mk}^2\end{array}\right)}, \tag{5.42}$$

[10] Our SE expressions match with those in the FD literature under special cases such as perfect channel estimation [24] and equal weight-based combining at the CPU [24, 92].

and

$$\eta_{\mathsf{d},n}(\boldsymbol{\kappa}, \boldsymbol{\mathcal{E}}_{\mathsf{u}}) = \frac{(N_{\mathsf{tx}} - \tau_p)\left(\sum_{j=1}^{M} \sqrt{\mathcal{E}_{\mathsf{d}}}\alpha_{\mathsf{d},jn}\kappa_{jn}\right)^2}{\mathtt{EST}_{\mathsf{d},n} + \mathtt{MUI}_{\mathsf{d},n} + \mathtt{IUE}_n + N_0}, \tag{5.43}$$

where $\mathtt{EST}_{\mathsf{u},k}$, $\mathtt{MUI}_{\mathsf{u},k}$ *and* $\mathtt{IAP}_k$ *correspond to interferences caused by the channel estimation error, multi-UE interference, and inter-AP interference. For DL,* $\mathtt{EST}_{\mathsf{d},n}$, $\mathtt{MUI}^{\mathsf{d}}_n$ *and* $\mathtt{IUE}_n$ *represent error due to channel estimation, the DL multi-UE interference and the UL UE to DL UE CLI, respectively. These terms can be evaluated as*

$$\begin{aligned}
\mathtt{EST}_{\mathsf{u},k} &= \sum_{k' \in \mathcal{U}_{\mathsf{u}}} \mathcal{E}_{\mathsf{u},k'} \sum_{m=1}^{M} |\omega^*_{mk}|^2 \alpha^2_{\mathsf{u},mk}(\beta_{\mathsf{u},mk'} - \alpha^2_{\mathsf{u},mk'}), \\
\mathtt{MUI}_{\mathsf{u},k} &= (N_{\mathsf{rx}} - \tau_p) \sum_{i \in \mathcal{P}_{l(k)} \setminus k} \mathcal{E}_{\mathsf{u},i} \Big(\sum_{m=1}^{M} \omega^*_{mk} \alpha^2_{\mathsf{u},mi} \Big)^2, \\
\mathtt{IAP}_k &= N_{\mathsf{tx}} \mathcal{E}_{\mathsf{d}} \sum_{n \in \mathcal{U}_{\mathsf{d}}} \sum_{m=1}^{M} \Big(\sum_{j=1, j \neq m}^{M} \kappa^2_{jn} \zeta^{\mathsf{InAI}}_{mj} |\omega^*_{mk}|^2 \alpha^2_{\mathsf{u},mk} + \kappa^2_{mn} |\omega^*_{mk}|^2 \alpha^2_{\mathsf{u},mk} \zeta^{\mathsf{SI}}_{mm} \Big), \\
\mathtt{EST}_{\mathsf{d},n} &= \sum_{q \in \mathcal{U}_{\mathsf{d}}} \sum_{j=1}^{M} \mathcal{E}_{\mathsf{d}} \kappa^2_{jq} (\beta_{\mathsf{d},jn} - \alpha^2_{\mathsf{d},jn}), \\
\mathtt{MUI}^{\mathsf{d}}_n &= (N_{\mathsf{tx}} - \tau_p) \mathcal{E}_{\mathsf{d}} \sum_{q \in \mathcal{P}_{l(n)} \setminus n} \Big(\sum_{j=1}^{M} \kappa_{jq} \alpha_{\mathsf{d},jn} \Big)^2, \\
\mathtt{IUE}_n &= \sum_{k \in \mathcal{U}_{\mathsf{u}}} \mathcal{E}_{\mathsf{u},k} \epsilon_{nk}.
\end{aligned}$$

Thus, the sum UL-DL SE of the FD enabled CF-system can be expressed as

$$\mathcal{R}_{\mathsf{s}}(\boldsymbol{\kappa}, \boldsymbol{\mathcal{E}}_{\mathsf{u}}) = \frac{\tau - \tau_p}{\tau} \left[\sum_{k \in \mathcal{U}_{\mathsf{u}}} \log(1 + \eta_{\mathsf{u},k}(\boldsymbol{\kappa}, \boldsymbol{\mathcal{E}}_{\mathsf{u}})) + \sum_{n \in \mathcal{U}_{\mathsf{d}}} \log(1 + \eta_{\mathsf{d},n}(\boldsymbol{\kappa}, \boldsymbol{\mathcal{E}}_{\mathsf{u}})) \right]. \tag{5.45}$$

Proof. See Appendix D.4 ■

From the expression for $\mathtt{IAP}_k$, we see that the DL signals from *all* the APs interfere with the UL signals of any AP, unlike DTDD. On the other hand, there is no need for scheduling APs in UL/DL in the FD system. Thus, we only need to consider power allocation for the FD system. However, it is easy to apply the UL and DL power allocation

protocols developed for the DTDD-enabled system in the FD case. As mentioned earlier, instead of the scheduled UL and DL AP subsets, we now have $\mathcal{A}_{\mathsf{u}} = \mathcal{A}_{\mathsf{d}} = \{1, 2, \ldots, M\}$. This only changes the limits of the summations in the beamforming gain and the interference terms. Secondly, due to IrAI, for the sub-problem of UL power allocation, the effective noise additionally includes the power of IrAI. To elaborate, in the FD case, we have $\mathsf{G}_{\mathsf{u},k}(\boldsymbol{\mathcal{E}}_{\mathsf{u}}) = (N - \tau_p)\mathcal{E}_{\mathsf{u},k}\left(\sum_{m=1}^{M} \omega_{mk}^{*}\alpha_{mk}^{2}\right)^{2}$, $\mathsf{I}_{\mathsf{u},k}(\boldsymbol{\mathcal{E}}_{\mathsf{u}}) = \mathtt{EST}_{\mathsf{u},k} + \mathtt{MUI}_{\mathsf{u},k} + \sigma^{2}_{\mathsf{eff.},\mathsf{u},k}$, and $\sigma^{2}_{\mathsf{eff.},\mathsf{u},k} \triangleq \left(\mathtt{IAP}_k + N_0 \sum_{m=1}^{M} |\omega_{mk}^{*}|^2 \alpha_{mk}^{2}\right)$. Recall that $\sigma^{2}_{\mathsf{eff.},\mathsf{u},k}$ is the power of the effective noise, which does not depend on the UL transmit powers. Here, $\mathtt{IAP}_k$ also includes the IrAI power, unlike DTDD. Thus, the original structure of the problem, as described for DTDD in Section 5.4.b, does not change. Similar arguments can also be made for the case of DL. Thus, the algorithms (namely Algorithm 7, Algorithm 8, and Algorithm 9) derived for DTDD directly apply to the FD system.

5.6 Orthgonal Pilots and Fixed Power Allocation: A Special Case

In this section, we present the achievable SEs with MRC in the UL and MFP in the DL, considering orthogonal pilot allocation and fixed power allocation. These results can be easily derived as special cases of the theories developed in the earlier sections. However, having a simplified model helps us understand the effects of various system parameters on the sum UL-DL SE, which is the purpose of this section. We first analyze the DTDD enabled CF-mMIMO system and then discuss the FD CF-mMIMO case.

5.6.a SE Analysis: DTDD

We first present a closed-form expression for the UL SINR.

Lemma 5.5. *The UL SINR of the kth UE can be expressed as*

$$\eta_{\mathsf{u},k} = \frac{N\mathcal{E}_{\mathsf{u},k}\left(\sum\limits_{m\in\mathcal{A}_{\mathsf{u}}}\alpha_{mk}^2\right)^2}{\mathtt{MUI}_k^{\mathsf{u}} + \mathtt{IAP}_k + N_0\sum\limits_{m\in\mathcal{A}_{\mathsf{u}}}\alpha_{mk}^2}, \tag{5.46}$$

where $\mathtt{MUI}_k^{\mathsf{u}}$ *represents multi-user interference and* $\mathtt{IAP}_k$ *represents inter-AP CLI. These are given by*

$$\mathtt{MUI}_k^{\mathsf{u}} = \sum_{m\in\mathcal{A}_{\mathsf{u}}}\sum_{n\in\mathcal{U}_{\mathsf{u}}}\mathcal{E}_{\mathsf{u},n}\alpha_{mk}^2\beta_{mn}, \tag{5.47a}$$

$$\mathtt{IAP}_k = N\sum_{n\in\mathcal{U}_{\mathsf{d}}}\sum_{m\in\mathcal{A}_{\mathsf{u}}}\sum_{j\in\mathcal{A}_{\mathsf{d}}}\mathcal{E}_{\mathsf{d},j}\kappa_{jn}^2\zeta_{mj}\alpha_{mk}^2\alpha_{jn}^2. \tag{5.47b}$$

Proof. The above result can be derived following the steps outlined in Chapter 4 ([33]) with c_{mk} replaced with $(\tau_p\mathcal{E}_{p,k}\beta_{mk}+N_0)^{-1}$, and ignoring the effect of pilot contamination. ■

Next, we present the DL SINR in the following lemma.

Lemma 5.6. *The DL SINR for the nth UE can be expressed as*

$$\eta_{\mathsf{d},n} = \frac{N^2\left(\sum\limits_{j\in\mathcal{A}_{\mathsf{d}}}\kappa_{jn}\sqrt{\mathcal{E}_{\mathsf{d},j}}\alpha_{jn}^2\right)^2}{\mathtt{MUI}_n^{\mathsf{d}} + \mathtt{IUE}_n + N_0}, \tag{5.48}$$

where $\mathtt{MUI}_n^{\mathsf{d}}$ *and* $\mathtt{IUE}_n$ *represent the DL multi-user interference and the UL UE to DL UE CLI, respectively, and read as*

$$\mathtt{MUI}_n^{\mathsf{d}} = N\sum_{q\in\mathcal{U}_{\mathsf{d}}}\sum_{j\in\mathcal{A}_{\mathsf{d}}}\mathcal{E}_{\mathsf{d},j}\kappa_{jq}^2\beta_{jn}\alpha_{jq}^2, \tag{5.49a}$$

$$\mathtt{IUE}_n = \sum_{k\in\mathcal{U}_{\mathsf{u}}}\mathcal{E}_{\mathsf{u},n}\epsilon_{nk}. \tag{5.49b}$$

With the above SINR expressions in hand, we can write the overall sum UL-DL SE of

the system as

$$\mathcal{R}_{\text{sum}}^{\text{DTDD}} = \frac{\tau - \tau_p}{\tau} \left[\sum_{k \in \mathcal{U}_{\mathsf{u}}} \mathcal{R}_{\mathsf{u},k} + \sum_{n \in \mathcal{U}_{\mathsf{d}}} \mathcal{R}_{\mathsf{d},n} \right], \tag{5.50}$$

where $\mathcal{R}_{\mathsf{u},k} = \log_2(1 + \eta_{\mathsf{u},k})$ and $\mathcal{R}_{\mathsf{d},n} = \log_2(1 + \eta_{\mathsf{d},n})$.

Note that, from Lemma 5.5 and Lemma 5.6, the gain and interference terms involved in the UL and DL SINRs are dependent on $\mathcal{A}_{\mathsf{u}}$ and $\mathcal{A}_{\mathsf{d}}$. Consequently, $\mathcal{R}_{\text{sum}}^{\text{DTDD}}$ depends on which APs are scheduled in the UL and DL. Clearly, the brute-force approach of listing out all the $2^{|\mathcal{A}_{\mathsf{u}} \cup \mathcal{A}_{\mathsf{d}}|}$ possible AP schedules and computing their achievable sum UL-DL SE using (5.50) makes the complexity of finding an optimal AP schedule exponential in the number of APs. As a low-complexity and pragmatic alternative, we use the greedy algorithm presented in [33]. In this approach, the incremental gain in sum UL-DL SE by activating each APs in the UL and DL modes is evaluated using (5.51a) and (5.51b),[11] and the AP that procures the maximum incremental gain in the sum UL-DL SE is scheduled in the corresponding mode; and this is repeated till all the APs are scheduled. It suffices to say that this greedy approach provides nearly identical performance as exhaustive search across all cases of our extensive simulation-based experiments.

5.6.b SE Analysis: FD

Now, we analyze the UL and DL SE of the FD CF-mMIMO system. We consider a similar distributed processing scheme as discussed in Section 5.6.a, except that each AP is now FD-enabled. Furthermore, each AP suffers from SI, incurring additional interference in the UL. We present our final closed-form expressions in the following Corollary.

[11] In (5.51a) and (5.51b), the scheduled AP set is denoted by $\mathcal{A}_s \subseteq \mathcal{A}$, consisting of UL and DL AP indices denoted by $\mathcal{A}_s^{\mathsf{u}}$ and $\mathcal{A}_s^{\mathsf{d}}$, with $\mathcal{A}_s^{\mathsf{u}} \cup \mathcal{A}_s^{\mathsf{d}} = \mathcal{A}_s$, respectively. Also, $\{j\} \notin \mathcal{A}_s$ denotes an unscheduled AP. $\delta_{\mathsf{u},j}$ and $\delta_{\mathsf{d},j}$ are the incremental gain obtained by scheduling the $\{j\}$th AP in UL and in DL, respectively. Thus, if $\delta_{\mathsf{u},j} > \delta_{\mathsf{d},j}$, we schedule the $\{j\}$th AP in the UL.

$$\delta_{\mathsf{u},j} = \sum_{k\in\mathcal{U}_{\mathsf{u}}} \log_2 \left[\left(1 + \frac{N\mathcal{E}_{\mathsf{u},k}\big(\sum\limits_{m\in\mathcal{A}_s^{\mathsf{u}}\cup j} \alpha_{mk}^2\big)^2}{\left(\begin{array}{c} \sum\limits_{m\in\mathcal{A}_s^{\mathsf{u}}\cup j}\sum\limits_{n\in\mathcal{U}_{\mathsf{u}}} \mathcal{E}_{\mathsf{u},n}\alpha_{mk}^2\beta_{mn} \\ +N\sum\limits_{n\in\mathcal{U}_{\mathsf{d}}}\sum\limits_{m\in\mathcal{A}_s^{\mathsf{u}}\cup j}\sum\limits_{j\in\mathcal{A}_s^{\mathsf{d}}} \mathcal{E}_{\mathsf{d},j}\kappa_{jn}^2\zeta_{mj}\alpha_{mk}^2\alpha_{jn} + N_0\sum\limits_{m\in\mathcal{A}_s^{\mathsf{u}}\cup j}\alpha_{mk}^2 \end{array} \right)} \right) \right.$$
$$\left. \times \left(1 + \frac{N\mathcal{E}_{\mathsf{u},k}\left(\sum\limits_{m\in\mathcal{A}_s^{\mathsf{u}}}\alpha_{mk}^2\right)^2}{\sum\limits_{m\in\mathcal{A}_s^{\mathsf{u}}}\sum\limits_{n\in\mathcal{U}_{\mathsf{u}}} \mathcal{E}_{\mathsf{u},n}\alpha_{mk}^2\beta_{mn} + N\sum\limits_{n\in\mathcal{U}_{\mathsf{d}}}\sum\limits_{m\in\mathcal{A}_s^{\mathsf{u}}}\sum\limits_{j\in\mathcal{A}_s^{\mathsf{d}}} \mathcal{E}_{\mathsf{d},j}\kappa_{jn}^2\zeta_{mj}\alpha_{mk}^2\alpha_{jn} + N_0\sum\limits_{m\in\mathcal{A}_s^{\mathsf{u}}}\alpha_{mk}^2} \right)^{-1} \right] \tag{5.51a}$$

$$\delta_{\mathsf{d},j} = \sum_{k\in\mathcal{U}_{\mathsf{u}}} \log_2 \left[\left(1 + \frac{N\mathcal{E}_{\mathsf{u},k}\big(\sum\limits_{m\in\mathcal{A}_s^{\mathsf{u}}} \alpha_{mk}^2\big)^2}{\left(\begin{array}{c} \sum\limits_{m\in\mathcal{A}_s^{\mathsf{u}}}\sum\limits_{n\in\mathcal{U}_{\mathsf{u}}} \mathcal{E}_{\mathsf{u},n}\alpha_{mk}^2\beta_{mn} \\ +N\sum\limits_{n\in\mathcal{U}_{\mathsf{d}}}\sum\limits_{m\in\mathcal{A}_s^{\mathsf{u}}}\sum\limits_{j\in\mathcal{A}_s^{\mathsf{d}}\cup j} \mathcal{E}_{\mathsf{d},j}\kappa_{jn}^2\zeta_{mj}\alpha_{mk}^2\alpha_{jn} + N_0\sum\limits_{m\in\mathcal{A}_s^{\mathsf{u}}}\alpha_{mk}^2 \end{array} \right)} \right) \right.$$
$$\left. \times \left(1 + \frac{N\mathcal{E}_{\mathsf{u},k}\left(\sum\limits_{m\in\mathcal{A}_s^{\mathsf{u}}}\alpha_{mk}^2\right)^2}{\left(\begin{array}{c} \sum\limits_{m\in\mathcal{A}_s^{\mathsf{u}}}\sum\limits_{n\in\mathcal{U}_{\mathsf{u}}} \mathcal{E}_{\mathsf{u},n}\alpha_{mk}^2\beta_{mn} \\ +N\sum\limits_{n\in\mathcal{U}_{\mathsf{d}}}\sum\limits_{m\in\mathcal{A}_s^{\mathsf{u}}}\sum\limits_{j\in\mathcal{A}_s^{\mathsf{d}}} \mathcal{E}_{\mathsf{d},j}\kappa_{jn}^2\zeta_{mj}\alpha_{mk}^2\alpha_{jn} + N_0\sum\limits_{m\in\mathcal{A}_s^{\mathsf{u}}}\alpha_{mk}^2 \end{array} \right)} \right)^{-1} \right]$$
$$+ \sum_{n\in\mathcal{U}_{\mathsf{d}}} \log_2 \left(1 + \frac{N^2\big(\sum_{j\in\mathcal{A}_s^{\mathsf{d}}\cup j}\kappa_{jn}\sqrt{\mathcal{E}_{\mathsf{d},j}}\alpha_{jn}^2\big)^2}{N\sum\limits_{q\in\mathcal{U}_{\mathsf{d}}}\sum\limits_{j\in\mathcal{A}_s^{\mathsf{d}}\cup j} \mathcal{E}_{\mathsf{d},j}\kappa_{jq}^2\beta_{jn}\alpha_{jq}^2 + \mathtt{IUE}_n + N_0} \right)$$
$$\times \left(1 + \frac{N^2\big(\sum_{j\in\mathcal{A}_s^{\mathsf{d}}}\kappa_{jn}\sqrt{\mathcal{E}_{\mathsf{d},j}}\alpha_{jn}^2\big)^2}{N\sum\limits_{q\in\mathcal{U}_{\mathsf{d}}}\sum\limits_{j\in\mathcal{A}_s^{\mathsf{d}}} \mathcal{E}_{\mathsf{d},j}\kappa_{jq}^2\beta_{jn}\alpha_{jq}^2 + \mathtt{IUE}_n + N_0} \right)^{-1} \tag{5.51b}$$

Corollary 5.3. *The sum UL-DL SE of the FD CF system is*

$$\mathcal{R}_{\text{sum}}^{\text{FD}} = \frac{\tau - \tau_p}{\tau} \left[\sum_{k \in \mathcal{U}_{\mathsf{u}}} \log_2(1 + \eta_{\mathsf{u},k}) + \sum_{n \in \mathcal{U}_{\mathsf{d}}} \log_2(1 + \eta_{\mathsf{d},n}) \right], \tag{5.52}$$

with the UL SINR of the kth UL UE and the DL SINR of the nth DL UE respectively evaluated as

$$\eta_{\mathsf{u},k} = \frac{N_{\text{rx}}^2 \mathcal{E}_{\mathsf{u},k} \left(\sum\limits_{m \in \mathcal{A}} \alpha_{mk}^{u2} \right)^2}{\mathtt{MUI}_k^{\mathsf{u}} + \mathtt{IAP}_k + N_{\text{rx}} N_0 \sum\limits_{m \in \mathcal{A}} \alpha_{mk}^{u2}} \tag{5.53a}$$

$$\eta_{\mathsf{d},k} = \frac{N_{\text{tx}}^2 \left(\sum_{j \in \mathcal{A}} \kappa_{jn} \sqrt{\mathcal{E}_{\mathsf{d},j}} \alpha_{jn}^{d2} \right)^2}{\mathtt{MUI}_n^{\mathsf{d}} + \mathtt{IUE}_n + N_0}, \tag{5.53b}$$

where $\mathcal{A} = \mathcal{A}_{\mathsf{u}} \cup \mathcal{A}_{\mathsf{d}}$. *The UL multi-user interference, inter-AP CLI, and the DL multi-user interference read as*

$$\mathtt{MUI}_k^{\mathsf{u}} = N_{\text{rx}} \sum_{m \in \mathcal{A}_{\mathsf{u}}} \sum_{n \in \mathcal{U}_{\mathsf{u}}} \mathcal{E}_{\mathsf{u},n} \alpha_{mk}^{u2} \beta_{mn}^{\mathsf{u}}, \tag{5.54a}$$

$$\begin{aligned} \mathtt{IAP}_k = {} & N_{\text{tx}} N_{\text{rx}} \sum_{n \in \mathcal{U}_{\mathsf{d}}} \sum_{m \in \mathcal{A}} \sum_{\substack{j \in \mathcal{A}, \\ j \neq m}} \mathcal{E}_{\mathsf{d},j} \kappa_{jn}^2 \zeta_{mj} \alpha_{mk}^{u2} \alpha_{jn}^{d2} \\ & + N_{\text{tx}} \sum_{n \in \mathcal{U}_{\mathsf{d}}} \sum_{m \in \mathcal{A}} \mathcal{E}_{\mathsf{d},m} \kappa_{mn}^2 \zeta_{mm} \alpha_{mk}^{u2} \alpha_{mn}^{d2} \mathtt{tr} \left(\mathbb{E} \left[\mathbf{G}_{mm}^{\text{SI}} \mathbf{G}_{mm}^{\text{SI}\ H} \right] \right), \end{aligned} \tag{5.54b}$$

$$\mathtt{MUI}_n^{\mathsf{d}} = N_{\text{tx}} \sum_{q \in \mathcal{U}_{\mathsf{d}}} \sum_{j \in \mathcal{A}} \mathcal{E}_{\mathsf{d},j} \kappa_{jq}^2 \beta_{jn}^{\mathsf{d}} \alpha_{jq}^{d2}, \tag{5.54c}$$

respectively. The inter-UE interference is given by (5.49b).

We can now comment on the benefits and challenges associated with FD and DTDD within the purview of CF-mMIMO. From Corollary 5.3, in FD, all the APs ($\mathcal{A}$) participate in UL as well in DL; unlike in DTDD where a subset of APs receive in the UL (the set $\mathcal{A}_{\mathsf{u}}$) and its complement set serves the DL UEs. This is an advantage of FD-enabled APs. However, if we consider similar antenna density per AP in both the schemes, i.e., $N_{\text{tx}} + N_{\text{rx}} = N$, the UL/DL array gain in DTDD scales with N; while in FD, it scales with N_{tx} or N_{rx}. Therefore, if the localized traffic demand at (or a set of) APs is asymmetric in

the UL and DL directions, DTDD can potentially procure much better system throughput.

5.7 Numerical Results

We consider that the UEs are dropped uniformly at random locations in a 1 km^2 square area. We take 5,000 random channel instantiations for Monte Carlo averaging. We consider 50% of the UEs to have UL data demands. The APs are deployed on a uniform rectangular grid for better coverage. The large scale fading between the mth AP and the kth UE is modeled as $\beta_{mk} = 10^{\frac{\mathsf{PL}_{mk} + \sigma_{\mathsf{sh.}} z_{mk}}{10}}$, where the path-loss PL_{mk} follows the three-slope model in [24], $\sigma_{\mathsf{sh.}} = 6$ dB, and $z_{mk} \sim \mathcal{N}(0,1)$. The system bandwidth and noise figure are taken as 20 MHz and 9 dB, respectively, which gives a noise variance of -92 dBm. The coherence interval consists of 200 channel uses [20]. The pilot SNR is taken as 20 dB. We set the algorithm parameters δ_{u}, δ_{d}, δ_{ADMM} and δ_{p} to 0.001. Other parameters, such as the number of APs, UEs, UL/DL data transmit powers, etc., are mentioned in the plots.

In Figure 5.4, we compare the cumulative distribution function (CDF) of the achievable UL SE with different power allocation schemes. We observe that FP-based power control added with weighted combing at the CPU (see $\mathsf{WC} + \mathsf{FP}$) uniformly outperforms only FP-based power control (see FP without WC) and only weighted combing at the CPU (see WC). This underlines the need for weighted combing along with UL power control rather than applying each individually. Further, we compare the proposed $\mathsf{WC} + \mathsf{FP}$ scheme with the estimated channel variance and large-scale fading-dependent power control scheme proposed by Nikbakht et al. in [104, 105], and we observe almost 4-fold improvement in 90%-likely UL SE rendered by our algorithm. Also, we verify the correctness of our derived closed-form expression for weighted combing given in Lemma 5.2 (see WC : Lemma 5.2) with that of Lemma 5.1 (see WC : Lemma 5.1), and see that SE achieved by derived weights matches the theoretical SE.

In Figure 5.5, we compare the CDFs of the achievable DL SE with our proposed FP and

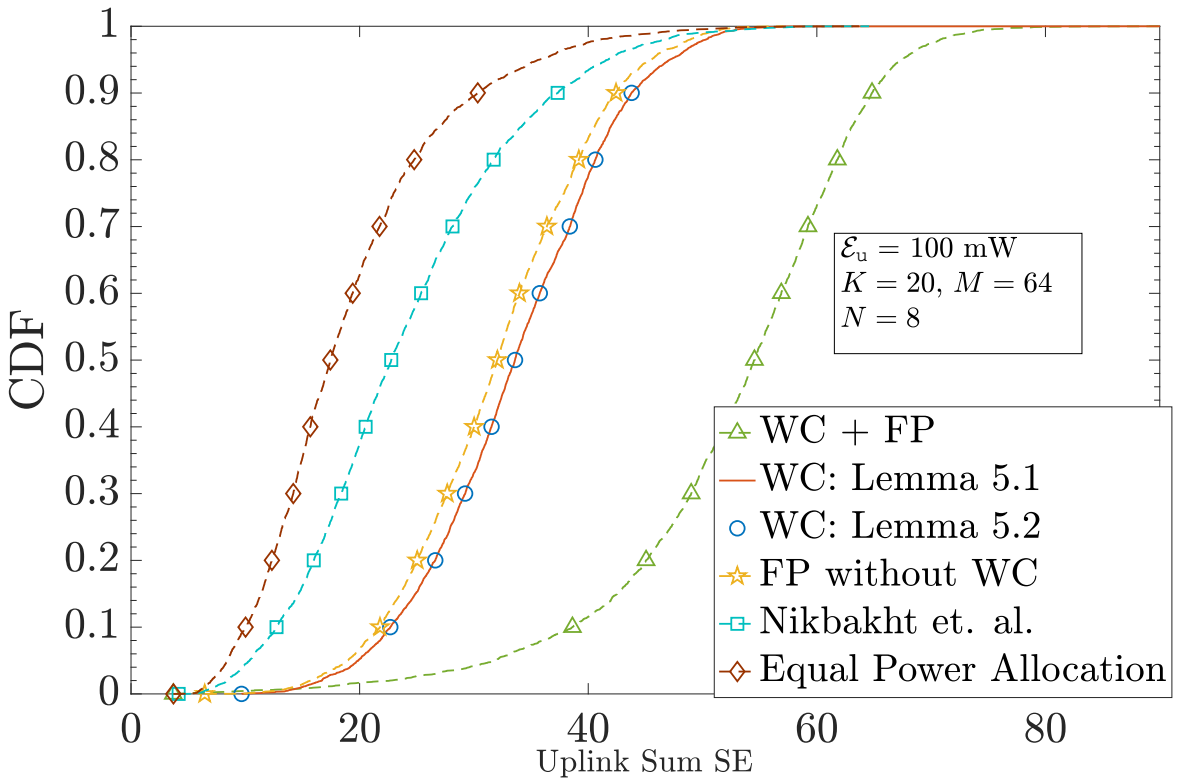

Figure 5.4: UL sum SE under the proposed power control algorithm and comparison with existing approaches [104, 105]. Optimal weighting at the CPU along with FP-based power control yields the best performance.

ADMM-based algorithm with equal power allocation and the scalable DL power allocation algorithm proposed by Interdonato et al. in [106]. We observe almost 43% improvement in the 90% sum DL SE attained by our proposed algorithm compared to the method in [106]. Further, compared to the equal power allocation scheme for DL outlined by Vu et al. in [24], Algorithm 9 procures almost 5-fold improvement in the SE. Also, as we increase the maximum DL transmit power budget per AP, the DL SE uniformly improves for all schemes.

We now compare the performances of DTDD and FD CF MIMO. In particular, we assume the InAI and IrAI are well suppressed, at -40 dB. Figure 5.6 compares the sum SEs under the two duplexing schemes considering different AP and antenna densities. We observe that an FD system with ($N_{\mathsf{tx}} = N_{\mathsf{rx}} = N, M = 64$) offers only 6% improvement

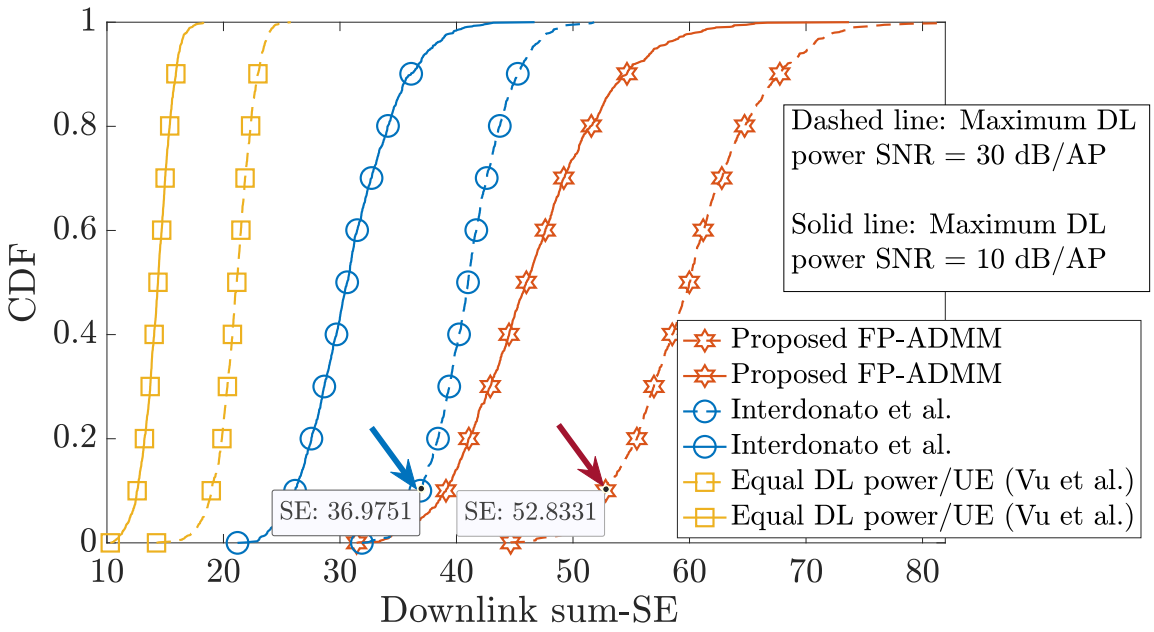

Figure 5.5: DL sum SE under the proposed power control algorithm and comparison with an existing approach [106]. This figure illustrates the improvement in DL sum SE that can be attained via our algorithm.

---

in the 90%-likely sum SE compared to a DTDD enabled CF-system with N antennas per 64 APs. However, the former system has double the antenna density compared to the DTDD CF system. If we consider the same antenna density in the two systems, then the 90%-likely sum SE of the DTDD CF system is 21% more than that of the FD system (see $(N_{\mathsf{tx}} = N_{\mathsf{rx}} = N/2, M = 64)$). This is because, in DTDD, the APs are scheduled based on the local UL/DL load in its vicinity, and hence, if there is more UL load near to one or a set of APs, those APs are scheduled in UL, which in turn leads to a beamforming gain in UL that scales with N. On the other hand, in the FD system, the beamforming gain scales with $N/2$. Recall that although in the FD system, all the APs are FD enabled, APs far away from the UEs contribute minimally to the overall sum SE. Thus, scheduling APs based on the localized traffic load is more beneficial.

In Figure 5.7, we illustrate the effect of IrAI on the performance of the FD CF system and contrast it with the DTDD CF system. When the IrAI is -20 dB, FD uniformly

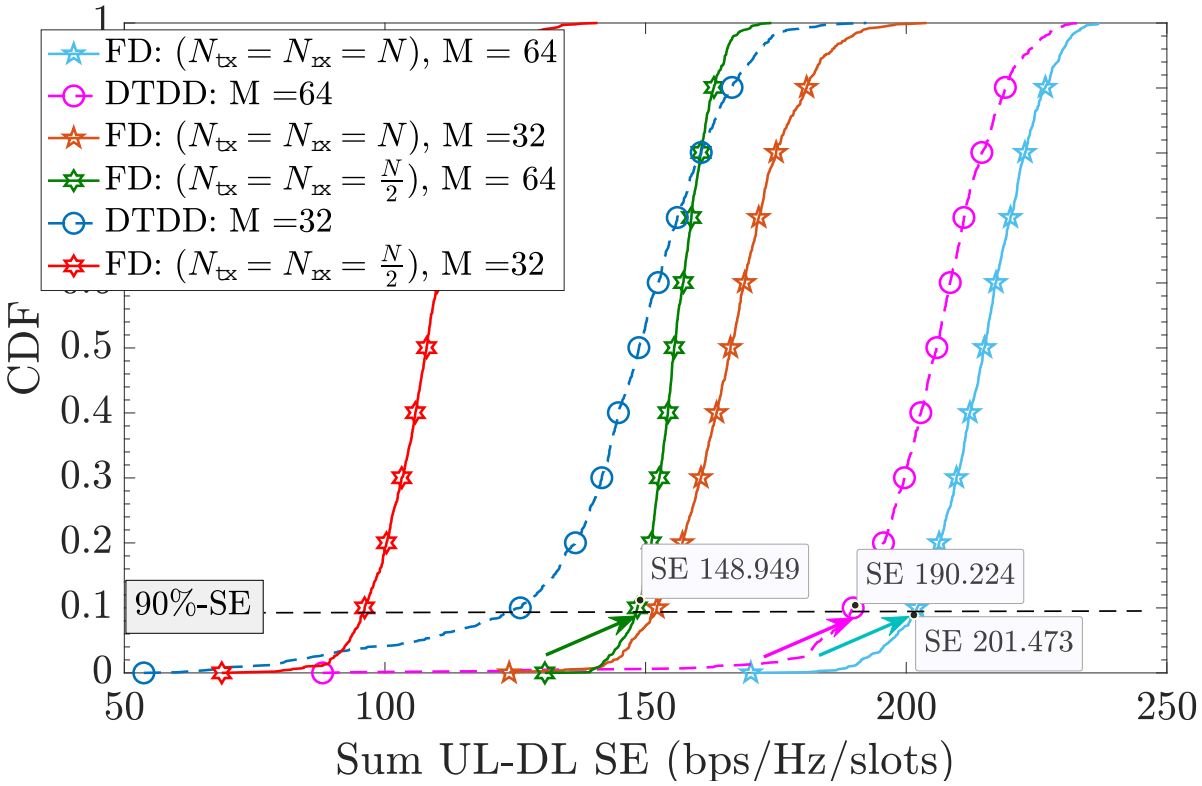

Figure 5.6: Performance comparison of DTDD and FD systems with various antenna and AP densities. We consider $K = 40$. Each HD AP is equipped with $N = 8$ antennas. InAI and IrAI strengths are taken as -40 dB.

outperforms the DTDD system even when the FD system has double the antenna density. However, as the IrAI strength increases, the sum SE of FD starts to deteriorate, achieving a 40% lower sum SE than DTDD when IrAI is 10 dB. Thus, the performance of FD is highly dependent on the level of IrAI suppression, while DTDD completely obviates the need for IrAI suppression and offers similar performance to that of an FD system having double the antenna density and low IrAI.

In Figure 5.8, we further inspect the variation of the sum SE over a wide range of IrAI for the FD system and compare the performance to the DTDD system. Even with double antenna density, the FD system can perform very poorly when IrAI strength becomes more pronounced (see the shaded region).

In Figure 5.9, we illustrate the effect of InAI on the sum SE. An FD system with ($M =$

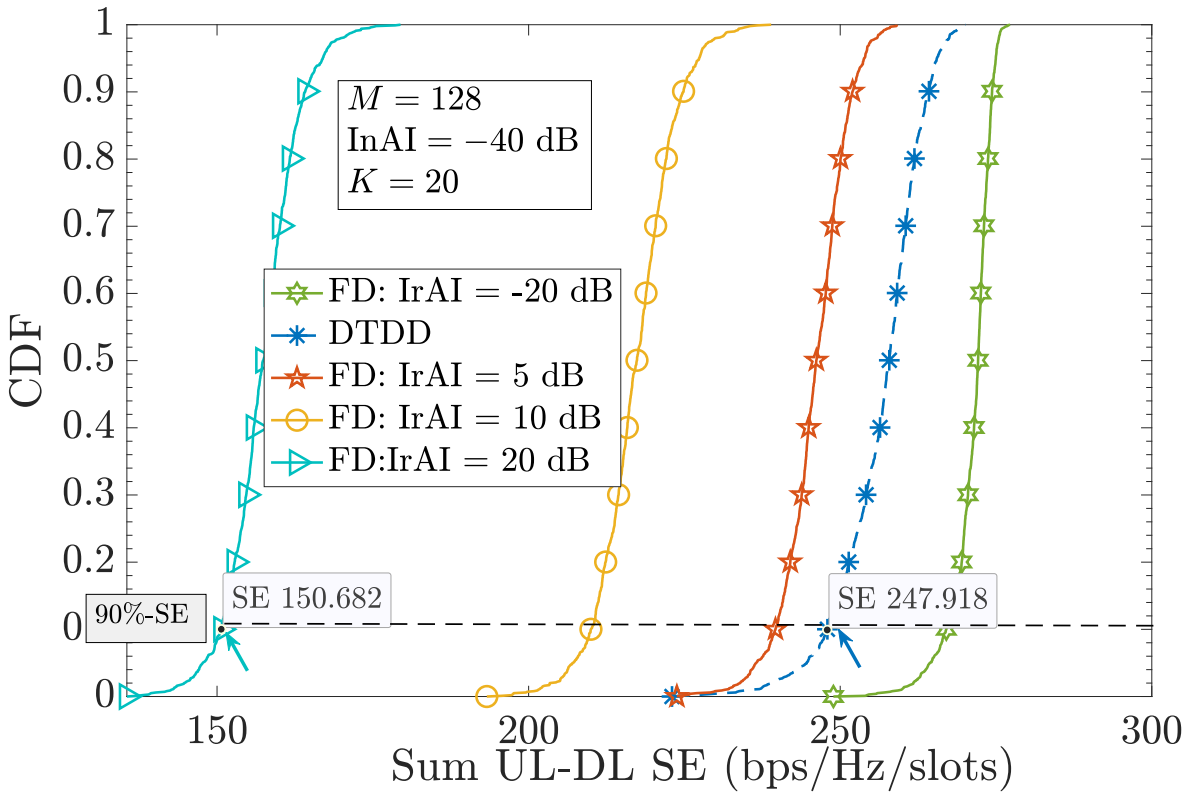

Figure 5.7: Effect of intra-AP interference (IrAI) on the performance of the FD system while InAI is maintained the same for both DTDD and FD systems.

$64, N_{\text{tx}} = N_{\text{rx}} = N = 8$) with IrAI -20 dB outperforms DTDD with ($M = 64, N = 8$) (i.e., half the antenna density compared to the FD system) when the InAI is no more than ≈ 11 dB above the noise floor. However, beyond an InAI of 11 dB, the sum SE of the FD system degrades compared to the DTDD system. This is because, in the FD system, all APs cause InAI, while in DTDD, only the DL-scheduled APs cause inter-AP interference.

Finally, in Figure 5.10, we plot the CDF of sum UL-DL SE of the DTDD and FD systems with MMSE combining in the UL and RZF precoding in the DL, and illustrate the effects of both power control and IrAI on the sum UL-DL SE. We obtain substantial benefits by applying the proposed power control algorithms compared to equal power allocation. This illustrates the applicability of the algorithms developed here to different precoder and combining schemes. Also, with similar antenna density, DTDD uniformly outperforms FD even with MMSE and RZF. This is because of the additional degrees of freedom DTDD

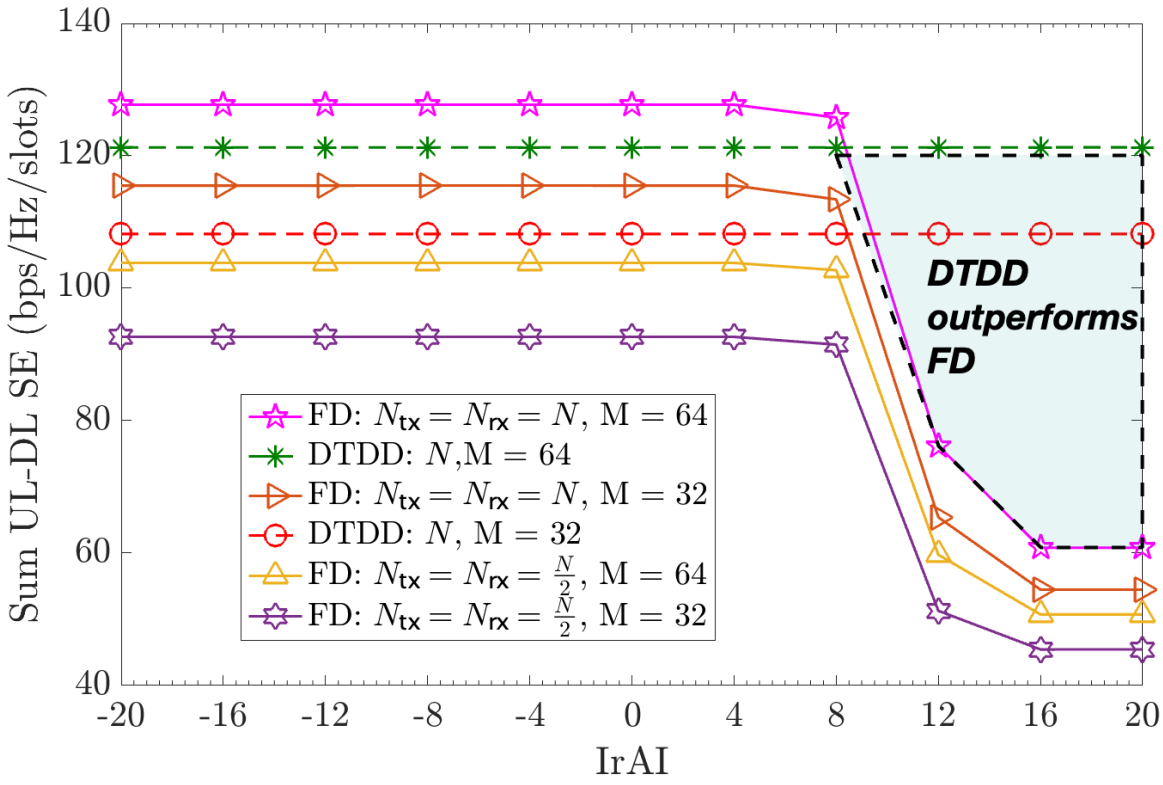

Figure 5.8: Sum UL-DL SE as a function of IrAI. DTDD can outperform FD even though the latter has double the antenna density

offers in terms of UL and DL AP scheduling and, consequently, mitigating the effects of InAI better than the FD system.

5.8 Chapter Summary

In this chapter, we presented a comparative study of DTDD and FD in CF systems. We first showed that the performance of these two duplexing schemes depends heavily on InAI, IrAI (for FD), and InUI, which in turn depends on the channel estimation error (and the pilot contamination level), UL and DL power allocation strategy, and the scheduled AP set (for DTDD). Then, we optimized the UL and DL power allocation and AP scheduling for DTDD, to maximize the sum UL-DL SE. We solved this NP-hard and non-convex problem by decoupling it into AP-scheduling, UL, and DL power allocation

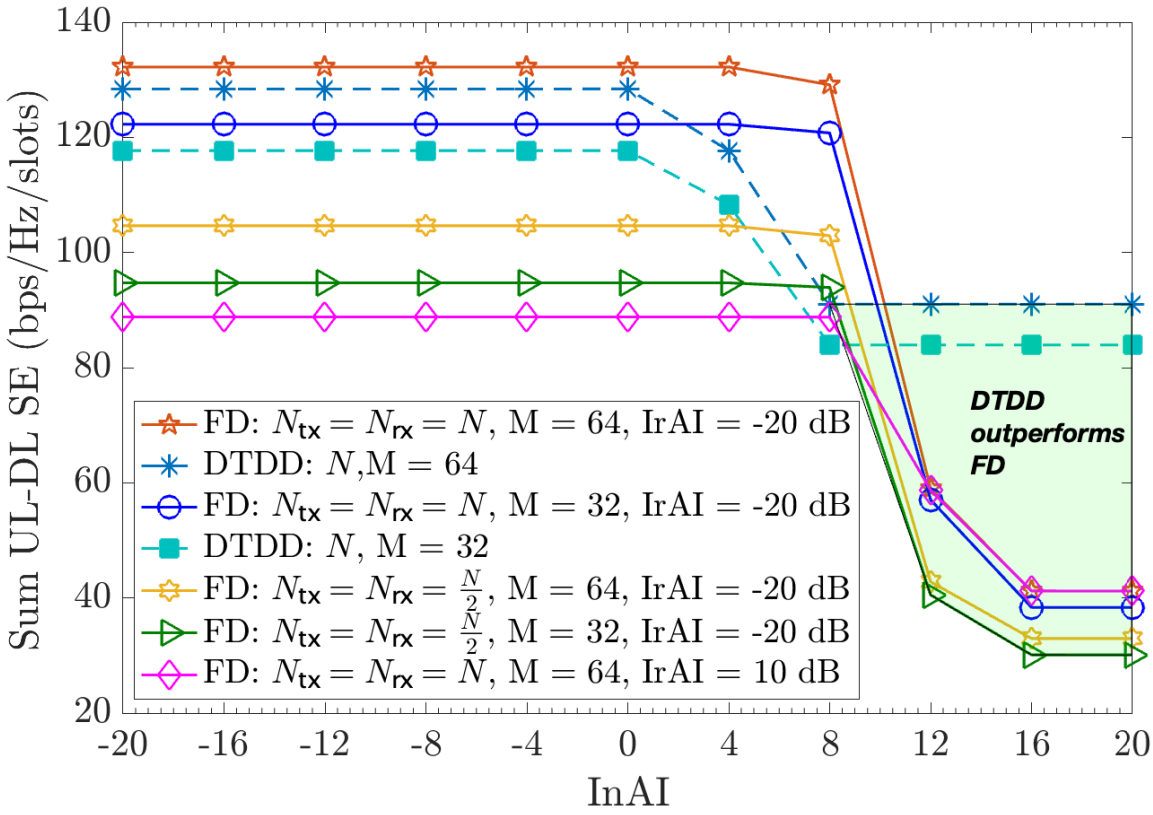

Figure 5.9: Effects of inter-AP interference (InAI) on the sum UL-DL SE. We observe that DTDD is more resilient to InAI.

sub-problems. We developed FP-based UL/DL power allocation algorithms and proved the convergence of the sub-problems to local optima. Further, we provided closed-form update equations using the Lagrange dual transform and ADMM for the sub-problems, making them easy to implement. We numerically illustrated the superiority of considering UL-DL power allocation and optimal weighting at the CPU over the case when either equal power allocation and/or only optimal weighting is considered (as were the scenarios in Chapter 3 and Chapter 4). Our experiments also underscored the interference suppression capabilities of MMSE-type combiners and precoders over ZF and MR-based combiners and precoders. Finally, we saw that DTDD outperforms FD when the two systems have a similar antenna density. This happens because DTDD can schedule the APs in UL or DL based on the localized traffic load and achieve better array gain for a given antenna density

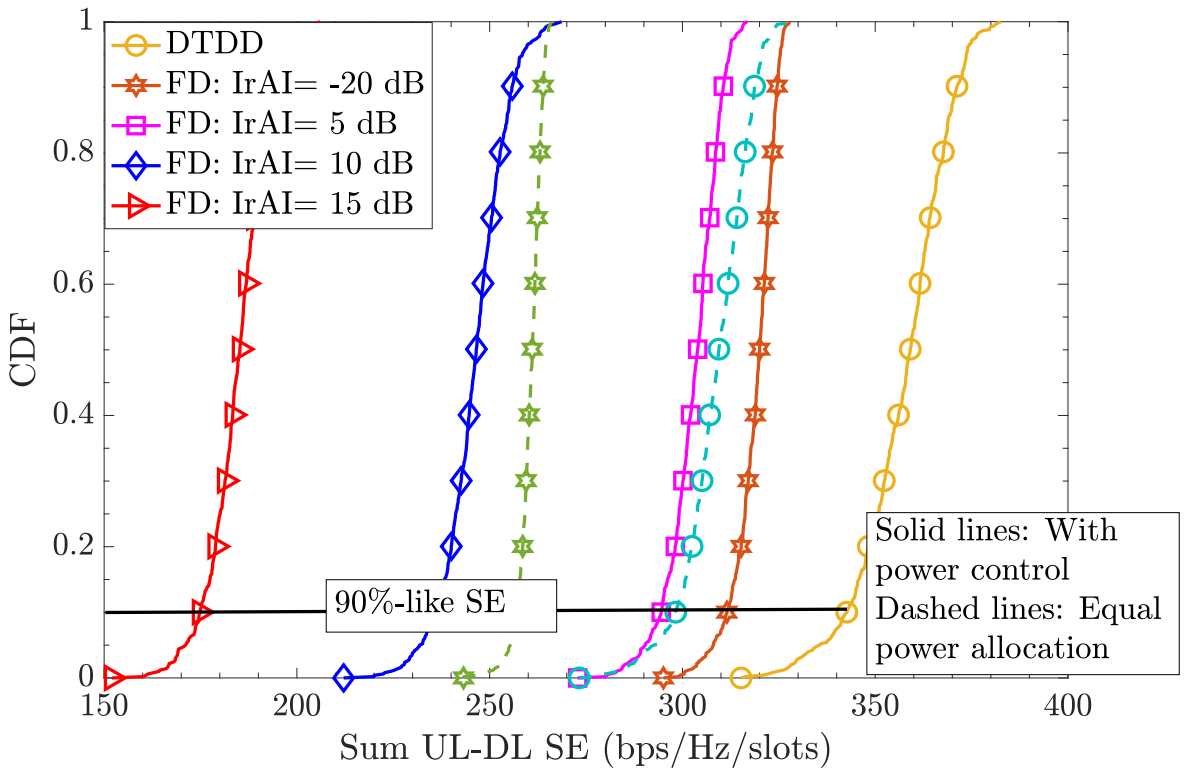

Figure 5.10: Effect of IrAI on the sum UL-DL SE with MMSE combiner in the UL and RZF precoder in the DL. InAI strength is taken as -40 dB, and we consider $K = 20, M = 64, N = 8, N_{\text{tx}} = N_{rx} = N/2$ (i.e., similar antenna density.)

---

and InAI suppression. Thus, we conclude that although both DTDD and FD enable the CF system to serve UL and DL UEs concurrently, DTDD is preferable because it can meet and even outperform FD without requiring the use of IrAI cancellation hardware. Fairness guarantees under the two duplexing schemes are a good direction for future work.

6 Modeling & Analysis of Asynchronism in UL Cell-Free Systems

Chapter Highlights

This chapter develops a mathematical framework to analyze the impact of ICI and ISI in the UL SE of the CF-mMIMO system using OFDM. In a CF-mMIMO system, geographically separated APs jointly serve a large number of UEs. The distributed nature of the overall system results in different propagation delays in the signals received at the APs. This delay in receiving signals from different UEs can exceed the CP duration, leading to interference from adjacent subcarriers and consecutive OFDM symbols. Our analysis shows that ignoring this crucial aspect leads to a gross overestimation of the achievable SE. We also develop an interference-aware combining scheme to alleviate ISI and ICI in addition to multi-UE interference. We also account for the scenario in which each UE performs a timing-advance with respect to its nearest AP. Numerically, we illustrate that ICI and ISI can significantly limit the achievable SE, but *we can considerably lessen the impacts of ICI and ISI by using the nearest AP-based timing advance and interference aware combining, and in many scenarios, obtain performance that is close to a time-aligned CF-mMIMO system.*

6.1 Introduction

CF-mMIMO systems, where distributed APs jointly serve multiple UEs, have been shown to provide multi-fold improvement in the SE compared to cellular mMIMO systems [19, 47, 107, 108]. However, the benefits of CF-mMIMO are obtained under the assumption that all the APs time-synchronously receive all the UEs' transmitted symbols [109, 110]. In a practical system, since every UE is at a different distance from every AP, it is not possible to ensure synchronous arrival of *all* the UEs' signals at *all* the APs. Accounting for this delay in receiving the signals at various APs and analyzing its impact on the SE is the goal of this work.

Recently, the authors in [109] evaluated the uplink SE of a CF-mMIMO system using OFDM. The authors in [110] proposed an opportunistic AP-selection scheme for efficient time-frequency resource utilization in a CF-OFDM system. Superimposed pilot-based channel estimation for CF-mMIMO OFDM has been explored in [111]. However, all these works assume that the uplink signals from all the UEs arrive time-synchronously at all the APs. In the sequel, we will refer to this as a *time-aligned* CF-mMIMO OFDM system.

In a cellular system, where each UE is attached to a specific base station (BS), the UEs can time-advance their transmit signals so that the BS synchronously receives the signals from all the UEs being served by it [112]. Due to this, in an OFDMA system where different UEs are allotted non-overlapping subcarriers, the multi-path signals from all the UEs arrive with a symbol start time that is contained within the CP duration. Hence, ICI and ISI are avoided at the BS. However, in a CF system, each UE is served by multiple APs, and thus, the propagation delays associated with each AP are different. Now, based on the distances between the APs and UEs, it is possible that the desired signal arrives at

an AP beyond the CP duration as per the timing reference at the AP.[1] This renders the OFDM sub-carriers non-orthogonal and, in turn, results in ICI and ISI. In this work, we analyze an uplink CF-mMIMO system accounting for the impact of ICI and ISI induced by signal propagation delays. Our key contributions and findings are as follows:

1. We first develop a model for a CF-mMIMO OFDM system that incorporates the effects of the propagation delays between all AP-UE pairs in the received signal at the APs. This, in turn, enables us to mathematically analyze the effects of ICI and ISI in the signal-to-interference-plus-noise ratio (SINR) at the central processing unit (CPU).

2. We then analyze a scheme where each UE time-advances its transmit signal with respect to the time reference at its nearest AP. This ensures that for every UE, there is no delay on the received signal in the nearest AP, and also reduces the propagation delays on the subsequent APs. The effectiveness of the scheme is validated via numerical experiments (see Figure 6.4).

3. We derive the achievable per-UE SE with maximal ratio and zero-forcing combing (MRC and ZFC). We extend our analysis to design an ICI and ISI-aware combiner that minimizes the mean square error (MSE) between the transmitted and the estimated symbols at the CPU.

4. Our numerical experiments show that the performance of a CF system can be severely limited by ICI and ISI. Increasing the CP length mitigates the ICI; this, however, reduces the fractional symbol duration. Further, an interference aware combining with the nearest AP-based timing-advance can reduce the effects of ICI and ISI (see

[1]For instance, 5G NR supports 30 kHz subcarrier spacing with the OFDM symbol duration being 33.3 μs and the CP duration being 2.3 μs. Thus, the propagation delay at an AP that is at an excess distance (relative to its nearest AP) of 750 m will be 2.5 μs, which exceeds the CP duration. Further, for 60 kHz subcarrier spacing and 1.2 μs CP duration, propagation delay at an AP at an excess distance of more than even 360 m will exceed the CP duration.

Figure 6.4) and offer a performance that almost matches with the time-aligned CF-system.

These results show that it is crucial to account for the effects of propagation delays in the design and analysis of CF-mMIMO systems. It is also important to perform appropriate timing-advance and ICI and ISI-aware signal processing at the CPU in order to mitigate the loss in SE due to ICI and ISI.

6.2 Signal and Channel Model

We consider an uplink CF-mMIMO OFDM system where M APs jointly serve K active UEs, all considered to be single antenna nodes, and $M > K$.[2] The APs are connected to a CPU, which performs joint data decoding based on the relayed data streams from the APs. The UEs simultaneously transmit their data over N_{s} sub-carriers. Let $\mathbf{S}_{i,k} = [S_{i,1,k}, S_{i,2,k}, \ldots, S_{i,N_{\mathsf{s}},k}]^T \in \mathbb{C}^{N_{\mathsf{s}} \times 1}$ be the ith OFDM symbol to be transmitted by the kth UE (before CP addition), where $S_{i,l,k}$ denotes the data transmitted over the lth sub-carrier. We consider that $\mathbb{E}\left[|S_{i,l,k}|^2\right] = \mathcal{E}_{i,l,k}$ and $\mathbb{E}\left[S_{i,l,k}S^*_{i',l',k'}\right] = 0, \forall i' \neq i, l' \neq l$, and $k' \neq k$. The time domain transmitted signal can be expressed as $\mathbf{C}_t\mathbf{F}^H\mathbf{S}_{i,k}$, where $\mathbf{F} \in \mathbb{C}^{N_{\mathsf{s}} \times N_{\mathsf{s}}}$ is the normalized discrete Fourier transform (DFT) matrix and the matrix $\mathbf{C}_t$ inserts the CP of length N_{cp}, which has the following structure:

$$\mathbf{C}_t = \begin{bmatrix} \mathbf{0}_{N_{\mathsf{cp}} \times (N_{\mathsf{s}} - N_{\mathsf{cp}})} & \mathbf{I}_{N_{\mathsf{cp}}} \\ & \mathbf{I}_{N_{\mathsf{s}}} \end{bmatrix} \in \mathbb{R}^{N_{\mathsf{o}} \times N_{\mathsf{s}}}. \tag{6.1}$$

Here, $N_{\mathsf{o}} = N_{\mathsf{cp}} + N_{\mathsf{s}}$ is the length of the time domain signal. Let $\mathbf{H}_{mk} \in \mathbb{C}^{N_{\mathsf{o}} \times N_{\mathsf{o}}}$ be the channel impulse response matrix between the mth AP and the kth UE, which has a Toeplitz structure [113] with first column being $[h_{mk}[0], h_{mk}[1], \ldots, h_{mk}[L_{h_{mk}} - 1], 0, \ldots, 0]^T \in \mathbb{C}^{N_{\mathsf{o}} \times 1}$, where $h_{mk}[n], \forall n = 1, 2, \ldots L_{h_{mk}}$ is the channel impulse response at the time sample

[2] This CF-MIMO system is referred to as *massive* as the total number of antenna elements is more than the number of active UEs, even if the APs are equipped with single antenna. This model has been considered in [19, 109].

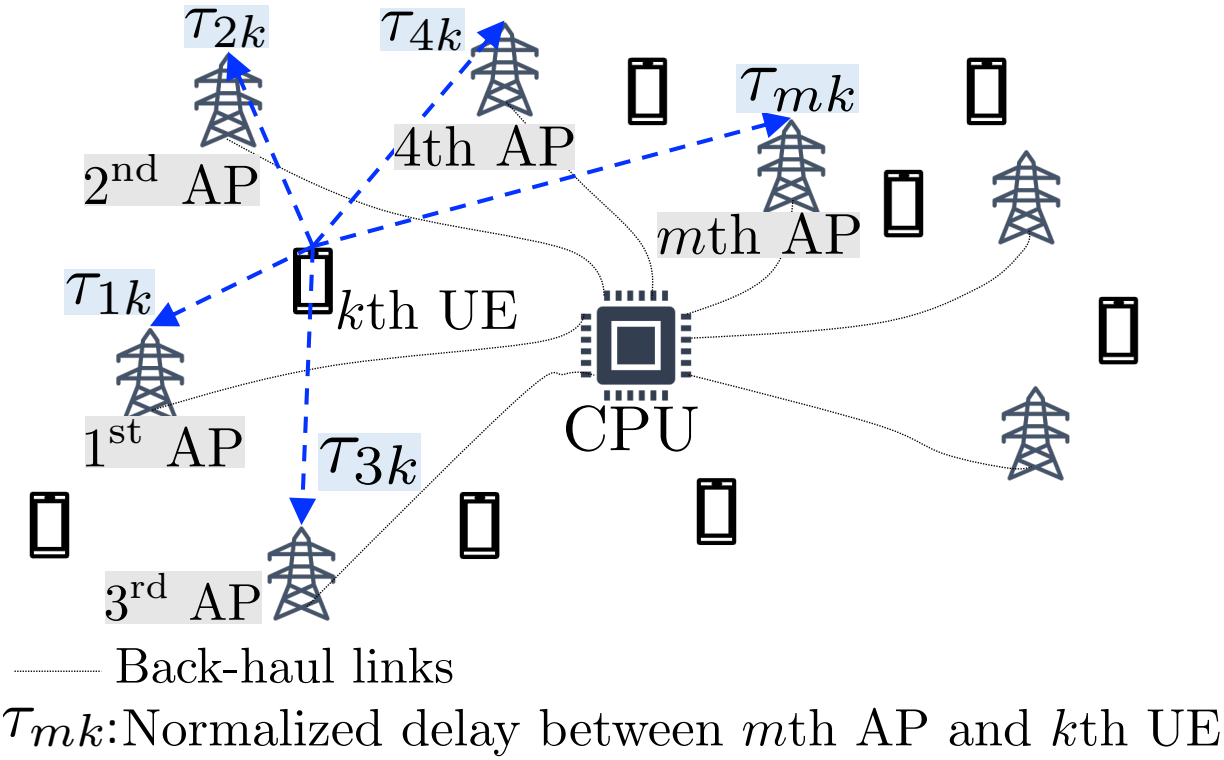

Figure 6.1: Different delay profiles with respect to the kth UE at different APs.

n, and $L_{h_{mk}}$, is the tap length of the channel. The impulse response $h_{mk}[n]$ includes the effects of path loss and follows an exponential power delay profile. Details on the modeling of $h_{mk}[n]$ are provided in Section 6.4.

Let the distance between the mth AP and the kth UE be denoted by l_{mk}. The uplink transmitted signal from the kth UE experiences a delay of l_{mk}/c seconds, where c denotes the speed of light. We define the normalized delay in receiving the uplink signals at the mth AP from the kth UE by

$$\tau_{mk} = \left\lfloor \frac{l_{mk}}{cT_s} \right\rceil, \tag{6.2}$$

where T_s is the sampling time. This is illustrated in Figure 6.1. We refer to this system as a *time-mismatched* CF-system.

We note that in a *cellular* system, each UE performs a timing-advance operation with

respect to the BS with which it is associated. This ensures that signals from the intra-cell UEs arrive at the BS synchronously (more precisely, within the CP duration), and hence, ICI and ISI can be avoided within the cell. However, in a CF system, since each UE is being served by multiple distributed APs, a nearest AP/BS-based timing-advance does not imply synchronous reception at all APs for all the UEs. Yet, if each UE performs timing-advance with respect to its nearest AP, ICI/ISI from UEs close to APs can be avoided. Hence, we analyze the performance of this judicious timing-advance scheme. Mathematically, if $m(k)$ is the index of the AP nearest to the UE k, then, after timing-advance, the normalized delay, denoted by $\tau_{mk}^{\mathtt{TA}}$, can be expressed as

$$\tau_{mk}^{\mathtt{TA}} = \left\lfloor \frac{l_{mk}}{cT_s} \right\rfloor - \left\lfloor \frac{l_{m(k)k}}{cT_s} \right\rfloor, \forall m = 1, 2, \ldots, M. \tag{6.3}$$

Needless to say, for $m = m(k)$, $\tau_{mk}^{\mathtt{TA}} = 0$. Later, we will show that this can significantly improve the performance compared to the system wherein no timing-advance is performed.

Now, in the uplink, the received signal corresponding to the ith OFDM symbol at the mth AP can be expressed as

$$\begin{aligned} \mathbf{y}_{i,m} = &\sum_{k=1}^{K} \mathbf{F}\mathbf{C}_r \boldsymbol{\Xi}_{mk} \mathbf{H}_{mk} \mathbf{C}_t \mathbf{F}^H \mathbf{S}_{i,k} \\ &+ \sum_{k=1}^{K} \mathbf{F}\mathbf{C}_r \overline{\boldsymbol{\Xi}}_{mk} \mathbf{H}_{mk} \mathbf{C}_t \mathbf{F}^H \mathbf{S}_{i-1,k} + \mathbf{F}\mathbf{C}_r \mathbf{n}_m, \end{aligned} \tag{6.4}$$

where

$$\boldsymbol{\Xi}_{mk} \triangleq \begin{bmatrix} \mathbf{0}_{\tau_{mk} \times N_\circ} \\ \mathbf{I}_{(N_\circ - \tau_{mk})} \quad \mathbf{0}_{(N_\circ - \tau_{mk}) \times \tau_{mk}} \end{bmatrix} \in \mathbb{R}^{N_\circ \times N_\circ}, \tag{6.5}$$

and

$$\overline{\boldsymbol{\Xi}}_{mk} \triangleq \begin{bmatrix} \mathbf{0}_{\tau_{mk} \times (N_\circ - \tau_{mk})} \quad \mathbf{I}_{\tau_{mk}} \\ \mathbf{0}_{(N_\circ - \tau_{mk}) \times N_\circ} \end{bmatrix} \in \mathbb{R}^{N_\circ \times N_\circ}, \tag{6.6}$$

encapsulate the effects of propagation delay between the mth AP and the kth UE, and

the interference from the previous OFDM symbol, respectively.[3] Here, similar to $\mathbf{C}_t$, the matrix $\mathbf{C}_r \triangleq \begin{bmatrix}\mathbf{0}_{N_\mathrm{s}\times N_{\mathrm{cp}}} & \mathbf{I}_{N_\mathrm{s}}\end{bmatrix} \in \mathbb{R}^{N_\mathrm{s}\times N_\mathrm{o}}$ performs the CP removal operation. Lastly, $\mathbf{n}_m \sim \mathcal{CN}(\mathbf{0}, \sigma^2_{\mathbf{n}}\mathbf{I}_{N_\mathrm{o}})$ is the additive receiver noise at the mth AP. Note that, setting $\tau_{mk} = 0, \forall m, k$, results in $\mathbf{\Xi}_{mk} = \mathbf{I}_{N_\mathrm{o}}$ and $\overline{\mathbf{\Xi}}_{mk} = \mathbf{0}_{N_\mathrm{o}}$, and reduces the system model to existing works on CF-mMIMO OFDM systems that do not consider the effects of propagation delays [109–111]. We refer to the system model obtained by setting $\tau_{mk} = 0$ as a *time-aligned* system. Now, the received stream corresponding to the lth sub-carrier of the ith OFDM symbol at the mth AP can be expressed as

$$y_{i,l,m} = \sum_{k=1}^{K} \mathbf{f}_l^T \mathbf{C}_r \mathbf{\Xi}_{mk} \mathbf{H}_{mk} \mathbf{C}_t \mathbf{f}_l^* S_{i,l,k} + \sum_{k=1}^{K} \sum_{\substack{n=1,\\ n\neq l}}^{N_\mathrm{s}} \mathbf{f}_l^T \mathbf{C}_r \mathbf{\Xi}_{mk} \mathbf{H}_{mk} \mathbf{C}_t \mathbf{f}_n^* S_{i,n,k}$$
$$+ \sum_{k=1}^{K} \sum_{n=1}^{N_\mathrm{s}} \mathbf{f}_l^T \mathbf{C}_r \overline{\mathbf{\Xi}}_{mk} \mathbf{H}_{mk} \mathbf{C}_t \mathbf{f}_n^* S_{i-1,k} + \mathbf{f}_l^T \mathbf{C}_r \mathbf{n}_m, \tag{6.7}$$

with $\mathbf{f}_l^T$ being the lth *row* of the DFT matrix and $\mathbf{f}_n^*$ being the nth *column* of the inverse DFT matrix.

Now, the CPU receives M data streams from all the APs corresponding to each sub-carrier index. Thus, the received signal at the CPU can be written as

$$\mathbf{y}_{i,l} = \begin{bmatrix} y_{i,l,1} \\ y_{i,l,2} \\ \vdots \\ y_{i,l,M} \end{bmatrix} = \begin{bmatrix} \sum_{k=1}^{K} \mathbf{f}_l^T \mathbf{C}_r \mathbf{\Xi}_{1k} \mathbf{H}_{1k} \mathbf{C}_t \mathbf{f}_l^* S_{i,l,k} \\ \sum_{k=1}^{K} \mathbf{f}_l^T \mathbf{C}_r \mathbf{\Xi}_{2k} \mathbf{H}_{2k} \mathbf{C}_t \mathbf{f}_l^* S_{i,l,k} \\ \vdots \\ \sum_{k=1}^{K} \mathbf{f}_l^T \mathbf{C}_r \mathbf{\Xi}_{Mk} \mathbf{H}_{Mk} \mathbf{C}_t \mathbf{f}_l^* S_{i,l,k} \end{bmatrix} + \mathbf{n}_{i,l}^{\mathtt{eff.}}. \tag{6.8}$$

We can rewrite (6.8) as

$$\mathbf{y}_{i,l} = \mathbf{G}_{i,ll} \mathbf{S}_{i,l} + \mathbf{n}_{i,l}^{\mathtt{eff.}}, \tag{6.9}$$

[3] We assume that $\max_{m,k} \tau_{mk} \leq N_\mathrm{o}, \forall m, k$. Thus, only the previous OFDM symbol causes ISI. For instance, if the farthest AP that can help with decoding a UE's signal is 1 km away, then the excess normalized delay (τ_{mk}) is 51 for a sampling time of 6.5 μsec. This is well within one symbol duration.

$$\mathbf{G}_{i,ll} = \begin{bmatrix} \mathbf{f}_l^T\mathbf{C}_r\boldsymbol{\Xi}_{11}\mathbf{H}_{11}\mathbf{C}_t\mathbf{f}_l^* & \mathbf{f}_l^T\mathbf{C}_r\boldsymbol{\Xi}_{12}\mathbf{H}_{12}\mathbf{C}_t\mathbf{f}_l^* & \dots & \mathbf{f}_l^T\mathbf{C}_r\boldsymbol{\Xi}_{1K}\mathbf{H}_{1K}\mathbf{C}_t\mathbf{f}_l^* \\ \mathbf{f}_l^T\mathbf{C}_r\boldsymbol{\Xi}_{21}\mathbf{H}_{21}\mathbf{C}_t\mathbf{f}_l^* & \mathbf{f}_l^T\mathbf{C}_r\boldsymbol{\Xi}_{22}\mathbf{H}_{22}\mathbf{C}_t\mathbf{f}_l^* & \dots & \mathbf{f}_l^T\mathbf{C}_r\boldsymbol{\Xi}_{2K}\mathbf{H}_{2K}\mathbf{C}_t\mathbf{f}_l^* \\ \vdots & \dots & \dots & \vdots \\ \mathbf{f}_l^T\mathbf{C}_r\boldsymbol{\Xi}_{M1}\mathbf{H}_{M1}\mathbf{C}_t\mathbf{f}_l^* & \mathbf{f}_l^T\mathbf{C}_r\boldsymbol{\Xi}_{M2}\mathbf{H}_{M2}\mathbf{C}_t\mathbf{f}_l^* & \dots & \mathbf{f}_l^T\mathbf{C}_r\boldsymbol{\Xi}_{MK}\mathbf{H}_{MK}\mathbf{C}_t\mathbf{f}_l^* \end{bmatrix}. \tag{6.10}$$

where $\mathbf{G}_{i,ll} \in \mathbb{C}^{M\times K}$ is shown in (6.10), $\mathbf{S}_{i,l} = [S_{i,l,1}, S_{i,l,2}, \dots, S_{i,l,K}]^T \in \mathbb{C}^{K\times 1}$, and $\mathbf{n}_{i,l}^{\mathtt{eff.}}$ being

$$\mathbf{n}_{i,l}^{\mathtt{eff.}} = \sum_{n=1, n\neq l}^{N_\mathtt{s}} \mathbf{G}_{i,ln}\mathbf{S}_{i,n} + \sum_{n=1}^{N_\mathtt{s}} \overline{\mathbf{G}}_{i,ln}\mathbf{S}_{i-1,n} + \overline{\mathbf{n}}_l, \tag{6.11}$$

with the kth column of $\mathbf{G}_{i,ln}$ and $\overline{\mathbf{G}}_{i,ln} \in \mathbb{C}^{M\times K}$ given by

$$[\mathbf{G}_{i,ln}]_{:,k} = \begin{bmatrix} \mathbf{f}_l^T\mathbf{C}_r\boldsymbol{\Xi}_{1k}\mathbf{H}_{1k}\mathbf{C}_t\mathbf{f}_n^* \\ \mathbf{f}_l^T\mathbf{C}_r\boldsymbol{\Xi}_{2k}\mathbf{H}_{2k}\mathbf{C}_t\mathbf{f}_n^* \\ \vdots \\ \mathbf{f}_l^T\mathbf{C}_r\boldsymbol{\Xi}_{Mk}\mathbf{H}_{Mk}\mathbf{C}_t\mathbf{f}_n^* \end{bmatrix} \in \mathbb{C}^{M\times 1}, \tag{6.12a}$$

$$[\overline{\mathbf{G}}_{i,ln}]_{:,k} = \begin{bmatrix} \mathbf{f}_l^T\mathbf{C}_r\overline{\boldsymbol{\Xi}}_{1k}\mathbf{H}_{1k}\mathbf{C}_t\mathbf{f}_n^* \\ \mathbf{f}_l^T\mathbf{C}_r\overline{\boldsymbol{\Xi}}_{2k}\mathbf{H}_{2k}\mathbf{C}_t\mathbf{f}_n^* \\ \vdots \\ \mathbf{f}_l^T\mathbf{C}_r\overline{\boldsymbol{\Xi}}_{Mk}\mathbf{H}_{Mk}\mathbf{C}_t\mathbf{f}_n^* \end{bmatrix} \in \mathbb{C}^{M\times 1}, \tag{6.12b}$$

respectively. The mth component of $\overline{\mathbf{n}}_m \in \mathbb{C}^{M\times 1}$ is $\mathbf{f}_l^T\mathbf{C}_r\mathbf{n}_m$.

Upon receiving the data streams from all the APs, the CPU combines the M streams for all the UEs at each sub-carrier to reconstruct the desired UE's signal from $\mathbf{y}_{i,l}$. The CPU utilizes the full CSI among all AP-UE links to design the combiner matrix, denoted

by $\mathbf{V}_{i,l} \triangleq [\mathbf{v}_{i,l,1}, \mathbf{v}_{i,l,2}, \ldots, \mathbf{v}_{i,l,K}]$, with the kth column being $\mathbf{v}_{i,l,k} \in \mathbb{C}^{M\times 1}$.[4] Thus, the estimate of the desired signal can be written as $\hat{\mathbf{S}}_{i,l} = \mathbf{V}_{i,l}^H \mathbf{y}_{i,l}$. Therefore, the estimated symbol on the kth stream of the ith OFDM symbol and the lth sub-carrier can be written as

$$\hat{S}_{i,l,k} = \mathbf{v}_{i,l,k}^H \mathbf{g}_{i,ll,k} S_{i,l,k} + \sum_{k'=1,k'\neq k}^{K} \mathbf{v}_{i,l,k}^H \mathbf{g}_{i,ll,k'} S_{i,l,k'} + \sum_{n=1,n\neq l}^{N_{\mathrm{s}}} \mathbf{v}_{i,l,k}^H \sum_{k'=1}^{K} \mathbf{g}_{i,ln,k'} S_{i,n,k'} + \sum_{n=1}^{N_{\mathrm{s}}} \mathbf{v}_{i,l,k}^H \sum_{k'=1}^{K} \overline{\mathbf{g}}_{i,ln,k'} S_{i-1,n,k'} + \mathbf{v}_{i,l,k}^H \overline{\mathbf{n}}_l, \tag{6.13}$$

where the second term is due to muti-UE interference, and the third and the fourth terms correspond to ICI and ISI arising due to timing misalignment in the uplink transmission, respectively. This is illustrated in Figure 6.2. Also, $\mathbf{g}_{i,ll,k}$, $\mathbf{g}_{i,ln,k}$, and $\overline{\mathbf{g}}_{i,ln,k}$ denote the kth column of $\mathbf{G}_{i,ll,k}$, $\mathbf{G}_{i,ln,k}$, and $\overline{\mathbf{G}}_{i,ln,k}$, respectively. Next, we present the performance analysis of this time-mismatched uplink CF-mMIMO system.

6.3 Performance Analysis

Based on (6.13), the instantaneous SINR of the kth UE on the lth sub-carrier and the ith OFDM symbol can be expressed as

$$\eta_{i,l,k} = \frac{\left|\mathbf{v}_{i,l,k}^H \mathbf{g}_{i,ll,k}\right|^2 \mathcal{E}_{i,l,k}}{\mathtt{MUI}_{i,l,k} + \mathtt{ICI}_{i,l,k} + \mathtt{ISI}_{i,l,k} + \sigma_{\mathbf{n}}^2 \|\mathbf{v}_{i,l,k}\|^2}, \tag{6.14}$$

where

$$\mathtt{MUI}_{i,l,k} = \sum_{k'=1,k'\neq k}^{K} \left|\mathbf{v}_{i,l,k}^H \mathbf{g}_{i,ll,k'}\right|^2 \mathcal{E}_{i,l,k'}, \tag{6.15a}$$

[4] This being the first work on the effects of propagation delays in uplink CF-systems, we consider availability of perfect CSI to focus attention on the effects of ICI and ISI due to timing mismatches. The incorporation of imperfect CSI adds to the interference due to the channel estimation error. Further, due to relative propagation delays, even the channel estimation procedure needs to be addressed with care, and can be a potential direction for future work.

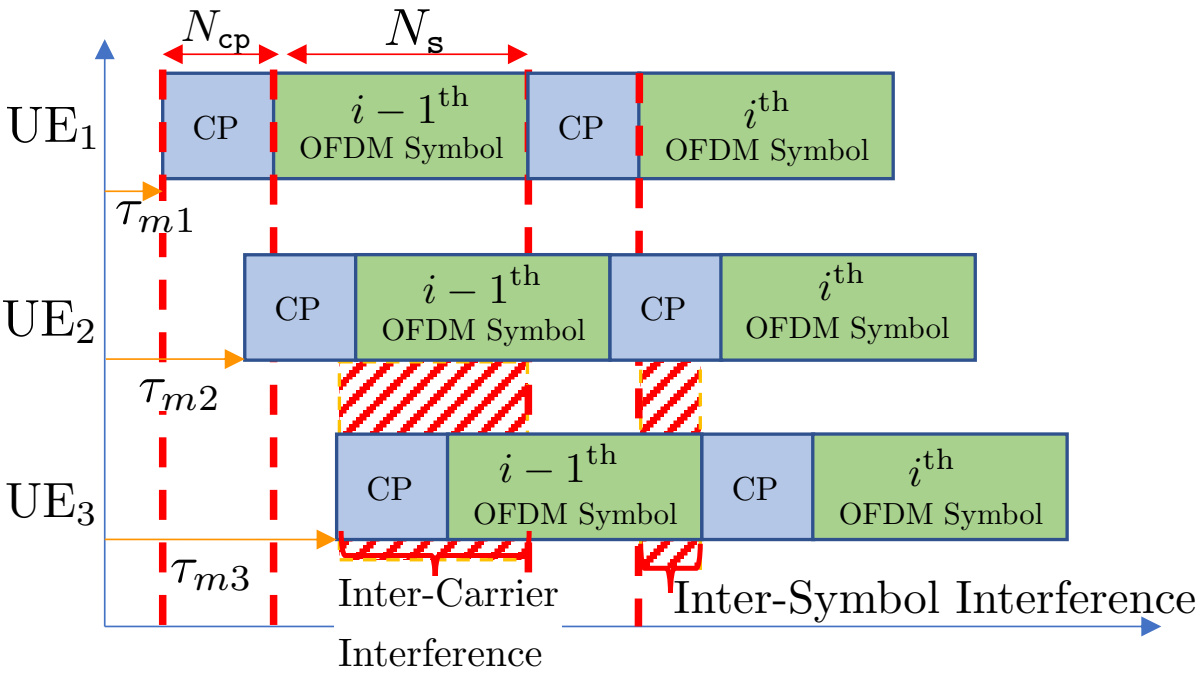

Figure 6.2: ICI and ISI resulting from delays in receiving the uplink signals at the mth AP due to the third UE (UE_3) whose signal arrives beyond the CP duration.

$$\texttt{ICI}_{i,l,k} = \sum_{k'=1}^{K} \sum_{n=1, n\neq l}^{N_{\text{s}}} \left| \mathbf{v}_{i,l,k}^{H} \mathbf{g}_{i,ln,k'} \right|^2 \mathcal{E}_{i,n,k'}, \tag{6.15b}$$

$$\texttt{ISI}_{i,l,k} = \sum_{k'=1}^{K} \sum_{n=1}^{N_{\text{s}}} \left| \mathbf{v}_{i,l,k}^{H} \overline{\mathbf{g}}_{i,ln,k'} \right|^2 \mathcal{E}_{i-1,n,k'}, \tag{6.15c}$$

where we have used the fact that the symbols are independent across UEs and across OFDM symbol indices in the frequency domain. Now, for MRC, $\mathbf{v}_{i,l,k} = \mathbf{g}_{i,ll,k}$ and for ZFC, $\mathbf{v}_{i,l,k} = \left[\mathbf{G}_{i,ll} \left(\mathbf{G}_{i,ll}^{H} \mathbf{G}_{i,ll} \right)^{-1} \right]_{:,k}$. We observe that although ZFC nullifies the effect of multi-UE interference, the performance would still suffer from ICI and ISI. In a time-aligned system, ZFC performs well in terms of the achievable SE at high SNR [Chapter 8, [113]], [108]. However, in our system, as we numerically show in Section 6.4, ZFC can perform poorly since it ignores the effects of ICI and ISI. Thus, we next provide an interference-aware combining scheme that takes ICI and ISI into account.

6.3.a Interference Aware Combining

To tackle the effects of ISI and ICI, the CPU can design a combiner which is MSE optimal with respect to the received symbol. Essentially, the optimal combiner is the solution of the following optimization problem:

$$\mathrm{P}_1: \quad \min_{\mathbf{v}_{i,l,k} \in \mathbb{C}^{M \times 1}} \mathbb{E}\left[\left|\hat{S}_{i,l,k} - S_{i,l,k}\right|^2\right], \ \forall i, l, k, \tag{6.16}$$

where our estimate $\hat{S}_{i,l,k}$ depends on the choice of the combiner $\mathbf{v}_{i,l,k}$. The expectation in (6.16) can be expanded as

$$\begin{aligned}\mathbb{E}\left[\left|S_{i,l,k} - \mathbf{v}_{i,l,k}^H \mathbf{y}_{i,l}\right|^2\right] &= \mathcal{E}_{i,l,k} - \mathcal{E}_{i,l,k}^2 \mathbf{g}_{i,ll,k}^H \mathbf{C}_{i,l,k}^{-1} \mathbf{g}_{i,ll,k} \\ &\quad + \left(\mathbf{v}_{i,l,k} - \mathcal{E}_{i,l,k} \mathbf{C}_{i,l,k}^{-1} \mathbf{g}_{i,ll,k}\right)^H \mathbf{C}_{i,l,k} \left(\mathbf{v}_{i,l,k} - \mathcal{E}_{i,l,k} \mathbf{C}_{i,l,k}^{-1} \mathbf{g}_{i,ll,k}\right), \end{aligned} \tag{6.17}$$

where $\mathbf{C}_{i,l,k}$ is defined as

$$\begin{aligned}\mathbf{C}_{i,l,k} = \Bigg(&\sum_{k'=1}^{K} \mathcal{E}_{i,l,k'} \mathbf{g}_{i,ll,k'} \mathbf{g}_{i,ll,k'}^H + \sum_{\substack{n=1, \\ n \neq l}}^{N_{\mathsf{s}}} \sum_{k=1}^{K} \mathcal{E}_{i,n,k} \mathbf{g}_{i,ln,k} \mathbf{g}_{i,ln,k}^H \\ &+ \sum_{n=1}^{N_{\mathsf{s}}} \sum_{k=1}^{K} \mathcal{E}_{i-1,n,k} \overline{\mathbf{g}}_{i,ln,k} \overline{\mathbf{g}}_{i,ln,k}^H + \sigma_{\mathbf{n}}^2 \mathbf{I}_M \Bigg). \end{aligned} \tag{6.18}$$

From (6.17), it is easy to show that the MSE optimal combiner is $\mathbf{v}_{i,k,l}^{\mathtt{opt}} = \mathcal{E}_{i,l,k} \mathbf{C}_{i,l,k}^{-1} \mathbf{g}_{i,ll,k}$.

6.3.b Spectral Efficiency

Under the different combining schemes discussed earlier, we can write the average per-UE SE expression as

$$\mathrm{R}_{\mathtt{avg}} = \frac{N_{\mathsf{s}}}{N_{\mathtt{cp}} + N_{\mathsf{s}}} \frac{1}{K N_{\mathsf{s}}} \sum_{k=1}^{K} \sum_{l=1}^{N_{\mathsf{s}}} \log_2\left(1 + \eta_{i,l,k}\right), \tag{6.19}$$

where $\eta_{i,l,k}$ is given by (6.14) and the pre-log factor $\dfrac{N_{\mathsf{s}}}{N_{\mathtt{cp}} + N_{\mathsf{s}}}$ captures the rate loss due to the CP duration [Chapter 3, [113]]. Also, the factor $1/KN_{\mathsf{s}}$ averages the SE over all

UEs and the subcarriers.

We next numerically illustrate the effects of propagation delays on the achievable SE under different combining schemes.

6.4 Numerical Results

We consider a CF-mMIMO system over an area of 1 km^2, where the APs are deployed in a rectangular grid for uniform coverage, and the UE locations are generated uniformly at random. All the numerical simulations are evaluated over 10^4 random instantiations of UEs. The channel impulse response, $h_{mk}[n]$ is generated according to $\mathcal{CN}(0, \sigma^2_{h_{mk}[n]}\beta_{mk})$, where β_{mk} captures the effects of large-scale fading which is frequency independent and remains constant for a relatively long period of time, and $\sigma^2_{h_{mk}[n]}$ is the channel tap variance that follows an exponential power delay profile with $\sum_{n=0}^{L_{h_{mk}}} \sigma^2_{h_{mk}[n]} = 1$. For numerical experiments, we consider $L_{h_{mk}} = L_h, \forall m = 1, \ldots, M$ and $k = 1, \ldots, K$. The large-scale fading coefficient $\beta_{mk} = 10^{\frac{\mathtt{PL}_{mk} + \zeta_{mk}}{10}}$, where $\mathtt{PL}_{mk}$ is the distance-dependent path loss component that follows the three slope COST-HATA model with breakpoint distances being 10 meters and 50 meters [109]. The shadow fading component is generated as $\zeta_{mk} \sim \mathcal{N}(0, \sigma^2_{\mathtt{sh.}})$, with $\sigma_{\mathtt{sh.}}$ being 6 dB [19, 107, 109]. We employ equal transmit power per subcarrier, and the symbol SNR is defined as $\mathcal{E}/\sigma^2_{\mathbf{n}}$, where $\mathcal{E}_{i,l,k} = \mathcal{E}, \forall i, l, k$. Other relevant parameters, such as number of sub-carriers ($N_{\mathtt{s}}$), APs (M), UEs (K), CP duration ($N_{\mathtt{cp}}$), and channel tap length (L_h) are plot-specific and are mentioned along with the figures. The acronyms used in the figures are as follows: (a) TA : time-aligned system (i.e. $\tau_{mk} = 0$), (b) TM : time-mismatched system where τ_{mk} is evaluated as (6.2); and (c) TM + TD : time-mismatched system employing nearest AP based timing-advance, where τ_{mk} is evaluated as (6.3).

In Figure 6.3, we plot the SE for different values of the symbol SNR considering ZFC at the CPU. We first observe that at low SNR (-30 to -10 dB), the system is noise-limited,

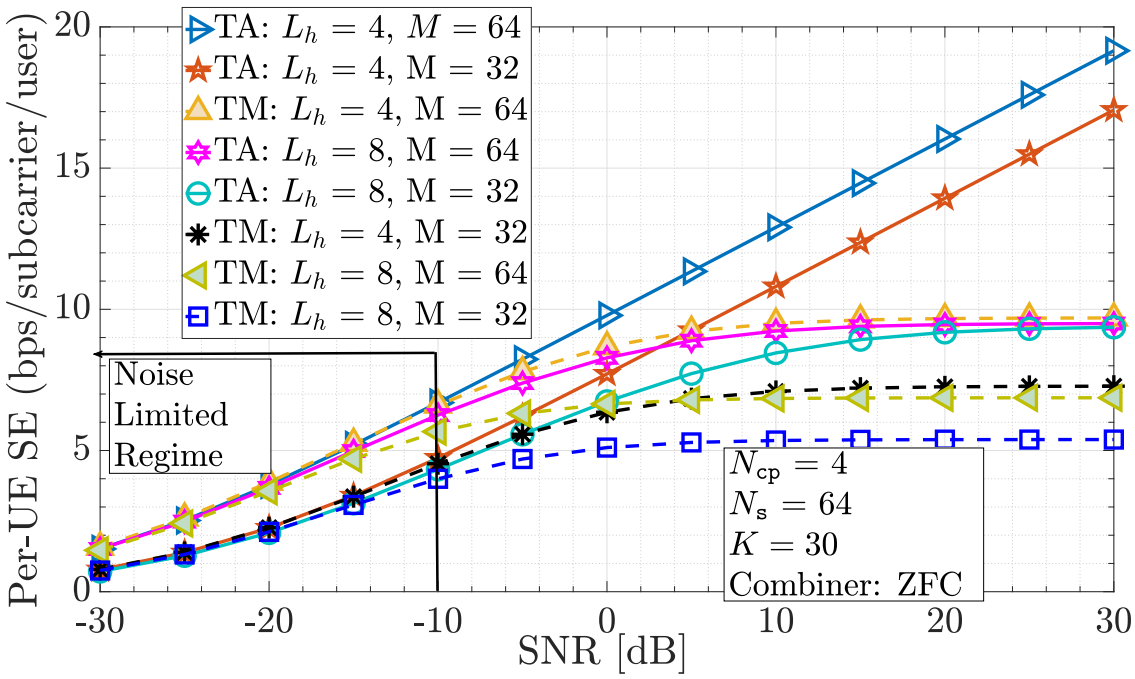

Figure 6.3: Plot of the SE vs. symbol SNR. We observe that in a time-mismatched (TM) system, the impact of ICI and ISI is significant, and the SE saturates at a lower value compared to the time-aligned (TA) system.

---

and thus, the difference between time-aligned or time-mismatched systems is negligible. In the case when $L_h = N_{\mathsf{cp}}$, after a symbol SNR of 10 dB, the SE of the time-mismatched system starts to saturate due to ICI and ISI at a considerably lower value (see, e.g., the curves corresponding to TM with $(L_h = 4, M = 32, 64)$) compared to the time-aligned system. Also, as the channel tap length increases, which in turn makes the system more frequency selective, the ICI and ISI become more pronounced, and the SE of the time-mismatched system deteriorates significantly (see $(L_h = 8, M = 32, 64)$). Finally, with an increase in the number of APs, the performance of the system uniformly improves for both time-aligned and time-mismatched systems.

Next, to illustrate the performance benefits of interference aware combining over conventional MRC and ZFC, in Figure 6.4, we plot the cumulative distribution function (CDF) of the SE under different combining schemes with and without timing-advance. Interference

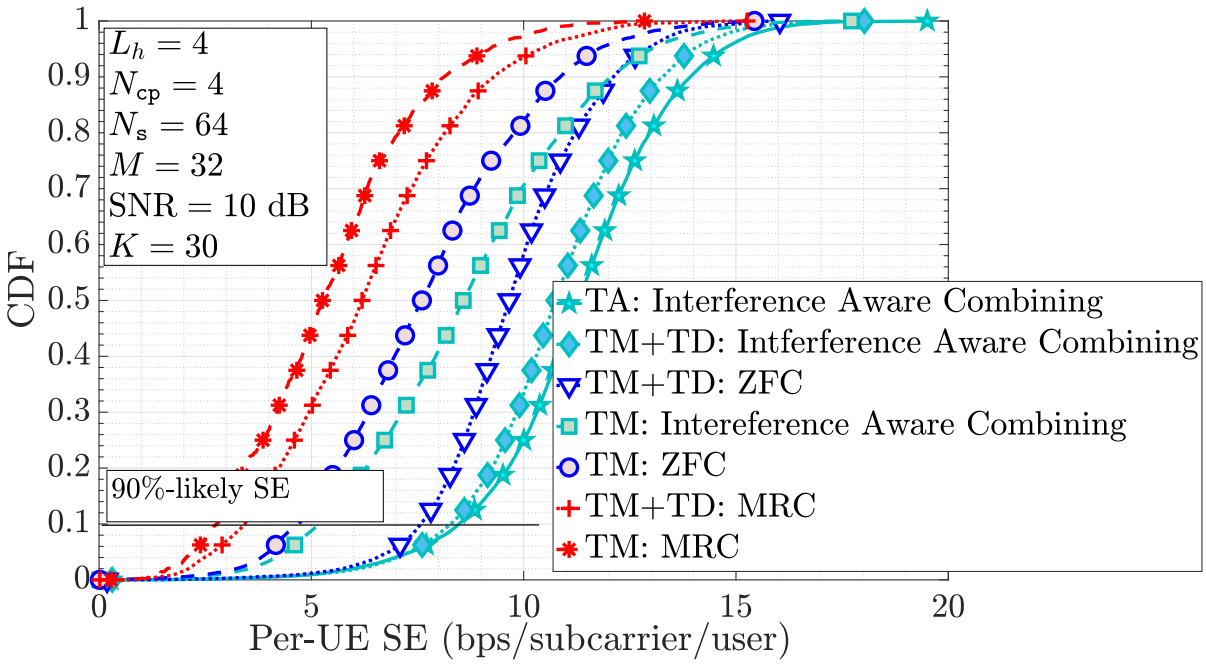

Figure 6.4: The CDFs of the uplink SE under different combining schemes. The figure underlines the effectiveness of interference aware combining along with the nearest AP-based timing-advance. (Acronym: TM + TD.)

aware combining considerably outperforms ZFC in the time-mismatched case; this highlights the ICI and ISI suppression ability of the scheme. Further, nearest AP-based timing advance along with interference-aware combining can potentially attain a performance close to that of a time-aligned system. The gap in the 90%-likely SEs attained by the interference aware scheme with timing-advance (see TM + TD : Interference Aware Combining) and the SE of the time-aligned system is marginal.[5]

One way to mitigate ICI is to increase the length of the CP. However, from (6.19), the pre-log factor $\frac{N_{\text{s}}}{N_{\text{cp}} + N_{\text{s}}}$ decreases as N_{cp} is increased. We experiment on this trade-off in Figure 6.5. For the time-aligned system and time-mismatched system employing time-advance with interference aware combining, choosing the CP length to equal the channel tap length is optimal, and any further increase results in a reduction of the SE. However,

[5]For the time-aligned system, ZFC and interference aware combing perform almost the same. Thus, to avoid clutter, we omit the CDF corresponding to the time-aligned system with ZFC.

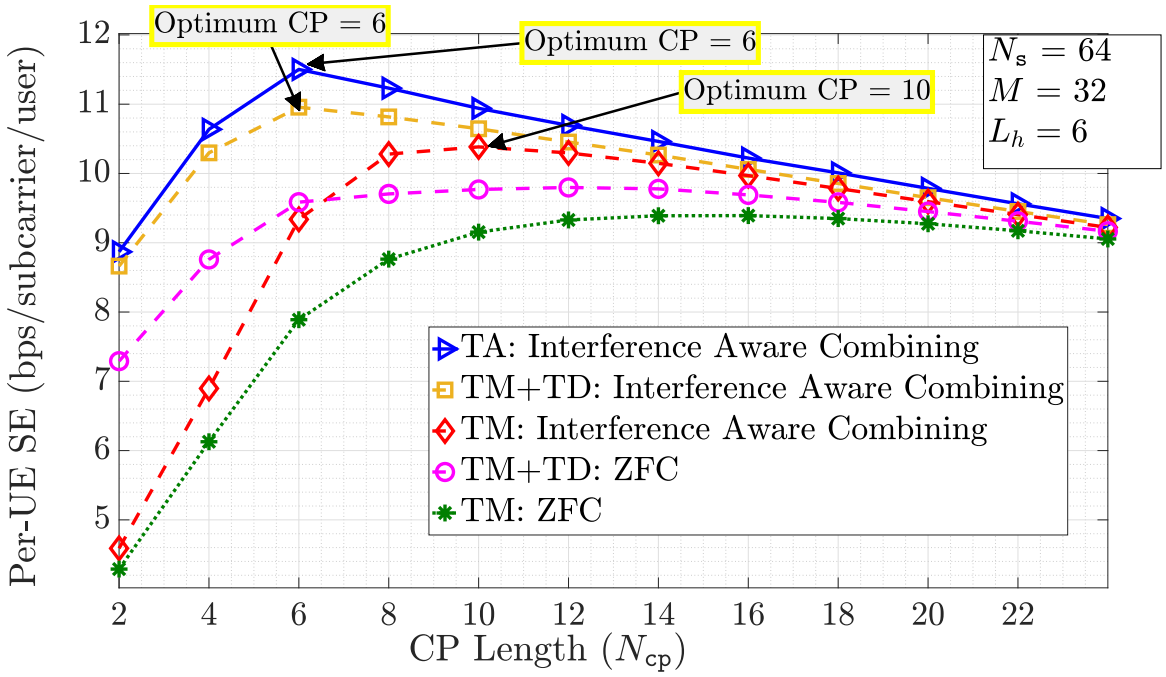

Figure 6.5: The behavior of SE with increasing CP duration under interference-aware combining. We observe a trade-off between the ICI suppression capability of an increased CP length and the rate loss incurred by it.

if we employ only ZFC or interference-aware combining without timing-advance, a larger CP length is required for optimum SE. For instance, we need a CP length of 10 for the time-mismatched system with interference aware combining without nearest AP-based timing-advance. Essentially, an increase in CP length reduces the effects of ICI and ISI and thus helps to improve the SE. However, beyond a certain CP length, the fractional SE loss overwhelms the ICI and ISI mitigation effect, and the SE starts to decrease.

6.5 Chapter Summary

In this chapter, we analyzed the impact of the signal propagation delays on the performance of an uplink CF-mMIMO OFDM system. The delays in receiving the uplink signals result in ICI and ISI, which we mathematically modeled and accounted for in our SE analysis. We investigated the performance with MRC and ZFC and also presented an interference-aware combining scheme. We showed that it is important to account for the

effects of ICI and ISI incurred due to signal propagation delays in CF mMIMO systems, as the propagation delays are inevitable due to the different relative distances between the APs and the UEs. We also saw that interference-aware combining coupled with nearest AP-based timing-advance can improve the system SE compared to a time-aligned system using classical ZFC or MRC. More sophisticated solutions based on uplink power control, sub-carrier allocation, and CP length optimization are potential directions for future work.

7 | Conclusion

Chapter Highlights

This chapter presents an overall summary of the thesis, underlining the key contributions and observations. This thesis addressed three facets of CF-mMIMO systems: channel estimation, DTDD, and UL synchronization. We first developed novel pilot design and allocation algorithms for CF-mMIMO systems. In particular, our algorithm based on graph coloring ensured no contamination among the UEs being served by one or more common AP(s) and simultaneously procured an optimal allocation with the least number of orthogonal pilots. Then, we analyzed the sum UL-DL SE of DTDD-enabled CF systems and developed algorithms for APs' UL/DL mode scheduling and UL-DL power allocation. Our major finding is that DTDD-enabled CF is more resilient to CLIs and can even outperform FD cellular and CF systems with similar antenna densities. Finally, we developed a theoretical framework to analyze the effects of asynchronous reception on the UL SE of the CF-mMIMO systems. Our analysis and experiments underscored the importance of the proposed interference-aware combining scheme, which mitigated the resulting ICI and ISI and resulted in a near synchronous/ideal performance. We benchmarked the performances of our proposed schemes with several existing comparable methods and illustrated the superiority of the developed algorithms in terms of achievable SE, complexity, and convergence. We conclude with a brief discussion of follow-up research that can be pursued in the future.

This thesis has, on the whole, focused on channel estimation, DTDD, and UL synchronization in CF-mMIMO systems. *On channel estimation*, one of the major contributions of this thesis is the development of a low-complexity pilot allocation algorithm that procures the pilot allocation with a minimum number of orthogonal pilots being reused across the UEs for CF-mMIMO systems. *On DTDD*, we found that the combination of DTDD and CF works like a virtual FD, offering a sum UL-DL SE that surpasses that of an FD CF system (without requiring SI or IrAI cancelation hardware.) Finally, *on UL synchronization*, we investigated the issue of the timing advance used for synchronization in UL cellular systems and how it affects the performance of CF systems.

In the following, we recapitulate our key findings in these three aspects of CF-mMIMO as they were developed and matured from chapter to chapter.

7.1 Summary of the Thesis

In Chapter 2, we demonstrated three approaches for pilot allocation for CF-mMIMO systems, each from a different and interesting viewpoint. In Section 2.2, we proposed channel estimation via quasi-orthonormal pilots (see Definition 2.1). We proved that pilots from MUOB codebooks minimize coherent interference among the set of quasi-orthogonal pilot sequences. Further, we pointed out that ZC-sequences could be used to construct MUOB pilot matrices, complying with the design specification of the 5G-NR standard. Then, we developed an AP-centric clustering algorithm that facilitated the allocation of pilots from MUOB codebooks to each cluster. One key advantage of MUOB-based pilot design is that once the initial AP-UE clusterings are formed, the pilots can be randomly assigned to each cluster from each MUOB codebook. Essentially, the strength of pilot contamination from the outer-cluster UEs is allocation-agnostic, thanks to the constant cross-correlation properties of the MUOB pilots. Hence, MUOB underlines the best (in terms of estimated channel quality) that can be achieved via random allocation of pilots to UEs. Our numerical findings illustrated that, in comparison to OPR, MUOB-based

pilots are superior in terms of achievable SE and UE fairness.

Next, we observed that an equivalent strategy (as developed for MUOB) can lead to high pilot contamination for orthogonal pilots. After AP-UE clustering, if we randomly assign orthogonal pilots to each cluster and reuse the same set of pilots across clusters, the cluster edge UEs can potentially share the same pilot orthogonal pilots. As a consequence, all the APs in the vicinity of the cluster-edge UEs would procure channel estimates with high MSE. Thus, to improve the performance of channel estimation via orthogonal pilots, we developed an iterative pilot allocation algorithm (see Algorithm 3) in Section 2.3. Our allocation strategy reduced the complexity compared to the previous algorithm (see Algorithm 1, Section 2.2.f) in the sense that it obviated the need for initial AP-centric clustering. However, the trade-off is the number of iterations required to procure channel estimates with low MSE at the APs. On the other hand, compared to the several existing schemes in literature for orthogonal pilot allocation, our algorithm does not require additional signaling overhead, e.g., SINR exchanges, for pilot assignment. We numerically illustrated the proposed algorithm's performance compared to existing schemes.

Next, we observed that the previous two methods and also the existing works in the literature focus on pilot design or pilot allocation given a predetermined length for the pilot sequences. In Section 2.4, we proposed a novel pilot design and allocation algorithm that ensures no pilot contamination among any pair of UEs that are proximal to a common AP, and this is guaranteed at all APs. Further, our algorithm (see Algorithm 4) procures the pilot allocation with a minimum number of orthogonal pilots being reused across the UEs. Specifically, we recast the problem as a graph-vertex coloring problem and solve it via a low-complexity algorithm known to be optimal for all bipartite graphs. Numerical results illustrated the superiority of the proposed technique over existing methods.

At this point of the thesis, we shifted our attention from the channel estimation problem and analyzed the performance of a DTDD-enabled CF-mMIMO system.

In Chapter 3, we derived the sum UL-DL SE of the DTDD-enabled CF-mMIMO system.

For ease of exposition, we assumed the availability of perfect CSI. We formulated a sum UL-DL SE maximization problem for scheduling the UL/DL mode of the APs based on UL/DL traffic demands of the UEs located in their vicinity. We proved that, with perfect CSI and perfect InAI cancelation, the sum UL-DL SE is a sub-modular function of the underlying AP set. We then employed a greedy algorithm to activate the APs in polynomial time. In the later part of the chapter (see Section 3.3.a and Section 3.3.b), we relaxed the assumption of perfect CSI and proved similar results considering statistical and estimated CSI with orthogonal pilots. Our numerical experiments revealed that DTDD-enabled CF-mMIMO substantially improves the sum SE compared to conventional TDD-based CF systems. The key reason for the performance improvement in DTDD compared to TDD-based systems is that the former duplexing scheme acts as a virtual FD system, simultaneously serving the UL and DL UEs.

Following this, in Chapter 4, we analyzed the performance of a DTDD CF-mMIMO system considering the effect of pilot contamination and imperfect InAI cancellation. As a consequence, the derivations of the sum UL-DL SE became more mathematically involved. Specifically, due to coherent interference (because of pilot contamination), the sum UL-DL SE becomes a non-linear function of the underlying UL and DL AP sets. Thus, for mathematical tractability, we derived a lower bound of the sum UL-DL SE and reformulated the AP-scheduling problem based on the maximization of the product of UL-DL SINRs. We then developed APs' mode selection algorithm based on the sub-modular nature of the product of UL-DL SINRs. We performed extensive numerical simulations to validate our theoretical findings. As a benchmark, we compared the performance of HD DTDD CF with an FD cellular system and observed that the HD DTDD CF-mMIMO can outperform an FD-cellular mMIMO system. Essentially, DTDD CF-mMIMO exploits the joint signal processing of a CF system coupled with the adaptive scheduling of UL-DL slots based on the localized traffic demands at the APs. On the other hand, the FD cellular system suffers from multi-cell interference and the SI at the BSs. Hence, a key advantage

of DTDD-enabled CF over the FD cellular system is that we no longer need additional hardware at each AP to cancel the SI.

In the previous chapters (i.e., Chapter 3 and Chapter 4), we considered full power allocation in UL and equal power allocation in DL. Next, in Chapter 5, we developed FP-based UL/DL power allocation algorithms and proved the convergence of the sub-problems to local optima. Further, we provided closed-form update equations using the Lagrange dual transform and ADMM for the sub-problems, making them easy to implement. Following this, we compared the performance of DTDD CF with the FD CF system, and we observed that DTDD outperforms FD when the two systems have a similar antenna density. This happens because DTDD can schedule the APs in UL or DL based on the localized traffic load and achieve better array gain for a given antenna density and InAI suppression. Thus, we conclude that although both DTDD and FD enable the CF system to serve UL and DL UEs concurrently, DTDD is preferable because it can meet and even outperform FD without requiring the use of IrAI cancellation hardware.

Finally, in Chapter 6, we analyzed the impact of the signal propagation delays on the performance of a UL CF-mMIMO OFDM system. The delays in receiving the uplink signals result in ICI and ISI, which we mathematically modeled and accounted for in our SE analysis. We investigated the performance with MR and ZF combining and presented an interference-aware combining scheme. We showed that it is important to account for the effects of ICI and ISI incurred due to signal propagation delays in CF mMIMO systems, as the propagation delays are inevitable due to the different relative distances between the APs and the UEs. We also saw that interference-aware combining coupled with nearest AP-based timing-advance can improve the system SE compared to a time-aligned system using classical ZF or MR combining.

Thus, in summary, the key take-home messages from this thesis are as follows:

(i) Pilot allocation is a challenging task for a CF-mMIMO system, and algorithms from

cellular setup cannot be directly reused in a CF system. Our proposed MUOB-based pilot design is allocation agnostic and provides the best performance obtainable via quasi-orthogonal pilots. On the other hand, our proposed vertex-coloring-based algorithm for orthogonal pilot reuse procures optimal allocation while minimizing the pilot length. It results in better performance in terms of NMSE of the estimated channels and the achievable SE compared to the state-of-the-art in the literature.

(ii) Our studies on the use of DTDD in a CF-mMIMO system considered a variety of practical system imperfections and generalizations, and our key finding is that DTDD is a promising duplexing scheme for the beyond 5G wireless systems, capable of serving both UL and DL traffic using only HD hardware. Our experiments revealed that DTDD CF is more resilient to CLIs and can outperform TDD CF & cellular, FD cellular, and even FD CF systems in terms of achievable sum UL-DL SE.

(iii) Finally, our work on asynchronous reception effects on UL CF systems showed that the assumption of perfect synchronism in a distributed system such as CF is a gross overestimate of the actual performance. We developed a mathematical framework to understand the effects of ICI and ISI on the UL SE. We also proposed a timing advance and an interference-aware combining scheme at the CPU, which procures near-synchronous performance.

As with most research, there is always room for further studies and improvement. We catalog a few promising directions.

7.2 Future Work

(i) An interesting extension of Chapter 2 is to characterize the optimal SNR threshold theoretically and explicitly determine the optimal pilot length that balances the loss in SE with the level of pilot contamination. Also, algorithms for pilot power

control can be developed to improve the performance of all the algorithms presented in Chapter 2.

(ii) The works presented in Chapter 3, Chapter 4, and Chapter 5, can be extended to incorporate fairness constraints. The system performance of CF-DTDD can be improved by incorporating UL-to-DL UE interference cancellation. Another aspect worth further investigating is a theoretical analysis of the latency performance of DTDD-enabled CF-mMIMO systems.

(iii) In Chapter 6, we numerically evaluated the optimal CP length. More sophisticated solutions based on UL power control, sub-carrier allocation, and CP length optimization are potential future directions of the current work. The results in Chapter 6 are for a centralized CF-mMIMO system, which can be extended to include distributed combining at the APs, considering perfect and imperfect channel estimation. Also, Chapter 6 only focused on UL asynchronism in CF systems. Exploring the effects of asynchronous reception in a DL CF-mMIMO system is equally pertinent.

(iv) Finally, the work on DTDD CF mMIMO can be extended to consider an OFDM framework, incorporating the effects of UL and DL synchronization/timing errors, to study the overall sum UL-DL SE and to analyze the effects of pilot contamination, power control, CLIs along with the ICI and ISI.

A | Appendix to Chapter 2

A.1 Derivation of MMSE Channel Estimate

Proof. Recall that we are considering a CF-mMIMO system where M APs, each equipped with N antennas, jointly serve K single antenna UEs. The channel vector between the mth AP and kth the UE is modeled as $\mathbf{f}_{mk} = \sqrt{\beta_{mk}}\mathbf{h}_{mk} \in \mathbb{C}^N$, where the path loss component β_{mk} is assumed to be constant for several coherence blocks, and the fast fading channel, $\mathbf{h}_{mk} \sim \mathcal{CN}(\mathbf{0}, \mathbf{I}_N)$, is to be estimated at the start of each coherence interval. Let $\mathcal{U} = \{1, 2, \ldots, K\}$ be the index set of all UEs, and the corresponding pilot sequences be $\mathbf{\Phi} \triangleq \{\boldsymbol{\varphi}_1, \boldsymbol{\varphi}_2, \ldots, \boldsymbol{\varphi}_K\}$. We consider the use of pilots of length τ_p.

Let, the kth UE transmits a pilot signal $\boldsymbol{\varphi}_k$ with an energy $\mathcal{E}_{p,k}$, then the received signal at the mth AP can be expressed as

$$\mathbf{Y}_{p,m} = \sqrt{\mathcal{E}_{p,k}\tau_p}\mathbf{f}_{mk}\boldsymbol{\varphi}_k^T + \sum\nolimits_{i\in\mathcal{U}\setminus\{k\}} \sqrt{\mathcal{E}_{p,i}\tau_p}\mathbf{f}_{mi}\boldsymbol{\varphi}_i^T + \mathbf{W}_{p,m} \in \mathbb{C}^{N\times\tau_p}, \tag{A.1}$$

where, each columns of $\mathbf{W}_{p,m}$ is distributed as $\mathcal{CN}(\mathbf{0}, N_0\mathbf{I}_N)$. Now, to estimate the kth UE's channel, the mth AP post-multiply (A.1) with $\boldsymbol{\varphi}_k^*$, and the processed becomes

$$\mathbf{y}_{p,m} = \mathbf{Y}_{p,m}\boldsymbol{\varphi}_k^* = \sqrt{\mathcal{E}_{p,k}\tau_p}\mathbf{f}_{mk} + \sum\nolimits_{i\in\mathcal{U}\setminus\{k\}} \sqrt{\mathcal{E}_{p,i}\tau_p}\langle\boldsymbol{\varphi}_i, \boldsymbol{\varphi}_k\rangle\mathbf{f}_{mi} + \mathbf{W}_{p,m}\boldsymbol{\varphi}_k^* \in \mathbb{C}^{N\times 1}, \tag{A.2}$$

with $\mathbf{W}_{p,m}\boldsymbol{\varphi}_k^* \sim \mathcal{CN}(\mathbf{0}, N_0\mathbf{I}_N)$. The MMSE estimate of the kth UE's channel at the mth

AP, denoted by $\hat{\mathbf{f}}_{mk}$, can be evaluated as [3]

$$\hat{\mathbf{f}}_{mk} = \frac{\mathbb{E}\left[\mathbf{f}_{mk}^H \mathbf{y}_{p,m}\right]}{\mathbb{E}\left[\mathbf{y}_{p,m}^H \mathbf{y}_{p,m}\right]} \mathbf{y}_{p,m} = \frac{\sqrt{\mathcal{E}_{p,k}\tau_p}\beta_{mk}}{N_0 + \mathcal{E}_{p,k}\beta_{mk}\tau_p + \sum_{i\in\mathcal{U}\setminus\{k\}} \mathcal{E}_{p,i}\tau_p\beta_{mi}\left|\langle\boldsymbol{\varphi}_i, \boldsymbol{\varphi}_k\rangle\right|^2} \mathbf{y}_{p,m} \tag{A.3}$$

Also, we can write, $\hat{\mathbf{f}}_{mk} = \mathbf{f}_{mk} - \tilde{\mathbf{f}}_{mk}$, where, $\tilde{\mathbf{f}}_{mk} \sim \mathcal{CN}(\mathbf{0}, (\beta_{mk} - \alpha_{mk}^2)\mathbf{I}_N)$, with

$$\alpha_{mk}^2 = \frac{\mathcal{E}_{p,k}\beta_{mk}^2\tau_p}{N_0 + \mathcal{E}_{p,k}\beta_{mk}\tau_p + \sum_{i\in\mathcal{U}\setminus\{k\}} \mathcal{E}_{p,i}\beta_{mi}\tau_p\left|\langle\boldsymbol{\varphi}_i, \boldsymbol{\varphi}_k\rangle\right|^2}. \tag{A.4}$$

Letting, $\texttt{Cont}_{mk} \triangleq \sum_{i\in\mathcal{U}\setminus\{k\}} \mathcal{E}_{p,i}\beta_{mi}\tau_p\left|\langle\boldsymbol{\varphi}_i, \boldsymbol{\varphi}_k\rangle\right|^2$, we can show that that [35]

$$\texttt{Cont.}_k = \begin{cases} \sum_{j\in\mathcal{U}\setminus\{\mathcal{O}_k\cup k\}} \mathcal{E}_{p,j}\beta_{mj}, & \boldsymbol{\Phi} \in \text{MUOB} \\ \sum_{j \text{ s.t.}\langle\boldsymbol{\varphi}_k,\boldsymbol{\varphi}_j\rangle=1} \tau_p\mathcal{E}_{p,j}\beta_{mj}, & \boldsymbol{\Phi} \in \text{OPR} \end{cases} \tag{A.5}$$

which is the pilot contamination experienced by the kth UE. ■

A.2 Proof of Theorem 2.2.

Proof. First, note that since the pilot length is τ_p and $L\tau_p = K$, we can always generate a pilot codebook $\boldsymbol{\Phi}_p \triangleq [\boldsymbol{\varphi}_k]_{k=1:\tau_p L} \in \mathbb{C}^{\tau_p\times K}$, such that pilots within each cluster are mutually orthogonal. Then, $\boldsymbol{\Phi}_p\boldsymbol{\Phi}_p^H = L\mathbf{I}_{\tau_p}$ follows from the fact that the intra-cluster pilots are orthonormal and there are L clusters. Hence, all nonzero singular values of $\boldsymbol{\Phi}_p$ are equal to $\sqrt{L}$, and consequently, $\|\boldsymbol{\Phi}_p^H\mathbf{x}\|^2 = L\|\mathbf{x}\|^2,\ \forall\mathbf{x} \in \mathbb{C}^{\tau_p}$. Therefore,

$$\|\boldsymbol{\Phi}_p^H\boldsymbol{\Phi}_p\|_{\text{F}}^2 = \sum\nolimits_{1\le i\le\tau_p L} \|\boldsymbol{\Phi}_p^H\boldsymbol{\varphi}_i\|_2^2 = L\sum\nolimits_{1\le i\le\tau_p L} \|\boldsymbol{\varphi}_i\|_2^2 = L^2\tau_p,$$

where the last equality follows from the fact that $\|\boldsymbol{\varphi}_i\|_2^2 = 1, \forall i$. Recall that $\mathcal{U}\setminus\{\mathcal{O}_k\cup k\}$ indicates the set of all UEs that do not share the same cluster as kth UE, then,

$$\begin{aligned} &\sum\nolimits_{k\in\mathcal{U}}\sum\nolimits_{j\in\mathcal{U}\setminus\{\mathcal{O}_k\cup k\}} \left|\langle\boldsymbol{\varphi}_j, \boldsymbol{\varphi}_k\rangle\right|^2 \\ &= \|\boldsymbol{\Phi}_p^H\boldsymbol{\Phi}_p\|_{\text{F}}^2 - \sum\nolimits_{k\in\mathcal{U}}\sum\nolimits_{j\in\mathcal{O}_k\cup\{k\}} \left|\langle\boldsymbol{\varphi}_j, \boldsymbol{\varphi}_k\rangle\right|^2 = \tau_p L(L-1). \end{aligned} \tag{A.6}$$

Since the summation in (A.6) contains $\tau_p^2 L(L-1)$ non-negative entries, it is easy to infer that

$$\max_{\substack{k\in\mathcal{U},\\ j\in\mathcal{U}\setminus\{\mathcal{O}_k\cup k\}}} |\langle\boldsymbol{\varphi}_j,\boldsymbol{\varphi}_k\rangle|^2 \geq \frac{\tau_p L(L-1)}{\tau_p^2 L(L-1)} = \frac{1}{\tau_p}. \tag{A.7}$$

Hence, $|\langle\boldsymbol{\varphi}_j,\boldsymbol{\varphi}_k\rangle|^2$ is lower bounded by $\frac{1}{\tau_p}$.

We now need to design pilots codebooks that satisfy $|\langle\boldsymbol{\varphi}_j,\boldsymbol{\varphi}_k\rangle|^2 = \frac{1}{\tau_p}$, $\forall k$, $\forall j \notin \mathcal{O}_k \cup k$. Invoking the definition of MUOB[1] [34], when τ_p is a prime or a power of a prime, MUOB codebooks exist provided $\sqrt{K} \leq \tau_p < K$. Then, (A.7) is satisfied with equality when $\boldsymbol{\varphi}_k$ and $\boldsymbol{\varphi}_j$ are chosen from two distinct MUOB-codebooks. ■

A.3 Proof of Theorem 2.3.

Proof. We now analyze the effect of pilot contamination on the system throughput. Our analysis applies to any random pilot codebook.

A.3.a UL SINR Analysis

Let the kth UE transmit the symbol $s_{u,k}$ ($\mathbb{E}[|s_{u,k}|^2] = 1$) in the UL with an energy of $\mathcal{E}_{u,k}$. Let $\mathcal{A}_k$ be the set of AP indices that jointly and coherently processes the kth UE's signal. After maximal ratio combining at those APs, the kth stream of the accumulated received signal at the CPU becomes

$$\begin{aligned} r_{u,k} = {} & \sqrt{\mathcal{E}_{u,k}} \sum\nolimits_{m\in\mathcal{A}_k} \mathbb{E}\left[\hat{\mathbf{f}}_{mk}^H \mathbf{f}_{mk}\right] s_{u,k} + \sqrt{\mathcal{E}_{u,k}} \sum\nolimits_{m\in\mathcal{A}_k} \left\{\hat{\mathbf{f}}_{mk}^H \mathbf{f}_{mk} - \mathbb{E}[\hat{\mathbf{f}}_{mk}^H \mathbf{f}_{mk}]\right\} s_{u,k} \\ & + \sum\nolimits_{i\in\mathcal{U}\setminus\{k\}} \sqrt{\mathcal{E}_{u,i}} \sum\nolimits_{m\in\mathcal{A}_k} \hat{\mathbf{f}}_{mk}^H \mathbf{f}_{mi} s_{u,i} + \sum\nolimits_{m\in\mathcal{A}_k} \hat{\mathbf{f}}_{mk}^H \mathbf{w}_m, \end{aligned} \tag{A.8}$$

where, $\mathbf{w}_m \sim \mathcal{CN}(\mathbf{0}, N_0\mathbf{I}_N)$ is the receiver noise added at the mth AP. The first and second term of (A.8) are commonly termed as array gain and beamforming uncertainty [19],

[1] A set of orthonormal bases $\{\Phi_j\}_{j=1,\ldots,L}$ of $\mathbb{C}^{\tau_p}$ are said to be *mutually unbiased* if $|\langle\boldsymbol{\varphi}_1,\boldsymbol{\varphi}_2\rangle|^2 = 1/\tau_p$ for any $\boldsymbol{\varphi}_1 \in \Phi_l$ and $\boldsymbol{\varphi}_2 \in \Phi_m$, $l \neq m$.

$$\gamma_k^u = \frac{\mathcal{E}_{u,k}\left|\sum\limits_{m\in\mathcal{A}_k}\mathbb{E}[\hat{\mathbf{f}}_{mk}^H\mathbf{f}_{mk}]\right|^2}{\mathcal{E}_{u,k}\mathtt{var}\left(\sum\limits_{m\in\mathcal{A}_k}\hat{\mathbf{f}}_{mk}^H\mathbf{f}_{mk}\right)+\sum\limits_{i\in\mathcal{U}\setminus\{k\}}\mathcal{E}_{u,i}\mathbb{E}\left[\left|\sum\limits_{m\in\mathcal{A}_k}\hat{\mathbf{f}}_{mk}^H\mathbf{f}_{mi}\right|^2\right]+N_0\sum\limits_{m\in\mathcal{A}_k}\mathbb{E}\|\hat{\mathbf{f}}_{mk}\|^2}. \quad \text{(A.9)}$$

respectively. Now, applying the use-and-then-forget technique [Chapter. 3, [3]], the UL SE of kth UE can be expressed[2] as $\lambda(1-\frac{\tau_p}{\tau})\log_2(1+\gamma_k^u)$, where, γ_k^u is given by (A.9), and the closed form expression is evaluated in the following lemma.

Lemma A.1. *In the UL, the SINR of the kth UE can written as*

$$\gamma_k^u = \frac{\mathcal{E}_{u,k}\mathtt{Gain}_{u,k}}{\mathcal{E}_{u,k}\mathtt{var}\left(\sum\limits_{m\in\mathcal{A}_k}\hat{\mathbf{f}}_{mk}^H\mathbf{f}_{mk}\right)+\sum\limits_{\substack{i\in\\ \mathcal{U}\setminus\{k\}}}\mathcal{E}_{u,i}\mathtt{I}_{ik}+N_0\sum\limits_{m\in\mathcal{A}_k}\alpha_{mk}^2}, \quad \text{(A.10)}$$

where,

$$\mathtt{Gain}_{u,k} = N^2\left(\sum\nolimits_{m\in\mathcal{A}_k}\alpha_{mk}^2\right)^2, \quad \text{(A.11a)}$$

$$\mathtt{var}\left(\sum\nolimits_{m\in\mathcal{A}_k}\hat{\mathbf{f}}_{mk}^H\mathbf{f}_{mk}\right) = \sum\nolimits_{m\in\mathcal{A}_k}N\alpha_{mk}^2\beta_{mk}, \quad \text{(A.11b)}$$

$$\mathtt{I}_{ik} = N^2\left(\sum\nolimits_{m\in\mathcal{A}_k}\alpha_{mk}^2\sqrt{\frac{\mathcal{E}_{p,i}}{\mathcal{E}_{p,k}}\frac{\beta_{mi}}{\beta_{mk}}}\right)^2|\langle\boldsymbol{\varphi}_i,\boldsymbol{\varphi}_k\rangle|^2+N\sum\nolimits_{m\in\mathcal{A}_k}\alpha_{mk}^2\beta_{mi}. \quad \text{(A.11c)}$$

Proof. The array gain in (A.9), can be written as

$$\mathbb{E}\left[\sum\nolimits_{m\in\mathcal{A}_k}\hat{\mathbf{f}}_{mk}^H\mathbf{f}_{mk}\right] = \mathbb{E}\left[\sum\nolimits_{m\in\mathcal{A}_k}\hat{\mathbf{f}}_{mk}^H\left[\hat{\mathbf{f}}_{mk}^H+\tilde{\mathbf{f}}_{mk}\right]\right] = \sum\nolimits_{m\in\mathcal{A}_k}\mathbb{E}\|\hat{\mathbf{f}}_{mk}\|^2 = N\sum\nolimits_{m\in\mathcal{A}_k}\alpha_{mk}^2$$

Thus, the numerator of (A.9), becomes

$$\mathcal{E}_{u,k}\left|\mathbb{E}[\sum\nolimits_{m\in\mathcal{A}_k}\hat{\mathbf{f}}_{mk}^H\mathbf{f}_{mk}]\right|^2 = \mathcal{E}_{u,k}N^2\left(\sum\nolimits_{m\in\mathcal{A}_k}\alpha_{mk}^2\right)^2, \quad \text{(A.12)}$$

[2]For a coherence interval of τ, we equally partition duration of $(\tau-\tau_p)$ channel uses for UL and DL link data transmission. Thus, the pre-log factor $\lambda(1-\frac{\tau_p}{\tau})$ for both UL implies a fraction λ ($\lambda\in[0,1]$) of the data transmission duration is alloted for UL.

which corroborates with (A.11a). Next,

$$\begin{aligned}
&\mathtt{var}\left(\sum\nolimits_{m\in\mathcal{A}_k}\hat{\mathbf{f}}_{mk}^H\mathbf{f}_{mk}\right)=\mathbb{E}\left[\left|\sum\nolimits_{m\in\mathcal{A}_k}\hat{\mathbf{f}}_{mk}^H\mathbf{f}_{mk}-\sum\nolimits_{m\in\mathcal{A}_k}\mathbb{E}\left[\hat{\mathbf{f}}_{mk}^H\mathbf{f}_{mk}\right]\right|^2\right]\\
&\overset{(a)}{=}\sum\nolimits_{m\in\mathcal{A}_k}\mathbb{E}\left[\left|\hat{\mathbf{f}}_{mk}^H\mathbf{f}_{mk}-\mathbb{E}\left[\hat{\mathbf{f}}_{mk}^H\mathbf{f}_{mk}\right]\right|^2\right]=\sum\nolimits_{m\in\mathcal{A}_k}\left\{\mathbb{E}\left[\left|\hat{\mathbf{f}}_{mk}^H\mathbf{f}_{mk}\right|^2\right]-\left|\mathbb{E}\left[\hat{\mathbf{f}}_{mk}^H\mathbf{f}_{mk}\right]\right|^2\right\}\\
&=\sum\nolimits_{m\in\mathcal{A}_k}\left\{\mathbb{E}\left[\left|\hat{\mathbf{f}}_{mk}^H\tilde{\mathbf{f}}_{mk}+\|\hat{\mathbf{f}}_{mk}\|^2\right|^2\right]-\left|\mathbb{E}\|\hat{\mathbf{f}}_{mk}\|^2\right|^2\right\}\\
&\overset{(b)}{=}\sum\nolimits_{m\in\mathcal{A}_k}\left\{\mathbb{E}\left[\left|\hat{\mathbf{f}}_{mk}^H\tilde{\mathbf{f}}_{mk}\right|^2\right]+\mathbb{E}\left[\|\hat{\mathbf{f}}_{mk}\|^4\right]-N^2\alpha_{mk}^4\right\}\\
&\overset{(c)}{=}\sum\nolimits_{m\in\mathcal{A}_k}\left\{N\alpha_{mk}^2(\beta_{mk}-\alpha_{mk}^2)+N(N+1)\alpha_{mk}^4-N^2\alpha_{mk}^4\right\}=\sum\nolimits_{m\in\mathcal{A}_k}N\alpha_{mk}^2\beta_{mk},
\end{aligned}\tag{A.13}$$

wherein, (a) follows as the variance of sum of independent random variables are sum of the respective variances. In (b), we note that $\mathbb{E}\left[\tilde{\mathbf{f}}_{mk}\right]=\mathbf{0}$ and is independent of $\hat{\mathbf{f}}_{mk}$, and therefore, apply Lemma. A.4. Finally, (c) is obtained using (A.39c). Thus, (A.11b) follows directly. Next, we derive the multi-user interference term. Prior to that, let us define the denominator of (A.3) as

$$d_{mk}^{-1}=N_0+\mathcal{E}_{p,k}\beta_{mk}\tau_p+\sum\nolimits_{i\in\mathcal{U}\setminus\{k\}}\mathcal{E}_{p,i}\tau_p\beta_{mi}\left|\langle\boldsymbol{\varphi}_i,\boldsymbol{\varphi}_k\rangle\right|^2,\tag{A.14}$$

and thus, $\hat{\mathbf{f}}_{mk}=\sqrt{\mathcal{E}_{p,k}\tau_p}\beta_{mk}d_{mk}\mathbf{y}_{p,m}$. For $i\neq k$, we can write,

$$\begin{aligned}
&\mathtt{I}_{ik}=\mathbb{E}\left[\left|\sum\nolimits_{m\in\mathcal{A}_k}\hat{\mathbf{f}}_{mk}^H\mathbf{f}_{mi}\right|^2\right]=\mathbb{E}\left[\left|\sum\nolimits_{m\in\mathcal{A}_k}\sqrt{\mathcal{E}_{p,k}\tau_p}\beta_{mk}d_{mk}\mathbf{y}_{p,m}^H\mathbf{f}_{mi}\right|^2\right]\\
&=\mathbb{E}\left[\left|\sum\nolimits_{m\in\mathcal{A}_k}\sqrt{\mathcal{E}_{p,k}\tau_p}\beta_{mk}d_{mk}\left(\sum\nolimits_{i'\in\mathcal{U}}\sqrt{\mathcal{E}_{p,i'}\tau_p}\langle\boldsymbol{\varphi}_{i'},\boldsymbol{\varphi}_k\rangle\mathbf{f}_{mi'}+\mathbf{W}_{p,m}\boldsymbol{\varphi}_k^*\right)^H\mathbf{f}_{mi}\right|^2\right]\\
&=\mathbb{E}\left[\left|\sum\nolimits_{m\in\mathcal{A}_k}\sqrt{\mathcal{E}_{p,k}\tau_p}\beta_{mk}d_{mk}\boldsymbol{\varphi}_k^T\mathbf{W}_{p,m}^H\mathbf{f}_{mi}\right|^2\right]\\
&+\mathbb{E}\left[\left|\sum\nolimits_{m\in\mathcal{A}_k}\sqrt{\mathcal{E}_{p,k}\tau_p}\beta_{mk}d_{mk}\left(\sum\nolimits_{i'\in\mathcal{U}}\sqrt{\mathcal{E}_{p,i'}\tau_p}\langle\boldsymbol{\varphi}_{i'},\boldsymbol{\varphi}_k\rangle\mathbf{f}_{mi'}\right)^H\mathbf{f}_{mi}\right|^2\right]\\
&=NN_0\sum\nolimits_{m\in\mathcal{A}_k}\mathcal{E}_{p,k}\tau_p d_{mk}^2\beta_{mk}^2\beta_{mi}+\mathtt{I}_1,
\end{aligned}\tag{A.15}$$

$$
\begin{aligned}
\mathtt{I}_1 &= \mathbb{E}\left[\left| \sum_{m\in\mathcal{A}_k} \sqrt{\mathcal{E}_{p,k}\tau_p}\beta_{mk}d_{mk}\left(\sum_{i'\in\mathcal{U}\setminus\{i\}} \sqrt{\mathcal{E}_{p,i'}\tau_p}\langle\boldsymbol{\varphi}_{i'},\boldsymbol{\varphi}_k\rangle\mathbf{f}_{mi'} + \sqrt{\mathcal{E}_{p,i}\tau_p}\langle\boldsymbol{\varphi}_i,\boldsymbol{\varphi}_k\rangle\mathbf{f}_{mi}\right)^H \mathbf{f}_{mi}\right|^2\right] \\
&\overset{(b)}{=} \mathbb{E}\left[\left| \sum\nolimits_{m\in\mathcal{A}_k} \sqrt{\mathcal{E}_{p,k}\tau_p}\beta_{mk}d_{mk}\sqrt{\mathcal{E}_{p,i}\tau_p}\langle\boldsymbol{\varphi}_i,\boldsymbol{\varphi}_k\rangle\|\mathbf{f}_{mi}\|^2\right|^2\right] \\
&+ \mathbb{E}\left[\left| \sum\nolimits_{m\in\mathcal{A}_k} \sqrt{\mathcal{E}_{p,k}\tau_p}\beta_{mk}d_{mk}\left(\sum\nolimits_{i'\in\mathcal{U}\setminus\{i\}} \sqrt{\mathcal{E}_{p,i'}\tau_p}\langle\boldsymbol{\varphi}_{i'},\boldsymbol{\varphi}_k\rangle\mathbf{f}_{mi'}\right)^H \mathbf{f}_{mi}\right|^2\right] \\
&= \mathtt{I}_2 + \underbrace{N\sum\nolimits_{m\in\mathcal{A}_k}\sum\nolimits_{i'\in\mathcal{U}\setminus\{i\}} \left\{\mathcal{E}_{p,k}\tau_p\beta_{mk}^2 d_{mk}^2\right\}\left\{\mathcal{E}_{p,i'}\tau_p\beta_{mi}\beta_{mi'}\right\}|\langle\boldsymbol{\varphi}_{i'},\boldsymbol{\varphi}_k\rangle|^2}_{\triangleq \mathtt{I}_3}
\end{aligned} \tag{A.17}
$$

(b): Using (A.40).

---

where $\mathtt{I}_1$ being the second expectation term involved in (A.15), and can be further manipulated as shown in (A.17), with

$$
\mathtt{I}_2 \triangleq \mathbb{E}\left[\left| \sum\nolimits_{m\in\mathcal{A}_k} \sqrt{\mathcal{E}_{p,k}\tau_p}\beta_{mk}d_{mk}\sqrt{\mathcal{E}_{p,i}\tau_p}\langle\boldsymbol{\varphi}_i,\boldsymbol{\varphi}_k\rangle\|\mathbf{f}_{mi}\|^2\right|^2\right]. \tag{A.16}
$$

Next, we expand $\mathtt{I}_2$ as shown in (A.18).

$$
\begin{aligned}
\mathtt{I}_2 &= \sum\nolimits_{m\in\mathcal{A}_k} \mathcal{E}_{p,k}\mathcal{E}_{p,i}\tau_p^2 d_{mk}^2\beta_{mk}^2|\langle\boldsymbol{\varphi}_i,\boldsymbol{\varphi}_k\rangle|^2\mathbb{E}\left[\|\mathbf{f}_{mi}\|^4\right] \\
&+ \mathcal{E}_{p,k}\mathcal{E}_{p,i}\tau_p^2|\langle\boldsymbol{\varphi}_i,\boldsymbol{\varphi}_k\rangle|^2\mathbb{E}\left[\sum\nolimits_{m\in\mathcal{A}_k}\sum\nolimits_{\substack{n\in\mathcal{A}_k,\\ m\neq n}} d_{mk}d_{nk}\beta_{mk}\beta_{nk}\|\mathbf{f}_{mi}\|^2\|\mathbf{f}_{ni}\|^2\right] \\
&= N(N+1)\sum\nolimits_{m\in\mathcal{A}_k} \mathcal{E}_{p,k}\mathcal{E}_{p,i}\tau_p^2 d_{mk}^2\beta_{mk}^2|\langle\boldsymbol{\varphi}_i,\boldsymbol{\varphi}_k\rangle|^2\beta_{mi}^2 \\
&+ N^2\mathcal{E}_{p,k}\mathcal{E}_{p,i}\tau_p^2|\langle\boldsymbol{\varphi}_i,\boldsymbol{\varphi}_k\rangle|^2\sum\nolimits_{m\in\mathcal{A}_k}\sum\nolimits_{\substack{n\in\mathcal{A}_k,\\ m\neq n}} d_{mk}d_{nk}\beta_{mk}\beta_{nk}\beta_{mi}\beta_{ni} \\
&= N^2\left(\sum\nolimits_{m\in\mathcal{A}_k} \mathcal{E}_{p,k}\mathcal{E}_{p,i}\tau_p^2 d_{mk}^2\beta_{mk}^2|\langle\boldsymbol{\varphi}_i,\boldsymbol{\varphi}_k\rangle|^2\beta_{mi}^2\right. \\
&\left.+\mathcal{E}_{p,k}\mathcal{E}_{p,i}\tau_p^2|\langle\boldsymbol{\varphi}_i,\boldsymbol{\varphi}_k\rangle|^2\sum\nolimits_{m\in\mathcal{A}_k}\sum\nolimits_{\substack{n\in\mathcal{A}_k,\\ m\neq n}} d_{mk}d_{nk}\beta_{mk}\beta_{nk}\beta_{mi}\beta_{ni}\right) \\
&+ \underbrace{N\sum\nolimits_{m\in\mathcal{A}_k} \mathcal{E}_{p,k}\mathcal{E}_{p,i}\tau_p^2 d_{mk}^2\beta_{mk}^2|\langle\boldsymbol{\varphi}_i,\boldsymbol{\varphi}_k\rangle|^2\beta_{mi}^2}_{\triangleq \mathtt{I}_4} \\
&= N^2\left(\sum\nolimits_{m\in\mathcal{A}_k} \sqrt{\mathcal{E}_{p,k}\tau_p}d_{mk}\beta_{mk}\sqrt{\mathcal{E}_{p,i}\tau_p}\beta_{mi}\right)^2|\langle\boldsymbol{\varphi}_i,\boldsymbol{\varphi}_k\rangle|^2 + \mathtt{I}_4.
\end{aligned} \tag{A.18}
$$

Now, the first term of (A.18) can be re-written as

$$\begin{aligned}
&N^2\left(\sum\nolimits_{m\in\mathcal{A}_k}\sqrt{\mathcal{E}_{p,k}\tau_p}d_{mk}\beta_{mk}\sqrt{\mathcal{E}_{p,i}\tau_p}\beta_{mi}\right)^2|\langle\boldsymbol{\varphi}_i,\boldsymbol{\varphi}_k\rangle|^2\\
&=N^2\left(\sum\nolimits_{m\in\mathcal{A}_k}\mathcal{E}_{p,k}\tau_p d_{mk}\beta_{mk}^2\sqrt{\frac{\mathcal{E}_{p,i}\tau_p}{\mathcal{E}_{p,k}\tau_p}}\frac{\beta_{mi}}{\beta_{mk}}\right)^2|\langle\boldsymbol{\varphi}_i,\boldsymbol{\varphi}_k\rangle|^2\\
&=N^2\left(\sum\nolimits_{m\in\mathcal{A}_k}\alpha_{mk}^2\sqrt{\frac{\mathcal{E}_{p,i}}{\mathcal{E}_{p,k}}}\frac{\beta_{mi}}{\beta_{mk}}\right)^2|\langle\boldsymbol{\varphi}_i,\boldsymbol{\varphi}_k\rangle|^2, \qquad \text{(A.19)}
\end{aligned}$$

which contributes to coherent interference. Thus, now using (A.17), (A.18), and (A.19), we have

$$\mathtt{I}_1=N^2\left(\sum\nolimits_{m\in\mathcal{A}_k}\alpha_{mk}^2\sqrt{\frac{\mathcal{E}_{p,i}}{\mathcal{E}_{p,k}}}\frac{\beta_{mi}}{\beta_{mk}}\right)^2|\langle\boldsymbol{\varphi}_i,\boldsymbol{\varphi}_k\rangle|^2+\mathtt{I}_4+\mathtt{I}_3. \qquad \text{(A.20)}$$

Now, we will simplify the second term of (A.17) as

$$\begin{aligned}
\mathtt{I}_3&=N\sum\nolimits_{m\in\mathcal{A}_k}\sum\nolimits_{\substack{i'\in\\ \mathcal{U}\setminus\{i\}}}\left\{\mathcal{E}_{p,k}\tau_p\beta_{mk}^2d_{mk}^2\right\}\left\{\mathcal{E}_{p,i'}\tau_p\beta_{mi}\beta_{mi'}\right\}|\langle\boldsymbol{\varphi}_{i'},\boldsymbol{\varphi}_k\rangle|^2\\
&=N\sum\nolimits_{m\in\mathcal{A}_k}\mathcal{E}_{p,k}\tau_p\beta_{mk}^2d_{mk}^2\beta_{mi}\times\left(\sum\nolimits_{i'\in\mathcal{U}}\mathcal{E}_{p,i'}\tau_p\beta_{mi'}|\langle\boldsymbol{\varphi}_{i'},\boldsymbol{\varphi}_k\rangle|^2-\mathcal{E}_{p,i}\tau_p\beta_{mi}|\langle\boldsymbol{\varphi}_i,\boldsymbol{\varphi}_k\rangle|^2\right)\\
&=\underbrace{N\sum\nolimits_{m\in\mathcal{A}_k}\mathcal{E}_{p,k}\tau_p\beta_{mk}^2d_{mk}^2\beta_{mi}\sum\nolimits_{i'\in\mathcal{U}}\mathcal{E}_{p,i'}\tau_p\beta_{mi'}|\langle\boldsymbol{\varphi}_{i'},\boldsymbol{\varphi}_k\rangle|^2}_{\triangleq\mathtt{I}_5}\\
&\quad-N\sum\nolimits_{m\in\mathcal{A}_k}\mathcal{E}_{p,k}\mathcal{E}_{p,i}\tau_p^2d_{mk}^2\beta_{mk}^2\beta_{mi}^2|\langle\boldsymbol{\varphi}_{i'},\boldsymbol{\varphi}_k\rangle|^2. \qquad \text{(A.21)}
\end{aligned}$$

Then,

$$\mathtt{I}_5=N\sum\nolimits_{m\in\mathcal{A}_k}\mathcal{E}_{p,k}\tau_p\beta_{mk}^2d_{mk}^2\beta_{mi}\left(\sum\nolimits_{i'\in\mathcal{U}}\mathcal{E}_{p,i'}\tau_p\beta_{mi'}|\langle\boldsymbol{\varphi}_{i'},\boldsymbol{\varphi}_k\rangle|^2\right), \qquad \text{(A.22)}$$

and we also observe here from (A.14) that

$$\sum\nolimits_{i'\in\mathcal{U}}\mathcal{E}_{p,i'}\tau_p\beta_{mi'}|\langle\boldsymbol{\varphi}_{i'},\boldsymbol{\varphi}_k\rangle|^2=\left(\frac{1}{d_{mk}}-N_0\right), \qquad \text{(A.23)}$$

which when substituted back in (A.22) results in

$$\mathtt{I}_5 = N \sum\nolimits_{m \in \mathcal{A}_k} \mathcal{E}_{p,k} \tau_p \beta_{mk}^2 d_{mk} \beta_{mi} - N N_0 \sum\nolimits_{m \in \mathcal{A}_k} \mathcal{E}_{p,k} \tau_p \beta_{mk}^2 d_{mk}^2 \beta_{mi}. \tag{A.24}$$

Therefore, inserting (A.24) into (A.21),

$$\begin{aligned} \mathtt{I}_3 =& N \sum\nolimits_{m \in \mathcal{A}_k} \mathcal{E}_{p,k} \tau_p \beta_{mk}^2 d_{mk} \beta_{mi} - N N_0 \sum\nolimits_{m \in \mathcal{A}_k} \mathcal{E}_{p,k} \tau_p \beta_{mk}^2 d_{mk}^2 \beta_{mi} \\ & - N \sum\nolimits_{m \in \mathcal{A}_k} \mathcal{E}_{p,k} \mathcal{E}_{p,i} \tau_p^2 d_{mk}^2 \beta_{mk}^2 \beta_{mi}^2 |\langle \boldsymbol{\varphi}_{i'}, \boldsymbol{\varphi}_k \rangle|^2 \end{aligned} \tag{A.25}$$

Now, substituting (A.20) into (A.15), we get

$$\begin{aligned} \mathtt{I}_{ik} =& N N_0 \sum\nolimits_{m \in \mathcal{A}_k} \mathcal{E}_{p,k} \tau_p d_{mk}^2 \beta_{mk}^2 \beta_{mi} \\ & + N^2 \left(\sum\nolimits_{m \in \mathcal{A}_k} \alpha_{mk}^2 \sqrt{\frac{\mathcal{E}_{p,i}}{\mathcal{E}_{p,k}}} \frac{\beta_{mi}}{\beta_{mk}} \right)^2 |\langle \boldsymbol{\varphi}_i, \boldsymbol{\varphi}_k \rangle|^2 + \mathtt{I}_4 + \mathtt{I}_3. \end{aligned} \tag{A.26}$$

Next, substituting for $\mathtt{I}_4$ and $\mathtt{I}_3$, we get,

$$\begin{aligned} \mathtt{I}_{ik} =& N N_0 \sum\nolimits_{m \in \mathcal{A}_k} \mathcal{E}_{p,k} \tau_p d_{mk}^2 \beta_{mk}^2 \beta_{mi} + N^2 \left(\sum\nolimits_{m \in \mathcal{A}_k} \alpha_{mk}^2 \sqrt{\frac{\mathcal{E}_{p,i}}{\mathcal{E}_{p,k}}} \frac{\beta_{mi}}{\beta_{mk}} \right)^2 |\langle \boldsymbol{\varphi}_i, \boldsymbol{\varphi}_k \rangle|^2 \\ & + N \sum\nolimits_{m \in \mathcal{A}_k} \mathcal{E}_{p,k} \mathcal{E}_{p,i} \tau_p^2 d_{mk}^2 \beta_{mk}^2 |\langle \boldsymbol{\varphi}_i, \boldsymbol{\varphi}_k \rangle|^2 \beta_{mi}^2 + N \sum\nolimits_{m \in \mathcal{A}_k} \mathcal{E}_{p,k} \tau_p \beta_{mk}^2 d_{mk} \beta_{mi} \\ & - N N_0 \sum\nolimits_{m \in \mathcal{A}_k} \mathcal{E}_{p,k} \tau_p \beta_{mk}^2 d_{mk}^2 \beta_{mi} - N \sum\nolimits_{m \in \mathcal{A}_k} \mathcal{E}_{p,k} \mathcal{E}_{p,i} \tau_p^2 d_{mk}^2 \beta_{mk}^2 \beta_{mi}^2 |\langle \boldsymbol{\varphi}_{i'}, \boldsymbol{\varphi}_k \rangle|^2, \end{aligned} \tag{A.27}$$

and, finally,

$$\mathtt{I}_{ik} = N^2 \left(\sum\nolimits_{m \in \mathcal{A}_k} \alpha_{mk}^2 \sqrt{\frac{\mathcal{E}_{p,i}}{\mathcal{E}_{p,k}}} \frac{\beta_{mi}}{\beta_{mk}} \right)^2 |\langle \boldsymbol{\varphi}_i, \boldsymbol{\varphi}_k \rangle|^2 + N \sum\nolimits_{m \in \mathcal{A}_k} \underbrace{\mathcal{E}_{p,k} \tau_p \beta_{mk}^2 d_{mk}}_{\alpha_{mk}^2} \beta_{mi}. \tag{A.28}$$

Lastly, the additive noise component of (A.10) trivially follows as $\hat{\mathbf{f}}_{mk} \sim \mathcal{CN}(\mathbf{0}, \alpha_{mk}^2 \mathbf{I}_N)$.

■

A.3.b DL SINR Analysis

Next, let $s_{d,k}$ be the intended DL signal for the kth UE. Let $\mathcal{E}_{d,m}$ be the total power budget

of mth AP, and the corresponding power control coefficient ζ_{mk} decides what fraction of power is intended for the kth UE. We employ reciprocity-based matched filter precoding in the DL. Now, the mth AP serves only a cluster of users indicated by the set $\tilde{\mathcal{U}}_m$, and therefore, the DL transmitted signal by the mth AP can be expressed as

$$\mathbf{r}_{d,m} = \sum\nolimits_{i\in\tilde{\mathcal{U}}_m} \sqrt{\mathcal{E}_{d,m}\zeta_{mi}}\hat{\mathbf{f}}^*_{mi}s_{d,i}. \tag{A.29}$$

Thus, the received signal at the kth UE can be expressed as

$$\begin{aligned} r_{d,k} &= \sum\nolimits_{m=1}^{M} \mathbf{f}^T_{mk}\mathbf{r}_{d,m} + w_k = \sum\nolimits_{m=1}^{M}\sum\nolimits_{i\in\tilde{\mathcal{U}}_m} \sqrt{\mathcal{E}_{d,m}\zeta_{mi}}\mathbf{f}^T_{mk}\hat{\mathbf{f}}^*_{mi}s_{d,k} + w_k \\ &= \sum\nolimits_{m\in\mathcal{A}_k} \sqrt{\mathcal{E}_{d,m}\zeta_{mk}}\mathbf{f}^T_{mk}\hat{\mathbf{f}}^*_{mk}s_{d,k} + \sum\nolimits_{i\in\mathcal{U}\setminus\{k\}}\sum\nolimits_{m\in\mathcal{A}_i} \sqrt{\mathcal{E}_{d,m}\zeta_{mi}}\mathbf{f}^T_{mk}\mathbf{f}^*_{mi}s_{d,i} + w_k, \end{aligned} \tag{A.30}$$

where, $w_k \sim \mathcal{CN}(0, N_0)$ is the receiver noise at the kth user. To apply Use-and-then-Forget bound, we re-write $r_{d,k}$ as

$$\begin{aligned} r_{d,k} &= \mathbb{E}\left[\sum\nolimits_{m\in\mathcal{A}_k} \sqrt{\mathcal{E}_{d,m}\zeta_{mk}}\mathbf{f}^T_{mk}\hat{\mathbf{f}}^*_{mk}\right] s_{d,k} + \Big\{\sum\nolimits_{m\in\mathcal{A}_k} \sqrt{\mathcal{E}_{d,m}\zeta_{mk}}\mathbf{f}^T_{mk}\hat{\mathbf{f}}^*_{mk} \\ &\quad -\mathbb{E}\left[\sum\nolimits_{m\in\mathcal{A}_k} \sqrt{\mathcal{E}_{d,m}\zeta_{mk}}\mathbf{f}^T_{mk}\hat{\mathbf{f}}^*_{mk}\right]\Big\} s_{d,k} + \sum\nolimits_{i\in\mathcal{U}\setminus\{k\}}\sum\nolimits_{m\in\mathcal{A}_i} \sqrt{\mathcal{E}_{d,m}\zeta_{mi}}\mathbf{f}^T_{mk}\mathbf{f}^*_{mi}s_{d,i} + w_k, \end{aligned}$$

and thus the DL SE becomes $(1-\lambda)(1-\frac{\tau_p}{\tau})\log_2(1+\gamma^d_k)$, where,

$$\begin{aligned} \gamma^d_k &= \left|\mathbb{E}\left[\sum\nolimits_{m\in\mathcal{A}_k} \sqrt{\mathcal{E}_{d,m}\zeta_{mk}}\mathbf{f}^T_{mk}\hat{\mathbf{f}}^*_{mk}\right]\right|^2 \Bigg(\mathtt{var}\left(\sum\nolimits_{m\in\mathcal{A}_k} \sqrt{\mathcal{E}_{d,m}\zeta_{mk}}\mathbf{f}^T_{mk}\hat{\mathbf{f}}^*_{mk}\right) \\ &\quad + \sum\nolimits_{i\in\mathcal{U}\setminus\{k\}} \mathbb{E}\left[\left|\sum\nolimits_{m\in\mathcal{A}_i} \sqrt{\mathcal{E}_{d,m}\zeta_{mi}}\mathbf{f}^T_{mk}\hat{\mathbf{f}}^*_{mi}\right|^2\right] + N_0\Bigg)^{-1}. \end{aligned} \tag{A.31}$$

We can apply the exact same analysis to derive the closed-form expressions of the DL signal gain and the beamforming error variance and show that

$$\mathbb{E}\left[\sum\nolimits_{m\in\mathcal{A}_k} \sqrt{\mathcal{E}_{d,m}\zeta_{mk}}\mathbf{f}^T_{mk}\hat{\mathbf{f}}^*_{mk}\right] = N\sqrt{\mathcal{E}_{d,m}\zeta_{mk}}\alpha^2_{mk} \tag{A.32a}$$

$$\mathtt{var}\left(\sum\nolimits_{m\in\mathcal{A}_k} \sqrt{\mathcal{E}_{d,m}\zeta_{mk}}\mathbf{f}^T_{mk}\hat{\mathbf{f}}^*_{mk}\right) = N\sum\nolimits_{m\in\mathcal{A}_k} \mathcal{E}_{d,m}\zeta_{mk}\alpha^2_{mk}\beta_{mk}. \tag{A.32b}$$

However, there is a subtle difference in the multi-user interference term as the kth UE

receives a signal from the ith UE ($i \neq k$) transmitted from the APs that serves ith UE ($m \in \mathcal{A}_i$). We derive the closed-form expression in the following lemma.

Lemma A.2. *It can be shown that the DL multi-user interference experienced by the kth UE due to the ith UE is*

$$\mathbb{E}\left[\left|\sum\nolimits_{m\in\mathcal{A}_i}\sqrt{\mathcal{E}_{d,m}\zeta_{mi}}\mathbf{f}_{mk}^T\hat{\mathbf{f}}_{mi}^*\right|^2\right] = N^2\left(\sum\nolimits_{m\in\mathcal{A}_i}\sqrt{\mathcal{E}_{d,m}\zeta_{mi}}\sqrt{\frac{\mathcal{E}_{p,k}}{\mathcal{E}_{p,i}}}\frac{\beta_{mk}}{\beta_{mi}}\alpha_{mi}^2\right)^2|\boldsymbol{\varphi}_i^H\boldsymbol{\varphi}_k|^2 + N\sum\nolimits_{m\in\mathcal{A}_i}\mathcal{E}_{d,m}\zeta_{mi}\beta_{mk}\alpha_{mi}^2. \tag{A.33}$$

Proof. The technique of the proof is the same as adopted in the UL case. The key difference is in the UL we substituted for the desired UE's estimated channel (i.e., $\hat{\mathbf{f}}_{mk}$) from (A.2), whereas here we substitute for $\hat{\mathbf{f}}_{mi}$. We show the key steps required to arrive at the final expression of (A.33).

$$\mathbb{E}\left[\left|\sum\nolimits_{m\in\mathcal{A}_i}\sqrt{\mathcal{E}_{d,m}\zeta_{mi}}\mathbf{f}_{mk}^T\hat{\mathbf{f}}_{mi}^*\right|^2\right] = \mathbb{E}\left[\left|\sum\nolimits_{m\in\mathcal{A}_i}\sqrt{\mathcal{E}_{d,m}\zeta_{mi}}\sqrt{\mathcal{E}_{p,i\tau_p}}\beta_{mi}d_{mi}\mathbf{f}_{mk}^T\times\right.\right.$$
$$\left.\left.\left(\sum\nolimits_{i'\in\mathcal{U}}\sqrt{\mathcal{E}_{p,i'\tau_p}}\langle\boldsymbol{\varphi}_{i'},\boldsymbol{\varphi}_i\rangle\mathbf{f}_{mi'} + \mathbf{W}_{p,m}\boldsymbol{\varphi}_i^*\right)^*\right|^2\right] = \mathcal{E}_{p,k}\tau_p\mathbb{E}\left[\left|\sum\nolimits_{m\in\mathcal{A}_i}\bar{d}_{mi}\|\mathbf{f}_{mk}\|^2\right|^2\right]|\langle\boldsymbol{\varphi}_k,\boldsymbol{\varphi}_i\rangle|^2$$
$$+\underbrace{\mathbb{E}\left[\left|\sum\nolimits_{m\in\mathcal{A}_i}\bar{d}_{mi}\mathbf{f}_{mk}^T\sum\nolimits_{\substack{i'\in\\ \mathcal{U}\setminus k}}\sqrt{\mathcal{E}_{p,i'\tau_p}}\langle\boldsymbol{\varphi}_{i'},\boldsymbol{\varphi}_i\rangle\mathbf{f}_{mi'}^*\right|^2\right]}_{\triangleq \mathtt{I}_5} + \underbrace{\mathbb{E}\left[\left|\sum\nolimits_{m\in\mathcal{A}_i}\bar{d}_{mi}\mathbf{f}_{mk}^T\mathbf{W}_{p,m}^*\boldsymbol{\varphi}_i\right|^2\right]}_{\triangleq \mathtt{I}_6}, \tag{A.34}$$

where in the last equality we substitute $\bar{d}_{mi} = \sqrt{\mathcal{E}_{d,m}\zeta_{mi}}\sqrt{\mathcal{E}_{p,i}\tau_p}\beta_{mi}d_{mi}$. Next, observe that, as the channel vectors of different users are uncorrelated and zero mean, and so are the channel vector and the noise component, the sum of the second and third expectations of (A.34) reduces to

$$\mathtt{I}_5 + \mathtt{I}_6 = N\sum\nolimits_{m\in\mathcal{A}_i}\sum\nolimits_{\substack{i'\in\\ \mathcal{U}\setminus k}}\bar{d}_{mi}^2\mathcal{E}_{p,i'\tau_p}\beta_{mk}\beta_{mi'}|\langle\boldsymbol{\varphi}_{i'},\boldsymbol{\varphi}_i\rangle|^2 + NN_0\sum\nolimits_{m\in\mathcal{A}_i}\bar{d}_{mi}^2\beta_{mk}. \tag{A.35}$$

Next, the first expectation (A.34) can be expanded as

$$\begin{aligned}
&\mathbb{E}\left[\left|\sum_{m\in\mathcal{A}_i}\bar{d}_{mi}\|\mathbf{f}_{mk}\|^2\right|^2\right] = \sum_{m\in\mathcal{A}_i}\bar{d}_{mi}^2\mathbb{E}\left[\|\mathbf{f}_{mk}\|^4\right] + \mathbb{E}\left[\sum\nolimits_{m\in\mathcal{A}_i}\sum\nolimits_{\substack{n\in\mathcal{A}_i\\n\neq m}}\bar{d}_{mi}\bar{d}_{ni}\|\mathbf{f}_{mk}\|^2\|\mathbf{f}_{nk}\|^2\right] \\
&= N(N+1)\sum\nolimits_{m\in\mathcal{A}_i}\bar{d}_{mi}^2\beta_{mk}^2 + N^2\sum\nolimits_{m\in\mathcal{A}_i}\sum\nolimits_{\substack{n\in\mathcal{A}_i\\n\neq m}}\bar{d}_{mi}\bar{d}_{ni}\beta_{mk}\beta_{nk} \\
&= N^2\left(\sum\nolimits_{m\in\mathcal{A}_i}\bar{d}_{mi}\beta_{mk}\right)^2 + N\sum\nolimits_{m\in\mathcal{A}_i}\bar{d}_{mi}^2\beta_{mk}^2. \qquad \text{(A.36)}
\end{aligned}$$

Finally, substituting (A.36),and (A.35) into (A.34), we get

$$\begin{aligned}
&\mathbb{E}\left[\left|\sum_{m\in\mathcal{A}_i}\sqrt{\mathcal{E}_{d,m}\zeta_{mi}}\mathbf{f}_{mk}^T\hat{\mathbf{f}}_{mi}^*\right|^2\right] = \mathcal{E}_{p,k}\tau_p\left\{N^2\left(\sum_{m\in\mathcal{A}_i}\bar{d}_{mi}\beta_{mk}\right)^2 + N\sum_{m\in\mathcal{A}_i}\bar{d}_{mi}^2\beta_{mk}^2\right\}|\langle\boldsymbol{\varphi}_k,\boldsymbol{\varphi}_i\rangle|^2 \\
&+ N\sum\nolimits_{m\in\mathcal{A}_i}\sum\nolimits_{\substack{i'\in\\\mathcal{U}\setminus k}}\bar{d}_{mi}^2\mathcal{E}_{p,i'}\tau_p\beta_{mk}\beta_{mi'}|\langle\boldsymbol{\varphi}_{i'},\boldsymbol{\varphi}_i\rangle|^2 + NN_0\sum\nolimits_{m\in\mathcal{A}_i}\bar{d}_{mi}^2\beta_{mk} \\
&= N^2\left(\sqrt{\mathcal{E}_{p,k}\tau_p}\sum\nolimits_{m\in\mathcal{A}_i}\bar{d}_{mi}\beta_{mk}\right)^2|\langle\boldsymbol{\varphi}_k,\boldsymbol{\varphi}_i\rangle|^2 \\
&+ N\sum\nolimits_{m\in\mathcal{A}_i}\bar{d}_{mi}^2\beta_{mk}\left\{\sum\nolimits_{i'\in\mathcal{U}}\mathcal{E}_{p,i'}\tau_p\beta_{mi'}|\langle\boldsymbol{\varphi}_{i'},\boldsymbol{\varphi}_i\rangle|^2\right\} + NN_0\sum\nolimits_{m\in\mathcal{A}_i}\bar{d}_{mi}^2\beta_{mk}. \qquad \text{(A.37)}
\end{aligned}$$

Now, (A.33) follows by substituting

$$\sqrt{\mathcal{E}_{p,k}\tau_p}\bar{d}_{mi}\beta_{mk} = \sqrt{\mathcal{E}_{d,m}\zeta_{mi}}\left\{\mathcal{E}_{p,i}\tau_p d_{mi}\beta_{mi}^2\right\}\frac{\beta_{mk}\sqrt{\mathcal{E}_{p,k}}}{\beta_{mi}\sqrt{\mathcal{E}_{p,i}}}, \qquad \text{(A.38a)}$$

$$\left\{\mathcal{E}_{p,i}\tau_p d_{mi}\beta_{mi}^2\right\} = \alpha_{mi}^2, \qquad \text{(A.38b)}$$

$$\text{and}\quad \left\{\sum\nolimits_{i'\in\mathcal{U}}\mathcal{E}_{p,i'}\tau_p\beta_{mi'}|\langle\boldsymbol{\varphi}_{i'},\boldsymbol{\varphi}_i\rangle|^2\right\} = \frac{1}{d_{mi}} - N_0 \qquad \text{(A.38c)}$$

appropriately on (A.37). ■

Finally, in the UL, γ_k^u of Lemma A.1 can be re-expressed as γ_k^u of Theorem 2.3. The first term of (A.28) corresponds to the first term on the denominator of γ_k^u in (2.8a), and merging (A.13) and $N\sum_{m\in\mathcal{A}_k}\alpha_{mk}^2\beta_{mi}$ from (A.28),we obtain the second term of γ_k^u. The rest of the terms follow directly from Lemma A.1. (2.8b) follows similarly from (A.32a), (A.32b), and Lemma A.2, and ρ_d be the maximum normalized (as a multiple of the noise variance N_0) power transmitted by each AP. ■

A.3.b.i Useful Lemma

Lemma A.3. *[3, Appendix. A] Let two independent random vectors* $\mathbf{x}$ *and* $\mathbf{y}$ *be distributed as* $\mathcal{CN}(\mathbf{0}, \sigma_x^2\mathbf{I}_N)$ *and* $\mathcal{CN}(\mathbf{0}, \sigma_y^2\mathbf{I}_N)$*, respectively. Then, the followings results follow*

$$\mathbb{E}\left[\|\mathbf{x}\|^2\right] = N\sigma_x^2 \tag{A.39a}$$

$$\mathbb{E}\left[\|\mathbf{x}\|^4\right] = N(N+1)\sigma_x^4 \tag{A.39b}$$

$$\mathbb{E}\left[\left|(\mathbf{x}+\mathbf{y})^H\mathbf{x}\right|^2\right] = N(N+1)\sigma_x^4 + N\sigma_x^2\sigma_y^2. \tag{A.39c}$$

Lemma A.4. *[19, (62)] If* $\mathbf{x}$ *and* $\mathbf{y}$ *are independent random vectors and* $\mathbb{E}[\mathbf{x}] = \mathbf{0}$*, then*

$$\mathbb{E}\left[|\mathbf{x}+\mathbf{y}|^2\right] = \mathbb{E}\left[|\mathbf{x}|^2\right] + \mathbb{E}\left[|\mathbf{y}|^2\right]. \tag{A.40}$$

B | Appendix to Chapter 3

B.1 Proof of Theorem 3.4

Proof. We first focus on the UL SE, considering the perfect CSI. If $\{j\} \notin \mathcal{A}_s$ is activated in the DL, then, from (3.12), the UL SINR remains unchanged, i.e., $\eta_{u,k}(\mathcal{A}_s \cup \{j\}) = \eta_{u,k}(\mathcal{A}_s)$, for $\{j\} \in \mathcal{A}_\mathsf{d}$. If jth AP is activated in the UL, then from (3.8)

$$\begin{aligned}\eta_{u,k}(\mathcal{A}_s \cup \{j\}) &= \sum_{m \in \mathcal{A}_s} \frac{N\mathcal{E}_{u,k}\beta_{mk}^2}{\sum_{k' \in \mathcal{U}_\mathsf{u} \setminus k} \mathcal{E}_{u,k'}\beta_{mk}\beta_{mk'} + N_0\beta_{mk}} \\ &\quad + \frac{N\mathcal{E}_{u,k}\beta_{jk}^2}{\sum_{k' \in \mathcal{U}_\mathsf{u} \setminus k} \mathcal{E}_{u,k'}\beta_{jk}\beta_{jk'} + N_0\beta_{jk}} \\ &= \eta_{u,k}(\mathcal{A}_s) + \eta_{u,k}(\{j\}) > \eta_{u,k}(\mathcal{A}_s), \end{aligned} \tag{B.1}$$

establishing the monotonicity. Also,

$$\begin{aligned}&\eta_{u,k}(\mathcal{A}_s \cup \{j\}) - \eta_{u,k}(\mathcal{A}_s) \\ &\quad = \begin{cases} 0, \text{ if } \{j\} \text{ operates in DL} \\ \eta_{u,k}(\{j\}), \text{ if } \{j\} \text{ operates in UL} \end{cases}, \end{aligned} \tag{B.2}$$

and therefore, it is easy to see that $\eta_{u,k}(\mathcal{A}_s \cup \{j\}) - \eta_{u,k}(\mathcal{A}_s) = \eta_{u,k}(\mathcal{A}_t \cup \{j\}) - \eta_{u,k}(\mathcal{A}_t)$. Thus, the UL SINR is a modular function of the underlying activated AP set. Finally, we can easily extend the above steps for the trained CSI case. ■

B.2 Proof of Theorem 3.5

Proof. Recall that $\mathcal{R}_{\mathsf{s}}(\mathcal{A}_s) = \mathcal{R}_{\mathsf{s}}(\mathcal{A}_{\mathsf{u}}) + \mathcal{R}_{\mathsf{s}}(\mathcal{A}_{\mathsf{d}})$, where $\mathcal{A}_{\mathsf{u}}$ and $\mathcal{A}_{\mathsf{d}}$ are mutually exclusive index sets. Hence, if the UL and DL sum SEs are sub-modular functions of the index set of activated APs, then the sum UL-DL SE is also sub-modular.

From Theorem 3.4, the UL SINR is a monotonically non-decreasing function of the activated AP set, and since $\log(1+x)$ is monotonically increasing for $x \geq 0$, the UL SE is also a monotonically non-decreasing function of the activated AP set. We now prove the sub-modular nature of the UL-SE. As the UL-SINR is modular, we can write $(1+\eta_{u,k}(\mathcal{A}_s \cup \{j\})) - (1+\eta_{u,k}(\mathcal{A}_s)) = (1+\eta_{u,k}(\mathcal{A}_t \cup \{j\})) - (1+\eta_{u,k}(\mathcal{A}_t))$, which implies $\dfrac{1+\eta_{u,k}(\mathcal{A}_s \cup \{j\})}{1+\eta_{u,k}(\mathcal{A}_s)} \geq \dfrac{1+\eta_{u,k}(\mathcal{A}_t \cup \{j\})}{1+\eta_{u,k}(\mathcal{A}_t)}$. Here, we use the fact that

$$\frac{1}{(1+\eta_{u,k}(\mathcal{A}_t))} \leq \frac{1}{(1+\eta_{u,k}(\mathcal{A}_t))},$$

due to the monotonic non-decreasing nature of the SINR. Also, as $\dfrac{1+\eta_{u,k}(\mathcal{A}_s \cup \{j\})}{1+\eta_{u,k}(\mathcal{A}_s)}$ and $\dfrac{1+\eta_{u,k}(\mathcal{A}_t \cup \{j\})}{1+\eta_{u,k}(\mathcal{A}_t)}$ are both ≥ 1, using the monotonicity of $\log(\cdot)$, we have

$$\begin{aligned} &\log\left(1+\eta_{u,k}(\mathcal{A}_s \cup \{j\})\right) - \log\left(1+\eta_{u,k}(\mathcal{A}_s)\right) \\ &\geq \log\left(1+\eta_{u,k}(\mathcal{A}_t \cup \{j\})\right) - \log\left(1+\eta_{u,k}(\mathcal{A}_t)\right), \end{aligned} \tag{B.3}$$

which establishes the sub-modularity of UL SE of kth UE, $\forall k \in \mathcal{U}_{\mathsf{u}}$. We can similarly prove the sub-modularity of the DL SINR, and as the linear sum of sub-modular functions is sub-modular [60], Theorem 3.5 holds true. ■

C | Appendix to Chapter 4

For the definitions of the notations used in the following proofs, the readers can refer to Table 4.1.

C.1 Proof of Theorem 4.1

Proof. The numerator of (4.5) can be written as

$$\mathbb{E}\Big[\sum_{m\in\mathcal{A}_{\mathsf{u}}}\hat{\mathbf{f}}_{mk}^{H}\hat{\mathbf{f}}_{mk}+\hat{\mathbf{f}}_{mk}^{H}\tilde{\mathbf{f}}_{mk}\Big]=\sum_{m\in\mathcal{A}_{\mathsf{u}}}\mathbb{E}\Big[\|\hat{\mathbf{f}}_{mk}\|^{2}\Big]=N\sum_{m\in\mathcal{A}_{\mathsf{u}}}\alpha_{mk}^{2}.$$

Next, we can show $\mathtt{var}\Big[\sum_{m\in\mathcal{A}_{\mathsf{u}}}\hat{\mathbf{f}}_{mk}^{H}\mathbf{f}_{mk}\Big]=\sum_{m\in\mathcal{A}_{\mathsf{u}}}N\alpha_{mk}^{2}\beta_{mk}$. Now, for the UEs that share their pilot sequences with the kth UE, i.e., for $n\in\mathcal{I}_p\backslash k$,

$$\begin{aligned}
&\mathbb{E}\big[\big|\sum_{m\in\mathcal{A}_{\mathsf{u}}}\hat{\mathbf{f}}_{mk}^{H}\mathbf{f}_{mn}\big|^{2}\big]=\mathbb{E}\big[\big|\sum_{m\in\mathcal{A}_{\mathsf{u}}}c_{mk}\sqrt{\tau_p\mathcal{E}_{p,k}}\beta_{mk}\times\big(\sum_{n'\in\mathcal{I}_p}\sqrt{\mathcal{E}_{p,n'}\tau_p}\mathbf{f}_{mn'}+\dot{\mathbf{w}}_{p,m}\big)^{H}\mathbf{f}_{mn}\big|^{2}\big]\\
&=N\sum_{m\in\mathcal{A}_{\mathsf{u}}}N_0c_{mk}^{2}\tau_p\mathcal{E}_{p,k}\beta_{mk}^{2}\beta_{mn}\\
&+\mathbb{E}\big[\big|\sum_{m\in\mathcal{A}_{\mathsf{u}}}c_{mk}\sqrt{\tau_p\mathcal{E}_{p,k}}\beta_{mk}\sum_{n'\in\mathcal{I}_p}\sqrt{\mathcal{E}_{p,n'}\tau_p}\mathbf{f}_{mn'}^{H}\mathbf{f}_{mn}\big|^{2}\big].
\end{aligned}\tag{C.1}$$

The last term in the above can be simplified as follows:

$$\begin{aligned}
&\mathbb{E}\big[\big|\sum_{m\in\mathcal{A}_{\mathsf{u}}}c_{mk}\sqrt{\tau_p\mathcal{E}_{p,k}}\beta_{mk}\big(\sum_{n'\in\mathcal{I}_p\backslash n}\sqrt{\mathcal{E}_{p,n'}\tau_p}\mathbf{f}_{mn'}+\sqrt{\mathcal{E}_{p,n}\tau_p}\mathbf{f}_{mn}\big)^{H}\mathbf{f}_{mn}\big|^{2}\big]\\
&=N\sum_{m\in\mathcal{A}_{\mathsf{u}}}c_{mk}^{2}\tau_p^{2}\mathcal{E}_{p,k}\beta_{mk}^{2}\mathcal{E}_{p,n}\beta_{mn}^{2}
\end{aligned}$$

$$+ N^2\Big(\sum_{m\in\mathcal{A}_\mathsf{u}} \alpha_{mk}^2 \frac{\beta_{mn}}{\beta_{mk}}\sqrt{\frac{\mathcal{E}_{p,n}}{\mathcal{E}_{p,k}}}\Big)^2 N \sum_{m\in\mathcal{A}_\mathsf{u}}\sum_{n'\in\mathcal{I}_p\setminus n} c_{mk}^2\tau_p^2\mathcal{E}_{p,k}\beta_{mk}^2\mathcal{E}_{p,n'}\beta_{mn'}\beta_{mn}.$$

Now $N \sum\limits_{m\in\mathcal{A}_\mathsf{u}}\sum\limits_{n'\in\mathcal{I}_p\setminus n} c_{mk}^2\tau_p^2\mathcal{E}_{p,k}\beta_{mk}^2\mathcal{E}_{p,n'}\beta_{mn'}\beta_{mn}$, can be further expanded as

$$\begin{aligned}
&N\sum_{m\in\mathcal{A}_\mathsf{u}} c_{mk}\sqrt{\tau_p\mathcal{E}_{p,k}}\beta_{mk}\beta_{mn}\Big\{c_{mk}\sqrt{\tau_p\mathcal{E}_{p,k}}\beta_{mk}\times\sum_{n'\in\mathcal{I}_p}\tau_p\mathcal{E}_{p,n'}\beta_{mn'}\Big\} - N\sum_{m\in\mathcal{A}_\mathsf{u}} c_{mk}^2\tau_p^2\mathcal{E}_{p,k}\beta_{mk}^2\mathcal{E}_{p,n}\beta_{mn}^2\\
&= N\sum_{m\in\mathcal{A}_\mathsf{u}}\tau_p\mathcal{E}_{p,k}c_{mk}\beta_{mk}^2\beta_{mn} - NN_0\sum_{m\in\mathcal{A}_\mathsf{u}} c_{mk}^2\tau_p\mathcal{E}_{p,k}\beta_{mk}^2\beta_{mn} - N\sum_{m\in\mathcal{A}_\mathsf{u}} c_{mk}^2\tau_p^2\mathcal{E}_{p,k}\beta_{mk}^2\mathcal{E}_{p,n}\beta_{mn}^2,
\end{aligned} \tag{C.2}$$

where, in the last step above, we used the fact

$$c_{mk}\sqrt{\tau_p\mathcal{E}_{p,k}}\beta_{mk}\sum_{n'\in\mathcal{I}_p}\tau_p\mathcal{E}_{p,n'}\beta_{mn'} = \sqrt{\tau_p\mathcal{E}_{p,k}}\beta_{mk} - N_0 c_{mk}\sqrt{\tau_p\mathcal{E}_{p,k}}\beta_{mk}.$$

Combining (C.1) and (C.2), with $\alpha_{mk}^2 = \tau_p\mathcal{E}_{p,k}c_{mk}\beta_{mk}^2$, we obtain

$$\sum_{n\in\mathcal{I}_p\setminus k}\mathcal{E}_{\mathsf{u},n}\mathbb{E}\big[\big|\sum_{m\in\mathcal{A}_\mathsf{u}}\hat{\mathbf{f}}_{mk}^H\mathbf{f}_{mn}\big|^2\big] = \sum_{n\in\mathcal{I}_p\setminus k}\mathcal{E}_{\mathsf{u},n}\Big(N^2\Big(\sum_{m\in\mathcal{A}_\mathsf{u}}\alpha_{mk}^2\frac{\beta_{mn}}{\beta_{mk}}\sqrt{\frac{\mathcal{E}_{p,n}}{\mathcal{E}_{p,k}}}\Big)^2 + N\sum_{m\in\mathcal{A}_\mathsf{u}}\alpha_{mk}^2\beta_{mn}\Big). \tag{C.3}$$

The first two terms above correspond to coherent interference (4.8b) and non-coherent interference, respectively, from UEs that share the kth UE's pilot. Next, considering the interference due to the UEs that do not share the kth UE's pilot, we obtain

$$\sum_{q\in\mathcal{U}_\mathsf{u}\setminus\mathcal{I}_p}\mathcal{E}_{\mathsf{u},n}\mathbb{E}\big[\big|\sum_{m\in\mathcal{A}_\mathsf{u}}\hat{\mathbf{f}}_{mk}^H\mathbf{f}_{mq}\big|^2\big] = N\sum_{q\in\mathcal{U}_\mathsf{u}\setminus\mathcal{I}_p}\mathcal{E}_{\mathsf{u},n}\sum_{m\in\mathcal{A}_\mathsf{u}}\tau_p\mathcal{E}_{p,k}c_{mk}\beta_{mk}^2\beta_{mq}. \tag{C.4}$$

Hence, (4.8a) follows via combining the beamforming uncertainty, the second term of (C.3), and (C.4). Finally, we can derive the inter-AP interference as

$$\begin{aligned}
&\sum_{n\in\mathcal{U}_\mathsf{d}}\mathbb{E}\big[\big|\sum_{m\in\mathcal{A}_\mathsf{u}}\sum_{j\in\mathcal{A}_\mathsf{d}}\sqrt{\mathcal{E}_{\mathsf{d},j}}\kappa_{jn}\hat{\mathbf{f}}_{mk}^H\mathbf{G}_{mj}\hat{\mathbf{f}}_{jn}^*\big|^2\big]\\
&= \sum_{n\in\mathcal{U}_\mathsf{d}}\sum_{m\in\mathcal{A}_\mathsf{u}}\sum_{j\in\mathcal{A}_\mathsf{d}}\mathcal{E}_{\mathsf{d},j}\kappa_{jn}^2\mathbb{E}\big[\mathtt{tr}\big(\mathbf{G}_{mj}\hat{\mathbf{f}}_{jn}^*\hat{\mathbf{f}}_{jn}^T\mathbf{G}_{mj}^H\hat{\mathbf{f}}_{mk}\hat{\mathbf{f}}_{mk}^H\big)\big]
\end{aligned}$$

$$\overset{(a)}{=} \sum_{n\in\mathcal{U}_\mathsf{d}}\sum_{m\in\mathcal{A}_\mathsf{u}}\sum_{j\in\mathcal{A}_\mathsf{d}} \mathcal{E}_{\mathsf{d},j}\kappa_{jn}^2 \mathtt{tr}\big(\mathbb{E}\big[\mathbf{G}_{mj}\hat{\mathbf{f}}_{jn}^*\hat{\mathbf{f}}_{jn}^T\mathbf{G}_{mj}^H\big]\mathbb{E}\big[\hat{\mathbf{f}}_{mk}\hat{\mathbf{f}}_{mk}^H\big]\big)$$
$$= N^2\sum_{m\in\mathcal{A}_\mathsf{u}}\sum_{j\in\mathcal{A}_\mathsf{d}}\sum_{n\in\mathcal{U}_\mathsf{d}} \kappa_{jn}^2\zeta_{mj}\alpha_{mk}^2\alpha_{jn}^2\mathcal{E}_{\mathsf{d},j}.$$

In (a), we apply the linearity of trace. Then we use the fact that $\mathbf{G}_{mj}$ and $\mathbf{f}_{jn}$ are independent, and therefore, $\mathbb{E}[\mathbf{G}_{mj}\hat{\mathbf{f}}_{jn}^*\hat{\mathbf{f}}_{jn}^T\mathbf{G}_{mj}^H] = \zeta_{mj}\mathbb{E}[\mathtt{tr}(\hat{\mathbf{f}}_{jn}^*\hat{\mathbf{f}}_{jn}^T)]\mathbf{I}_N = N\alpha_{jn}^2\zeta_{mj}\mathbf{I}_N$, and $\mathbb{E}[\hat{\mathbf{f}}_{mk}\hat{\mathbf{f}}_{mk}^H] = \alpha_{mk}^2\mathbf{I}_N$, which yields the final result in (4.8c). ■

C.2 Proof of Theorem 4.2

Proof. We note that from (4.9), we can write the effective DL SINR as

$$\eta_{\mathsf{d},n} = \Big[\Big|\sum_{j\in\mathcal{A}_\mathsf{d}}\kappa_{jn}\sqrt{\mathcal{E}_{\mathsf{d},j}}\mathbb{E}\big[\mathbf{f}_{jn}^T\hat{\mathbf{f}}_{jn}^*\big]\Big|^2\Big]\times\Bigg(\mathtt{var}\Big\{\sum_{j\in\mathcal{A}_\mathsf{d}}\kappa_{jn}\sqrt{\mathcal{E}_{\mathsf{d},j}}\mathbf{f}_{jn}^T\hat{\mathbf{f}}_{jn}^*\Big\}$$
$$+\sum_{q\in\mathcal{I}_p\backslash n}\mathbb{E}\Big[\Big|\sum_{j\in\mathcal{A}_\mathsf{d}}\kappa_{jq}\sqrt{\mathcal{E}_{\mathsf{d},j}}\mathbf{f}_{jn}^T\hat{\mathbf{f}}_{jq}^*\Big|^2\Big]+\sum_{q\in\mathcal{U}_\mathsf{d}\backslash\mathcal{I}_p}\mathbb{E}\Big[\Big|\sum_{j\in\mathcal{A}_\mathsf{d}}\kappa_{jq}\sqrt{\mathcal{E}_{\mathsf{d},q}}\mathbf{f}_{jn}^T\hat{\mathbf{f}}_{jq}^*\Big|^2\Big]$$
$$+\sum_{k\in\mathcal{U}_\mathsf{u}}\mathcal{E}_{\mathsf{u},n}\mathbb{E}\big|\mathsf{g}_{nk}\big|^2+N_0\Bigg)^{-1}. \tag{C.5}$$

The gain and the variance of the beamforming uncertainty related terms, i.e., the numerator term and the first term in the denominator of (C.5), can be obtained via steps similar to those in the UL case. The second term in the denominator of (C.5), which is the inter-UE interference due to data streams of the UEs that share pilots with the nth UE, i.e., $q\in\mathcal{I}_n\backslash n$, can be expressed as (C.6). Further algebraic manipulations yield

$$\sum_{q\in\mathcal{I}_p\backslash n}\mathbb{E}\Big[\Big|\sum_{j\in\mathcal{A}_\mathsf{d}}\kappa_{jq}\sqrt{\mathcal{E}_{\mathsf{d},j}}\mathbf{f}_{jn}^T\hat{\mathbf{f}}_{jq}^*\Big|^2\Big]+\sum_{q\in\mathcal{U}_\mathsf{d}\backslash\mathcal{I}_p}\mathbb{E}\Big[\Big|\sum_{j\in\mathcal{A}_\mathsf{d}}\kappa_{jq}\sqrt{\mathcal{E}_{\mathsf{d},q}}\mathbf{f}_{jn}^T\hat{\mathbf{f}}_{jq}^*\Big|^2\Big]$$
$$= N^2\sum_{q\in\mathcal{I}_p\backslash n}\Big(\sum_{j\in\mathcal{A}_\mathsf{d}}\sqrt{\mathcal{E}_{\mathsf{d},j}}\kappa_{jq}\alpha_{jq}^2\sqrt{\frac{\mathcal{E}_{p,n}}{\mathcal{E}_{p,q}}\frac{\beta_{jn}}{\beta_{jq}}}\Big)^2+N\sum_{q\in\mathcal{U}_\mathsf{d}\backslash n}\sum_{j\in\mathcal{A}_\mathsf{d}}\mathcal{E}_{\mathsf{d},j}\kappa_{jq}^2\beta_{jn}\alpha_{jq}^2. \tag{C.7}$$

The first term in (C.7) equates to (4.11b). The second term together with the nth UE's beamforming uncertainty corresponds to (4.11a), and (4.11c) follows from $\mathbb{E}\big|\mathsf{g}_{nk}\big|^2 = \epsilon_{nk}$.

$$\mathbb{E}\big[\big|\sum_{j\in\mathcal{A}_{\mathsf{d}}}\kappa_{jq}\sqrt{\mathcal{E}_{\mathsf{d},j}}\mathbf{f}_{jn}^{T}\hat{\mathbf{f}}_{jq}^{*}\big|^{2}\big]=\mathbb{E}\big[\big|\sum_{j\in\mathcal{A}_{\mathsf{d}}}\kappa_{jq}\sqrt{\mathcal{E}_{\mathsf{d},j}}\tau_{p}\sqrt{\mathcal{E}_{p,n}\mathcal{E}_{p,q}}c_{jq}\beta_{jq}\|\mathbf{f}_{jn}\|^{2}\big|^{2}\big]$$
$$+\mathbb{E}\big[\big|\sum_{j\in\mathcal{A}_{\mathsf{d}}}\kappa_{jq}\sqrt{\mathcal{E}_{\mathsf{d},j}}c_{jq}\sqrt{\tau_{p}\mathcal{E}_{p,q}}\beta_{jq}\mathbf{f}_{jn}^{T}\big(\sum_{q'\in\mathcal{I}_{p}\backslash n}\sqrt{\tau_{p}\mathcal{E}_{p,q'}}\mathbf{f}_{jq'}+\dot{\mathbf{w}}_{p,j}\big)\big|^{2}\big]$$
$$=N(N+1)\tau_{p}^{2}\mathcal{E}_{p,n}\mathcal{E}_{p,q}\sum_{j\in\mathcal{A}_{\mathsf{d}}}\kappa_{jq}^{2}\mathcal{E}_{\mathsf{d},j}c_{jq}^{2}\beta_{jq}^{2}\beta_{jn}^{2}$$
$$+N^{2}\tau_{p}^{2}\mathcal{E}_{p,n}\mathcal{E}_{p,q}\big(\sum_{j\in\mathcal{A}_{\mathsf{d}}}\sqrt{\mathcal{E}_{\mathsf{d},j}}\kappa_{jq}c_{jq}\beta_{jq}\beta_{jn}\big)\big(\sum_{j'\in\mathcal{A}_{\mathsf{d}},j'\neq j}\sqrt{\mathcal{E}_{\mathsf{d},j'}}\kappa_{j'q}c_{j'q}\beta_{j'q}\beta_{j'n}\big)$$
$$+N\tau_{p}\mathcal{E}_{p,q}\sum_{j\in\mathcal{A}_{\mathsf{d}}}\kappa_{jq}^{2}\mathcal{E}_{\mathsf{d},j}c_{jq}^{2}\beta_{jq}^{2}\big(\sum_{q'\in\mathcal{I}_{p}\backslash n}\tau_{p}\mathcal{E}_{p,q'}\beta_{jq'}+N_{0}\big)\beta_{jn}. \tag{C.6}$$

■

C.3 Proof of Theorem 4.3

Proof. We present an inductive proof. Let us assume we schedule the APs in $\mathcal{A}_s$ such that $f_{mk}(\mathcal{A}_s)$ is maximized. Now consider the set $\mathcal{A}_t$, such that $\mathcal{A}_s \subseteq \mathcal{A}_t$. We need to prove that, if we schedule any AP $\{j\} \notin \mathcal{A}_t$ next, the incremental gain obtained by adding $\{j\}$ to $\mathcal{A}_t$ is smaller than the incremental gain achieved by adding $\{j\}$ to $\mathcal{A}_s$. Now, by our hypothesis, the set $\mathcal{A}_s$ is determined first to maximize $f_{mk}(.)$. Therefore, since AP $\{j\}$ is not part of $\mathcal{A}_s$, the product SINR under $\mathcal{A}_s$ is greater than that attained via only activating the $\{j\}$th AP in either of the mode of transmissions, that is, $\prod_{k=1}^{K}\frac{\sum_{m\in\mathcal{A}_s}\mathtt{G}_{mk}(\mathcal{A}_s)}{\sum_{m\in\mathcal{A}_s}\mathtt{I}_{mk}(\mathcal{A}_s)}\geq\prod_{k=1}^{K}\frac{\mathtt{G}_{jk}(\{j\})}{\mathtt{I}_{jk}(\{j\})}$.

Using the monotonic nondecreasing property in Definition 4.1, we can write

$$\prod_{k=1}^{K}\frac{\sum_{m\in\mathcal{A}_t}\mathtt{G}_{mk}(\mathcal{A}_t)}{\sum_{m\in\mathcal{A}_t}\mathtt{I}_{mk}(\mathcal{A}_t)}\geq\prod_{k=1}^{K}\frac{\sum_{m\in\mathcal{A}_s}\mathtt{G}_{mk}(\mathcal{A}_s)}{\sum_{m\in\mathcal{A}_s}\mathtt{I}_{mk}(\mathcal{A}_s)}\Rightarrow\frac{\prod_{k=1}^{K}\sum_{m\in\mathcal{A}_t}\mathtt{G}_{mk}(\mathcal{A}_t)-\prod_{k=1}^{K}\sum_{m\in\mathcal{A}_t}\mathtt{G}_{mk}(\mathcal{A}_s)}{\prod_{k=1}^{K}\sum_{m\in\mathcal{A}_t}\mathtt{I}_{mk}(\mathcal{A}_t)-\prod_{k=1}^{K}\sum_{m\in\mathcal{A}_s}\mathtt{I}_{mk}(\mathcal{A}_s)}$$
$$\geq\frac{\prod_{k=1}^{K}\sum_{m\in\mathcal{A}_s}\mathtt{G}_{mk}(\mathcal{A}_s)}{\prod_{k=1}^{K}\sum_{m\in\mathcal{A}_s}\mathtt{I}_{mk}(\mathcal{A}_s)}\geq\prod_{k=1}^{K}\frac{\mathtt{G}_{jk}(\{j\})}{\mathtt{I}_{jk}(\{j\})}$$
$$\Rightarrow-\prod_{k=1}^{K}\mathtt{I}_{jk}(\{j\})\prod_{k=1}^{K}\sum_{m\in\mathcal{A}_s}\mathtt{G}_{mk}(\mathcal{A}_s)+\prod_{k=1}^{K}\mathtt{G}_{jk}(\{j\})\prod_{k=1}^{K}\sum_{m\in\mathcal{A}_s}\mathtt{I}_{mk}(\mathcal{A}_s)$$

$$
\begin{aligned}
&- \prod_{k=1}^{K} \left(\mathtt{I}_{jk}(\{j\}) + \sum_{m \in \mathcal{A}_s} \mathtt{I}_{mk}(\mathcal{A}_s) \right) \prod_{k=1}^{K} \sum_{m \in \mathcal{A}_s} \mathtt{G}_{mk}(\mathcal{A}_s) \\
&+ \prod_{k=1}^{K} \left(\mathtt{G}_{jk}(\{j\}) + \sum_{m \in \mathcal{A}_s} \mathtt{G}_{mk}(\mathcal{A}_s) \right) \prod_{k=1}^{K} \sum_{m \in \mathcal{A}_s} \mathtt{I}_{mk}(\mathcal{A}_s) \\
&\geq - \prod_{k=1}^{K} \left(\mathtt{I}_{jk}(\{j\}) + \sum_{m \in \mathcal{A}_t} \mathtt{I}_{mk}(\mathcal{A}_t) \right) \prod_{k=1}^{K} \sum_{m \in \mathcal{A}_t} \mathtt{G}_{mk}(\mathcal{A}_t) \\
&+ \prod_{k=1}^{K} \left(\mathtt{G}_{jk}(\{j\}) + \sum_{m \in \mathcal{A}_t} \mathtt{G}_{mk}(\mathcal{A}_t) \right) \prod_{k=1}^{K} \sum_{m \in \mathcal{A}_t} \mathtt{I}_{mk}(\mathcal{A}_t). \qquad \text{(C.9)}
\end{aligned}
$$

$$
\geq - \prod_{k=1}^{K} \mathtt{I}_{jk}(\{j\}) \prod_{k=1}^{K} \sum_{m \in \mathcal{A}_t} \mathtt{G}_{mk}(\mathcal{A}_t) + \prod_{k=1}^{K} \mathtt{G}_{jk}(\{j\}) \prod_{k=1}^{K} \sum_{m \in \mathcal{A}_t} \mathtt{I}_{mk}(\mathcal{A}_t) \qquad \text{(C.8)}
$$

Next, adding and subtracting $\prod_{k=1}^{K} \sum_{m \in \mathcal{A}_s} \mathtt{G}_{mk}(\mathcal{A}_s) \prod_{k=1}^{K} \sum_{m \in \mathcal{A}_s} \mathtt{I}_{mk}(\mathcal{A}_s)$ on the left hand side and $\prod_{k=1}^{K} \sum_{m \in \mathcal{A}_t} \mathtt{G}_{mk}(\mathcal{A}_t) \prod_{k=1}^{K} \sum_{m \in \mathcal{A}_t} \mathtt{I}_{mk}(\mathcal{A}_t)$ on the right hand side of (C.8), we get (C.9), equivalently

$$
\begin{aligned}
&- \prod_{k=1}^{K} \sum_{m \in \mathcal{A}_s \cup \{j\}} \mathtt{I}_{mk}(\mathcal{A}_s \cup \{j\}) \prod_{k=1}^{K} \sum_{m \in \mathcal{A}_s} \mathtt{G}_{mk}(\mathcal{A}_s) + \prod_{k=1}^{K} \sum_{m \in \mathcal{A}_s \cup \{j\}} \mathtt{G}_{mk}(\mathcal{A}_s \cup \{j\}) \prod_{k=1}^{K} \sum_{m \in \mathcal{A}_s} \mathtt{I}_{mk}(\mathcal{A}_s) \\
&\geq - \prod_{k=1}^{K} \sum_{m \in \mathcal{A}_t \cup \{j\}} \mathtt{I}_{mk}(\mathcal{A}_t \cup \{j\}) \prod_{k=1}^{K} \sum_{m \in \mathcal{A}_t} \mathtt{G}_{mk}(\mathcal{A}_t) + \prod_{k=1}^{K} \sum_{m \in \mathcal{A}_t \cup \{j\}} \mathtt{G}_{mk}(\mathcal{A}_t \cup \{j\}) \prod_{k=1}^{K} \sum_{m \in \mathcal{A}_t} \mathtt{I}_{mk}(\mathcal{A}_t).
\end{aligned}
$$

Using the fact that

$$
\prod_{k=1}^{K} \sum_{m \in \mathcal{A}_s \cup \{j\}} \mathtt{I}_{mk}(\mathcal{A}_s \cup \{j\}) \prod_{k=1}^{K} \sum_{m \in \mathcal{A}_s} \mathtt{I}_{mk}(\mathcal{A}_s) \leq \prod_{k=1}^{K} \sum_{m \in \mathcal{A}_t \cup \{j\}} \mathtt{I}_{mk}(\mathcal{A}_t \cup \{j\}) \prod_{k=1}^{K} \sum_{m \in \mathcal{A}_t} \mathtt{I}_{mk}(\mathcal{A}_t),
$$

we can finally write,

$$
\frac{\prod_{k=1}^{K} \sum_{m \in \mathcal{A}_s \cup \{j\}} \mathtt{G}_{mk}(\mathcal{A}_s \cup \{j\})}{\prod_{k=1}^{K} \sum_{m \in \mathcal{A}_s \cup \{j\}} \mathtt{I}_{mk}(\mathcal{A}_s \cup \{j\})} - \frac{\prod_{k=1}^{K} \sum_{m \in \mathcal{A}_s} \mathtt{G}_{mk}(\mathcal{A}_s)}{\prod_{k=1}^{K} \sum_{m \in \mathcal{A}_s} \mathtt{I}_{mk}(\mathcal{A}_s)}
$$

$$\geq \frac{\prod_{k=1}^{K} \sum_{m \in \mathcal{A}_t \cup \{j\}} \mathtt{G}_{mk}(\mathcal{A}_t \cup \{j\})}{\prod_{k=1}^{K} \sum_{m \in \mathcal{A}_t \cup \{j\}} \mathtt{I}_{mk}(\mathcal{A}_t \cup \{j\})} - \frac{\prod_{k=1}^{K} \sum_{m \in \mathcal{A}_t} \mathtt{G}_{mk}(\mathcal{A}_t)}{\prod_{k=1}^{K} \sum_{m \in \mathcal{A}_t} \mathtt{I}_{mk}(\mathcal{A}_t)},$$

which reduces to Theorem 4.3. ■

D | Appendix to Chapter 5

D.1 Proof of Lemma 5.2

Proof. With ZF combining, the mth term of $\mathbb{E}[\mathbf{u}_{kk}]$ in (**??**) evaluates to

$$\gamma_{mk}\mathbb{E}[\mathbf{e}_{l(k)}^T(\mathbf{Z}_{\mathsf{u},m}^H\mathbf{Z}_{\mathsf{u},m})^{-1}\mathbf{Z}_{\mathsf{u},m}^H\mathbf{f}_{mk}] = \alpha_{mk}^2. \tag{D.1}$$

Next, we evaluate $\mathbb{E}[\mathbf{u}_{ki}\mathbf{u}_{ki}^H] \in \mathbb{C}^{|\mathcal{A}_\mathsf{u}|\times|\mathcal{A}_\mathsf{u}|}$ in closed form. First, we consider the UEs that use the same pilot as the kth UE, i.e., the UEs indexed by $i \in \mathcal{P}_{l(k)}, i \neq k$. In this case, the mth diagonal entry of $\mathbb{E}[\mathbf{u}_{ki}\mathbf{u}_{ki}^H]$ can be expanded as

$$\begin{aligned}\mathbb{E}[\mathbf{v}_{mk}^H\mathbf{f}_{mi}\mathbf{f}_{mi}^H\mathbf{v}_{mk}] &= \mathbb{E}[\mathbf{v}_{mk}^H\hat{\mathbf{f}}_{mi}\hat{\mathbf{f}}_{mi}^H\mathbf{v}_{mk}] + \mathbb{E}[\mathbf{v}_{mk}^H\tilde{\mathbf{f}}_{mi}\tilde{\mathbf{f}}_{mi}^H\mathbf{v}_{mk}] \\ &\overset{(a)}{=} \alpha_{mk}^4 + \mathbb{E}[\mathbf{v}_{mk}^H\mathbb{E}[\tilde{\mathbf{f}}_{mi}\tilde{\mathbf{f}}_{mi}^H]\mathbf{v}_{mk}].\end{aligned} \tag{D.2}$$

Here, in (a) we use the fact that $\mathbb{E}[\mathbf{v}_{mk}^H\hat{\mathbf{f}}_{mi}\hat{\mathbf{f}}_{mi}^H\mathbf{v}_{mk}] = \alpha_{mk}^4$ if $i \in \mathcal{P}_{l(k)}$. Next, since $\tilde{\mathbf{f}}_{mi} \sim \mathcal{CN}(\mathbf{0}, (\beta_{mi} - \alpha_{mi}^2)\mathbf{I}_N)$ and $\mathbb{E}[\mathbf{v}_{mk}^H\mathbf{v}_{mk}] = \dfrac{\alpha_{mk}^2}{N-\tau_p}$, $\mathbb{E}[\mathbf{v}_{mk}^H\mathbb{E}[\tilde{\mathbf{f}}_{mi}\tilde{\mathbf{f}}_{mi}^H]\mathbf{v}_{mk}] = \dfrac{1}{N-\tau_p}\alpha_{mk}^2(\beta_{mi} - \alpha_{mi}^2)$. The off-diagonal (m,n)th element of $\mathbb{E}[\mathbf{u}_{ki}\mathbf{u}_{ki}^H]$ can be calculated as $[\mathbb{E}[\mathbf{u}_{ki}\mathbf{u}_{ki}^H]]_{m,n} = \mathbb{E}[\mathbf{v}_{mk}^H\hat{\mathbf{f}}_{mi}\hat{\mathbf{f}}_{ni}^H\mathbf{v}_{nk}] + \mathbb{E}[\mathbf{v}_{mk}^H\tilde{\mathbf{f}}_{mi}\tilde{\mathbf{f}}_{ni}^H\mathbf{v}_{nk}] = \alpha_{mk}^2\alpha_{ni}^2$. Next, for the UEs that do not share the same pilot as the kth UE ($\forall i' \notin \mathcal{P}_{l(k)}$), it is easy to show that the off-diagonal entries of $\mathbb{E}[\mathbf{u}_{ki'}\mathbf{u}_{ki'}^H]$ are zero. The mth diagonal entry can be evaluated as $\mathbb{E}[\mathbf{v}_{mk}^H\mathbf{f}_{mi'}\mathbf{f}_{mi'}^H\mathbf{v}_{mk}] = \mathbb{E}[\mathbf{v}_{mk}^H\mathbb{E}[\tilde{\mathbf{f}}_{mi'}\tilde{\mathbf{f}}_{mi'}^H]\mathbf{v}_{mk}] = \dfrac{\alpha_{mk}^2(\beta_{mi'} - \alpha_{mi'}^2)}{(N-\tau_p)}$.

Next, we can show that $\mathbb{E}[|\mathbf{v}_{mk}^H\tilde{\mathbf{G}}_{mj}\mathbf{p}_{jn}|^2] = \dfrac{N\zeta_{mj}^{\mathsf{InAP}}\alpha_{mk}^2}{(N-\tau_p)}$. It is easy to argue that due to the independence of the channel vectors involved, the off-diagonal entries of $\mathbb{E}[\mathbf{d}_{kn}\mathbf{d}_{kn}^H]$ are

zero. Finally, $\mathbf{N}_{\text{eff.}} = N_0 \texttt{diag}\left(\frac{\alpha_{1k}^2}{N-\tau_p}, \ldots, \frac{\alpha_{|\mathcal{A}_\mathsf{u}|k}^2}{N-\tau_p}\right)$. This completes the key steps in the derivation of $\boldsymbol{\omega}_k^{\text{opt.}}$. With a little algebraic manipulation, we arrive at the expressions in the Lemma. ■

D.2 Proof of Lemma 5.4

Proof. Here, we provide the important steps involved in the proof. The beamforming gain, $\left|\sum_{j\in\mathcal{A}_\mathsf{d}} \kappa_{jn}\sqrt{\mathcal{E}_\mathsf{d}}\mathbf{f}_{jn}^H\mathbf{p}_{jn}\right|^2$, after substituting for $\mathbf{p}_{jn}$, with $\mathbb{E}\left[\|\mathbf{Z}_{\mathsf{d},j}(\mathbf{Z}_{\mathsf{d},j}^H\mathbf{Z}_{\mathsf{d},j})^{-1}\mathbf{e}_{l(n)}\|^2\right] = \frac{c_{jn}}{(N-\tau_p)}$ and $\hat{\mathbf{f}}_{jn} = c_{jn}\sqrt{\tau_p\mathcal{E}_{p,j}}\beta_{jn}\mathbf{Z}_{\mathsf{d},j}\mathbf{e}_{l(n)}$, can be evaluated as follows:

$$\begin{aligned}&\mathcal{E}_\mathsf{d}\left|\sum_{j\in\mathcal{A}_\mathsf{d}}\kappa_{jn}\sqrt{(N-\tau_p)c_{jn}^{-1}}\hat{\mathbf{f}}_{jn}^H\mathbf{Z}_{\mathsf{d},j}\left(\mathbf{Z}_{\mathsf{d},j}^H\mathbf{Z}_{\mathsf{d},j}\right)^{-1}\mathbf{e}_{l(n)}\right|^2\\ &= (N-\tau_p)\mathcal{E}_\mathsf{d}\left(\sum_{j\in\mathcal{A}_\mathsf{d}}\kappa_{jn}\alpha_{jn}\right)^2. \end{aligned} \tag{D.3}$$

Next, from the denominator of (3.12), we can rewrite $\mathcal{E}_\mathsf{d}\Big(\texttt{var}\{\boldsymbol{\kappa}_n^T\mathbf{d}_{nn}\}+\sum_{q\in\mathcal{U}_\mathsf{d}\setminus n}\mathbb{E}[|\boldsymbol{\kappa}_q^T\mathbf{d}_{nq}|^2]\Big)$ as $\mathcal{E}_\mathsf{d}\Big(\sum_{q\in\mathcal{U}_\mathsf{d}}\mathbb{E}[|\boldsymbol{\kappa}_q^T\mathbf{d}_{nq}|^2] - |\mathbb{E}[\boldsymbol{\kappa}_n^T\mathbf{d}_{nn}]|^2\Big)$. Substituting for $\mathbf{d}_{nq}$ and $\boldsymbol{\kappa}_q$, we get

$$\sum_{q\in\mathcal{U}_\mathsf{d}}\mathbb{E}\left[\left|\boldsymbol{\kappa}_q^T\mathbf{d}_{nq}\right|^2\right] = \sum_{q\in\mathcal{U}_\mathsf{d}}\mathbb{E}\left[\left|\sum\nolimits_{j\in\mathcal{A}_\mathsf{d}}\kappa_{jq}\mathbf{f}_{jn}^T\mathbf{p}_{jq}\right|^2\right], \tag{D.4}$$

which can be evaluated as $(N-\tau_p)\sum_{q\in\mathcal{P}_{l(n)}}\left(\sum_{j\in\mathcal{A}_\mathsf{d}}\kappa_{jq}\alpha_{jn}\right)^2 + \sum_{q\in\mathcal{U}_\mathsf{d}}\sum_{j\in\mathcal{A}_\mathsf{d}}\kappa_{jq}(\beta_{jn}-\alpha_{jn}^2)$. Then, with $\left|\mathbb{E}[\boldsymbol{\kappa}_n^T\mathbf{d}_{nn}]\right|^2 = (N-\tau_p)\left(\sum_{j\in\mathcal{A}_\mathsf{d}}\kappa_{jn}\alpha_{jn}\right)^2$, we get (5.16a) and (4.11a). ■

D.3 Proof of Proposition 5.2

Proof. First, optimizing $f\left(\boldsymbol{\mathcal{E}}_\mathsf{u}, \boldsymbol{\varpi}_\mathsf{u}\right)$ is equivalent to optimizing $f\left(\boldsymbol{\mathcal{E}}_\mathsf{u}, \boldsymbol{\varpi}_\mathsf{u}, \tilde{\boldsymbol{\varpi}}_\mathsf{u}\right)$, where

$$f\left(\boldsymbol{\mathcal{E}}_\mathsf{u}, \boldsymbol{\varpi}_\mathsf{u}, \tilde{\boldsymbol{\varpi}}_\mathsf{u}\right) = \sum\nolimits_{k\in\mathcal{U}_\mathsf{u}}\ln\left(1+\varpi_{\mathsf{u},k}\right) - \sum\nolimits_{k\in\mathcal{U}_\mathsf{u}}\varpi_{\mathsf{u},k} + f(\boldsymbol{\mathcal{E}}_\mathsf{u}, \tilde{\boldsymbol{\varpi}}_\mathsf{u}), \tag{D.5}$$

due to the equivalence of $\sum_{k\in\mathcal{U}_\mathsf{u}} \dfrac{(1+\varpi_{\mathsf{u},k})\mathsf{G}_{\mathsf{u},k}\left(\boldsymbol{\mathcal{E}}_\mathsf{u}\right)}{\mathsf{G}_{\mathsf{u},k}\left(\boldsymbol{\mathcal{E}}_\mathsf{u}\right)+\mathsf{I}_{\mathsf{u},k}\left(\boldsymbol{\mathcal{E}}_\mathsf{u}\right)}$ and $f(\boldsymbol{\mathcal{E}}_\mathsf{u},\tilde{\boldsymbol{\varpi}}_\mathsf{u})$. Next, we observe that $f\left(\boldsymbol{\mathcal{E}}_\mathsf{u}^{\mathtt{iter}+1},\boldsymbol{\varpi}_\mathsf{u}^{\mathtt{iter}+1},\tilde{\boldsymbol{\varpi}}_\mathsf{u}^{\mathtt{iter}+1}\right)\geq f\left(\boldsymbol{\mathcal{E}}_\mathsf{u}^{\mathtt{iter}},\boldsymbol{\varpi}_\mathsf{u}^{\mathtt{iter}},\tilde{\boldsymbol{\varpi}}_\mathsf{u}^{\mathtt{iter}}\right)$, because at iteration indexed by $\mathtt{iter}+1$, each of these variables optimally solves the equivalent *convex surrogate* $f(\cdot)$ while keeping the other two variables fixed. Since $f\left(\boldsymbol{\mathcal{E}}_\mathsf{u},\boldsymbol{\varpi}_\mathsf{u},\tilde{\boldsymbol{\varpi}}_\mathsf{u}\right)$ has a finite upper bound, the algorithm is globally convergent. ■

D.4 Proof of Corollary 5.2

Proof. The proof follows using similar techniques as in Lemmas 5.3 and 5.4. We only explain the proof for IrAI. The power of the IrAI with ZF is $\mathbb{E}\left[\left|\sqrt{\mathcal{E}_\mathsf{d}}\kappa_{mn}\mathbf{v}_{mk}^H\mathbf{G}_m^{\mathsf{SI}}\mathbf{p}_{mn}\right|^2\right]=\mathcal{E}_\mathsf{d}\kappa_{mn}^2\mathbb{E}\left[\mathtt{tr}\left\{\mathbf{v}_{mk}^H\mathbf{G}_m^{\mathsf{SI}}\mathbf{p}_{mn}\mathbf{p}_{mn}^H{\mathbf{G}_m^{\mathsf{SI}}}^H\mathbf{v}_{mk}\right\}\right]=\mathcal{E}_\mathsf{d}\kappa_{mn}^2\mathtt{tr}\left\{\mathbb{E}\left[\mathbf{v}_{mk}^H\mathbb{E}\left[\mathbf{G}_m^{\mathsf{SI}}\mathbf{p}_{mn}\mathbf{p}_{mn}^H{\mathbf{G}_m^{\mathsf{SI}}}^H\right]\mathbf{v}_{mk}\right]\right\}=N_\mathtt{tx}\mathcal{E}_\mathsf{d}\kappa_{mn}^2\zeta_{mm}^{\mathsf{SI}}\mathtt{tr}\left\{\mathbb{E}\left[\|\mathbf{v}_{mk}\|^2\right]\right\}=\dfrac{N_\mathtt{tx}\mathcal{E}_\mathsf{d}\kappa_{mn}^2\zeta_{mm}^{\mathsf{SI}}\alpha_{mk}^2}{N_\mathtt{rx}-\tau_p}$, where for the inner expectation, we note that the ith diagonal entry, $\mathbb{E}\left[\mathbf{G}_m^{\mathsf{SI}}\mathbf{p}_{mn}\mathbf{p}_{mn}^H{\mathbf{G}_m^{\mathsf{SI}}}^H\right]_{ii}$, can be evaluated as

$$\begin{aligned}&\mathbb{E}\left[\mathbf{G}_m^{\mathsf{SI}}\left[i,:\right]\mathbf{p}_{mn}\mathbf{p}_{mn}^H{\mathbf{G}_m^{\mathsf{SI}}}^H\left[i,:\right]\right]\\&=\mathtt{tr}\left\{\mathbb{E}\left[\mathbf{p}_{mn}\mathbf{p}_{mn}^H\right]\mathbb{E}\left[{\mathbf{G}_m^{\mathsf{SI}}}^H\left[i,:\right]\mathbf{G}_m^{\mathsf{SI}}\left[i,:\right]\right]\right\}=N_\mathtt{tx}\zeta_{mm}^{\mathsf{SI}}.\end{aligned}$$

Here, $\mathbf{G}_m^{\mathsf{SI}}\left[i,:\right]$ denotes the ith row of $\mathbf{G}_m^{\mathsf{SI}}$. It is easy to show that the off-diagonal terms evaluate to zero. Thus, $\mathbb{E}\left[\mathbf{G}_m^{\mathsf{SI}}\mathbf{p}_{mn}\mathbf{p}_{mn}^H{\mathbf{G}_m^{\mathsf{SI}}}^H\right]=N_\mathtt{tx}\zeta_{mm}^{\mathsf{SI}}\mathbf{I}_{N_\mathtt{rx}}$. Finally, with ZF combining, $\mathbb{E}\left[\|\mathbf{v}_{mk}\|^2\right]=\dfrac{\alpha_{mk}^2}{N_\mathtt{rx}-\tau_p}$. ■

D.5 Numerical experiments on the convergence of Algorithm 7 and Algorithm 9

Now, we validate the rate of convergence (we define this as the difference in the iterates/cost function between two consecutive iterations of the algorithms) of the iterates (i.e., $\boldsymbol{\kappa}$ and $\boldsymbol{\mathcal{E}}_u$) as a function of the iteration count. We evaluate the UL and DL power allocation algorithms with different initializations of $\boldsymbol{\kappa}$ and $\boldsymbol{\mathcal{E}}_\mathsf{u}$, and observe convergence within

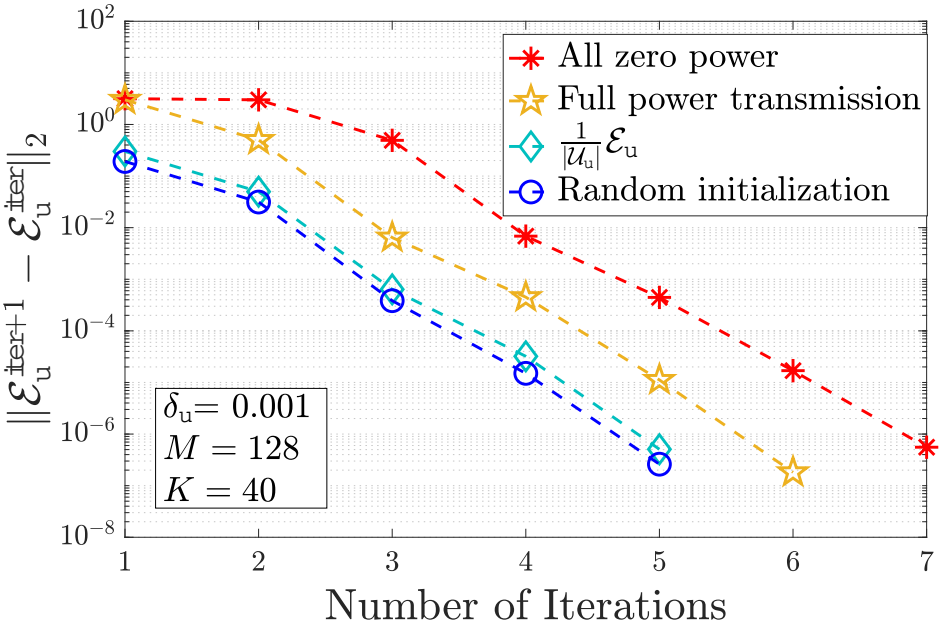

Figure D.1: Rate of convergence of UL power control coefficients

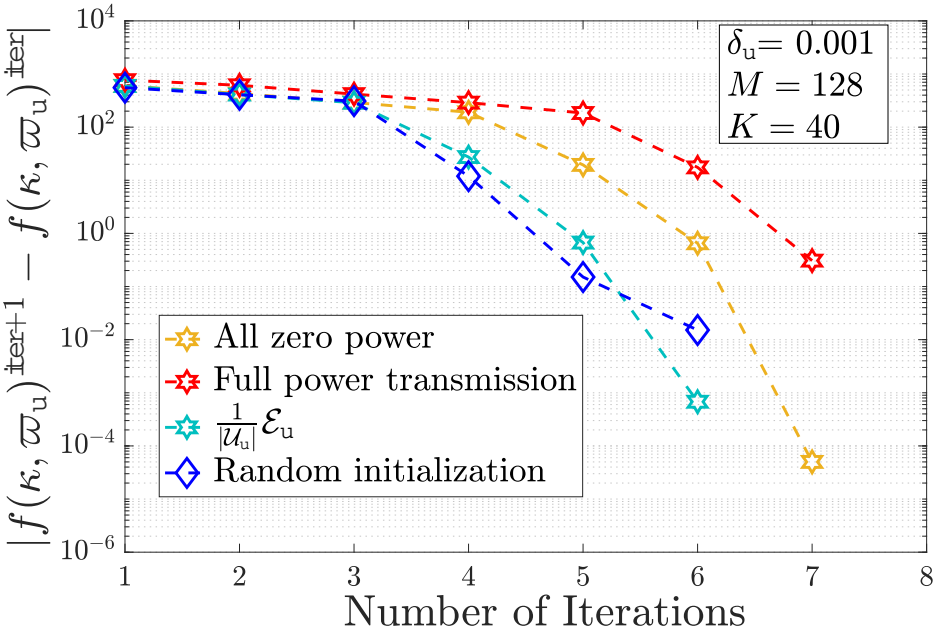

Figure D.2: Rate of convergence of the equivalent cost given in (5.20)

6/7 iterations while ensuring the gap between two consecutive iterates no more than 0.001

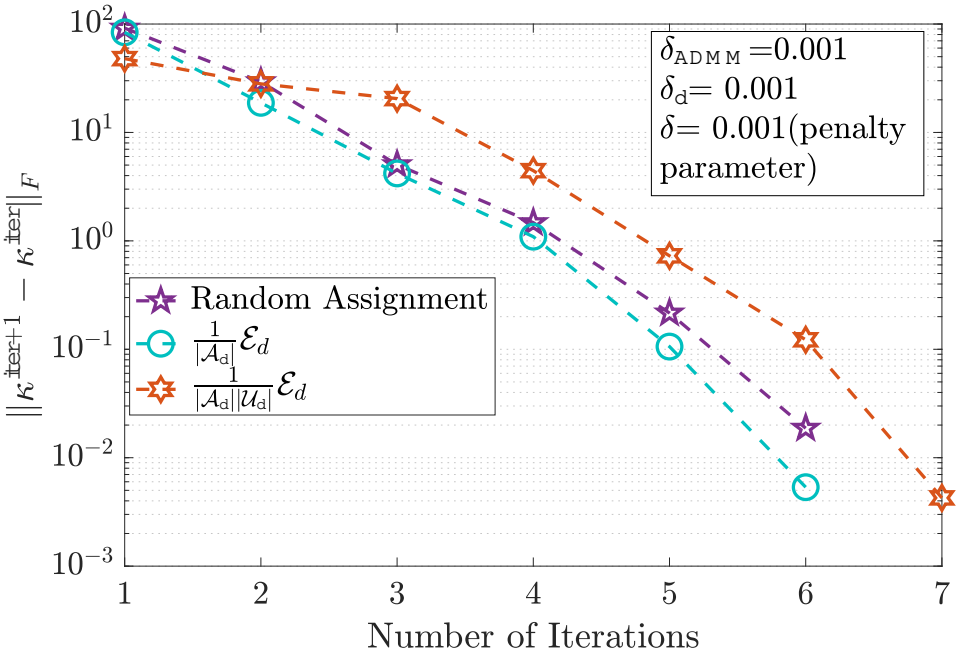

Figure D.3: Rate of convergence of DL power control coefficients

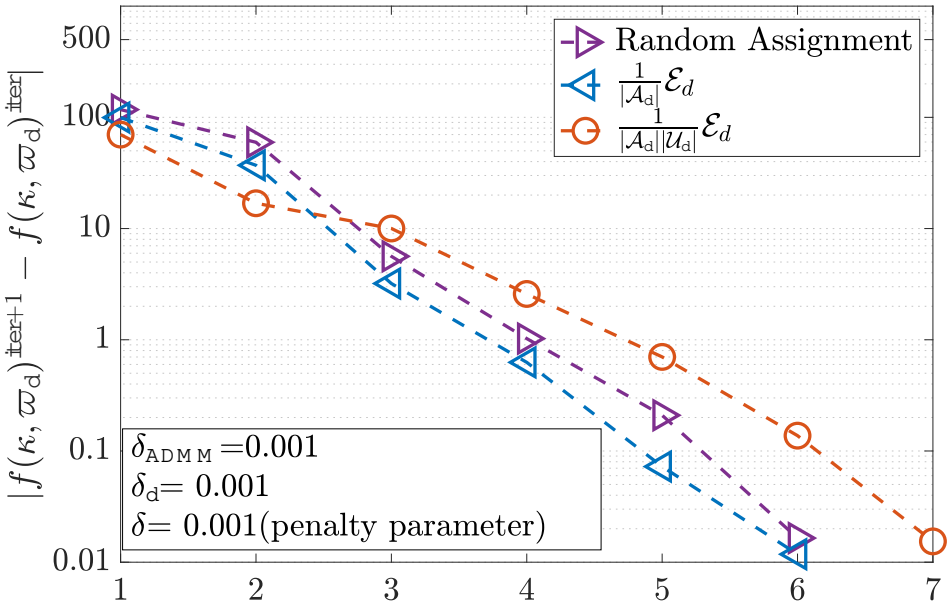

Figure D.4: Rate of convergence of the equivalent cost, i.e., $f(\boldsymbol{\kappa}, \boldsymbol{\varpi}_{\text{d}})$.

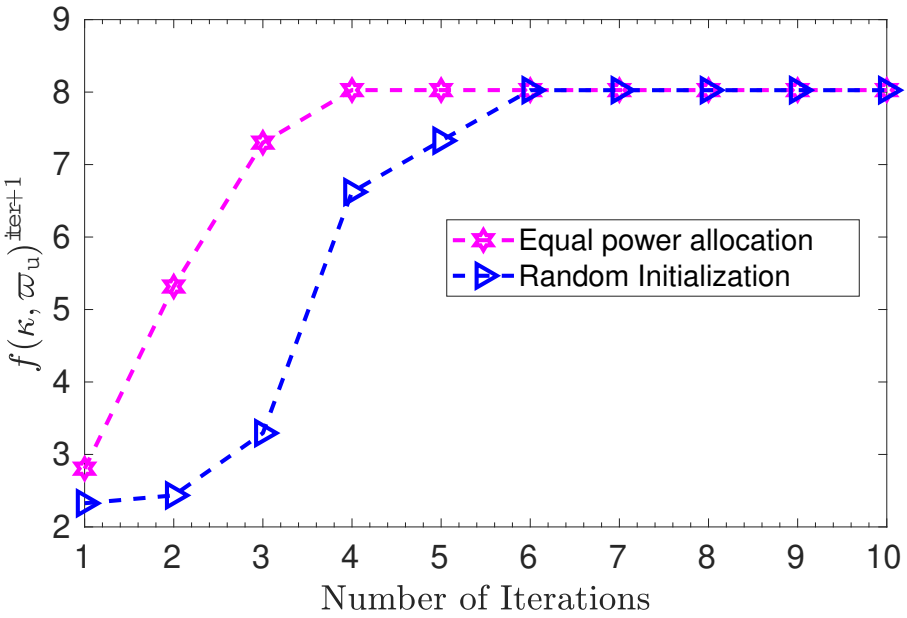

Figure D.5: Convergence of the UL cost function for two different initializations. The legends indicate the initial power allocation.

upon convergence. Specifically, Figure D.5 illustrates the convergence claimed in Proposition 5.2 in the revised manuscript. Similar results can be generated for DL, but we omit it to avoid repetition. Convergence properties of the overall AO of UL and DL power allocation are illustrated in Figure D.6, Figure D.7, and Figure D.8. These experiments reveal fast convergence of the proposed algorithms in terms of cost function as well as the iterates involved in the algorithm, even with a large number of APs and UEs in the system.

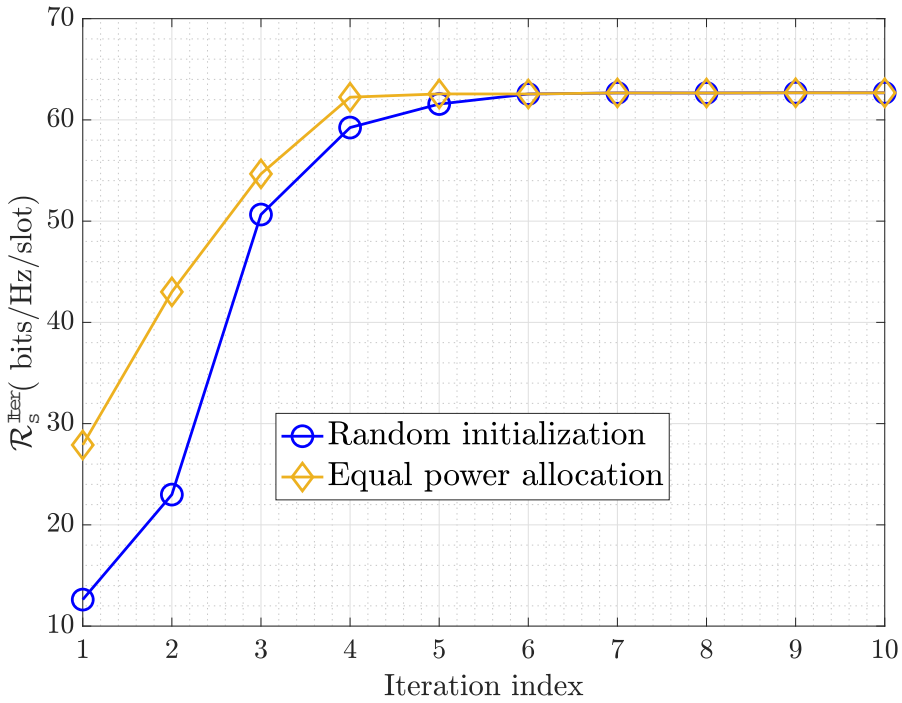

Figure D.6: Convergence of the AO of sum UL-DL SE (cost function) for two different initializations. The legends indicate the initial power allocation

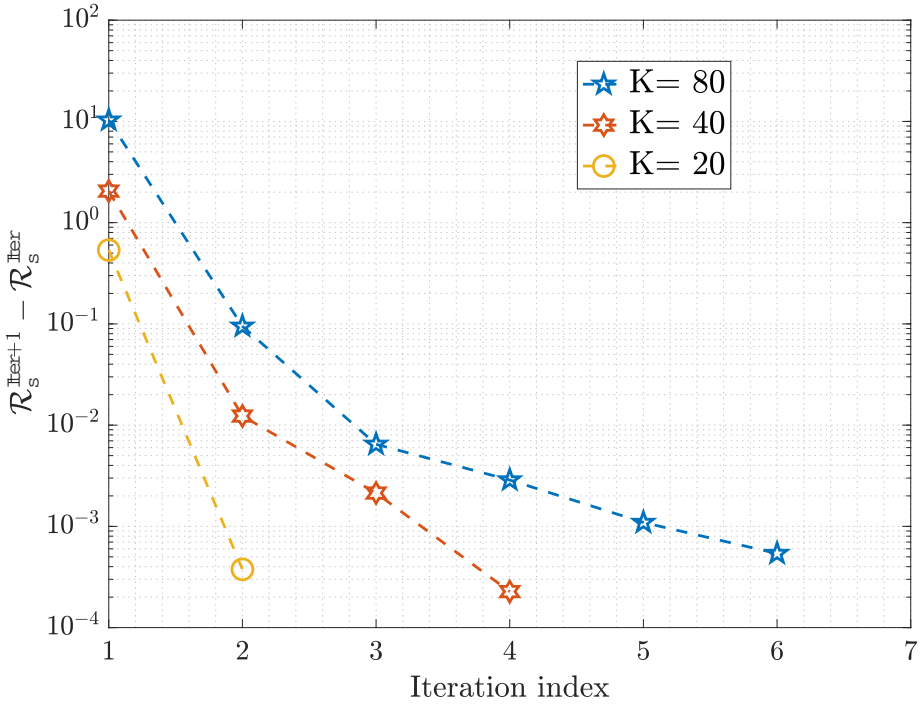

Figure D.7: Rate of convergence of overall alternating optimization with different number of UEs in the system.

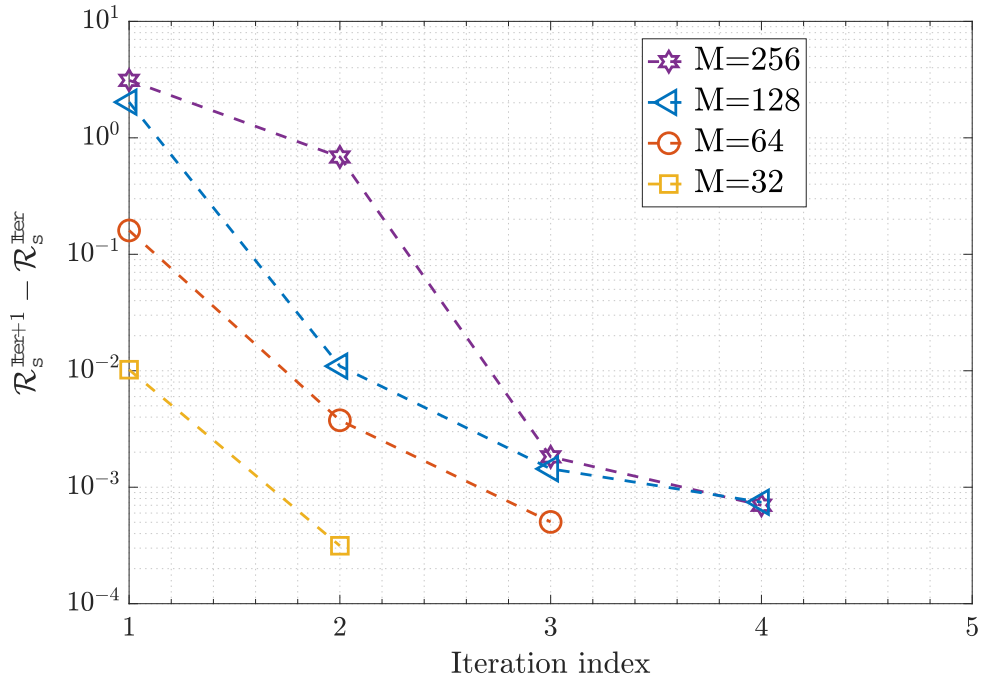

Figure D.8: Rate of convergence of overall alternating optimization with different number of APs in the system.

Bibliography

[1] E. G. Larsson, O. Edfors, F. Tufvesson, and T. L. Marzetta, "Massive MIMO for next generation wireless systems," *IEEE Commun. Mag.*, vol. 52, no. 2, pp. 186–195, Feb. 2014. [Cited on page: 2.]

[2] T. L. Marzetta, "Noncooperative cellular wireless with unlimited numbers of base station antennas," *IEEE Trans. Wireless Commun.*, vol. 9, no. 11, pp. 3590–3600, Nov. 2010. [Cited on page: 2.]

[3] T. L. Marzetta, E. G. Larsson, H. Yang, and H. Q. Ngo, *Fundamentals of Massive MIMO*. Cambridge University Press, 2016, doi:10.1017/CBO9781316799895. [Cited on pages: 2, 82, 198, 200, and 208.]

[4] S. Parkvall, E. Dahlman, A. Furuskar, and M. Frenne, "NR: The new 5G radio access technology," *IEEE Commun. Standards Mag.*, vol. 1, no. 4, pp. 24–30, Dec. 2017. [Cited on page: 2.]

[5] B. Hochwald, T. Marzetta, and V. Tarokh, "Multiple-antenna channel hardening and its implications for rate feedback and scheduling," *IEEE Trans. Inf. Theory*, vol. 50, no. 9, pp. 1893–1909, Sep. 2004. [Cited on page: 2.]

[6] H. Q. Ngo and E. G. Larsson, "No downlink pilots are needed in TDD massive MIMO," *IEEE Trans. Wireless Commun.*, vol. 16, no. 5, pp. 2921–2935, May 2017. [Cited on page: 2.]

[7] D. Lee, H. Seo, B. Clerckx, E. Hardouin, D. Mazzarese, S. Nagata, and K. Sayana, "Coordinated multipoint transmission and reception in LTE-advanced: deployment scenarios and operational challenges," *IEEE Commun. Mag.*, vol. 50, no. 2, pp. 148–155, Feb. 2012. [Cited on page: 2.]

[8] W. Feng, Y. Wang, N. Ge, J. Lu, and J. Zhang, "Virtual MIMO in multi-cell distributed antenna systems: Coordinated transmissions with large-scale CSIT," *IEEE J. Sel. Areas Commun.*, vol. 31, no. 10, pp. 2067–2081, Oct. 2013. [Cited on page: 2.]

[9] W. Choi and J. G. Andrews, "Downlink performance and capacity of distributed antenna systems in a multicell environment," *IEEE Trans. Wireless Commun.*, vol. 6, no. 1, pp. 69–73, Jan. 2007. [Cited on page: 2.]

[10] S. Venkatesan, A. Lozano, and R. Valenzuela, "Network MIMO: Overcoming intercell interference in indoor wireless systems," in *Proc. 41st Asilomar Conf. Signals, Syst., Comput.*, Nov. 2007, pp. 83–87. [Cited on page: 2.]

[11] A. Lozano, R. W. Heath, and J. G. Andrews, "Fundamental limits of cooperation," *IEEE Trans. Inf. Theory*, vol. 59, no. 9, pp. 5213–5226, Sep. 2013. [Cited on page: 3.]

[12] S. Stefanatos and A. Alexiou, "Access point density and bandwidth partitioning in ultra dense wireless networks," *IEEE Trans. Commun.*, vol. 62, no. 9, pp. 3376–3384, Sep. 2014. [Cited on page: 3.]

[13] J. Zhang, S. Chen, Y. Lin, J. Zheng, B. Ai, and L. Hanzo, "Cell-free massive MIMO: A new next-generation paradigm," *IEEE Access*, vol. 7, pp. 99 878–99 888, 2019. [Cited on page: 3.]

[14] E. Nayebi, A. Ashikhmin, T. L. Marzetta, and H. Yang, "Cell-free massive MIMO systems," in *Proc. 49th Asilomar Conf. Signals, Syst. Comput.*, Nov. 2015, pp. 695–699. [Cited on pages: 4 and 76.]

[15] Z. Chen and E. Björnson, "Channel hardening and favorable propagation in cell-free massive MIMO with stochastic geometry," *IEEE Trans. Commun.*, vol. 66, no. 11, pp. 5205–5219, Nov. 2018. [Cited on pages: 4 and 93.]

[16] G. Interdonato, E. Björnson, H. Quoc Ngo, P. Frenger, and E. G. Larsson, "Ubiquitous cell-free massive MIMO communications," *EURASIP J. Wireless Commun. Netw.*, vol. 2019, no. 1, p. 197, Dec. 2019. [Cited on pages: 4, 48, 93, 95, 98, 103, 117, 129, and 137.]

[17] Özlem Tugfe Demir, E. Björnson, and L. Sanguinetti, "Foundations of user-centric cell-free massive MIMO," *Foundations and Trends® in Signal Processing*, vol. 14, no. 3-4, pp. 162–472, 2021. [Online]. Available: http://dx.doi.org/10.1561/2000000109 [Cited on pages: 4 and 130.]

[18] A. Wyner, "Shannon-theoretic approach to a Gaussian cellular multiple-access channel," *IEEE Trans. Inf. Theory*, vol. 40, no. 6, pp. 1713–1727, Nov. 1994. [Cited on page: 5.]

[19] H. Q. Ngo, A. Ashikhmin, H. Yang, E. G. Larsson, and T. L. Marzetta, "Cell-free massive MIMO versus small cells," *IEEE Trans. Wireless Commun.*, vol. 16, no. 3, pp. 1834–1850, Mar. 2017. [Cited on pages: xvi, 5, 7, 24, 48, 51, 56, 57, 60, 63, 74, 75, 76, 82, 84, 91, 93, 98, 101, 103, 117, 132, 175, 177, 185, 199, and 208.]

[20] E. Björnson and L. Sanguinetti, "Making cell-free massive MIMO competitive with MMSE processing and centralized implementation," *IEEE Trans. Wireless Commun.*, vol. 19, no. 1, pp. 77–90, Jan. 2020. [Cited on pages: 7, 60, 98, 111, 113, 117, 129, 130, 131, 135, 140, 141, and 166.]

[21] J. Denis and M. Assaad, "Improving cell-free massive MIMO networks performance: A user scheduling approach," *IEEE Trans. Wireless Commun.*, vol. 20, no. 11, pp. 7360–7374, Nov. 2021. [Cited on pages: 7, 48, and 101.]

[22] R. Sabbagh, C. Pan, and J. Wang, "Pilot allocation and sum-rate analysis in cell-free massive MIMO systems," in *Proc. IEEE Int. Conf. Commun. (ICC)*, May 2018, pp. 1–6. [Cited on pages: 7, 24, 51, 56, and 132.]

[23] A. Sabharwal, P. Schniter, D. Guo, D. W. Bliss, S. Rangarajan, and R. Wichman, "In-band full-duplex wireless: Challenges and opportunities," *IEEE J. Sel. Areas Commun.*, vol. 32, no. 9, pp. 1637–1652, Sep. 2014. [Cited on pages: 7 and 56.]

[24] T. T. Vu, D. T. Ngo, H. Q. Ngo, and T. Le-Ngoc, "Full-duplex cell-free massive MIMO," in *Proc. IEEE Int. Conf. Commun. (ICC)*, May 2019, pp. 1–6. [Cited on pages: 7, 56, 98, 131, 132, 136, 138, 159, 166, and 167.]

[25] "IEEE standard for a precision clock synchronization protocol for networked measurement and control systems," *IEEE Std 1588-2008 (Revision of IEEE Std 1588-2002)*, pp. 1–269, Jul. 2008. [Cited on page: 8.]

[26] R. Rogalin, O. Y. Bursalioglu, H. Papadopoulos, G. Caire, A. F. Molisch, A. Michaloliakos, V. Balan, and K. Psounis, "Scalable synchronization and reciprocity calibration for distributed multiuser MIMO," *IEEE Trans. Wireless Commun.*, vol. 13, no. 4, pp. 1815–1831, Apr. 2014. [Cited on page: 8.]

[27] S. Elhoushy, M. Ibrahim, and W. Hamouda, "Cell-free massive MIMO: A survey," *IEEE Commun. Surv. Tutor.*, vol. 24, no. 1, pp. 492–523, Firstquarter 2022. [Cited on page: 9.]

[28] S.-N. Hong and G. Caire, "Virtual full-duplex relaying with half-duplex relays," *IEEE Trans. Inf. Theory*, vol. 61, no. 9, pp. 4700–4720, Sep. 2015. [Cited on page: 14.]

[29] F. Riera-Palou, G. Femenias, A. G. Armada, and A. Pérez-Neira, "Clustered cell-free massive MIMO," in *Proc. IEEE Globecom Workshops (GC Wkshps)*, Dec. 2018, pp. 1–6. [Cited on pages: 24, 56, and 132.]

[30] H. Liu, J. Zhang, X. Zhang, A. Kurniawan, T. Juhana, and B. Ai, "Tabu-search-based pilot assignment for cell-free massive MIMO systems," *IEEE Trans. Veh. Technol.*, vol. 69, no. 2, pp. 2286–2290, Feb. 2020. [Cited on pages: 24, 51, and 56.]

[31] Y. Zhang, H. Cao, P. Zhong, C. Qi, and L. Yang, "Location-based greedy pilot assignment for cell-free massive MIMO systems," in *Proc. IEEE 4th Int. Conf. Comput. Commun. (ICCC)*, Dec. 2018, pp. 392–396. [Cited on pages: xvi, 24, 57, 63, 64, and 132.]

[32] T. C. Mai, H. Q. Ngo, M. Egan, and T. Q. Duong, "Pilot power control for cell-free massive MIMO," *IEEE Trans. Veh. Technol.*, vol. 67, no. 11, pp. 11 264–11 268, Nov. 2018. [Cited on pages: 24, 51, and 132.]

[33] A. Chowdhury, R. Chopra, and C. R. Murthy, "Can dynamic TDD enabled half-duplex cell-free massive MIMO outperform full-duplex cellular massive MIMO?" *IEEE Trans. Commun.*, vol. 70, no. 7, pp. 4867–4883, Jul. 2022. [Cited on pages: xvi, 24, 51, 56, 57, 60, 63, 129, 130, 132, 136, 162, and 163.]

[34] W. K. Wootters and B. D. Fields, "Optimal state-determination by mutually unbiased measurements," *Annals of Physics*, vol. 191, no. 2, pp. 363 – 381, 1989. [Cited on pages: 26, 27, 35, and 199.]

[35] A. Chowdhury, P. Sasmal, and C. R. Murthy, "Comparison of orthogonal vs. union of subspace based pilots for multi-cell massive MIMO systems," in *Proc. IEEE 21st Int. Workshop Signal Process. Adv. Wireless Commun. (SPAWC)*, May 2020, pp. 1–5. [Cited on pages: 26, 27, 37, 44, and 198.]

[36] A. Klappenecker and M. Roetteler, "Constructions of mutually unbiased bases," 2003. [Cited on pages: 26 and 27.]

[37] Z. Zhang, J. Liu, and K. Long, "Low-complexity cell search with fast PSS identification in LTE," *IEEE Trans. Veh. Technol.*, vol. 61, no. 4, pp. 1719–1729, May 2012. [Cited on page: 27.]

[38] R.-A. Pitaval, B. M. Popović, P. Wang, and F. Berggren, "Overcoming 5G PRACH capacity shortfall: Supersets of zadoff–chu sequences with low-correlation zone," *IEEE Tran. Commun.*, vol. 68, no. 9, pp. 5673–5688, Sep. 2020. [Cited on pages: 27 and 36.]

[39] E. Björnson, J. Hoydis, and L. Sanguinetti, "Massive MIMO networks: Spectral, energy, and hardware efficiency," *Foundations and Trends® in Signal Processing*, vol. 11, no. 3-4, pp. 154–655, 2017. [Cited on pages: 27, 103, 113, and 124.]

[40] R. Jain, D. Chiu, and W. Hawe, "A quantitative measure of fairness and discrimination for resource allocation in shared computer systems," *CoRR*, vol. cs.NI/9809099, 1998. [Online]. Available: https://arxiv.org/abs/cs/9809099 [Cited on page: 29.]

[41] W. C. Jakes and D. C. Cox, *Microwave Mobile Communications*. Wiley-IEEE Press, 1994. [Cited on page: 30.]

[42] N. Akbar, E. Björnson, N. Yang, and E. G. Larsson, "Max-min power control in downlink massive MIMO with distributed antenna arrays," *IEEE Trans. Commun.*, vol. 69, no. 2, pp. 740–751, Feb 2021. [Cited on pages: 32, 33, 34, 37, and 43.]

[43] N. Akbar, E. Bjoernson, E. G. Larsson, and N. Yang, "Downlink power control in massive MIMO networks with distributed antenna arrays," in *Proc. IEEE Int. Conf. Commun. (ICC)*, May 2018, pp. 1–6. [Cited on pages: 32, 33, and 37.]

[44] S. Zhou, M. Zhao, X. Xu, J. Wang, and Y. Yao, "Distributed wireless communication system: a new architecture for future public wireless access," *IEEE Commun. Mag.*, vol. 41, no. 3, pp. 108–113, Mar. 2003. [Cited on page: 32.]

[45] H. Q. Ngo, L. Tran, T. Q. Duong, M. Matthaiou, and E. G. Larsson, "On the total energy efficiency of cell-free massive MIMO," *IEEE Trans. Green Commun. Netw.*, vol. 2, no. 1, pp. 25–39, Mar. 2018. [Cited on pages: 37 and 41.]

[46] H. Liu, J. Zhang, S. Jin, and B. Ai, "Graph coloring based pilot assignment for cell-free massive MIMO systems," *IEEE Trans. Veh. Technol.*, vol. 69, no. 8, pp. 9180–9184, Aug 2020. [Cited on pages: xvi, 43, 57, 63, 64, and 132.]

[47] E. Nayebi, A. Ashikhmin, T. L. Marzetta, H. Yang, and B. D. Rao, "Precoding and power optimization in cell-free massive MIMO systems," *IEEE Trans. Wireless Commun.*, vol. 16, no. 7, pp. 4445–4459, Jul. 2017. [Cited on pages: 48, 76, 93, 98, 117, and 175.]

[48] H. Q. Ngo, A. Ashikhmin, H. Yang, E. G. Larsson, and T. L. Marzetta, "Cell-free massive MIMO: Uniformly great service for everyone," in *Proc. IEEE 16th Int. Workshop Signal Process. Adv. Wireless Commun. (SPAWC)*, Jun. 2015, pp. 201–205. [Cited on pages: xvi, 51, 57, and 63.]

[49] M. Attarifar, A. Abbasfar, and A. Lozano, "Random vs structured pilot assignment in cell-free massive MIMO wireless networks," in *Proc. IEEE Int. Conf. Commun. Workshops (ICC Workshops)*, May 2018, pp. 1–6. [Cited on pages: xvi, 51, 57, 63, 64, and 132.]

[50] E. Björnson and L. Sanguinetti, "Scalable cell-free massive MIMO systems," *IEEE Trans. Commun.*, vol. 68, no. 7, pp. 4247–4261, Jul. 2020. [Cited on page: 51.]

[51] M. Garey and D. Johnson, *Computers and Intractability: A Guide to the Theory of NP-completeness*, ser. Mathematical Sciences Series. Freeman, 1979. [Online]. Available: https://books.google.co.in/books?id=fjxGAQAAIAAJ [Cited on page: 55.]

[52] D. Brélaz, "New methods to color the vertices of a graph," *Commun. ACM*, vol. 22, no. 4, p. 251–256, Apr. 1979, doi: 10.1145/359094.359101. [Cited on page: 56.]

[53] J. Bai and A. Sabharwal, "Asymptotic analysis of MIMO multi-cell full-duplex networks," *IEEE Trans. Wireless Commun.*, vol. 16, no. 4, pp. 2168–2180, Apr. 2017. [Cited on pages: 56, 98, 99, 115, 116, 129, 136, and 138.]

[54] H. H. Yang, G. Geraci, Y. Zhong, and T. Q. S. Quek, "Packet throughput analysis of static and dynamic TDD in small cell networks," *IEEE Wireless Commun. Lett.*, vol. 6, no. 6, pp. 742–745, Dec. 2017. [Cited on page: 67.]

[55] G. RP-110450, "Study item description for further enhancements to LTE TDD for DL-UL interference management and traffic adaptation," 2011. [Cited on pages: 67 and 94.]

[56] R1-1713969, "Discussion on duplexing flexibility and cross-link interference mitigation schemes," *3GPP TSG RAN WG1 Meeting #90*, Aug. 2017. [Cited on pages: 67 and 94.]

[57] "3rd generation partnership project; technical specification group radio access network; NR; physical layer procedures for control (release 15) V15.5.0," 3GPP Standard TS 38.213, Mar. 2019. [Cited on page: 67.]

[58] H. Kim, J. Kim, and D. Hong, "Dynamic TDD systems for 5G and beyond: A survey of cross-link interference mitigation," *IEEE Commun. Surveys Tutor.*, vol. 22, no. 4, pp. 2315–2348, Jul. 2020. [Cited on pages: 67, 94, and 129.]

[59] J. Winters, "Optimum combining in digital mobile radio with cochannel interference," *IEEE Trans. Veh. Technol.*, vol. 33, no. 3, pp. 144–155, Aug. 1984. [Cited on pages: 81 and 83.]

[60] S. Fujishige, Ed., *Chapter I - Introduction, Submodular Functions and Optimization*, ser. Annals of Discrete Mathematics. Elsevier, 2005, vol. 58. [Cited on pages: 86, 87, 106, and 210.]

[61] D. Wang, M. Wang, P. Zhu, J. Li, J. Wang, and X. You, "Performance of network-assisted full-duplex for cell-free massive MIMO," *IEEE Trans. Commun.*, vol. 68, no. 3, pp. 1464–1478, Mar. 2020. [Cited on pages: 88, 95, 98, 111, 112, and 113.]

[62] M. Matthaiou, O. Yurduseven, H. Q. Ngo, D. Morales-Jimenez, S. L. Cotton, and V. F. Fusco, "The road to 6G: Ten physical layer challenges for communications engineers," *IEEE Commun. Mag.*, vol. 59, no. 1, pp. 64–69, Jan. 2021. [Cited on page: 93.]

[63] M. Duarte, C. Dick, and A. Sabharwal, "Experiment-driven characterization of full-duplex wireless systems," *IEEE Trans. Wireless Commun.*, vol. 11, no. 12, pp. 4296–4307, Dec. 2012. [Cited on pages: 93 and 94.]

[64] M. M. Razlighi, N. Zlatanov, S. R. Pokhrel, and P. Popovski, "Optimal centralized dynamic-time-division-duplex," *IEEE Trans. Wireless Commun.*, vol. 20, no. 1, pp. 28–39, Jan. 2021. [Cited on page: 93.]

[65] R1-1701616, "Discussion on duplexing flexibility and cross-link interference mitigation schemes," *3GPP TSG RAN WG1 Meeting #88*, Feb. 2017. [Cited on page: 94.]

[66] L. Xue, Y. Cheng, Y. Zhou, and B. Qu, "Next generation TDD cellular communication," in *Proc. 49th Asilomar Conf. Signals, Syst. Comput.*,, Nov. 2015, pp. 1036–1040. [Cited on page: 94.]

[67] J. Liu, R. Fan, H. Wang, J. Liu, and F. Wang, "Dynamic TDD testbed and field measurements," in *Proc. IEEE Conf. Veh. Technol. (VTC)*, May 2016, pp. 1–5. [Cited on page: 94.]

[68] H. Kamboj, B. Anand, S. Gupta, A. Meshram, S. Balijepalli, and C. Murthy, "Hardware implementation of cell-free MIMO and dynamic TDD using the OAI 5G NR codebase," in *Proc. 25th Int. ITG Workshop Smart Antennas*, Eurecom, French Riviera, France, 2021. [Cited on page: 94.]

[69] J. Liu, S. Han, W. Liu, and C. Yang, "The value of full-duplex for cellular networks: A hybrid duplex-based study," *IEEE Trans. Commun.*, vol. 65, no. 12, pp. 5559–5573, Dec. 2017. [Cited on page: 94.]

[70] J. Liu, S. Han, W. Liu, Y. Teng, and N. Zheng, "Performance gain of full duplex over half duplex under bidirectional traffic asymmetry," in *Proc. IEEE Int. Conf. Commun. Workshops, (ICC)*, May 2016, pp. 98–103. [Cited on page: 94.]

[71] R1-1702113, "Discussion on duplexing flexibility and cross-link interference mitigation schemes," *3GPP TSG RAN WG1 Meeting #88*, Sophia Antipolis, France, Feb. 2017. [Cited on page: 95.]

[72] P. Jayasinghe, A. Tölli, J. Kaleva, and M. Latva-aho, "Bi-directional beamformer training for dynamic TDD networks," *IEEE Trans. Signal Process.*, vol. 66, no. 23, pp. 6252–6267, Dec. 2018. [Cited on page: 95.]

[73] K. Lee, Y. Park, M. Na, H. Wang, and D. Hong, "Aligned reverse frame structure for interference mitigation in dynamic TDD systems," *IEEE Trans. Wireless Commun.*, vol. 16, no. 10, pp. 6967–6978, Oct. 2017. [Cited on page: 95.]

[74] A. Chowdhury, R. Chopra, C. R. Murthy, and H. A. Suraweera, "On the achievable rates of full-duplex massive MIMO systems under channel aging," in *Proc. IEEE 20th Int. Workshop Signal Process. Adv. Wireless Commun. (SPAWC)*, Jul. 2019, pp. 1–5. [Cited on pages: 98, 99, and 116.]

[75] A. C. Cirik, Y. Rong, and Y. Hua, "Achievable rates of full-duplex MIMO radios in

fast fading channels with imperfect channel estimation," *IEEE Trans. Signal Process.*, vol. 62, no. 15, pp. 3874–3886, Aug. 2014. [Cited on page: 98.]

[76] M. Bashar, K. Cumanan, A. G. Burr, M. Debbah, and H. Q. Ngo, "On the uplink max–min SINR of cell-free massive MIMO systems," *IEEE Trans. Wireless Commun.*, vol. 18, no. 4, pp. 2021–2036, Apr. 2019. [Cited on pages: 101 and 103.]

[77] Y. Gao, H. Vinck, and T. Kaiser, "Massive MIMO antenna selection: Switching architectures, capacity bounds, and optimal antenna selection algorithms," *IEEE Trans. Signal Process.*, vol. 66, no. 5, pp. 1346–1360, Mar. 2018. [Cited on pages: 106 and 147.]

[78] S. Ma, L. Xu, C. Du, X. Cheng, and S. Li, "A novel dynamic user admission scheme for multi-cell massive MIMO systems," in *Proc. IEEE Int. Symp. Broadband Multimedia Syst. Broadcast. (BMSB)*, Oct. 2020, pp. 1–4. [Cited on page: 107.]

[79] R. Vaze and H. Ganapathy, "Sub-modularity and antenna selection in MIMO systems," *IEEE Commun. Lett.*, vol. 16, no. 9, pp. 1446–1449, Sep. 2012. [Cited on page: 107.]

[80] J. Wang, H. Zhu, L. Dai, N. J. Gomes, and J. Wang, "Low-complexity beam allocation for switched-beam based multiuser massive MIMO systems," *IEEE Trans. Wireless Commun.*, vol. 15, no. 12, pp. 8236–8248, Dec. 2016. [Cited on page: 107.]

[81] C. R. Srivatsa and C. R. Murthy, "On the impact of channel estimation on the design and analysis of IRSA based systems," *IEEE Trans. Sig. Process.*, vol. 70, pp. 4186–4200, 2022. [Cited on page: 113.]

[82] C. Peel, B. Hochwald, and A. Swindlehurst, "A vector-perturbation technique for near-capacity multiantenna multiuser communication-part I: channel inversion and regularization," *IEEE Trans. Commun.*, vol. 53, no. 1, pp. 195–202, Jan. 2005. [Cited on page: 113.]

[83] J. Zhang, C.-K. Wen, S. Jin, X. Gao, and K.-K. Wong, "Large system analysis of cooperative multi-cell downlink transmission via regularized channel inversion with imperfect CSIT," *IEEE Trans. Wireless Commun.*, vol. 12, no. 10, pp. 4801–4813, Oct. 2013. [Cited on page: 114.]

[84] S. Fukue, H. Iimori, G. T. F. De Abreu, and K. Ishibashi, "Joint access configuration and beamforming for cell-free massive MIMO systems with dynamic TDD," *IEEE Access*, vol. 10, pp. 40 130–40 149, 2022. [Cited on page: 129.]

[85] J. Zheng, J. Zhang, H. Du, D. Niyato, B. Ai, M. Debbah, and K. B. Letaief, "Mobile cell-free massive MIMO: Challenges, solutions, and future directions," *IEEE Wireless Commun.*, to appear, 2023. [Cited on page: 129.]

[86] J. Zheng, J. Zhang, J. Cheng, V. C. M. Leung, D. W. K. Ng, and B. Ai, "Asynchronous cell-free massive MIMO with rate-splitting," *IEEE J. Sel. Areas Commun.*, vol. 41, no. 5, pp. 1366–1382, May 2023. [Cited on page: 129.]

[87] Y. Zhu, J. Li, P. Zhu, H. Wu, D. Wang, and X. You, "Optimization of duplex mode selection for network-assisted full-duplex cell-free massive MIMO systems," *IEEE Commun. Lett.*, vol. 25, no. 11, pp. 3649–3653, Nov. 2021. [Cited on pages: 129, 130, and 133.]

[88] X. Xia, P. Zhu, J. Li, H. Wu, D. Wang, Y. Xin, and X. You, "Joint user selection and transceiver design for cell-free with network-assisted full duplexing," *IEEE Trans. Wireless Commun.*, vol. 20, no. 12, pp. 7856–7870, Dec. 2021. [Cited on pages: 129, 132, and 156.]

[89] Y. Hu, H. Ge, H. Wang, and D. Wang, "Spectral efficiency of network-assisted full-duplex for cell-free massive MIMO system under pilot contamination," *IEEE Access*, vol. 9, pp. 110 826–110 841, 2021. [Cited on pages: 130 and 132.]

[90] X. Xia, P. Zhu, J. Li, H. Wu, D. Wang, and Y. Xin, "Joint optimization of spectral efficiency for cell-free massive MIMO with network-assisted full duplexing," *Sci. China Inf. Sci.*, vol. 64, pp. 1–16, Aug. 2021. [Cited on pages: 130 and 133.]

[91] X. Xia, Z. Fan, W. Luo, A. Lu, D. Wang, X. Zhao, and X. You, "Joint uplink power control, downlink beamforming, and mode selection for secrecy cell-free massive MIMO with network-assisted full duplexing," *IEEE Syst. J.*, vol. 17, no. 1, pp. 720–731, Mar. 2023. [Cited on pages: 130 and 133.]

[92] M. Mohammadi, T. T. Vu, B. Naderi Beni, H. Q. Ngo, and M. Matthaiou, "Virtually full-duplex cell-free massive MIMO with access point mode assignment," in *Proc. IEEE 23rd Int. Workshop Signal Process. Adv. Wireless Commun. (SPAWC)*, Jul. 2022, pp. 1–5. [Cited on pages: 130, 131, 132, 133, 134, 150, 156, and 159.]

[93] M. Mohammadi, T. T. Vu, H. Q. Ngo, and M. Matthaiou, "Network-assisted full-duplex cell-free massive MIMO: Spectral and energy efficiencies," *IEEE J. Sel. Areas Commun.*, vol. 41, no. 9, pp. 2833–2851, Sep. 2023. [Cited on pages: 131, 132, 134, and 142.]

[94] H. V. Nguyen, V.-D. Nguyen, O. A. Dobre, S. K. Sharma, S. Chatzinotas, B. Ottersten, and O.-S. Shin, "On the spectral and energy efficiencies of full-duplex cell-free massive MIMO," *IEEE J. Sel. Areas Commun.*, vol. 38, no. 8, pp. 1698–1718, Aug. 2020. [Cited on pages: 131 and 133.]

[95] P. Anokye, R. K. Ahiadormey, and K.-J. Lee, "Full-duplex cell-free massive MIMO with low-resolution ADCs," *IEEE Trans. Veh. Technol.*, vol. 70, no. 11, pp. 12 179–12 184, Nov. 2021. [Cited on pages: 131, 132, and 136.]

[96] A. Chowdhury and C. R. Murthy, "Comparative study of dynamic TDD with full-duplex in cell-free massive MIMO systems," in *Proc. Nat. Conf. Commun. (NCC), Guwahati, India*, Feb. 2023, pp. 1–6. [Cited on pages: 131 and 132.]

[97] Q. Ding, Y. Lian, and Y. Jing, "Performance analysis of full-duplex massive MIMO systems with low-resolution ADCs/DACs over Rician fading channels," *IEEE Trans. Veh. Technol.*, vol. 69, no. 7, pp. 7389–7403, Jul. 2020. [Cited on pages: 132, 136, and 138.]

[98] K. Shen and W. Yu, "Fractional programming for communication systems—part I: Power control and beamforming," *IEEE Trans. on Signal Process.*, vol. 66, no. 10, pp. 2616–2630, May 2018. [Cited on pages: 133, 148, 151, 152, and 157.]

[99] S. Boyd, N. Parikh, E. Chu, B. Peleato, and J. Eckstein, "Distributed optimization and statistical learning via the alternating direction method of multipliers," *Found. Trends Mach. Learn.*, vol. 3, no. 1, p. 1–122, jan 2011. [Online]. Available: https://doi.org/10.1561/2200000016 [Cited on pages: 133 and 153.]

[100] T. Riihonen, S. Werner, and R. Wichman, "Mitigation of loopback self-interference in full-duplex MIMO relays," *IEEE Trans. Signal Process.*, vol. 59, no. 12, pp. 5983–5993, Dec. 2011. [Cited on page: 136.]

[101] S. M. Kay, *Fundamentals of Statistical Signal Processing: Estimation Theory*. Englewood Cliffs, NJ, USA: Prentice-Hall, Inc., 1993. [Cited on page: 138.]

[102] A. Lozano, A. Tulino, and S. Verdu, "Multiple-antenna capacity in the low-power regime," *IEEE Trans. Inf. Theory*, vol. 49, no. 10, pp. 2527–2544, Oct. 2003. [Cited on page: 143.]

[103] S. Buzzi, C. D'Andrea, A. Zappone, and C. D'Elia, "User-centric 5G cellular networks: Resource allocation and comparison with the cell-free massive MIMO approach," *IEEE Trans. Wireless Commun.*, vol. 19, no. 2, pp. 1250–1264, Feb. 2020. [Cited on page: 157.]

[104] R. Nikbakht, R. Mosayebi, and A. Lozano, "Uplink fractional power control and

downlink power allocation for cell-free networks," *IEEE Wireless Commun. Lett.*, vol. 9, no. 6, pp. 774–777, Jun. 2020. [Cited on pages: xvii, 166, and 167.]

[105] R. Nikbakht and A. Lozano, "Uplink fractional power control for cell-free wireless networks," in *Proc. IEEE Int. Conf. Commun. (ICC)*, May 2019, pp. 1–5. [Cited on pages: xvii, 166, and 167.]

[106] G. Interdonato, P. Frenger, and E. G. Larsson, "Scalability aspects of cell-free massive MIMO," in *Proc. IEEE Int. Conf. Commun. (ICC)*, May 2019, pp. 1–6. [Cited on pages: xvii, 167, and 168.]

[107] M. Karlsson, E. Björnson, and E. G. Larsson, "Techniques for system information broadcast in cell-free massive MIMO," *IEEE Trans. Commun.*, vol. 67, no. 1, pp. 244–257, Jan. 2019. [Cited on pages: 175 and 185.]

[108] Özlem Tugfe Demir, E. Björnson, and L. Sanguinetti, "Foundations of user-centric cell-free massive MIMO," *Foundations and Trends® in Signal Processing*, vol. 14, no. 3-4, pp. 162–472, 2021. [Online]. Available: http://dx.doi.org/10.1561/2000000109 [Cited on pages: 175 and 183.]

[109] W. Jiang and H. D. Schotten, "Cell-free massive MIMO-OFDM transmission over frequency-selective fading channels," *IEEE Commun. Lett.*, vol. 25, no. 8, pp. 2718–2722, Aug. 2021. [Cited on pages: 175, 177, 180, and 185.]

[110] ——, "Opportunistic AP selection in cell-free massive MIMO-OFDM systems," in *Proc. IEEE 95th Veh. Technol. Conf. (VTC- Spring)*, Jun. 2022, pp. 1–5. [Cited on pages: 175 and 180.]

[111] H. Ge, N. Garg, and T. Ratnarajah, "Channel estimation for generalized superimposed cell-free massive MIMO-OFDM systems," in *Proc. IEEE 23rd Int. Workshop Signal Process. Adv. Wireless Commun. (SPAWC)*, Jul. 2022, pp. 1–5. [Cited on pages: 175 and 180.]

[112] "Evolved Universal Terrestrial Radio Access (E-UTRA); Physical Channels and Modulation," 3GPP TS 36.211 release 10 (v10.7.0), Feb., 2013. [Cited on page: 175.]

[113] D. Tse and P. Viswanath, *Fundamentals of Wireless Communication*. Cambridge University Press, 2005. [Cited on pages: 177, 183, and 184.]